CRANFIELD UNIVERSITY

G.A. FLYNN

EXPERIMENTAL INVESTIGATION OF ATTACHMENT LINE TRANSITION ON A LARGE SWEPT CYLINDER

CRANFIELD COLLEGE OF AERONAUTICS

PhD THESIS

CRANFIELD UNIVERSITY

CRANFIELD COLLEGE OF AERONAUTICS

PhD THESIS

Academic year 1996-7

G.A. FLYNN

Experimental investigation of attachment line transition on a large swept cylinder

Supervisor : **R.I. Jones**

January 1997

ABSTRACT

Transition of the attachment line boundary layer was investigated using a large swept cylinder. Results for natural transition and transition tripping with two-dimensional trip wires were similar to those obtained by Poll using a similar, but smaller, model. Lower displacement thickness Reynolds numbers but larger trip sizes, than for the flat-plate boundary layer, were required for transition. The investigation of transition tripping was then extended to involve three-dimensional trips. The attachment line boundary layer was less susceptible to three-dimensional trips than to two-dimensional trips but upper and lower bounds of attachment line Reynolds number for transition were identical. It was also found that the roughness Reynolds numbers for fully effective three-dimensional trips were similar for the attachment line and flat-plate boundary layers. Another common feature was the more abrupt upstream movement of the transition front with increasing Reynolds number for three-dimensional trips than for two-dimensional trips. Turbulence spreading downstream of a three-dimensional trip was also examined and, as in the flat-plate boundary layer, was found to be heavily dependent on Reynolds number (varying from 3° at low Reynolds number to a value approaching 10° as Reynolds number exceeded the value for natural transition), but was also dependent on either the trip size or the initial conditions at which the trip first introduced turbulent spots. The effects of higher levels of freestream turbulence were then investigated for both two-dimensional and three-dimensional trips. With a small increase in freestream turbulence the conditions for transition with two-dimensional trips were affected far more than those for three-dimensional trips, for which only the transition completion conditions were affected significantly, resulting in a reduced extent of the transition region. Larger levels of turbulence appeared to have similar effects on the two trip types. Restrictions in model length and windspeed for the higher turbulence tests prevented an accurate investigation of the effects of turbulence on the upper and lower bounds for transition tripping and on the influence of spanwise distance at higher levels of turbulence. Finally, the interaction between two trips positioned on the attachment line was examined. The effect of the second trip on the transition Reynolds number was found to a function of the streamwise separation distance between the two trips.

ACKNOWLEDGEMENT

I would like to thank my supervisor, Dr. R.I. Jones, for his guidance throughout a long project and for his optimism when things were looking bleak. I would also like to thank Professor D.I.A. Poll and Dr. K.P. Garry for their advice regarding both my wind tunnel tests and some of my more speculative conclusions. In addition, special thanks go to Malcolm Goodridge and his workshop staff for the excellent work and constant repairs performed on my model.

Finally, I would like to thank my mother for her limitless support throughout my many years as student.

Dedicated to my father.

CONTENTS

LIST OF FIGURES

NOTATION

C^*	-	Reynolds number = $\bar{R}^2$
C	-	Chord
Cp	-	Pressure coefficient
d	-	Trip wire or sphere diameter
k	-	Trip height (= d)
K	-	Relaminarisation parameter
P	-	Stagnation pressure
p	-	Static pressure
Q_∞	-	Freestream velocity
q_∞	-	Freestream dynamic pressure
r	-	Leading edge radius
$\bar{R}$	-	Characteristic Reynolds number (= $V_e.\eta/\upsilon$)
R_k	-	Reynolds number based on height k of roughness element and velocity V_e
R_{kk}	-	Reynolds number based on height k of roughness element and velocity V_k
R_{δ^*}	-	Reynolds number w.r.t laminar boundary layer displacement thickness (= $1.026\bar{R}$)
R_θ	-	Reynolds number w.r.t laminar boundary layer momentum thickness (= $0.404\bar{R}$)
s	-	Distance between trip wire and transition detection location
s_{12}	-	Distance between first and second trips
t	-	Time
U_1	-	Velocity gradient normal to leading edge
U	-	Chordwise component of velocity
V	-	Spanwise component of velocity
V_{rms}	-	Root-mean-square of hot-wire output voltage
x	-	Chordwise distance, perpendicular to attachment line
y	-	Spanwise distance, parallel to attachment line
z	-	Distance normal to surface
α	-	Turbulence spreading semi-angle
Γ	-	Intermittency factor
δ	-	Boundary layer thickness
δ^*	-	Displacement thickness
ϵ	-	Blockage correction factor
ζ	-	Normalised co-ordinate for intermittency distributions
η	-	Characteristic length
θ	-	Momentum thickness

Λ	-	Sweep angle
ν	-	Kinematic viscosity
ρ	-	Density
ϕ	-	Chordwise position expressed as angle round model ($\approx$ x/r)
ψ	-	Angle between external streamline and attachment line
2D	-	Two-dimensional
3D	-	Three-dimensional

Suffices

∞	-	Free stream
e	-	At outer edge of boundary layer
w	-	At wall
r	-	At reattachment
k	-	Height of tripping element
a.l.	-	At attachment line

Acronyms

CSV	-	Comma separated values
ASCII	-	American standard code for information interchange
RMS	-	Root mean square
DVM	-	Digital voltmeter
ADC	-	Analogue to digital converter

Note

k is also used to represent a constant in chapter 1 and appendix A

INTRODUCTION

In early studies of transition on swept wings, Gray('52) observed transition occurring very close to the leading edge of several swept wings. He concluded that the transition was caused by instabilities linked to the streamline curvature in the flow downstream of the leading edge. Owen & Randall('52&'53) investigated this further and discovered that the transition near the leading edge was indeed caused by a mechanism later named cross-flow instability, a conclusion supported by Gregory('60). Thus, in 1965, the teams, including Gaster at Handley Page and Pfenninger at Northrop Norair, investigating transition on swept wings had expected the main transition problem to be cross-flow instability. During the tests, however, it was discovered that the turbulent boundary layer from the fuselage was contaminating the attachment line boundary layer at the root junction and the resulting turbulence was spreading along the attachment line resulting in a turbulent wing. This process was named attachment line contamination. Gaster('67), Gregory & Love('65) and Pfenninger('65) immediately started to investigate the problem and several possible solutions were proposed. Gaster developed a 'bump' which produced a local stagnation point and prevented the turbulence from advancing along the attachment line, while Pfenninger used a combination of boundary layer suction and fences to remove the turbulence. However, these investigations were terminated at an early stage, before the processes involved in attachment line transition could be investigated in detail.

In the 1970's, with the occurrence of the oil crisis, interest in laminar flow was rekindled and investigations into swept wing flows and attachment line transition were reintroduced. Although numerous companies and research institutes, including NASA, Boeing, McDonnell Douglas and Airbus, have examined aspects of laminar flow wings the majority of the work investigating attachment line transition has been performed by Poll('78-'92) at Cranfield and Manchester Universities and, to a lesser extent, Arnal('88&'92) at ONERA.

Although Poll's work examined attachment line transition fairly comprehensively, covering semi-infinite wings, tapered wings, effects of compressibility, etc., it was limited to 2D trip wires at low levels of freestream turbulence. The present investigation is intended to extend the work of Poll to include transition tripping using 3D trips (in this case spheres) and the effects of higher levels of freestream turbulence on a semi-infinite wing in incompressible flows. Gregory & Love('65) and Firmin & Cook(unpublished) briefly examined attachment line transition with 3D trips but the results were very limited. The present investigation covers a wider range of 3D trip sizes and Reynolds numbers, with the 3D trips positioned both on and downstream of the attachment line. The latter allowed the spreading angle of the turbulent wedge formed downstream of the trip to be examined and thus give an indication of the influence of the trips on the attachment line boundary layer. No previous investigations of attachment line transition with high levels of freestream

turbulence could be found, however, the effects of freestream turbulence on attachment line transition are of interest, especially with respect to internal flows and in particular transition on turbine blades. Finally, the affect of interaction between two trips, on transition Reynolds numbers, was briefly investigated.

The experiments carried out in the present investigation were intended to cover a wide variety of topics and provide information on the conditions for attachment line transition for each of these. Mechanisms involved were not investigated and in some cases restrictions in the facilities, and their availability, prevented as complete an investigation as would have been liked.

1 - THE ATTACHMENT LINE BOUNDARY LAYER

The attachment line boundary layer forms along the leading edge of a swept wing at the loci of the points where the flow attaches to the wing before diverging over the upper and lower surfaces. As a result of the wing sweep, a flow exists along this line and hence the attachment line boundary layer is formed. A sketch of the attachment line boundary layer, taken from Poll('83b), is presented in Fig 1.1, where the line AA represents the attachment line. The axis system is also shown.

From the sketch it is clear that the flow in the vicinity of the attachment line is highly three-dimensional and the attachment line boundary layer is heavily influenced by the flow divergence. In order to simplify this complicated problem, the attachment line boundary layer is often studied using models where infinite swept wing conditions can be assumed.

The infinite swept wing flow is an idealised situation that is often a close approximation to conditions on the leading edge of a high aspect ratio untapered wing. In this case the attachment line boundary layer quickly reaches an asymptotic condition where boundary layer growth is cancelled by flow divergence on to the upper and lower surfaces of the wings. Due to this balance between the fluid that enters the layer from the freestream and that which is removed by the divergence, all spanwise variations are eliminated. Thus the attachment line boundary layer must have constant properties along the span, e.g. constant thickness, constant skin friction coefficient, etc.

Since the fluid that is withdrawn from the attachment line forms part of the developing chordwise boundary layer flow, attachment line transition is the critical transition mechanism and must be dealt with before further transition mechanisms downstream can be considered. If the attachment line boundary layer is turbulent then the whole wing boundary layer will be turbulent, unless there is relaminarisation in the favourable pressure gradient immediately downstream of the attachment line.

The present investigation is limited to the case of a cylinder with a constant section and a large spanwise extent and can therefore be assumed to be semi-infinite. Poll *et al*('92) argued that since differences between the values of sweep back, transition location and chordwise velocity-gradient for aircraft and wind-tunnel models have no particular significance (provided that the value of the non-dimensional characteristic parameter, $\bar{R}$, is reproduced in the experiment), then accurate flight scale information can be obtained on a highly swept model, with a large leading edge radius, in a large low-speed wind-tunnel. Thus the criteria developed for infinite swept cylinders can be applied to swept wings and slender bodies at incidence.

It has already been mentioned that in the case of an untapered, high aspect ratio cylinder the external inviscid flow and the boundary layer are independent of spanwise position. In addition, Poll('78) stated that freestream turbulence levels are also unimportant

unless the turbulence intensity is greater than 0.8% (although this was based on studies of the effect of turbulence on heat transfer) and Poll *et al*('92) showed that for a typical civil aircraft at cruise condition the spanwise Mach number is approximately 0.3. Compressibility is therefore unlikely to present a problem and it is not necessary to examine attachment line transition in a transonic wind tunnel. The attachment line boundary layer can therefore by completely specified by the Reynolds number $\bar{R}$. This conclusion was previously made for low speed flows by Cumpsty & Head('67) for their similarity parameter C^*. Poll later rejected this parameter since the length scale is not directly related to the boundary layer thickness. He introduced the parameter $\bar{R}$ $(= C^{*1/2})$ where :

$$\bar{R} = \frac{V_e \eta}{\nu_e}$$

and η is the characteristic length scale, which for the attachment line boundary layer is related to the flow divergence and is defined by :

$$\eta = \left(\frac{\nu_e}{(dU_e/dx)_{x=0}}\right)^{1/2}$$

In the present investigation the attachment line boundary layer is tripped, using trip wires and spheres, to cause premature transition. These trips lead to an additional two parameters related to the trip height, d, and the distance, s, from the trip to the transition detection location. Three independent non-dimensional groups are therefore required to describe the transition conditions, namely :

$$\bar{R}\,,\ d/\eta\,,\ s/\eta$$

In order to derive a simple relation between the experimental conditions (model sweep, windspeed etc.) and the parameters $\bar{R}$ and η, it is necessary to examine the flow in the vicinity of the attachment line. On and immediately downstream of the attachment line there is a region where the flow at the edge of the boundary layer may be estimated by the following relations :

$$U_e = kx \qquad\qquad V_e = V_\infty = constant$$

where k is a constant and can be obtained from :

$$k = \frac{U_\infty U_1}{C} \qquad and \qquad U_1 = \left[\frac{d(U_e/U_\infty)}{d(x/C)} \right]_{x=0}$$

These relations allow the derivation of the characteristic length scale η, and also therefore the Reynolds number $\bar{R}$, in terms of leading edge sweep and radius, and freestream parameters for the particular case of the swept cylinder. Appendix A shows the calculation of η, the result of which is :

$$\eta = \sqrt{\frac{\nu_e r}{2 Q_\infty \cos\Lambda}}$$

this gives

$$\bar{R} = \sqrt{\frac{Q_\infty r \sin\Lambda \tan\Lambda}{2 \nu_e}}$$

Cumpsty & Head('69) investigated the use of a similar equation, for their swept cylinder model, given that the effective values of the model dimensions were not known. The method they used to obtain the effective value of C^* ($= \bar{R}^2$) is detailed in their report. From their results Cumpsty & Head concluded that the geometric value of C^* could be taken as the effective value. Thus C^* can be calculated on the assumption that the velocity gradient around a leading edge is the same as that around a similar leading edge in two-dimensional potential flow.

Cumpsty & Head also concluded that, since the boundary layer properties on the leading edge were uniquely defined by the value of C^*, only a single experimental arrangement with a range of tunnel speeds was required to obtain results which would be valid for all combinations of sweep, leading edge radius and stream velocity.

Since the majority of work investigating transition mechanisms is done using flat-plate models, it is necessary to compare the attachment line boundary layer to the flat-plate boundary layer.

Due to the asymptotic condition created by the flow divergence, the attachment line boundary layer is closer to the asymptotic suction layer or the fully developed pipe flow than the flat-plate boundary layer. However, several authors, including Arnal & Juillen('88) and Cumpsty & Head('67), have stated that the attachment line profile is almost indistinguishable from the Blasius flat-plate profile. The theoretical attachment line laminar velocity profile from Rosenhead('63) was plotted against the Blasius profile and presented

in Fig 1.2. It can be seen that while the profiles are indeed similar, the attachment line profile is slightly fuller and hence a slightly more stable velocity profile.

The relations between the non-dimensional parameters used in attachment line investigations and the standard non-dimensional parameters used for laminar boundary layers in flat-plate studies can be obtained from tabulated data in Rosenhead('63), leading to the following relations :

$$\delta_{.99} = 3.055 \,.\, \eta \quad \text{and} \quad R_{\delta.99} = 3.055 \,.\, \bar{R}$$

$$\delta^{*} = 1.026 \,.\, \eta \quad \text{and} \quad R_{\delta^{*}} = 1.026 \,.\, \bar{R}$$

$$\theta = 0.404 \,.\, \eta \quad \text{and} \quad R_{\theta} = 0.404 \,.\, \bar{R}$$

2 - TRANSITION ON SWEPT WINGS

2.1 NATURAL ATTACHMENT LINE TRANSITION

Attachment line transition was first discovered due to contamination from the turbulent boundary layer of the fuselage. In the absence of these upstream disturbances and with a smooth surface, attachment line transition may occur due to amplification of small-scale turbulent and acoustic fluctuations present in the freestream. The process is the same as natural transition on a flat plate and involves selective amplification of small disturbances, characterised by their frequency and wave number, leading to the creation of wave packets. The wave packets consist of predominately two-dimensional travelling waves normally referred to as Tollmein-Schlichting (TS) waves.

Many authors, including Poll, Cumpsty & Head('69), and Hall & MacKerrell('88) have studied natural attachment line transition and a critical value of $\bar{R}$ of about 600 has been generally agreed upon. For values of $\bar{R}$ above 600, the disturbance amplitude of the wave packets increase as they are convected downstream eventually leading to breakdown and the formation of turbulent spots. It is the appearance of these turbulent spots that mark the onset of transition. As the value of $\bar{R}$ is increased, the amplification ratios get larger and the transition point moves upstream towards the wing root. For values of $\bar{R}$ below 600 the waves decay and the flow remains laminar.

Natural transition was briefly examined in the present tests during both the 2D trip and 3D trip work, although this does not constitute a major part of the present investigation and was done primarily to check the model.

As described in chapter 1, $\bar{R}$ can readily be converted to a Reynolds number based on more familiar boundary layer characteristics. The above value of $\bar{R} = 600$ is equivalent to $R_{\delta^*} = 615$. For the flat-plate boundary Poll('89) gave $R_{\delta^*} = 425$ as the minimum value for the onset of instabilities. However, due to the large streamwise distance required for the disturbances to breakdown into turbulent spots, and the increase in R_{δ^*} with increasing streamwise distance, Poll obtained a value of $R_{\delta^*} = 2500$ as a minimum for transition onset on a flat plate.

2.2 TRANSITION TRIPPING

Fasel showed that if disturbances whose magnitude exceeds approximately 1% of the freestream velocity are introduced into the flat-plate boundary layer (Blasius profile) then they may be amplified at Reynolds numbers where only damping was predicted by

linear stability theory, i.e. at Reynolds numbers below the linear stability limit. In this case the large amplitude disturbances undergo non-linear amplification and rapidly breakdown to form turbulent spots. Morkovin referred to the process as bypass transition, where the relatively gradual linear amplification part of the transition process is bypassed. Attachment line contamination is an example of bypass transition. Other causes of bypass transition are high levels of freestream turbulence and surface roughness (or trips).

In practical situations transition can be tripped by surface imperfections such as waviness, steps and gaps at structural junctions, and three-dimensional roughness elements linked to the surface (screws, rivets, etc.) or generated by environmental factors (insects, ice crystals, etc.). Hardy('88), who studied attachment line transition in a high lift situation, cited isolated roughness (e.g. surface imperfections) as a possible reason for the observed erratic behaviour of the boundary layer state with a change in incidence. Pfenninger & Groth('61b) also demonstrated, during flight tests, that both large gusts and rain clouds could cause transition, on the attachment line, at Reynolds numbers where laminar flow had previously been present. The gust caused the occurrence of a negative pressure peak and an adverse pressure gradient close to the leading edge. In both cases laminar flow was recovered shortly after leaving the disturbance source. In the same tests, flyspecks on the wing leading edge were found to cause transition at lower altitudes. However, as the altitude increased and the unit Reynolds number decreased, the surface roughness caused by the flyspecks became more and more immersed within the boundary layer until eventually the flyspeck roughness became subcritical and full chord laminar flow was again established.

In experiments, common tripping devices are 2D wires and 3D spheres, cylinders or cones. There are several other experimental methods commonly used to introduce disturbances. Poll('78) used a turbulent end plate, Gaster('67) used a spark (generated between a small pair of electrodes on the model surface) and also an earphone in a small hole on the model surface, and several authors have used a thin flat vibrating ribbon near the surface of a flat-plate. Sparks are mostly used in studies of the turbulent spot since the introduction of the turbulent spots can be controlled, unlike trip wires where the spots occur randomly at a certain Reynolds number. Both the earphone and the vibrating ribbon are used to excite travelling waves in the boundary layer thus allowing the investigation of Tollmein-Schlichting waves, although the vibrating ribbon is unsuitable for use on curved surfaces.

Trips used in the present tests consist of 2D wires and 3D spheres. The flow downstream of both 2D and 3D trips, and the mechanisms by which they introduce turbulence, have been studied in detail on flat plates. Klebanoff *et al*('92) stated that 2D and 3D roughness elements behave in a similar manner, at least qualitatively, in inducing transition. However, the mechanisms by which the two trip types cause transition are quite different and will be described in more detail in the chapters on 2D and 3D tripping. Briefly,

it would appear that both trip types are capable of causing transition via two mechanisms. The first, for smaller trips, involves the introduction of large, but laminar, disturbances which breakdown to form turbulent spots at some point downstream. A 2D trip introduces 2D vortices that develop into a 3D configuration before breaking down into turbulence. A 3D trip produces the 3D vortices more directly, but may involve some interaction with the horseshoe vortex also created by the trip. The second mechanism for each trip type enables sufficiently large trips to cause transition at, or at least immediately downstream of, itself. In this case the trip is referred to as 'fully effective'.

In addition to different mechanisms being responsible for tripping, 2D trips and 3D trips also exhibit differing critical conditions. A 3D trip is less effective in causing transition and so larger 3D trips are required to produce transition, at similar Reynolds numbers, than 2D trips. However, 3D trips are of a more critical nature and transition moves forward more quickly than with 2D trips as soon as critical conditions, for producing transition downstream, are exceeded.

A common parameter used in examination of transition tripping is the roughness Reynolds number, R_{kk}, based on the height, k, of the trip and the velocity V_k at the trip height.

$$R_{kk} = \frac{V_k k}{\nu}$$

Critical values of R_{kk} normally refer to the minimum value for fully effective tripping and provided the trips are fully immersed in the boundary layer, critical conditions can be fairly well represented by a constant value of R_{kk}.

Critical values of R_{kk} for fully effective tripping of the attachment line boundary layer were given in Poll('89) as R_{kk} = 400 - 500 for transition onset with 2D trips. Poll('89) also presented values for 3D trips from work done by Gregory & Love and Firmin & Cook, for transition onset R_{kk} = 500 - 600.

Comparing the tripping process on the attachment line and the flat plate, Poll demonstrated that although the attachment line boundary layer is more stable and is less susceptible to 2D trips, it can be tripped at values of R_{δ^*} considerably lower than the flat-plate boundary layer. The attachment line boundary layer is less susceptible to 2D trips since a trip wire placed on a flat plate will cause an increase in the momentum thickness, θ, by an amount equivalent to the drag of the wire. In contrast, on the attachment line no such increase in θ occurs downstream. The flow, with reduced momentum, is removed in the chordwise direction by the flow divergence. Therefore the trip merely acts as a source of disturbance and transition is not induced by an artificial increase in θ. Tolerable heights for

3D trips appear to be similar for the two flows.

Although the actual values vary slightly from text to text, the critical values for transition tripping on a flat plate are of the order of $R_{kk} = 200$ for 2D trips and $R_{kk} = 600$ for 3D trips, where these values refer to transition onset.

Although, as has been discussed, the boundary layer can be tripped to cause transition at Reynolds number below the linear stability limit, a minimum Reynolds number exists for the turbulence created to be self sustaining. This Reynolds number, referred to here as the lower limit for transition tripping, represents a limit for stability to the larger disturbances introduced via the bypass mechanisms.

On the attachment line, large trips, referred to as gross disturbances, are capable of causing turbulent spots at Reynolds numbers below this lower bound for transition tripping. Numerous authors, including Arnal & Juillen('88), Poll, Cumpsty & Head('69), Gaster('67) and Gregory & Love('65) have examined this lower bound. Values of $\bar{R}$ for transition onset ranged from 223 to 260 but a value of approximately 250 is generally accepted. This is equivalent to a value of $R_{\delta^*} = 254$, which is considerably lower than the flat-plate value.

It is widely accepted that the stability limit for the flat-plate boundary layer, of the order of $R_{\delta^*} = 400 - 500$, also represents a lower bound for transition tripping of the boundary layer.

For Reynolds number greater than the lower bound turbulent spots expand as they travel downstream while for Reynolds number below the limit the spots contract. Gaster studied the relative velocity of the leading and trailing edges of the turbulent spots on the attachment line. He confirmed that for large Reynolds numbers ($\bar{R} > 280$) the leading edge moves faster than the trailing edge so that the spots expand, while below this critical speed they contract. Between values of $\bar{R}$ of 250 and 320, Arnal & Juillen were able follow the movement of individual spots and calculate convection velocities of the upstream and downstream fronts of the spots. The velocities remain close to $0.7V_e$ but the downstream fronts moves slightly faster resulting in the growth of the spots.

For fully turbulent flow the lower bound is slightly greater, with observed values of between 292 and 318. $\bar{R} = 300$ is the accepted value, although Cumpsty & Head demonstrated that the fully turbulent law of the wall could not be applied until $\bar{R} = 374$.

For transition caused by gross disturbances, the mean flow is heavily distorted by the trip and the boundary layer retains a long memory of disturbances introduced. However, at large distances along the attachment line there is no distinction between disturbances introduced by a turbulent boundary layer and those introduced by a very large trip wire.

In the case of attachment line contamination all surfaces are smooth but the intersection of the wing and fuselage flows can constitute a source of gross disturbance for the developing attachment line flow on the wing.

2.3 INTERMITTENCY

The intermittency factor, Γ, can be defined as the measure of the probability that the flow at a given point in the boundary layer will be turbulent. Thus Γ is zero for laminar flow and unity for fully turbulent flow. During transition the turbulent intermittency must vary along the attachment line even when $\bar{R}$ is fixed, i.e. the completion of turbulence is always dependent on s.

Poll('78) examined the intermittency distribution on the attachment line for various experimental configurations and showed that although $\bar{R}$ for transition onset is a function of d and s, the intermittency distribution could be represented by a single function if Γ was plotted against the normalised co-ordinates ζ_1 or ζ_2, where both coordinates are functions of $\bar{R}$ as follows :

$$\zeta_1 = \frac{\bar{R} - \bar{R}_{\Gamma=0.5}}{\bar{R}_{\Gamma=0.75} - \bar{R}_{\Gamma=0.25}}$$

and

$$\zeta_2 = \frac{\bar{R} - \bar{R}_{Transitiononset}}{\bar{R}_{\Gamma=0.75} - \bar{R}_{\Gamma=0.25}}$$

Poll('83b) demonstrated that Narasimha's('57) universal flat-plate intermittency distribution can also be applied to the attachment line boundary layer. Thus Narasimha's distribution can be expressed as a function of both ζ_1 and ζ_2 :

$$\Gamma = 1 - EXP(-0.412(\zeta_1 + 1.3)^2)$$

and

$$\Gamma = 1 - EXP(-0.412\,\zeta_2^2)$$

The above equations allow an estimation of the intermittency distribution given measured values of $\bar{R}$ at the three specific values of Γ.

Poll('78) also developed an equation to estimate Γ for the specific condition of attachment line transition due to gross contamination. The experimental data used to obtain this equation was very limited and Stewart('87), having obtained more extensive experimental data, altered the equation slightly to obtain the following :

$$\Gamma = 1 - \exp\left[-\left(\frac{\bar{R} - 245}{106}\right)^2 \left(\frac{s}{\bar{R}\eta} + 2\right) \right]$$

The applicability of this equation is limited to measurement positions at greater than $s/\eta = 2000$ downstream of the gross disturbance source.

Intermittency distributions from the present tests were compared with each of these universal distributions and the also with Poll's and Stewart's prediction for gross contamination.

2.4 RELAMINARISATION

Relaminarisation was not investigated in the present tests, however the possibility of the flow from a turbulent attachment line relaminarising in the favourable pressure gradient area downstream of the attachment line is an important feature of leading edge flows. A brief review of previous tests is therefore presented.

The relaminarisation of a turbulent boundary layer to the laminar state in regions of strong favourable pressure gradients has been studied in detail and is a well established phenomenon in two-dimensional and axisymmetric flows. Critical values of pressure gradient have been calculated for both two-dimensional and infinite swept wings.

A review of relaminarisation criteria is presented in Poll('78). The relaminarisation parameter $K = \upsilon.(dU_e/dx)/U_e^2$ was defined for two-dimensional flows. When applied to the attachment line boundary layer and the possibility of relaminarisation in the favourable pressure gradient just downstream, this parameter is inversely proportional to the square of the leading edge similarity parameter $\bar{R}$. The critical value of K for 2D flow was given by Beasley('73) as 5×10^{-6}, while Arnal *et al*('92) suggested 10^{-6} as a possible value for the beginning of relaminarisation, but 5×10^{-6} as the value required for complete relaminarisation. Arnal also assumed that the value for three-dimensional boundary layers would be of the same order if the velocity and its derivative were evaluated along the external streamline.

By applying these expressions at the attachment line and considering the characteristics of the attachment line region, Poll('83a) derived the simple criteria of $\bar{R} < 265$ for relaminarisation downstream of the attachment line. It was therefore concluded that turbulence resulting from either attachment line contamination or cross-flow instability is unlikely to be relaminarised in the strong favourable pressure gradient existing in the leading edge region.

Other authors have determined that relaminarisation is possible in certain situations,

most important of these is a high-lift configuration. In this case a pronounced velocity peak is observed on the upper surface close to the leading edge. The acceleration parameter attains a very large value, larger than at the attachment line location. In his experiment Arnal *et al*('92) obtained a value of K of about 10^{-5} (double the required value) at the suction peak, with a high lift configuration. Arnal's measurements were performed at the wall and he concluded that the relaminarisation was not necessarily complete up to the outer edge of the boundary layer.

Both Hardy('88) and Bertelrud('83) also found evidence of relaminarisation of turbulent attachment line boundary layers in high lift configurations.

Relaminarisation would be extremely unlikely to occur downstream of the attachment line on the present model.

2.5 CROSS-FLOW INSTABILITY

Investigations of attachment line transition and cross-flow instability have in the past been closely linked. In fact attachment line transition was discovered while investigating cross-flow instability. In the present tests cross-flow instability is not investigated, however, it was necessary to briefly consider the possibility that cross-flow instability may affect the tests involving 3D trips positioned downstream of the attachment line. For this reason a brief review of cross-flow instability was performed.

Cross-flow instability occurs downstream of the attachment line and is a consequence of the rapid acceleration of the flow in the chordwise direction. A combination of the spanwise flow and the accelerating chordwise flow, produces an imbalance between pressure forces and centrifugal forces within the boundary layer, in planes drawn parallel to the surface. The result is the formation of a velocity distribution in the direction normal to the local streamline direction at the edge of the boundary layer. This is the cross-flow velocity profile. It has a zero component at the wall and at the boundary layer edge, with a maximum at some intermediate position. Most importantly, the profile has a point of inflection between the locations of the maximum cross-flow velocity and the edge of the boundary layer. According to Rayleigh, the existence of an inflection point is a sufficient condition for flow instability in the limit of infinite Reynolds number (inviscid instability). In practise, the existence of an inflection point usually results in instability and subsequent transition to turbulence at very low Reynolds numbers.

The existence of zero-frequency, stationary waves in the laminar flow is a characteristic feature of cross-flow instability. In experiments cross-flow instability is easily identifiable using visualisation techniques. The cross-flow waves, which are actually co-

rotating vortices within the boundary layer, take the form of streamwise, streak lines. These waves are amplified by the cross-flow instability.

Many authors have studied cross-flow instability, including Hall *et al*('84), Poll, Arnal, Cumpsty & Head('67), Flores *et al*('91), Pfenninger & Groth('61b) etc. Owen & Randall('52) developed a cross-flow Reynolds number and a critical value above which cross-flow instability, in the absence of attachment line transition, dominates the transition process.

3 - INTRODUCTION TO MODEL, INSTRUMENTATION AND WIND TUNNEL, AND GENERAL PRELIMINARY TESTS

3.1 8'x6' WIND TUNNEL

The 8'x6' wind-tunnel is a closed working section, closed return tunnel with the following working section dimensions:

Length	5.18m
Width	2.43m
Height	1.82m

A diagram of the tunnel is presented in Fig 3.1. The tunnel speed range extends from $3ms^{-1}$ up to approximately $40ms^{-1}$ (for the present model). The tunnel has a longitudinal turbulence intensity of 0.09% on the centre line at $40ms^{-1}$, while the flow velocity uniformity is ±0.7% over 93% of the horizontal centre line and ±1.1% over 91% of the vertical centre line. Flow angularity on the centre line (for $Q_\infty = 5 - 60ms^{-1}$) was quoted as 0.25° (yaw) and 0.75° (pitch). Finally, the static pressure gradient is negligible.

The tunnel freestream turbulence was checked using a hot-wire probe, held on a large and steady strut in an otherwise empty test section. The raw hot-wire output was sampled at 10kHz for 10 seconds at a range of windspeeds. The sampled files of data were then reduced, using part of the 'Streamware' software* (see section 3.3.1.) to give mean perturbation components, and the freestream turbulence was calculated. Over the range of windspeeds used in this test, which was representative of the range to be used during the transition tests, the measured freestream turbulence remained at a fairly constant level slightly below the specified value given above (i.e. slightly less than 0.09%).

The windspeed during the tests was measured using the tunnel static rings, which are connected to a Furness FC016 digital manometer that was calibrated by comparing the output to that from a Pitot-static probe positioned in the centre of the empty test section. The following linear relation was obtained :

$$q_\infty\ (N/m^2) = 10.88 \times \Delta P\ (mmH_2O)$$

where ΔP is the Furness reading.

This value was re-confirmed at a later date mid-way through the tests.

* - StreamWare Version 1.00D, by Dantec MT

3.2 SWEPT CYLINDER MODEL

3.2.1 MODEL DESIGN

The model is a swept, faired cylinder of span 2.6m and chord 0.68m. Fig 3.2 shows a sketch of the model and it's dimensions. Initially the model was built in two spanwise sections (1.6m lower & 1.0m upper). This allowed the model to also be used in Cranfield's 8'x4' Tunnel, where the effects of medium and high levels of freestream turbulence were investigated (for details of 8'x4' Tunnel, see chapter 7). The leading edge radius is 0.17m and the thickness/chord ratio is 0.5. The design sweep is 60°, however the model is mounted on a pivot that allows a sweep range of 55° - 72°.

Initial tests examining transition onset, without any trips present, indicated that there was a problem with the model in the leading edge tip region. It appeared that the model's base plate, added to protect the sharp leading edge, was leading to the presence of a separation bubble. This problem was more evident at higher sweep angles and was at a minimum at the design sweep. The separation bubble problem appeared to be confirmed when the hot-wire probe was positioned near the leading edge tip and turbulent spots were detected at low Reynolds numbers.

The model's leading edge tip was reshaped by the addition of a bulbous nose. This gave a smooth attachment point and was blended into the rest of the model to ensure that no steps had been introduced. Further transition detection tests with no trips present yielded transition onset Reynolds number of the same order as Poll's('78) results. It was therefore assumed that the bulbous nose had corrected the leading edge tip problem.

For pressure measurements, the model is equipped with three sets of static pressure taps with each set consisting of 46 taps between ±1° and ±110°. The three sets of taps are positioned along the span at 0.90m, 1.40m and 2.00m from the leading edge tip.

Elsenaar('90) expressed concerns over transition tripping by the model static pressure taps, due to inflow and outflow of air from the tap tubing. Authors examining suction and blowing have likened the holes to 3D trips of a size dependent on the size of the hole and the suction velocity. Elsenaar recommended a maximum hole size of 0.25mm, although this value referred to a 2D aerofoil.

The pressure taps on the present model are greater than 0.25mm. The possibility that the taps may influence transition was therefore examined during the initial tests. Several hot-wire locations along the attachment line were used with the upstream location upstream of the pressure taps. At various sweeps with no trips present, the transition onset Reynolds numbers from this upstream location were compared with values obtained from extrapolation of results from the hot-wire locations downstream of the static taps. Good

agreement was obtained and the pressure taps are not, therefore, thought to represent a problem with regards to the flow stability.

3.2.2 MODEL MOUNTING

The model was mounted on a pivoting block, positioned on the tunnel floor upstream of the centre of the test section. The actual pivot is 160mm above the floor so that at the design sweep of 60° the leading edge tip is 250mm above the tunnel floor. At the minimum sweep, where the leading edge tip is closest to the floor, it was still considered to be safely outside the tunnel floor boundary layer. The rear of the model sat on a block of appropriate size for the sweep angle and the top of the model was held tight using wire and turnbuckles. This set-up allowed easy fine tuning of the model alignment and in conjunction with the model's weight kept model vibration to a minimum. Poll('78) used a similar configuration.

Initial tests indicated that slight model vibration was present at the lower sweep angles with the higher windspeeds. With the greater windspeeds required for transition at smaller sweep angles, it was perhaps unsurprising that problems with model vibration increased as the sweep was reduced. Transition onset results for zero and very small trips clearly demonstrated the effect of the vibration, with values of $\bar{R}$ smaller at smaller sweep angles. The effect therefore presented itself as a sweep effect. The fact that even with zero trip and minimum sweep the vibration was only just detectable, by observing the trailing edge tip, suggested that this may only be a problem at higher windspeed. Supporting this was the absence of the apparent sweep effect with medium and even small trips. Since the vast majority of the work was performed at low enough windspeeds to avoid vibration, it was decided to proceed with the existing set-up. For the case of zero and very small trips, the results obtained with the maximum sweep agreed with Poll's results, suggesting again that at higher sweep there is no effective model vibration. The low values of $\bar{R}$ at lower sweep angles with zero and very small trips were therefore neglected (though they will be required in the turbulence spreading tests in chapter 5).

The apparent sweep effect with very small trips was observed while using both 2D and 3D trips.

3.2.3 MODEL ALIGNMENT AND ATTACHMENT LINE POSITION

The attachment line was marked on the model using a felt-tip marker pen such that it did not affect the model surface in any way. Each of the ±1° static taps were used as

references and the attachment line was marked midway between each pair. A large rule was then used and the attachment line was drawn. The reference positions for trips and hot-wire locations were also marked on the surface. Subsequent pressure distribution tests, where the attachment line position can be identified as the point where Cp achieves a maximum, and checks on accuracy requirements (where the change in transition onset conditions due to 3D trips and/or the hot-wire being slightly off the attachment line were found to be negligible) suggested that the line marked in this way was entirely satisfactory.

During the actual tests the model sweep angle was changed very often and it was felt that it was too time consuming to check the model pressure distribution to ensure model alignment after each alteration. Instead, each time the model was inserted into the tunnel at the start of session the model alignment was checked and a reference position marked on the floor (this was necessary due to the fact that the floorboards were removable and their positions could alter very slightly from previous sessions). This reference position was then used with a plumbline from the model trailing edge to check the alignment for each test. From preliminary tests, where the pressure distribution was routinely checked after each change in sweep, the plumbline proved satisfactory. Despite this, a brief test was performed using a medium 3D trip to check the affect of model alignment. At a sweep angle of 66°, after first burst conditions had been obtained, the rear of the model was moved laterally by approximately 5mm (using the turnbuckles). Transition onset was re-examined, and the value of $\bar{R}$ for transition onset was found to be within 1% of the original value. Thus it appears that even very large errors in alignment have little effect on the transition Reynolds number for the present model and experimental set-up.

3.3 INSTRUMENTATION

3.3.1 HOT-WIRE ANEMOMETRY

The transition detection tests were performed using a Dantec 90C10 hot-wire anemometer with a 1D straight-pronged TSI hot-wire (due to availability). The Dantec anemometer was controlled using Dantec's 'Streamware' software on a Dell 486 PC. The hot-wire probe was inserted in a short probe holder which was held in a cradle at an angle of 20° to the model surface. The probe holder could be moved through the cradle in order to adjust the hot-wire probe height, while the cradle sat on the model surface held by adhesive tape. The hot-wire anemometer output, which remained uncalibrated, was fed into a root-mean-square (RMS) meter, the range of which was kept at a constant value appropriate for the whole transition region, with peak values of the RMS voltage, V_{rms}, about mid-scale on the meter. The RMS meter output was observed on an oscilloscope. A scopadaptor was used to obtain a time base for the oscilloscope of 1sec/div and a sensitivity

of 0.1V/div.

Transition onset was easily observable as the appearance of turbulent bursts was usually very clear. In a few cases the turbulent bursts were quite small (this was more of a problem in the 8'x4' tunnel) but transition onset was taken to be the condition where, on average, 1 clear burst of turbulence occurred approximately every 15 seconds, as defined by Poll. It should be noted however that in some cases transition onset is quite sudden and only a very small increase in windspeed is required to move from no spots to numerous spots. This is particularly true for medium and large trips. In fact, for the largest trip this change in windspeed can be too small to alter the actual Furness reading for windspeed. For small and zero trips transition onset is more gradual and large changes in windspeed only increases the rate of turbulent spots slightly, for example with one set-up an increase in $\bar{R}$ from 515 to 560 resulted in an increase in the rate of turbulent bursts from 1 every 15 seconds to 1 every 5 seconds.

The fully turbulent signal was more difficult to define. Obviously complete turbulence should refer to the minimum conditions at which laminar spots disappear, however this is not easily observed. Poll & Paisley('85) also expressed difficulty in defining a fully turbulent signal and concluded that a simple visual examination of a fluctuating signal is insufficient when dealing with essentially turbulent flows. However, in the absence of a viable alternative, it was decided to proceed with determination of fully turbulent conditions by observing the RMS output on an oscilloscope. The fully turbulent RMS signal should be similar in appearance to the laminar signal. This could be easily obtained in the case of small and zero trips but with larger trips small peaks (possibly laminar spots) were difficult to exclude entirely, even at very high windspeeds. Complete turbulence was therefore accepted as a roughly 'laminar-like' signal where small peaks were not treated as laminar spots -, i.e. only large and obvious laminar spots led to the windspeed being increased again. In some tests the mean value of V_{rms} appeared to continue decreasing (though only very slightly) with further increases in windspeed after conditions for complete turbulence had been recorded.

Thus the complete transition region, as observed using the RMS output, can be described as follows : with increasing Reynolds number, the appearance of turbulent spots is followed by a steady increase in the rate of these spots, as the spots begin to merge the RMS signal becomes smoother (since V_{rms} no longer returns to zero after each spot) and eventually can attain quite a smooth signal not much rougher than the laminar signal. The mean value of V_{rms} reaches a peak at this point and then begins to decrease as laminar spots appear, resulting in a loss of the smooth signal. The laminar spots appear relatively quickly and then slowly decrease in frequency until the flow is fully turbulent resulting in a fairly smooth signal and V_{rms} reaches a minimum (but still greater than the laminar value).

This change in V_{rms} is due to the rapid increase in amplitude of turbulence to a

maximum value, at the point where the intermittency is approximately 0.5, and the subsequent reduction in the amplitude of turbulent fluctuations as fully turbulent flow is approached.

Observation of the raw hot-wire signal would simply show an increase in the rate of generation of turbulent spots leading to merging of spots until eventually the laminar regions between them disappear and the signal is fully turbulent.

A comparison between results obtained by observing the RMS meter output and the raw hot-wire output, showed that the results for transition onset were identical and, with the RMS meter range at the range used during tests, the size of turbulent spots was similar. Conditions for complete turbulence were, in general, also similar.

Depending on the experimental set-up, the extent of the transition region can vary and different parts can pass unobserved. Thus the calm signal at peak V_{rms} was often too short to be noticed. It appeared that the calm signal was more difficult to observe with the hot-wire closer to the trip. In addition, the fully turbulent signal appeared rougher with the hot-wire nearer the trip, perhaps further downstream the turbulent boundary layer was better developed.

The Dantec anemometer was also used to sample the hot-wire signal. Via the 'Streamware' software on the Dell 486, the Dantec could be set up to sample the signal at a specified frequency for a specified duration. Each run was started manually and the data was stored on the Dell's hard-drive in a format useable only with the 'Streamware' software. These files could then either be exported as an ASCII file (American Standard Code for Information Interchange) or used as an input to various functions within the 'Streamware' software. Two sample frequencies were used and in each case it was the uncalibrated, raw hot-wire output which was sampled.

For frequency spectra, data was sampled at 14kHz for 10 seconds. This was performed for transition onset and completion conditions for several experimental set-ups which covered each region of the $\bar{R}$ vs d/η graph for each block of tests. The sampled data was then input into 'Streamware's' own frequency spectra program and the resulting graph printed as a hard copy (file sizes made storage of files on disk problematic).

For calculation of the intermittency distribution, data was sampled at 2kHz for 20 seconds. This was performed at several points across the transition region for several experimental set-ups covering each region of the $\bar{R}$ vs d/η graph for each block of tests. The intermittency data was exported as CSV files (Comma Separated Values) and were then input into a program written to calculate the intermittency factor for each file. Details of the program and equations used are given in Appendix B. Briefly, this program worked by calculating the second derivative of the hot-wire output (with respect to time), the value of which was then compared to a specified value equal to the maximum derivative observed in laminar flow. If the derivative was greater then that particular period of time was

declared turbulent, if the derivative was less it was declared laminar. By totalling up all the turbulent regions of time the intermittency factor was obtained.

3.3.2 CHECKS ON HOT-WIRE INSTRUMENTS

A few brief initial tests were performed to check the effects of instrument sensitivity and the possibility that the hot-wire cradle assembly may cause intrusion effects.

A test was performed with an older anemometer (a DISA 55M anemometer) and the signal appearance compared with that from the Dantec. It was observed in the check that turbulent bursts were smaller in amplitude and background fluctuations were greater for the DISA. This led to the turbulent bursts being more difficult to identify and having a different appearance - more of an increase and then slow decrease of turbulence than a single burst of turbulence. Perhaps as a result of this, transition onset Reynolds numbers obtained were about 8% greater. It appears that the Dantec anemometer is, in some way, more sensitive to the disturbances. The difficulty in identifying turbulent spots with the DISA anemometer also leads to the conclusion the Dantec also produces the more accurate results.

The effect of the RMS meter was also investigated using the Dantec anemometer. Transition onset conditions with various trip sizes were observed with the RMS meter range set to 30mV, 100mV, 300mV and 1V. For some tests the smallest RMS range led to overloading while in others the turbulent bursts were too small to be distinguished when V_{rms} was at 1V. In all cases, a smaller RMS range led to lower transition onset Reynolds numbers although it should be noted that typical changes in $\bar{R}$ were only of the order of 3 - 5 (i.e. about 1%), although in a few tests with very small or zero trips larger decreases were obtained. The 300mV range was chosen since this gave a range suitable for the whole transition region.

The observed oscilloscope signal could also be altered by changing the sensitivity of the scopadaptor. Although a final value of 0.1V/div was settled on, a brief test indicated that altering the scopadaptor sensitivity could have a similar effect to altering the RMS range.

In conclusion, it appeared that small disturbances, observable at Reynolds numbers below first burst conditions, could take on the appearance of turbulent spots with increased instrument sensitivity. Therefore, only turbulent spots which were evident (and whose shape was evident) with the defined instrumentation sensitivity were regarded as true turbulent spots. Small blips in the signal which took on the appearance of a turbulent spots only when the instrumentation sensitivity was increased were assumed to be either laminar disturbances or turbulent spots in the very early stages of development. In order to obtain a consistent

and repeatable definition of transition onset these blips were disregarded.

For the fully turbulent signal, any increase in sensitivity made the signal appear rougher.

In order to check that the probe holder/cradle assembly did not affect the flow at the hot-wire probe position, the model static pressure at 1° off the attachment line was measured at a range of windspeeds. The probe was then placed immediately downstream of the tap and the static pressure re-measured. The static pressure in each case was identical, it was therefore concluded that the probe holder/cradle had a negligible effect on the flow at the probe location.

During the tests it was necessary to frequently move the hot-wire probe and since the surface is not completely flat (to scale discussed here as 10's of μm) the probe height varied slightly when relocated. It was also decided that to help ensure the safety of the probe it would be better to move the probe away from the surface within the cradle before moving the actual cradle. It was therefore necessary to check the effect of the probe height. This was investigated using several experimental set-ups over a few sessions. In each test the transition onset and completion conditions were examined while varying the hot-wire probe height over a small range (though greater than the range which may occur during actual tests where the probe is moved to different spanwise locations).

In each case no detectable changes in the results were found although the magnitude of the turbulent spots varied very slightly, first increasing as the probe height increased and then, when the probe was higher than used in any tests, decreasing. This variation in the magnitude of the turbulent spots is not surprising, it is well known that measured intermittency varies with the position within the boundary layer. Cumpsty & Head('69) also observed a change in length of turbulent spots at different heights within the attachment line boundary layer. In addition, one of their tests produced a situation where a fully turbulent boundary layer was observed with the hot-wire in the centre of the boundary layer, while some areas of non-turbulent flow were observed both towards the surface and towards the edge of the boundary layer. In Cumpsty & Head's tests, however, the change in hot-wire height was far greater than used in these preliminary tests, which were greater than the unintentional variations during the actual tests. Since the observed variations were very small, errors in measured intermittency should also be very small. It was, therefore, decided that it was sufficient to use just the operator's judgement (i.e. naked eye) in positioning the probe as close to surface as possible without risking damage to the probe.

It was estimated that the probe height was maintained at a height of between 0.25mm and 0.4mm.

3.3.3 OTHER INSTRUMENTATION

The pressure distribution was measured at the first and third set of static taps (i.e. 0.9m & 2.0m). Only two sets of taps were used due to restrictions in instrumentation and number of channels available. The taps were connected via scanivalves to the total ports of two ±0.5psi pressure transducers that were previously calibrated using a Druck pressure calibrator. The tunnel static rings were connected to the static ports of the transducers, thus providing a freestream static pressure which was later corrected to the freestream static pressure in the test section in the presence of the model (i.e. for static pressure gradient and blockage). The transducer output was filtered through a low-pass bandwidth filter (to remove noise) within Dana amplifiers (with gain = 1) and then input to an ADC (Analogue to Digital Converter). The ADC output was sampled using a microcomputer (typically 200 samples for the zeroes and 50 samples for each port) and the average voltage for each port was stored in an ASCII file.

Velocity profiles were measured using a traversable flattened Pitot probe. This consisted of a probe holder mounted on 'skis', the Pitot probe could then be moved through the holder, at an angle of 27° to the model surface, by turning a control nut. The external dimensions of the inlet of the Pitot probe are 1.67mm wide and 0.23mm thick. The probe holder was taped securely to the surface of the model. It should be noted that due to the very slight flexibility in the ski legs the angle to the model may have been altered slightly during application of the base and may have also allowed a very slight movement during tests. Great care was taken to ensure that the probe was always parallel to the surface. The control nut moves the probe 0.66mm per full revolution of the nut, at the angle of 27° to the surface. Thus the vertical movement of the probe is 0.3mm per full revolution of the control nut. Accurate measurement of the probe height therefore required that the initial height be known accurately.

During the tests, the initial height involved the probe being in contact with the surface. Care was taken to insure that the probe was only just in contact. This was checked by lightly tapping on the head and watching for any deflection and was also checked at the end of each set of tests by lowering the probe by the same number of control nut revolutions to verify that the probe returned to the surface. Any error at this point was minimised by averaging the reference zeros from the start and end of the test. Typical differences in number of revolution to return the probe to the surface were between 0 and $^1/_3$, equal to 0.1mm.

The dynamic pressure was measured at a range of windspeeds for each probe height. Measurements were made using one of the ±0.5psi pressure transducers, with the output being read on a DVM (Digital VoltMeter). The Pitot probe was connected to the total port of the transducer while the nearest available model static tap was generally connected to the

static port. The probe was usually used in positions on the model suitable for use with a model tap without causing possible intrusion effects at the tap. During these tests the transducer was positioned inside the model and the tube connecting the probe gained access through one of the access hatches. For these tests a special hatch cover was made which allow the tube to pass at the corner.

Atmospheric conditions were measured using the tunnel's thermometer probe and a barometer.

Model sweep angle was measured using an inclinometer.

3.4 PRELIMINARY MEASUREMENTS

3.4.1. PRESSURE DISTRIBUTION AND ATTACHMENT LINE PRESSURE GRADIENT

The model pressure distribution was measured at two speeds for each of the working sweep angles (i.e. 55°, 60°, 65° and 70°). Examples of the distributions obtained are presented in Fig 3.3. From these plots the measured distribution could be checked against the theoretical distribution. This is particularly important since η is calculated from the theoretical value.

As described in Appendix C, the measured model pressure distributions, without correction for model blockage or flow angularity, were used in conjunction with the measured values of static pressure at the attachment line, in order to estimate the model blockage correction factors and the effective sweep angle. With these corrections applied the measured pressure distribution, as shown in Fig 3.3, matches very closely the theoretical pressure distribution. The same corrections also led to good matching between measured and calculated value of V_e, where the measured values of V_e were obtained from the Pitot probe used in the velocity profile measurements. It can therefore be assumed that the simplified equations for $\bar{R}$ and η (which depend on the theoretical pressure distribution) give accurate values, provided the correction for blockage and sweep angle are applied. Using the measured pressure distributions and static pressure on the attachment line, estimated errors in V_e and dU/dx, calculated assuming the theoretical pressure distribution, are generally of the order of 1%. The slightly larger error in V_e at lower windspeeds suggests that this error may be closer to 3% at small Reynolds numbers, an error comparable to that experienced by Poll('78) during his swept cylinder tests.

The attachment line pressure gradient was also obtained from the pressure

distribution tests. A direct measurement of the pressure difference, between the 1° ports at the first and third set of model static taps, was considered. However, it was felt that since only one port from each set of taps would be used, the error in Δp would be greater than that from the pressure distribution measurement, where several values on either side of the attachment line are used to obtain the Cp on the actual attachment line. From the plots of pressure distribution it can be seen the attachment line pressure gradient is only of the order of -0.3% of the freestream dynamic pressure. This compares favourably with the model used by Poll('78) which had a gradient of +2.9%, while Cumpsty & Head('69) disregarded an even larger pressure gradient as having negligible effects.

3.4.2 VELOCITY PROFILES

The laminar velocity profiles were measured at several positions on the model at several sweep angles, using the traversable flattened Pitot probe mentioned earlier. This was done primarily to check the measured profile against the theoretical profile and thus verify the validity of the relations between η and δ, δ^* and θ expressed in chapter 1. The corrections for viscous effects and wall displacement effects are detailed in Appendix D.

Initial plots of the laminar velocity profiles showed some slight scatter and appeared to confirm the initial concern over the accuracy of the probe/cradle assembly. However, the scatter was consistent, i.e. profiles from various tests were of consistent shape but were displaced vertically by various amounts. It therefore appeared that the scatter was due to the assumed initial height of the probe. It was mentioned above that differences of up to 0.1mm in the apparent reference height at the start and the end of the tests were observed. This however fails to account for the possibility that, despite the care taken to insure that the probe was only just in contact with the surface, the probe may have been lowered too far and while in contact with the surface had actually deflected slightly. This would lead to all subsequent measurement heights being slightly lower than dictated. This problem was recognised at the time of the tests but, given the initial doubt over the whole instrument, the method used was deemed to be at least as accurate as the rest of the instrument's operation and was sufficient for the results required. The laminar velocity profiles were therefore corrected for initial probe height by translating each profile vertically to obtain a best match with the theoretical profile. Since, for each profile, each point was translated by the same distance any differences in the shape of the measured profiles and the theoretical profile would still be present.

Fig 3.4 shows the velocity profiles measured on the attachment line at various Reynolds numbers and corrected for the initial probe height. These profiles were obtained just downstream of the first set of model static taps at sweep angles of 55°, 60° and 70°.

The calculated profile from Rosenhead('63) is also presented. The measured profiles and the theoretical profile show very good agreement. From the measured values no sweep or Reynolds number effect could be observed. This agrees with Cumpsty & Head('67&'69), who studied the attachment line boundary layer in detail and showed that for the laminar attachment line boundary layer the velocity profiles, with the coordinate normal to the surface suitably transformed, is independent of C^* ($= \bar{R}^2$). Similar behaviour is observed with the Blasius solution for the flat-plate boundary layer which, expressed in suitable non-dimensional terms, is also independent of Reynolds number.

Accurate estimation of the boundary layer thickness from measured profiles remains a problem due to the thinness of the boundary layer. However the similarity between the measured and theoretical velocity profiles show that the values of δ (and indeed δ^* and θ) in terms of η, obtained from the theoretical profile and quoted in chapter 1, may be used.

Laminar velocity profiles were also measured just downstream of the third set of model static taps at sweep angles of 55° and 70° and similarly good agreement with the theoretical profile was obtained. This suggests that the asymptotic assumption is verified.

Velocity profiles parallel to the attachment line were also measured at points downstream of the attachment line, although it is well documented that the non-dimensionalised spanwise velocity profiles, in the vicinity of the leading edge of an infinite swept wing, are independent of x and y. Examples of the measured profiles, obtained just downstream of the first set of static taps at sweep angles of 55° and 70°, are presented in Fig 3.5 with the theoretical attachment line velocity profile. Each profile is non-dimensionalised using V_e and η on at the attachment line. The main purpose of these measurements was to check on boundary layer growth, an estimate of which was required for later tests involving trips positioned downstream of the attachment line. The similarity between profiles measured at various distances from the attachment line suggest no significant boundary layer growth occurs within the range of the tests. This may be different from the situation on an actual wing, Flores *et al*('91) commented on the thinness of the attachment line boundary layer compared to further downstream.

Finally, turbulent velocity profiles were measured at various sweep angles and Reynolds numbers. The boundary layer was tripped using a large trip to ensure fully turbulent flow. The Pitot probe was then positioned well downstream of the trip to ensure that the boundary layer had indeed taken on turbulent characteristics. Without a theoretical profile for comparison, the correction for initial probe height were obviously more difficult to apply. For the profiles presented in Fig 3.6, two sweep angles were used which allowed matching of profiles at $\bar{R} = 425$ from the two sweeps. The minimum correction was applied to one of the profiles and this was then used to obtain a best guess for corrections to the other profiles in the graph. As stated by Cumpsty & Head('67), the turbulent attachment line velocity profiles, and thus the various boundary layer characteristics, are functions of $\bar{R}$.

This is similar to turbulent flat-plate flow behaviour. As with the laminar profiles, no sweep effect was noticeable.

3.4.3 BOUNDARY LAYER DEVELOPMENT LENGTH

From Poll('78) it was calculated that the fully developed boundary layer (i.e. distance from leading edge tip to asymptotic conditions) was obtained at the point where s/η was of similar magnitude to $\bar{R}$. In the worst test case this gave a length of 0.25m. Despite this calculation, a brief test was performed to check that the trip was not in a developing boundary layer thus leading to premature transition. The trip and hot-wire were moved 200mm downstream and transition onset compared with values for the original positions. Tests were performed at each sweep angle using a medium 3D trip. With this trip any change in d/η would result in a large change in $\bar{R}$, however no significant change in the transition onset Reynolds numbers were observed. The trip location used can therefore safely be assumed to be within the fully developed asymptotic boundary layer.

3.4.4 TEMPERATURE EFFECTS

During tests with no trip or the very smallest trips, it was observed that the transition onset Reynolds number appeared to increase slightly as the air in the tunnel increased in temperature, as occurred when the tunnel was run at high speeds for long durations.

It was frequently observed for experiments with small or no trips, that turbulent bursts could be detected at relatively low windspeeds while (or shortly after) the velocity was increasing (or decreasing). When the flow was left to settle these turbulent bursts would fairly quickly die away. However, in situations where the tunnel air temperature at the start of the test was low, turbulent bursts could be detected at even lower windspeeds and took longer to die away. At higher velocities the turbulent spots took a lot longer to die out (in some cases as much as three minutes). During tests where the tunnel air was already warm, the early non-sustainable turbulent spots were less evident. Thus it appears that two separate effects result in premature appearance of turbulent spots which cannot be sustained ; flow acceleration where the spots die out quickly after the flow settles and low air temperature where the spots die out slowly as the air temperature increases.

Lasseigne *et al*('92) studied the effects of temperature on instabilities within the attachment line boundary layer. He concluded that a small amount of cooling of the surface had a significant stabilising effect on the streamwise disturbances provided the instability was due to viscous effects (there was little influence on instabilities due an inflection point).

Presumably an increase in the air temperature will have a similar effect since it is the temperature difference which induces density variations and causes a change in the mean flow. This supports the observed temperature effects.

Some tests performed in very cold conditions (during winter on a day when the building was unheated) produced slightly lower values for transition onset Reynolds number with a larger range of 2D trips including some medium trips.

Pfenninger & Bacon('69) also experienced some experimental scatter due to temperature fluctuations in the tunnel under different atmospheric conditions. However, they obtained higher transition Reynolds numbers when the temperature was lower and the weather was cloudy and overcast.

In conclusion, a great deal of care was taken during each test to insure that the flow was fully settled and the turbulent spots were sustainable before the conditions for transition onset were recorded. The first appearance of the turbulent spots could occur at values of $\bar{R}$ as much as 10% below the accepted value for transition onset (i.e.$\Delta\bar{R} \approx 60$).

4 - ATTACHMENT LINE TRANSITION INITIATED BY 2D TRIPS

Attachment line transition initiated by 2D trip wires was comprehensively investigated by Poll and reported on in a series of papers (Poll'78 - Poll'92). The main purpose of repeating these tests is to verify the validity of both the model and the instrumentation by checking results against those of Poll. Similar results, while validating the model, will also support Poll's results, particularly with respect to the 'kink' in the $\bar{R}$ vs d/η graph. The results with 2D trips were also required for comparison with attachment line transition due to 3D trips and for the investigation into the effect of freestream turbulence.

4.1 PREVIOUS EXPERIMENTAL WORK

Many authors have studied transition initiated by two-dimensional trip wires on flat plates and this includes nearly all of the work examining the processes by which 2D trips cause transition. These investigations include Gibbings *et al*('86a), Klebanoff & Tidstrom('72), Morkovin('69&'89) and Tani('61). The bulk of the work studying tripping of the attachment line boundary layer has been done by Cumpsty & Head('69) and Poll('78) using the same faired swept cylinder.

From the investigations using flat plates a good understanding of the flow around 2D trip wires and the subsequent tripping of boundary layer transition has been gained.

Provided the trip wire is not too large, the flow will separate from the trip wire and reattach to the model surface at some distance downstream creating a closed separation bubble, consisting mainly of a single large eddy. The separated inflectional velocity profile created by small trips has a very low critical Reynolds numbers. The small amplitude disturbances present in the freestream may therefore be amplified at Reynolds number where the upstream attached boundary layer was stable to the small disturbances. The degree of amplification depends on the local shear layer Reynolds number, the streamwise distance to the reattachment point and the local disturbance level (boundary layer receptivity to sound and turbulence is very efficient at the trip). Provided these amplified disturbances have achieved a certain magnitude within the separated region, given by Fasel as 1% of the freestream velocity, they may be amplified further as they are convected downstream. This may occur at Reynolds numbers below the linear stability limit, eventually leading to breakdown and the formation of turbulent spots.

With a larger trip size the amplification by the free shear layer may be sufficient to cause breakdown to turbulent spots prior to reattachment of the flow downstream of the trip or, alternatively, eddies may be shed from the wire in the form of a Karman Street.

The position of the reattachment point of the separation bubble varies with both the boundary layer state at reattachment and the trip diameter. Gibbings *et al*('86a) demonstrated that an asymptotic value for the distance to reattachment of about 10 trip diameters is approached as the trip size increases and the flow becomes fully turbulent at reattachment. For some distance downstream of the reattachment point a distorted boundary layer velocity profile exists. The profile gradually returns to an undistorted state at the 'recovery position'.

Poll('78) contains a fairly complete study of attachment line transition due to a large range of 2D trip sizes. Figs 4.1 and 4.2 present his results as graphs of $\bar{R}$ vs d/η for transition onset and completion. Poll split these graphs into four regions each governed by a different transition process. A brief summary of the different transition processes present is given below.

For zero or very small trips ($d/\eta < 0.8$), the trips have no influence on the conditions for the appearance of turbulent spots. Transition is therefore indistinguishable from natural transition (as described in section 2.1) and linearised theory is still valid. A minimum critical Reynolds number is required for the packets of Tollmein-Schlichting waves, initiated by small disturbances in the freestream, to amplify as they travel along the attachment line before eventually reaching some threshold condition beyond which they break down to form turbulent spots. This critical Reynolds number is referred to as the upper bound for boundary layer tripping and for the attachment line boundary layer has a value of about $\bar{R} = 600$. This value also represents the upper bound for transition completion.

$\bar{R} = 600$ is the accepted value here. Poll reported a value of 570 in earlier papers and 600 in later papers. Hall & MacKerrell('88) gave a value of 583 and Cumpsty & Head('69) gave 606. Pfenninger & Bacon('69) detected high frequency (regular sinusoidal) oscillations at $\bar{R} = 562$ leading to transition onset at $\bar{R} = 624$ at the most downstream of the measuring stations, a lower value may therefore have been obtained as the spanwise distance tends to infinity - giving the upper limit.

With greater Reynolds number the amplification of disturbances increases and the transition front moves upstream. Thus transition onset is dependent on $\bar{R}$ and s/η.

At finite s/η, changes in $\bar{R}$ from transition onset to a fully turbulent boundary layer (at the same spanwise location) were given by Hardy('88) as around 80.

The maximum value of $d/\eta = 0.8$, bounding this region, represents a criterion for the maximum tolerable roughness height. For values of d/η greater than this limiting height the transition location is determined by disturbances introduced at the wire.

With small trips wires ($0.8 < d/\eta < 1.6$) disturbances from the trip dominate the transition process and the value of $\bar{R}$ for transition lies between 400 and 600. The trip wire

introduces a small disturbance that is still essentially laminar although no packets of Tollmein-Schlichting waves were observed by Poll. Instead, isolated perturbations were observed travelling along the attachment line. Thus the free shear layer produced by the trip remains laminar to attachment whilst providing disturbance levels which are sufficiently large to undergo non-linear amplification and consequently produce transition in the quoted range of $\bar{R}$. Poll suggested that a laminar vortex was being shed from the trip wire and this undergoes some form of amplification or three-dimensional stretching before breaking down to form turbulent spots. The turbulent spots form initially at a large distance downstream of the trip, but as the trip size, or $\bar{R}$, increases the transition front moves upstream towards the trip. Thus transition onset is dependent on $\bar{R}$, d/η and s/η.

With medium trip wires ($1.6 < d/\eta < 2.0$), the trip dominates the transition process for values of $\bar{R}$ lying between 250 and 400. The trip wire diameters are now sufficiently large so that the turbulent bursts originate at the trip wire, i.e. the shear layer undergoes transition to turbulence prior to reattachment at the wall. The turbulent spots then propagate indefinitely along the span with transition onset observed at all spanwise stations at the same value of $\bar{R}$. Thus transition onset is mainly dependent on $\bar{R}$ and d/η. Fig 4.1 from Poll('78) suggests a very small dependence on s/η although the present results suggest no dependence (see Fig 4.8). Transition completion, however, remains dependent on s/η due to the dependence of spot growth rate on $\bar{R}$ and thus the variation in intermittency with spanwise position.

The change in the transition process from the smaller trips results in a discontinuity in the relation between $\bar{R}$ and d/η. This is clearly seen as a kink on the $\bar{R}$ vs d/η graph.

With large trip wires ($d/\eta > 2.0$) turbulent spots again originate within the free shear layer immediately downstream of the trip. In this case, however, the turbulent spots may be produced at much lower Reynolds numbers and if $\bar{R}$ is below 250 the turbulent spots decay and eventually disappear at some point downstream. A value of $\bar{R} = 250$ is therefore accepted as representing a lower limit for the indefinite propagation of turbulence along the attachment line, i.e. the minimum Reynolds number at which turbulent spots can sustain themselves by the generation of an adequate turbulence production rate. Poll also concluded that the same value represents a critical value for relaminarisation and, in the case of a turbulent boundary layer upstream, there is no laminar flow at any point on the attachment line before conditions drop below the critical level. It therefore appears that, for $\bar{R} < 250$, the laminar layer is stable to those disturbances whose amplitudes are typical of those found in turbulent flows.

For a fully turbulent boundary layer, Poll determined a lower limit for transition tripping of $\bar{R} = 300$.

These values for the lower limit for transition onset and completion are approximate

values taken from the results of a whole series of tests. Poll obtained values of $\bar{R}$ in the range 245 to 260 for transition onset and 292 to 300 for fully turbulent flow. Pfenninger('65) obtained values of $\bar{R}$ in the range 225 to 260 for transition onset and $\bar{R}$ in the range 260 to 272 for a fully turbulent attachment line. Cumpsty & Head('69), also using trip wires, obtained values of 245 for transition onset and 283 for fully turbulent flow. Arnal *et al*('92) used two models and obtained lower bounds for transition onset of $\bar{R} = 258\pm18$ and $\bar{R} = 251\pm11$, while complete turbulence was obtained at $\bar{R} = 309\pm12$ and $\bar{R} = 318\pm22$. Overall, this gives a difference in $\bar{R}$ for onset and completion of turbulence of approximately 50 to 80 for large trips. Hardy('88) gave a value of 50 and calculated a value from Poll's data of 55. Cumpsty & Head('69) found that a fully turbulent 'law of the wall' region was not established until $\bar{R}$ reaches approximately 374.

From these, the accepted values for the purpose of comparison with the present tests were taken as $\bar{R} = 250$ for transition onset and $\bar{R} = 300$ for transition completion.

Within this region of the $\bar{R}$ vs d/η graph, transition onset is initially dependent on $\bar{R}$, d/η and s/η and for smaller values of s/η, $\bar{R}$ continues to decrease although a limit exists for complete turbulence. At larger values of d/η and s/η the dependence on the trip size diminishes and there exists a limiting value of d/η (= 4.0) beyond which the transition process is effectively independent of d/η - a condition called 'gross contamination'. Poll('78) stated that when transition is induced by a gross disturbance the transition criterion should depend upon turbulent flow properties.

Poll('78) also examined attachment line contamination by a turbulent flat-plate boundary layer at the junction with the swept wing model. This also represented a gross disturbance and produced a similar value for the lower bound for tripping. Poll concluded that, far downstream, the source of the turbulence is irrelevant. Thus the lower bound for transition tripping is the same irrespective of the tripping device used. From the values quoted above, Arnal also used a turbulent flat-plate boundary layer to contaminate the attachment line boundary at the junction.

Poll('89) compared the values for the lower bound for attachment line flow and flat-plate flow. He concluded that in the case of the attachment line, the lower bound occurs at a value of R_{δ^*} of about 270, considerably lower than the lower bound for flat-plate tripping of R_{δ^*}=425. However, Poll considered that since this bound is related to turbulence, then turbulent flow parameters should be used to compare the two values. Thus he compared the value of the local turbulent momentum thickness Reynolds numbers for onset of transition close to the lower bound condition. He found that these values were similar for the attachment line and flat-plate flows, and also independent of trip size. A similar value was also obtained for a pipe flow.

A brief comparison between the flat-plate boundary layer and the attachment line boundary layer was made in sections 2.1 and 2.2. Essentially, the attachment line velocity profile is similar in appearance to the Blasius profile but is slightly fuller and thus more stable.

The other difference discussed earlier was that the attachment line boundary layer is less susceptible to 2D trips. This is because any momentum defect from the trip is lost due to flow divergence while on a flat plate the trip results in an increase in θ. Poll('78) examined the critical roughness height for the flat-plate boundary layer at a specific Reynolds number and compared it to the critical roughness height for the attachment line at an equivalent Reynolds number. The roughness height was about 50% greater for the attachment line boundary layer, proving that it was less sensitive to 2D trips than the flat-plate boundary layer.

In comparing the two boundary layers, $\bar{R}$ cannot be used and several other criteria have been examined. A common parameter in studies of transition tripping is R_{kk}, the Reynolds number based on a trip of height k and the velocity at that height V_k. The critical value of R_{kk} is that required for transition to occur at the trip. R_{kk} can be calculated from the equation

$$R_{kk} = \bar{R} .(d/\eta).(V_k/V_e)$$

The ratio V_k/V_e is obtained from the theoretical laminar velocity profile, for the attachment line, from Rosenhead('63). A graph of $R_{\delta*}$ vs R_{kk} for both the attachment line and the flat-plate boundary layers, obtained from Poll('89), is presented in Fig 4.3. In the case of the attachment line boundary layer this criterion gives fairly constant values for both transition onset and completion, and can be applied for values of d/η between 0.8 and 2.0. Poll gave the following values for R_{kk} for 2D trips :

R_{kk} = 400-500	transition onset	4.1
R_{kk} = 550-650	complete turbulence	

Poll also quoted values of R_{kk}, for transition onset, of between 150 and 400 for the flat-plate boundary layer, while Tani('61) gave a value of between 150 and 300 and Klebanoff *et al*('55) gave a value of between 200 and 300. Gibbings *et al*('86a) gave values of R_k (roughness Reynolds number with V_k replaced by V_e) for onset and completion of turbulence at the reattachment point downstream of the trip on the flat-plate as 230 and 500 respectively, the corresponding values of $R_{\delta*}$ were 425 and 740.

Thus conditions for transition at the trip wire can be fairly well represented by a critical value of R_{kk}. For the attachment line boundary layer, Gaster('67) determined an alternative critical roughness criterion. From a graph of freestream velocity versus trip wire

diameter he concluded that the critical trip wire size could be determined from the equation:

$$(V_e.d/\upsilon)_{crit} = 47.R_\theta^{1/2} = 30.\bar{R}^{1/2} \qquad 4.2$$

This equation is referred to as Gaster's criterion and corresponds to transition onset with 2D trips.

Finally, Poll('78) examined the variation of $\bar{R}$ with d/η for very large s/η. The width of the transition region was found to be essentially constant ($\Delta\bar{R} = 60$) over the whole range of d/η and for the range $d/\eta = 0.8$ to 2.0, $\bar{R}$ can be well represented by :

$$\bar{R} = 830 - 294.(d/\eta) \quad - \quad \text{first burst} \qquad 4.3$$
$$\bar{R} = 890 - 294.(d/\eta) \quad - \quad \text{complete turbulence}$$

As was mentioned above, the main purpose of the present investigation of attachment line transition initiated by 2D trips was to confirm the validity of the present model and instrumentation. Good agreement with the large amount of data and approximate relations listed above should be sufficient for this purpose.

4.2 PRESENT INVESTIGATION

For the present investigation, definitions of transition onset and completion were the same as suggested by Poll. Thus, transition onset was taken as the point at which 1 turbulent burst occurs every 15 seconds and transition completion was taken as the absence of any laminar bursts during a period of approximately two minutes.

For each trip size / sweep angle combination used, three spanwise locations were used for the hot-wire probe. The positions used were 0.2m, 1.0m and 1.8m downstream of the trip. It was felt that this would provide enough data to interpolate results to appropriate values of s/η.

The trip wires were stretched beyond the yielding point in order to ensure the removal of all kinks from the wire and were then glued to the surface using a water based glue. This glue held the trips firmly in place and was easily removed without causing any damage to the model. The trips were positioned 0.5m from the leading edge tip.

A range of the experimental set-ups, covering the $\bar{R}$ vs d/η graph, were chosen for repeat tests. The first attempt at these repeat tests yielded transition onset Reynolds numbers that were much lower. However, it was noted that the set-ups with the greatest

change in $\bar{R}$ were those which, when plotted on the $\bar{R}$ vs d/η graph, occupied the area where the gradient is steepest. Thus it appear that perhaps the large changes in $\bar{R}$ were due to small changes in d/η (or a change in d of approximately 0.1mm). A subsequent study revealed a very slight flat spot on the model, where the surface was very smooth and hard, just off the attachment line. This was due to repairs of damage caused by the application and removal of the 3D trips, performed between the original 2D trip tests and the repeat tests. In the very smooth hard region the glue, used to hold down the trip wire, did not appear to bond properly with the surface thus allowing the trip to move away very slightly, from the surface, in the flat spot region. As a result of these observations, later repeat tests were performed with the 2D trips applied further along the model's attachment line in an unworked, and thus unrepaired, area. These repeat test produced satisfactory results.

It was concluded that while these tests demonstrated that good repeatability could be achieved they also demonstrated the great care required to obtain accurate results from these type of tests.

As well as determining transition onset and completion conditions, four set-ups were used for data sampling for subsequent calculation of frequency spectra and intermittency distributions. The four set-ups used corresponded to the four regions on the $\bar{R}$ vs d/η graph, as described by Poll('78), i.e. zero trip, small trip (introducing laminar disturbances), medium trip (introducing turbulence directly) and large trip (introducing turbulence at $\bar{R}$ < 250). The hot-wire was used in both the upstream and downstream locations for each. For the frequency spectra, data was sampled at first burst conditions and at fully turbulent conditions. Data for the intermittency distribution was sampled at nine windspeeds ranging from just below first burst conditions to just above fully turbulent conditions.

Prior to commencing the investigation of transition, the flow in the vicinity of the trip was briefly studied.

4.3 FLOW AROUND A 2D TRIP WIRE

Some doubt existed as to the extent of the separation region behind a 2D trip on the attachment line. Therefore, to obtain a more complete comparison with the flat-plate boundary layer, the flow in the vicinity of a 2D trip was briefly examined prior to investigating the transition conditions.

Methods of flow visualisation were considered for studying the region but the use of smoke and laser was considered inappropriate due to the proximity of the surface and reflections off it, while oil flow techniques also had problems ; namely the period required to increase the windspeed to test conditions and the effect it would have on the model

surface. It was therefore decided to study the pressure field around the trips.

The static pressure gradient around a 2D trip and the velocity profiles at several points downstream of the trip were examined using the model static pressure taps and the traversable Pitot probe, used earlier to measure the attachment line velocity profiles. Details of calculations involved are given in Appendix E.

The static pressure gradient was examined by positioning the trip at various distances (mostly upstream) from the second set of model static taps. A ±0.5psi pressure transducer was then used to measure the pressure difference between the 1° ports on the first and second set of taps. This was done at a range of windspeeds for two trip wires and two sweep angles. The transducer output was simply read on a DVM and the value noted along with the windspeed. A brief check with no trip present was also performed to verify the magnitude of the small natural attachment line pressure gradient between the two measurement points.

Fig 4.4 shows the results for a few of these tests in terms of ΔCp against s/η where:

$$\Delta C_p = \frac{p_{trip} - p_{undisturbed}}{q_{undisturbed}}$$

The point of maximum ΔCp represents the reattachment point. In each of the cases on this graph the Reynolds number and trip size were sufficient for a fully turbulent flow at the reattachment point.

The reattachment distances from all the measurements were plotted in Fig 4.5 in the form of d/δ^* against s_t/d. This graph clearly shows that an asymptotic reattachment distance of approximately 10d is approached as the trip sizes become large. A similar behaviour was found with 2D trip wires on a flat plate by Gibbings *et al*('86a) and their graph is shown in Fig 4.6. It appears that a similar separation distance of about 10d is obtained with a large trip on the flat plate. The major difference is the sizes of trips required to approach this asymptotic value. For the flat plate d/δ^* is of the order of 2, while for the attachment line d/δ^* is of the order of 4. Transition tripping of the attachment line boundary layer by a 2D trip wire also requires a bigger trip than the flat-plate boundary layer. The reason for this is that the attachment line flow containing the momentum deficit is removed by flow divergence in the chordwise direction and R_θ is not therefore artificially increased by the momentum deficit downstream of the trip. This would also therefore appear responsible for the difference in d/δ^* for the asymptotic reattachment distance.

Another clear observation from Fig 4.4 is that while larger trips lead to smaller values of s_t/d, the value of s_t/η remains in a small range of between 25 and 40. Also, larger trips lead to larger changes in pressure and longer recovery lengths, since the recovery rate downstream of trip appears fairly constant.

Most of the values in Fig 4.5 were obtained at conditions sufficient to cause a fully turbulent boundary layer, although in the case of the smaller trips this may occur downstream of the reattachment point. This switch from transitional to turbulent reattachment results in a similar trend with increasing d/η to Gibbing's work on a flat plate, which also involved reattachment points of varying conditions. He suggested that the maximum value of s_t/d coincides with a point corresponding to the beginning of transition occurring at the reattachment point.

The velocity profiles were measured using the traversable Pitot probe. The trip was positioned well downstream from the first set of model static taps and the probe was then positioned at several distances downstream of the trip. The probe was connected to the total port of the pressure transducer and the 1° port from the first set of static taps (well upstream of the trip) was connected to the static port. The measurement of the profiles and traversing of the probe was handled in an identical manner to the earlier velocity profile tests, in section 3.4.2. The upstream model static pressure tap was used to avoid having to move the trip relative to probe and pressure tap during these tests. The probe could then be moved further from the trip and the static pressure corrected using the static pressure gradient tests performed earlier. The Reynolds number and trip size combinations were large enough to ensure a fully turbulent flow at the reattachment point. No corrections were applied for the small possible errors in reference height of the probe as discussed in section 3.4.2.

With the probe only a short distance downstream of the trip and the head of the Pitot probe within the separation bubble, errors were very large. In these cases the Pitot probe was measuring a base pressure rather than the total pressure when near to the wall and even as the probe moved higher and into the downstream flow there was considerable intrusion on the upstream flow passing beneath. In addition, no correction for variation in static pressure from the wall to the outer part of the bubble was applied. However, since errors decreased as the probe moved downstream, it was felt that the positive parts of the approximate profiles would give some insight into the boundary layer development. Around and slightly downstream of the reattachment point variations in pressure readings, leading to possible errors, may have been present due to the unsteadiness of the reattachment. In fact, it was noted during numerous tests that the DVM readings at a single point varied by as much as 10%. Due to the nature of the set-up, with corrections required between undisturbed static pressure and static pressure at the probe position, these variations in the readings could introduce variable errors. With the probe far from the wall the velocities were relatively high and the variation in velocity was of the order of 3%. Near the wall where velocities were low possible errors of 20% occurred.

Fig 4.7 shows an example of some of the profiles obtained. Even allowing for the approximate nature of the tests the features of the flow downstream of the 2D trips are

clearly seen. As s/η increases the height of the separation bubble and the magnitude of the free shear layer reduces until the flow is reattached. Additional profiles suggest that the point of inflection then reduces in severity as it moves relatively quickly towards the surface and a short distance downstream of the reattachment point, the point of inflection is lost. The boundary layer then gradually becomes fuller as dV/dz at the wall increases and the boundary layer tends towards the turbulent velocity profile. At some distance downstream, at the recovery position, the fully turbulent velocity profile is achieved and Gibbing *et al*('86a) suggested that this coincides with the end of transition. In the present case of a semi-infinite attachment line boundary layer the turbulent velocity profile then remains constant along the remainder of the wing. The exact shape of this profile was shown in Fig 3.6 to be dependent on the Reynolds number. Provided critical conditions are exceeded, the trip size should not influence the final profile, although it will certainly influence the recovery position.

4.4 TRANSITION RESULTS

Conditions for transition onset and completion are presented Figs 4.8 and 4.9, respectively. Results are plotted in terms of the attachment line Reynolds number, $\bar{R}$, for transition onset (or completion) against the corresponding trip size, d/η. On both graphs, curves are plotted for constant spanwise distances, s/η, between the trip and the hot-wire. Prior to plotting these graphs, results, for both $\bar{R}$ and d/η, from experiments for each trip and sweep angles combination were plotted against the values of s/η (for the different hot-wire locations). The values of $\bar{R}$ and d/η at the specified values of s/η were then obtained from interpolation of these graphs. For $\bar{R}$ values between 250 and 600, the variation with s/η is very small or zero. Outside this range the variation is greater and more care was required with plots of $\bar{R}$ (or d/η) vs s/η.

Some of the actual experimental data was not used in obtaining the final graphs. Values obtained with zero trip and the smallest trip at low sweep angles were neglected due to the slight model vibration observed at high windspeeds with the lower sweep angles, as described in section 3.2.2. In addition, results for transition completion from higher sweep angle tests with large trips (such that $d/\eta > 2.0$) were also neglected. This was due to a sizeable variation in $\bar{R}$ with changes in sweep angle for constant values of $d/\eta > 2.0$. If graphs of experimental data points interpolated to specific values of s/η are plotted and curves linking the values obtained at each sweep angle are drawn, then for both transition onset and completion these curves for constant sweep take on an appearance similar to the final $\bar{R}$ vs d/η graph. The transition onset curves blend together well to form the data for the final curve of best fit for all the data, with little scatter. For transition completion curves, the displacement between curves for each sweep angle also result in good matching

provided $d/\eta < 2.0$. Above this value of d/η the curve for each sweep angle attains a different constant value of $\bar{R}$ as the dependence on trip size is removed. The graph is presented in Fig 4.10, minus the zero and very small trip results at lower sweep angles.

A tentative explanation for the large difference in values of $\bar{R}$ with sweep angle and the reason for neglecting the higher values are linked to the initial tests detailed in section 3.3.2 concerning the effect of hot-wire height, as examined for transition conditions. It was concluded that small alterations in the probe height had little influence on detection of a turbulent burst. Many authors have, however, pointed out that intermittency must be a function of height within the boundary layer and studies of turbulent spots on flat plates have shown that turbulent spots become narrower near to the wall. Indeed, the value of $\bar{R} = 374$ determined by Cumpsty & Head to be the lower limit for the turbulent law of the wall to be valid was considerably higher than the accepted lower limit for a fully turbulent boundary layer and Poll attributed this to the narrower spots near the wall. In section 1 it was shown that η, and thus the boundary layer thickness, is a function of both freestream velocity and sweep angle. Using the equation for η, it can be shown that the boundary layer at $\Lambda = 70°$ is 30% thicker than at $\Lambda = 55°$, and an increase in windspeed from $12ms^{-1}$ to $24ms^{-1}$ results in a reduction in boundary layer thickness of 40%. So although the physical hot-wire height must have varied very slightly each time it was moved this variation is small in comparison to the possible changes in relative height due to changes in boundary layer thickness. The good agreement between values of $\bar{R}$ for $d/\eta < 2.0$ where windspeeds are higher and the good agreement between the low sweep values of $\bar{R}$ for $d/\eta > 2.0$ and those obtained in previous investigations, suggest that for thinner boundary layers the hot-wire probe is at a suitable height such that small alterations do not greatly alter the intermittency. In contrast conditions where the thickest boundary layers are achieved, i.e. at lower windspeeds and greater sweep angles, result in the hot-wire probe attaining a position lower in the boundary layer. It appears then that for a hot-wire probe below a certain height in the boundary layer the intermittency becomes heavily dependent on that height.

In conclusion, it is assumed that values of $\bar{R}$ for transition completion with large trips and high sweep angles are too dependent on the effective hot-wire height to produce results suitable for comparison with other investigations. The values obtained with the lower sweep angles agree with results of other investigations. Since the main purpose of this investigation of 2D trips is to validate the model prior to extending the test to cover new ground, it is clear that in order to obtain a meaningful comparison with both the present 2D trip tests and previous investigations, the results for transition completion with high sweep angles and large trips will also have to be neglected in the following tests involving 3D trips and high levels of freestream turbulence.

For the accepted data, both scatter and repeatability were within acceptable limits. Scatter (expressed as function of $\bar{R}$) resulted in experimental data within ±4% of the curve

of best fit, across both the transition onset and transition completion graphs.

Poll discussed two bounds on value of $\bar{R}$ for transition tripping, the upper bound (or maximum value of $\bar{R}$ for stability to small disturbance) and the lower bound (or minimum value of $\bar{R}$ for turbulence to be self-sustaining). Here a third value of $\bar{R}$ was considered, namely the value corresponding to the smallest fully effective trip, i.e. the smallest trip for turbulent spots to be introduced directly at the trip. This value of $\bar{R}$ coincides with the kink on the $\bar{R}$ vs d/η graph. These three values, applicable to transition onset, are referred to as $\bar{R}_{upper}$, $\bar{R}_{kink}$ and $\bar{R}_{lower}$.

As was mentioned above, graphs of $\bar{R}$ vs s/η for each trip size and sweep angle combination were used to obtain the values of $\bar{R}$ at specific values of s/η. Each of these graphs for which $d/\eta > 2.0$ were used to examine $\bar{R}_{lower}$, where $\bar{R}_{lower}$ is the value obtained as $s/\eta \rightarrow \infty$. These curves were plotted on a single graph and are presented in Fig 4.11. The values obtained for $\bar{R}_{lower}$ were within the range $\bar{R} = 236$ to $\bar{R} = 262$.

A graph of $\bar{R}$ vs s/η was also used to estimate $\bar{R}_{upper}$. In this case $\bar{R}$ was plotted against s/η for $d/\eta = 0.0$. $\bar{R}_{upper}$ represents the value of $\bar{R}$ as $s/\eta \rightarrow \infty$ and from Fig 4.12 it appears that in the present tests the upper bound for transition tripping is of the order of $\bar{R} = 660$. This value is significantly greater than the value obtained by Poll('78). However comparison of the actual data points available showed that, for $s/\eta > 4000$, measured values of $\bar{R}$ for transition onset matched almost exactly. Since Poll's model allowed a far greater range of s/η values to be examined it is logical to assume that the large difference in $\bar{R}_{upper}$ is simply due to the extrapolation required with the present results. It is therefore concluded that if larger values of s/η had been attainable in the present tests, it is likely that a value of $\bar{R}_{upper}$ of approximately 600 would have been obtained. Larger values of s/η were available at lower sweep angles, however, as was discussed in section 3.2.2, slight model vibration at higher windspeeds and lower sweep angles prevented their use for tests with zero and very small trips.

Using the assumed value for $\bar{R}_{upper} = 600$, it is possible to project a curve for $s/\eta \rightarrow \infty$ onto the $\bar{R}$ vs d/η graph. From this curve the maximum tolerable roughness is obtained as the value of d/η at which $\bar{R}$ starts to decrease. A value of approximately $d/\eta = 0.9$ was obtained.

The value for $\bar{R}_{kink}$ was taken from the $\bar{R}$ vs d/η graph where it was obtained as the intersection of two curves of best fit, one for small trips and one for larger trips. From this graph $\bar{R}_{kink} = 376$ and this occurs at a value of $d/\eta = 1.67$.

These values of $\bar{R}$ were also examined for transition completion. Unfortunately the restrictions on maximum Reynolds number imposed by the model and the wind tunnel resulted in insufficient data to examine the upper bound for transition completion. However, for $\bar{R} > 600$ the intermittency will increase downstream of the transition onset location until

eventually the flow is fully turbulent. Since the upper bound refers to conditions for infinite s/η the value for transition completion is essentially the same as for transition onset. Within the limited range for the present model, for natural transition, an increase in $\bar{R}$ of approximately 80 from the transition onset value is required for transition completion at the same location.

From plots of $\bar{R}$ vs s/η for transition completion with large trip sizes, the lower bound was estimated to be approximately $\bar{R} = 300$.

Due to the dependence of $\bar{R}$, for transition completion, on s/η, the kink did not occur at a single point but moved with changing s/η. $\bar{R}_{kink}$ was not therefore examined.

Projected curves for $s/\eta \rightarrow 0$ and $s/\eta \rightarrow \infty$ for both transition onset and completion are presented in Figs 4.13 and 4.14. These curves were obtained using a combination of extrapolation of the $\bar{R}$ vs d/η graphs and extrapolation of experimental data for each trip/sweep combination. Approximate relations, of similar form to equations 4.1 and 4.3, for the present data together with Gaster's criterion for transition onset as $s/\eta \rightarrow 0$ (equation 4.2) are also shown.

Intermittency distributions were measured for several points on the $\bar{R}$ vs d/η graph. The graph obtained for natural transition is presented in Fig 4.18a, while the graphs obtained with various trips are presented in Fig 4.18b. All of the distributions are plotted, together with Narasimha's universal intermittency distribution, against ζ_1 and ζ_2 in Figs 4.19. Details of Narasimha's intermittency distribution and the parameters ζ_1 and ζ_2 are given in section 2.4 together with the equation from Stewart('87) for predicting the intermittency factor far downstream of a gross disturbance. The intermittency distribution given by this equation is presented in Fig 4.20 together with the measured distribution for the largest trip with the greatest values of s/η.

Finally, frequency spectra were obtained for a number of test configurations with varying boundary layer conditions. Examples of the spectra obtained are presented in Figs 4.21.

4.5 DISCUSSION

Attachment line transition due to 2D trip wires was investigated essentially to verify the validity of the model and instrumentation. This mainly involved comparisons with results from Poll('78). Figs 4.1 and 4.2, taken from Poll('78), and Figs 4.8 and 4.9, obtained from the present tests, are clearly very similar, although small difference do exist.

The present results, for transition onset, suggest a slightly greater value of $\bar{R}$ for

natural transition at smaller s/η. The difference decreases with increasing spanwise distance until for s/η > 4000 a good match is achieved with Poll's data. It therefore appears that the present model has a greater dependence on the spanwise distance in the absence of trips. This greater dependence on s/η is also evident, although not as clearly, in the presence of small trips. With large trips, where dependence on s/η returns, the spanwise distance appears to have slightly smaller effect for the present model. Thus differences in s/η's effect between the two models appears to vary with Reynolds number.

For transition completion, the present results again suggest a greater change in $\bar{R}$ with increasing s/η for small trips. For large trips Poll demonstrated that $\bar{R}$ quickly approached a minimum value. However, the present results suggest that $\bar{R}$ continues to decrease, although only slightly, with increasing d/η.

To obtain a clearer comparison the $\bar{R}$ vs d/η curves at s/η = 2000 were taken from each of the transition onset and completion graphs and plotted in Fig 4.15. This graph demonstrates the good agreement for transition onset with the only significant difference being the value of $\bar{R}$ at d/η = 0. Other differences, including the position of the kink and the gradient of the curve immediately below the kink are extremely small and are well within the experimental scatter range for the present tests. Agreement between the curves for transition completion is less satisfactory with values from the present investigation being consistently higher. This suggests that a slightly larger transition region occurs with the present model.

The small differences between the two sets of results obviously lead to slightly different values bordering the four distinct regions evident on both Poll's and the present $\bar{R}$ vs d/η graphs. The following values were obtained for transition onset :

Zero trip : $d/\eta < 0.9$ $\bar{R} > 600$

Any trip present is too small to have any influence and natural transition occurs due amplification of the small disturbances, present in the freestream, at high Reynolds number. Thus d/η = 0.9 represent the maximum tolerable roughness value and $\bar{R}$ = 600 represent the upper bound for transition tripping or the upper limit for stability to small scale disturbances. Values of $\bar{R}$ are heavily dependent on s/η.

Small trips : $0.9 < d/\eta < 1.67$ $600 > \bar{R} > 376$

The small trips introduce laminar disturbances. These disturbances are expanded and amplified as they travel downstream and eventually breakdown to form turbulent spots. s/η still influences $\bar{R}$ but not as much as in the zero trip region and by a diminishing amount as d/η increases.

Medium trips : $1.67 < d/\eta < 1.97$ $376 > \bar{R} > 250$

The trips are fully effective and turbulent spots are introduced within the free shear layer. $\bar{R}$ is high enough for the turbulent spots to sustain themselves indefinitely and they expand as they travel downstream. Indeed, it was observed during the experiments that the bursts of turbulence are of greater magnitude at larger distances downstream of the trip. Thus any turbulent spots present at $s/\eta = 0$ will also be present at $s/\eta = \infty$, and vice versa. $\bar{R}$ for transition onset is therefore no longer dependent on s/η, $\bar{R}$ for transition completion is however still dependent on s/η.

Large trips : $d/\eta > 1.97$ $\bar{R} < 250$

The trips are again fully effective and turbulent spots are introduced within the free shear layer. $\bar{R}$, however, is too low to sustain an adequate turbulence production rate and the turbulent spots contract as they travel downstream and eventually die out. $\bar{R} = 250$ therefore represent the lower limit for transition tripping. Since the rate of decay increases with decreasing $\bar{R}$, the value of $\bar{R}$ for detection of turbulent spots is dependent on s/η. For transition completion, $\bar{R}$ approaches a minimum relatively quickly and s/η has less effect on its value.

As has already been mentioned, the change from the small trip to the fully effective trip results in a kink in curves of $\bar{R}$ vs d/η. This kink is apparently a result of a discontinuity as the transition process changes. This will be discussed in more detail in section 5.6 incorporating results obtained using 3D trips. In the case of the 2D trips, the change in transition process involves the transition front moving from downstream of the reattachment point into the free shear layer.

Overall, the values of d/η bordering each of the regions are in good agreement with the values proposed by Poll('78). The upper bound was assumed using data obtained by Poll but the excellent agreement between experimental results at high s/η for the present and Poll's tests suggest that a greater range of s/η for the present model would lead to a similar value for $\bar{R}_{upper}$. Thus accepted values for the upper and lower bounds for transition tripping achieve good agreement, with values of $\bar{R}_{upper} = 600$, $\bar{R}_{lower} = 250$ for transition onset and $\bar{R}_{lower} = 300$ for transition completion matching the accepted values from numerous other reports.

The other values of Reynolds numbers from previous investigations described in section 4.1 was the critical roughness Reynolds number. The graphs of $\bar{R}$ vs d/η for $s/\eta \rightarrow 0$, presented in Fig 4.13, suggest critical values of R_{kk}, applicable within the range $1.1 < d/\eta < 2.4$, of :

R_{kk} = 450 transition onset
R_{kk} = 630 transition completion

These values are within the range defined by Poll in equation 4.1.

In addition, curves of $R_{\delta*}$ vs R_{kk} for the present tests together with previous attachment line and flat-plate investigations are presented in Figs 4.16 and 4.17. These graphs suggest a slight increase in roughness Reynolds numbers for the present tests, in comparison with Poll's results, for both transition onset and completion. The greater values of R_{kk} for the attachment line boundary layer than the flat-plate boundary layer are also evident, while the two graphs together suggest an approximately similar extent of transition region for both Poll's and the present data, and indeed the flat-plate data from Gibbings *et al*('86a). It is noted, however, that the extent of the transition region is more difficult to estimate from these graphs than from the $\bar{R}$ vs d/η graphs.

Transition was also studied for $s/\eta \to \infty$ and the graph of $\bar{R}$ vs d/η for $s/\eta \to \infty$ is presented in Fig 4.14. The approximate relation between $\bar{R}$ and d/η for transition, given in equation 4.3, matches the transition onset curve well, within the range $0.5 < d/\eta < 2.0$. For the transition completion curve, the equation had to be altered slightly. The gradient of the approximate curve remained the same but the constant was increased by 20, thus shifting the curve upwards. While this suggests a considerably greater extent of transition region, the actual difference in transition regions is much smaller since both $\bar{R}$ and d/η increase across the transition region. Thus the extent of the transition region is only slightly greater for the present model, as was observed in Fig 4.15.

It was partly to confirm the extent of the transition region that the intermittency distributions were measured. The intermittency distribution for natural transition is presented in Fig 4.18a while distributions for three trip sizes are presented in Fig 4.18b. The three trips used, covered the three tripped regions of the $\bar{R}$ vs d/η graph, with the large trip used at a low sweep angle. The extent of the transition region for the various trip sizes can be estimated from the graphs.

The very limited results available for natural transition from both the transition detection and the intermittency tests suggested a similar extent of transition region to Poll and Hardy('88). However, from the more extensive data for tripped transition, it appears that values of $\Delta\bar{R}$ (i.e. the difference between $\bar{R}$ for transition completion and $\bar{R}$ for transition onset) range from about 90 for small trips to about 65 for fully effective trips, with some variation for different s/η. This agrees fairly well with the $\bar{R}$ vs d/η graphs for the present tests and again suggests a slightly larger transition region than observed in previous tests by Poll and Hardy. In comparing these intermittency graphs and the values of $\Delta\bar{R}$ with the $\bar{R}$ vs d/η graphs it must be remembered that d/η is increasing across the intermittency region.

The affect of s/η on the extent of the transition region was also examined though the full transition region for zero trip and small s/η could not be covered due to tunnel restrictions. In the case of the other trips s/η only has a significant influence on the results when $\bar{R}$, for transition onset, is less than 250, i.e. in the case of the large trip. Here the extent of the transition region is greater with smaller s/η. This is due to the fact that, with gross disturbances, transition onset can be observed a short distance downstream of the trips at Reynolds numbers well below the lower bound, while for transition completion a minimum Reynolds number exists even for small s/η. For transition onset there are therefore large differences in $\bar{R}$ with s/η when $\bar{R} < 250$ while for transition completion there are only small differences in $\bar{R}$ with s/η, due to the minimum value required for fully turbulent flow.

The data from each of the three trip sizes were also plotted on a single graph against the normalised co-ordinate ζ_1 together with Narasimha's universal flat-plate intermittency distribution, described in section 2.4. This graph is presented in Fig 4.19a. As with Poll's data, good agreement was achieved. The alternative form of Narasimha's distribution was also plotted with the present data against ζ_2. There was considerably more scatter using this normalised co-ordinate, probably due to the sensitivity to $\bar{R}$ for transition onset, which is less well defined within the intermittency distribution than the other values used in calculation of ζ_1 and ζ_2.

An attempt was also made to plot the intermittency distribution obtained with the largest trip and large s/η together with the theoretical distribution for gross disturbances, proposed by Stewart('87), in Fig 4.20. Although, in the present tests, transition onset occurs at $\bar{R} < 245$ there is a fairly good agreement between the measured and predicted distributions. The shape and extent of the distribution appear to match very well and translating the measured distribution by increasing $\bar{R}$ for each point measured by a constant value of 12 leads to a very good agreement. It therefore appears that Stewart's equation can accurately predict the intermittency distribution provided transition onset occurs at $\bar{R} = 245$. This was the value Stewart obtained for $\bar{R}_{lower}$ and it would appear that it was applicable for $s/\eta > 2000$. For the present model $\bar{R}_{lower}$ was accepted as 250 and dictated transition onset conditions for $s/\eta > 3000$.

Finally, frequency spectra were examined for the same three trips as used in the intermittency distribution. The expected variation in the spectra with intermittency was observed, with the range of fluctuation frequencies increasing with intermittency. However, other slight differences in frequency spectra for first burst conditions between the three 2D trips appeared to be more a function of the Reynolds number and possibly the measurement height than the actual trips. Examples of the frequency spectra obtained are presented in Figs 4.21. It appears that the shift to higher Reynolds numbers, associated with the smaller trip, has a similar effect to increasing the intermittency, in that the range of fluctuation frequencies increases slightly.

The 2D trip tests alone did not provide enough information to reach this conclusion. However, the frequency spectra were investigated primarily to check if any differences existed between the transition regions initiated by 2D trips and 3D trips. Similar trends in frequency spectra were obtained in the 3D trips tests, in chapter 5, and also those measured in the higher freestream turbulence tests in chapter 7. Since no obvious trends in the frequency spectra due to differences in trip type or freestream turbulence could be spotted, all the frequency spectra were taken together to reach the conclusion that Reynolds number (and possibly the measurement height), at which the first burst conditions were obtained, influenced the frequency spectra for the turbulent spots.

With these observations, it was realised that a far greater range of tests would be required to investigate possible variations in the frequency spectra with trip types, since larger variations due to other factors would have to be accounted for first. Unfortunately there was insufficient time to do this.

4.6 CONCLUSIONS

From the graph of $\bar{R}$ vs d/η it can be deduced that the main aims of the 2D trip tests, i.e. to confirm the validity of the model and instrumentation, have been met. The existence of the kink, which had concerned Poll, is even more evident in the present tests, which demonstrate a definite step change as the transition mechanism changes. The slight differences between the present results and Poll's results appear to be most significant in three areas ; transition onset in the absence of trips at low s/η, the extent of the transition region and the gradual decrease in $\bar{R}$ for transition completion with large trips. However, even these differences are small and do not suggest any problems with the model or instrumentation.

5 - ATTACHMENT LINE TRANSITION INITIATED BY 3D TRIPS

The previous chapter examined attachment line transition initiated by 2D trips and obtained similar results to that obtained in a similar study by Poll('78). The investigation of attachment line transition is now extended to cover 3D trips positioned on the attachment line. The flow downstream of a 3D trip and the mechanisms by which transition occurs are quite different from those with 2D trips. A brief review of the effects of 3D trips from previous investigations using flat plates is given first.

5.1 PREVIOUS EXPERIMENTAL WORK

A three-dimensional, isolated roughness element is an irregularity the height of which is of the same order as the chordwise and spanwise extent. Little work has been done on attachment line transition initiated by 3D trips. However, the mechanisms by which 3D trips cause transition have been studied, at some length, in the flat-plate boundary layer. These include investigations by Gibbings *et al*('86b), Morkovin('89), Klebanoff *et al*('92), Motohashi *et al*('91&'93) and Gregory & Walker('50). From these and other studies, critical Reynolds numbers based on trip heights have been developed for the flat-plate boundary layer and a fairly good understanding of the flow around the trips has been developed.

The complex 3D structure of the flow downstream of 3D roughness elements varies with the roughness Reynolds number, however the effect of the exact trip shape is less clear. Klebanoff *et al*('92) suggested that the trip shape affected the flow stability, with a spherical roughness element having a more destabilising effect than a cylindrical one. In contrast, Gregory & Walker('50) observed that the critical height was unaffected by the roughness shape. The actual transition process is not well understood but Motohashi *et al*('91) stated that the fundamental nature of the transition process was the same for both spherical and cylindrical roughness elements. Furthermore, it is widely accepted that, provided the trip meets the definitions of a 3D trip given above, the trip's shape has little effect on the topology of the flow downstream, although Morkovin('89) suggested that the Reynolds number of events changed with the 3D trip shape.

The flow around a 3D roughness element consists of several distinguishing features. As mentioned above, the exact structure and the effect of each feature varies with the roughness Reynolds number. At low Reynolds numbers a horseshoe vortex is formed by the downwash at the front of the roughness resulting from the static pressure gradient across the boundary layer. The horseshoe vortex wraps around the roughness and forms streamwise vortices, which for the flat-plate case are stable for $R_{kk} < 300$. In addition, a short separated region forms in the wake of the trip, the length of which was quoted by

Morkovin('89) as being of the order of 3k - 6k. As a result of the separation region and the horseshoe vortices, the boundary layer has both spanwise and vertical shear layers. Slightly further downstream a pair of spiral vortices form which move up away from the surface and then trail downstream at the trip height.

At slightly higher Reynolds numbers, of the order of R_{kk} = 350 - 450 the separated shear layer at the top of the roughness becomes unstable and starts shedding disturbances or hairpin eddies. It appears that these replace, or evolve from, the spiral vortices. As R_{kk} increases, the horseshoe vortices and the stretching interlacing hairpin eddies grow stronger. At R_{kk} values from 450 to 600 transition occurs at first rather far downstream but then moves upstream rapidly with small increases in the Reynolds number. The turbulent spots then spread by lateral contamination from the source point, a process that is reviewed in chapter 6.

Despite this detailed knowledge of the flow around 3D trips, it is still unclear whether the turbulent spots are due to the shed eddies, breakdown of the horseshoe vortices or the interaction of the full multiple vortex system. Klebanoff *et al*('92) observed the shed eddies inducing, or evolving into, turbulent spots. This agreed with the earlier suggestion of Von Doenhoff & Braslow('61) that transition results from the formation of discrete eddies or disturbances originating at the trip. Motohashi *et al*('93) also appeared to agree with this, stating that the initial stages of transition were characterised by the appearance of velocity fluctuations that had originated at the shear layer created by the separation region. However, Motohashi *et al*('91) concluded that these disturbances interacted with the horseshoe vortices prior to transition onset. Morkovin('89) also concluded that transition was a result of interaction between the vortex systems but Gibbings *et al*('86b) found that duplication and re-duplication of the horseshoe vortices themselves led to the final breakdown to turbulence.

Despite this lack of agreement concerning the actual process which leads to turbulent spots, the critical conditions for the transition front to move up to the trip have been studied in some detail and, despite the slightly differing definitions of transition, agreement between the various investigations is fairly good. For investigations using flat plates it has been found that the critical value of R_{kk} varies with the Reynolds number based on the trip's position relative to the leading edge of the plate, or with R_{δ^*}. Smaller values of R_{kk} were obtained for trips positioned further downstream.

Numerous authors have examined the roughness Reynolds number, R_{kk}, for transition onset at the trip on a flat plate. Gibbings *et al*('86b) obtained a range of values of R_{kk} of between 520 and 615. Klebanoff *et al*('55) gave values for R_{kk} of between 490 and 578. Von Doenhoff & Braslow('61) also gave a value of R_{kk} of the order of 500 - 600, while Tani('61) suggested a larger range of R_{kk} = 500 - 800. Gibbings *et al* also examined the critical conditions for transition completion and obtained a range of R_{kk} = 630 - 675.

These values of critical R_{kk} are significantly higher than those quoted in section 4.1 for 2D trips. However, the forward movement of the transition position from the natural transition location to the roughness location with increasing freestream velocity is more rapid for a 3D roughness element than for a trip wire. Tani('61) has explained this as being due to the type of disturbances introduced by each trip. A 3D trip introduces 3D disturbances directly. In contrast, a 2D trip introduces 2D disturbances that must deform three-dimensionally before breaking down to turbulence. The process is therefore more gradual for 2D trips.

The only previous study of 3D trips in the attachment line boundary layer were done by Gregory & Love('65) and Firmin & Cook (unpublished but presented in Poll'89). They briefly examined attachment line contamination by fully effective 3D trips consisting of a cone and a glass sphere. Firmin & Cook found that in the presence of a large sphere the transition region extended from $\bar{R} = 238$ to $\bar{R} = 273$. Poll('89) contained a comparison between various forms of 2D and 3D trips on the attachment line and flat plates, although the data on attachment line transition by 3D trips was limited to the Gregory & Love and Firmin & Cook results. The graph of R_{δ^*} vs R_{kk} obtained by Poll is presented in Fig 5.1. He concluded that the different tripping characteristics of trip wires and isolated, or 3D, roughness elements are principally related to the character of the disturbance that is introduced i.e. two-dimensional type for the wire and a three-dimensional type for the sphere. Poll concluded, from the experimental data, that these differences were small and that for both transition onset and completion, the criteria for tripping of the infinite swept attachment line boundary layer were the same, to a first approximation, for fully effective trip wires, single spheres and single conical roughness elements. These criteria were expressed as values of R_{kk} for transition onset ($R_{kk} = 550$) and completion ($R_{kk} = 650$) at the trip. Comparing the effect of a single isolated roughness element on a flat plate and on the attachment line, Poll concluded that the results (in terms of critical value of R_{kk}) showed reasonable agreement, provided that the roughness element was controlling the transition, for both transition onset and completion. However, in terms of local laminar displacement thickness Reynolds numbers, the attachment line flow can be tripped to turbulence at conditions well below the minimum for flat-plate flow.

5.2 PRESENT INVESTIGATION

As with the investigation using 2D trips, a range of 3D trips were used with a range of sweep angles to obtain a wide range of values of d/η. For each trip size / sweep angle combination, three hot-wire locations along the attachment line were used and the conditions for transition onset and completion were determined. The same definitions for

transition onset and completion conditions were also used, namely, one burst of turbulence approximately every fifteen seconds for transition onset, while transition completion involves the lack of any laminar bursts for a period of approximately two minutes.

The 3D trips consisted of ball bearings of various diameters. They were attached to the model surface at the attachment line, 0.5m from the leading edge tip, using SuperGlue. It was concluded from previous tests that the actual shape of the 3D roughness element has little influence. Therefore great care was only taken, when applying the trip, to insure the trip was pressed down through the glue and flush with the surface. Thus with the glue forming a crown round the bottom of the ball bearing, the effective shape of the trip varied with ball size and quantity of glue used, i.e. a large trip appeared more like a sphere while a small trip more like a dome. Efforts were made to apply less glue when using small trips.

A brief test also revealed that the trip could be placed up to 5mm downstream of the attachment line without altering the results. This is obviously a far greater distance than could occur due to errors during the experiments.

Later tests involving repeats of the initial 3D trip tests demonstrated good repeatability for both transition onset and completion.

Data sampling was performed for similar set-ups over similar ranges as in the 2D trip tests. Thus data for frequency spectra was sampled at conditions for transition onset and transition completion. Data for intermittency distributions was sampled at nine windspeeds covering the transition region for small, medium and large trips. In addition the experimental set-up which produced points on the $\bar{R}$ vs d/η graph just above the 'kink' was also sampled.

As with the 2D trip tests, a brief investigation of the flow in the vicinity of the 3D trips was performed prior to studying the transition conditions.

5.3 FLOW AROUND 3D TRIPS

As with 2D trips, some doubt existed as to the extent of the separation region behind a 3D trip. The static pressure gradient around a 3D trip and the velocity profiles at several points downstream of the trip were therefore examined using the model static pressure taps and the traversable Pitot probe. The experiments were performed using an identical set-up and technique as with the 2D trip tests, the sole exception being the positioning of the trip relative to the static tap in the static pressure gradient tests. Two trips and two sweep angles were used in these tests.

The static tap used in the static pressure gradient tests is 3mm downstream of the

attachment line. The external streamline through the static tap was therefore estimated and each trip was positioned at various distances upstream of the tap, along this line. The trips were also positioned either side of the line to check that the maximum affected static pressure was being measured.

Results for the smallest trip were unclear but with larger trips the static pressure distribution, expressed as a value of ΔCp (= static pressure behind trip - static pressure without trip), has a similar appearance to those obtained using 2D trips. The static pressure distribution for one of the larger trips used is presented in Fig 5.2. It can be seen that the changes in static pressure due to the trips are smaller than those caused by 2D trips, as are the recovery distances downstream of trips. The similarity of the pressure distributions' appearance to those for 2D trips indicates the presence of a small region of separation behind each trip. The separation distance, as a function of the trip diameter, was less clear than for 2D trips and was not therefore plotted against the trip size. It appears, however, that an approximate separation distance of $s_r/d = 4$ is approached as the trips become large. With the exception of the smallest value of d/η, the Reynolds numbers used were large enough to ensure at least a transitional flow immediately downstream of the trip and in most cases the flow was fully turbulent.

Morkovin('89) suggested that on a flat plate the reattachment distance, downstream of a 3D trip, is of the order of $^1/_{10}$th of that of 2D trips. In this case the 3D trip value is about $^2/_5$th of the trip value. However, Morkovin was working with results that gave a reattachment distance of the order of 40d for 2D trips.

The numerous flat plate investigations have demonstrated that a complex set of vortices is set up behind the 3D trip. The present tests were in no way adequate to observe each of the vortex structures. However, it was felt that the tests would certainly show the overall effect on the mean attachment line velocity profile.

For the velocity profile measurements, both the trip and the Pitot probe were positioned on the attachment line. The experimental procedure was identical to that used in section 4.3 for 2D trips. The profiles obtained with the largest trip are presented in Fig 5.3a and the similarity with the profiles for 2D trips presented in Fig 4.7 is clear. However, with the exception of this single test involving the largest value of d/η, the velocity profiles obtained were very different. More typical examples of the profiles obtained are shown in Fig 5.3b.

The profiles in Fig 5.3a suggests that the largest 3D trips resulted in a recirculation region, with the profiles further downstream tending towards fully turbulent velocity profiles, as with the 2D trips. The majority of the tests did not however produce evidence of a separation region, although this would appear to be due to the small extent of the bubble as demonstrated by the static pressure distributions above. Thus most of the tests appear to have started downstream of the reattachment point. As can be seen in Fig 5.3b,

these profiles, obtained with smaller trips, clearly show a large distortion of the mean velocity profiles on the attachment line. The profiles suggest double points of inflection at locations shortly downstream of the expected reattachment point. These inflection points appear to move higher in the boundary layer and reduce in severity, as distance downstream of the trip increases. Returning to Fig 5.3a, similar distortions can be seen in the intermediate profile while the downstream profile, which is further downstream than those in Fig 5.3b, shows that eventually these points of inflection disappear and the velocity profile continues to fill out, developing towards the fully turbulent velocity profile. Gibbings *et al*('86b) found that the undistorted velocity profiles are recovered sooner by using larger fully effective trips, although a forward limit existed to which the recovery position could be moved.

The potentially large errors discussed in section 4.3 may raise doubts over the observed profiles however the similarity of profiles between different values of $\bar{R}$ and d/η, and the good repeatability of the few profiles re-tested, suggest that these profile are indeed representative of the flow downstream of a 3D trip. It is therefore concluded that these distortions are caused by the complex sets of vortices described in section 5.1.

5.4 TRANSITION RESULTS

Conditions for transition onset and completion are presented in Figs 5.4 and 5.5, respectively. The results are plotted in terms of the attachment line Reynolds number, $\bar{R}$, for transition onset (or completion) against the corresponding value of d/η. On both graphs, curves of constant s/η are plotted. As with the 2D trip results, the values of $\bar{R}$ and d/η at each specified value of s/η were obtained from interpolation of experimental results obtained with various hot-wire locations for similar sweep angle / trip size combinations.

Also in common with the 2D trip tests, some results had to be neglected before producing the final graphs of $\bar{R}$ vs d/η. The slight model vibration present with lower sweep angles at higher windspeeds results in data obtained at lower sweep angles with the smallest trip (and zero trip) being neglected for both transition onset and completion. In addition, data for transition completion with large trips ($d/\eta > 3.0$) and high sweep angles was also neglected. The reason for this is discussed in detail in section 4.4. Briefly, the cause is linked to variations in intermittency with height within the boundary layer and the relatively thick boundary layers obtained with low windspeeds and high sweep angles.

The experimental data used in obtaining the curves of best fit for the final $\bar{R}$ vs d/η graphs show very little scatter ($< \pm 4\%$ in terms of $\bar{R}$).

It has already been stated that the critical values of $\bar{R}$ representing the upper and

lower bounds for transition tripping should be similar for both 2D and 3D trips. Certainly the value for $\bar{R}_{upper}$ must be identical, since this is the value for natural transition. However, the critical roughness sizes associated with the two bounds were expected to be different for the 3D trips and were therefore examined. In addition, the value of $\bar{R}_{lower}$ was investigated to confirm the similarity and the value of $\bar{R}_{kink}$, associated with the minimum fully effective trip size, was also investigated.

From the 2D trip tests a value of approximately $\bar{R}_{upper} = 660$ was obtained with the present results. However, as mentioned in section 4.4, within the more limited range of s/η values for the present tests, the results agreed with Poll's results. With his extended range of s/η, Poll's results suggested a value of $\bar{R} = 600$. This value was accepted as the correct value and using this value for $\bar{R}_{upper}$ of 600, the maximum tolerable roughness was calculated by projecting a curve for $s/\eta \rightarrow \infty$ onto the $\bar{R}$ vs d/η graph. From this curve the maximum tolerable roughness was obtained as the value of d/η at which $\bar{R}$ started to decrease. A value of approximately $d/\eta = 1.33$ was obtained.

To investigate the lower bound, the graphs of $\bar{R}$ vs s/η for each trip with $d/\eta > 2.6$ were plotted on a single graph and presented in Fig 5.6. The lower bound for transition tripping, associated with transition onset, was obtained from this graph as the value of $\bar{R}$ as $s/\eta \rightarrow \infty$. This gives values for $\bar{R}_{lower}$ within the range $\bar{R} = 241$ to $\bar{R} = 260$. The lower bound for transition completion was also obtained from this graph, with values for $\bar{R}_{lower}$ in the range $\bar{R} = 304$ to 318.

The value for $\bar{R}_{kink}$ was only examined for transition onset, since the kink does not occur at a single point for transition completion. It was obtained from the $\bar{R}$ vs d/η graph as the point of intersection of the two curves of best fit for small trips, that produce transition well downstream, and larger trips, which result in transition immediately downstream. From this graph $\bar{R}_{kink} = 451$ and occurs at a value of $d/\eta = 1.82$.

For further comparison with 2D trip results, projected curves for $s/\eta \rightarrow 0$ and $s/\eta \rightarrow \infty$ for both transition onset and completion are presented in Figs 5.7 and 5.8. These curves were obtained using a combination of extrapolation of the $\bar{R}$ vs d/η graphs and extrapolation of experimental data for each trip/sweep combination. Approximate curves in the form of constant values of R_{kk} and a modified form of Gaster's criterion are also included in graph for $s/\eta \rightarrow 0$, while an approximate relation of a similar form to equation 4.3 is included in the graph for $s/\eta \rightarrow \infty$.

Intermittency distributions were measured for several points on the $\bar{R}$ vs d/η graph and are presented in Figs 5.13. Figs 5.14 show the distributions plotted against ζ_1 and ζ_2, together with the two forms of Narasimha's universal intermittency distribution.

5.5 DISCUSSION

It is immediately obvious from the graphs of $\bar{R}$ v d/η for transition onset and completion with 3D trips, presented in Fig 5.4 and 5.5, that the behaviour of the attachment line boundary layer subjected to disturbances from 3D trips is very similar to that observed using 2D trips. The graphs can again be split in to four distinct regions and the upper and lower limits for transition tripping are identical. There are however slight differences. The graph of R_{δ^*} vs R_{kk} from Poll('89), presented in Fig 5.1, demonstrated that the attachment line boundary layer, like the flat-plate boundary layer, was less susceptible to 3D trips than to 2D trips. This fact can be clearly seen in the present $\bar{R}$ vs d/η graphs. Fig 5.9 shows the curve for $s/\eta = 2000$ from both the 2D trips test and the 3D trip tests, and demonstrates that the values of d/η are greater for the 3D trips in each of the four regions of the $\bar{R}$ vs d/η graphs. The values of $\bar{R}$ and d/η, for transition onset, bordering each of the regions are listed below :

Zero trip : $d/\eta < 1.33$ $\bar{R} > 600$

Natural transition occurs. $\bar{R}$ is a function of s/η.

Small trips : $1.33 < d/\eta < 1.82$ $600 > \bar{R} > 451$

Transition occurs at some distance downstream of the trip but moves upstream rapidly with small increases in Reynolds number or trip size. The exact transition mechanism involved is unknown, but it would appear to be linked to eddies (or disturbances) originating at the trip and possibly some vortex interaction downstream of the trip. $\bar{R}$ is a function of s/η, but this diminishes with increasing d/η.

Medium trips : $1.82 < d/\eta < 2.63$ $451 > \bar{R} > 250$

Turbulent spots are created at, or immediately downstream of, the trip. For transition onset, $\bar{R}$ is no longer a function of s/η, though the dependence remains for transition completion.

Large trips : $d/\eta > 2.63$ $\bar{R} < 250$

Turbulent spots are created at the trip but decay and eventually die out as they convect downstream of the trip. $\bar{R}$ is once again a function of s/η and at low s/η turbulent spots can be obtained at very low $\bar{R}$. For transition completion a minimum exists and there is less dependence on s/η.

Thus, as expected, $\bar{R}_{upper}$ and $\bar{R}_{lower}$ are identical for transition onset with 2D and 3D trips. However, the trip sizes differ and the maximum tolerable roughness for 3D trips is approximately $d/\eta = 1.33$, this compares with a value of $d/\eta = 0.9$ for the 2D trips. There is also a large difference in values of d/η at $\bar{R} = 250$, from $d/\eta = 1.97$ for 2D trips to 2.63 for 3D trips. Thus, from values of $\bar{R}$ and d/η for transition onset, the most obvious differences between the transition conditions with 2D and 3D trips is the larger values of d/η for 3D trips.

For transition completion a similar comparison between 2D trip and 3D trip results was obtained, with larger values of d/η across each of the four regions of the $\bar{R}$ vs d/η graph, although $\bar{R}_{upper}$ could not be investigated directly (it is assumed equal to $\bar{R}_{upper}$ for transition onset) and $\bar{R}_{lower}$ was very slightly higher, at a value of $\bar{R} = 310$.

In the 2D trip tests, approximate relations for $\bar{R}$ vs d/η for $s/\eta \to 0$, in terms of critical values of R_{kk}, and for $s/\eta \to \infty$, in terms of linear relations between $\bar{R}$ and d/η, were determined for both transition onset and completion. Similar graphs for 3D trips are presented in Figs 5.7 and 5.8. From the graph of $\bar{R}$ vs d/η for $s/\eta \to 0$, the approximate curves represented by constant R_{kk} are applicable within the range $1.4 < d/\eta < 3.2$, and are fairly well represented by :

$R_{kk} = 650$	transition onset
$R_{kk} = 925$	transition completion

These values are considerably greater than the values obtained for 2D trips (= 450 for transition onset and 600 for transition completion). It is also apparent that there is a larger difference between the transition completion and transition onset conditions. This suggests that, at least for $s/\eta \to 0$, the transition region is larger for 3D trips than for 2D trips. Close inspection of the $\bar{R}$ vs d/η graphs does show a greater difference between transition onset and completion conditions for fully effective 3D trips than for 2D trips. This can be clearly seen in Fig 5.9. However, these graphs also suggest a smaller transition region for small 3D trips than for small 2D trips, which may be connected to the more rapid upstream movement of transition, with increasing Reynolds number, for 3D trips. The differences between the extent of the transition regions for fully effective 2D trips and 3D trips may be simply due to the different flow fields downstream of the trip or the mechanisms involved in transition. However, it cannot be ruled out that these small differences are due to experimental error. It has already been pointed out that transition completion conditions are difficult to define accurately from observation of a hot-wire signal. However, from a comparison between the present and previous investigations using 3D trips, in Fig 5.10, it appears that the extent of the transition region in the present investigation is similar to that of Gregory & Love('65).

The graph of $\bar{R}$ vs d/η for $s/\eta \rightarrow 0$, in Fig 5.7, also suggests that the modified form of Gaster's criterion matches the results fairly well. The original equation for 2D trips is given in equation 4.2. This was altered, for 3D trips, to :

$$(V_e.d/\upsilon) = 61.R_\theta^{1/2}$$

From the graph of $\bar{R}$ vs d/η for $s/\eta \rightarrow \infty$, in Fig 5.8, the following approximate relations, applicable within the range $1.1 < d/\eta < 2.5$, were determined :

$$\bar{R} = 985 - 294.(d/\eta) \qquad \text{transition onset}$$
$$\bar{R} = 1065 - 294.(d/\eta) \qquad \text{transition completion}$$

Comparing these approximate relations with those for 2D trips, it can be seen that the gradients are unchanged but the curves have been shifted upwards.

The extent of the transition region given by these approximations is also similar to that obtained in the tests with 2D trips. This differed from results for transition at the trip where the extent of the transition region for 3D trips was apparently greater. In this aspect at least, therefore, the attachment line boundary layers tripped by 2D trips and 3D trips behave more alike as the observation point moves further downstream.

Comparing the value of R_{kk} for transition onset, given above, with the values given in section 5.1 for the flat-plate boundary layer, it is apparent that the roughness Reynolds number for the attachment line boundary layer is slightly greater. However, Fig 5.10 also suggests that the values are slightly greater than those obtained in previous investigations for the attachment line boundary layer by Gregory & Love('65) and Firmin & Cook. A similar observation was made with the results for 2D trips when compared to Poll's data.

Further comparisons between 2D trips and 3D trips in flat plate and the attachment line boundary layers were made in Figs 5.11 and 5.12. These graphs of $R_{\delta*}$ vs R_{kk} are taken from Fig 5.1 (from Poll('89)) with the results from the present investigation for 2D trips and 3D trips added. Aspects concerning solely the 2D trips on these graphs were discussed in section 4.5 where it was established that the attachment line boundary layer is more stable than the flat-plate boundary layer and is less susceptible to 2D trips, due to the removal of the momentum deficit by the flow divergence. The attachment line boundary layer can, however, be tripped at lower Reynolds numbers.

Fig 5.11 shows that with 3D trips, the attachment line can again be tripped at lower Reynolds numbers ($R_{\delta*}$) than the flat plate but, although the accepted values of critical R_{kk} given above are very slightly greater for the attachment line results, Reynolds numbers based on the trip height are quite similar for transition onset. This agrees with the explanations for differences obtained with 2D trips. The momentum deficit, experienced

downstream of a 2D trip on a flat plate, has negligible effect downstream of a 3D trip on either a flat plate or the attachment line. It is therefore not surprising that flat plate and the attachment line boundary layers are susceptible to similarly sized 3D trips. This does not mean to suggest that the differences in susceptibility to 2D and 3D trips, on the flat plate, are due to the momentum loss. The attachment line boundary layer shows similar behaviour to the flat-plate boundary layer in being less susceptible to 3D trips than to 2D trips. These differences are far greater than any difference caused solely by the momentum deficit and are due to the basic differences in the flow downstream of the trips and the mechanisms by which transition is induced.

The results from Fig 5.12, for transition completion, are more difficult to explain. While values of R_{kk} for transition onset with 3D trips were very similar for the attachment line boundary layer and the flat-plate boundary layer, the graph for transition completion suggests that significantly larger values of R_{kk} are required for a fully turbulent attachment line boundary layer at the trip. It was mentioned above that the extent of the transition region, for transition at the trip, was greater for the present results with 3D trips than with 2D trips. It now appears that the present results also suggest a greater transition region, with 3D trips, for the attachment line boundary layer than the flat-plate boundary layer. Comparison between the attachment line results of Gregory & Love and the flat-plate results of Gibbings *et al*, in Figs 5.1a and 5.1b, suggest a similar occurrence. It is not clear why the extent of the transition region is greater for attachment line boundary layer, especially when the length of transition regions is similar for the two boundary layers with 2D trips, however the good agreement with the data of Gregory & Love does support the observation.

From previous investigations using flat plates, it was determined that another difference existed between transition induced by 2D trips and 3D trips, namely that for small trips the upstream movement of the transition front with increasing Reynolds number is more abrupt with 3D trips than with 2D trips. The present results provide several observations to suggest that similar behaviour occurs on the attachment line.

The influence of s/η could be observed in the graphs of $\bar{R}$ vs s/η used to obtain values of $\bar{R}$ at set values of s/η, for each trip size and sweep angle combination, for use in plotting the $\bar{R}$ vs d/η graphs. From these $\bar{R}$ vs s/η graphs it was observed that in the case of small trips the rate of increase in $\bar{R}$ with decreasing s/η was smaller for 3D trips, i.e. a smaller increase in Reynolds number was required to move the transition front upstream. Although the difference was not great, it can be seen in the graphs of $\bar{R}$ vs d/η, presented in Figs 4.8 and 5.4, that the curves for constant s/η do lie slightly closer together for small 3D trips than for small 2D trips. For both trip types, the influence of s/η for transition onset is removed at the kink and must also be identical for trip sizes below the minimum tolerable roughness. This ensures that only small differences are evident in the small trip region of the

$\bar{R}$ vs d/η graphs.

The influence of s/η may be more clearly detected from the difference between the projected curve for s/η → 0 and the curves for s/η > 400, for $\bar{R} > \bar{R}_{kink}$ on the $\bar{R}$ vs d/η graph. The kink in the graph for 3D trips is less severe, thus the change in $\bar{R}$ from measured values to the projected value for s/η → 0 is significantly smaller than for 2D trips. This again suggests that the upstream movement of the transition front with increasing Reynolds number is indeed more abrupt for 3D trips than with 2D trips. This assumption has important consequences for an observed feature of 3D tripping discussed in section 5.6. It is noted now that this feature also supports the present assumption. It therefore appears that very similar behaviour, in terms of the movement of the transition front with increasing Reynolds number, is again observed for the attachment line and flat-plate boundary layers.

Further consideration of the shape of the $\bar{R}$ vs d/η graph in the region of the kink revealed further evidence to support the idea of the more abrupt movement of the transition front. If the position of the kink for both 2D and 3D trips are examined it can been seen that, compared to the differences in the maximum tolerable roughness and in the values of d/η at $\bar{R}$ = 250, the differences in value of d/η at the kink is small (1.67 for 2D trips compared to 1.82 for 3D trips). Far more significant is the large difference in values of $\bar{R}_{kink}$ of 376 for 2D trips and 451 for 3D trips. The upper limit for transition tripping is the same in each case. If the maximum tolerable roughness is now taken as an effective zero, then it is clear that a smaller increase in trip size and a smaller decrease in Reynolds number is required to move to the kink on the 3D trip graph. This is in effect a smaller movement along the curves for $\bar{R}$ vs d/η. Since the kink represents the point at which the transition front first reaches the trip, then a smaller increase in d/η was required to move the transition front from far downstream up to the 3D trip.

An interesting feature of this is that ratio of $\Delta\bar{R}/\Delta(d/\eta)$, from the position of maximum tolerable roughness (associated with s/η → ∞) to the kink (associated with s/η → 0), was almost identical for the 2D trip and 3D trip graphs. This simply means that the gradient of $\bar{R}$ vs d/η curve was similar. However, examination of $\bar{R}$ vs d/η graph, shows that the curve linking these two points is associated with very large s/η and it has already been pointed out that the projection of the s/η → 0 curve above the kink has a far steeper gradient, compared to curves for s/η > 400, for the 2D trips than the 3D trips. It therefore appears that the similarity between 2D trips and 3D trips in terms of the relation between $\bar{R}$ and d/η improves with distance downstream. A similar conclusion has already been reached with regards to the length of the transition region and it is well documented that, for gross disturbances, the behaviour of the boundary layer far downstream is independent of the source of turbulence. Returning to the graphs of $\bar{R}$ vs d/η for s/η → 0 and s/η → ∞ for 2D trips and 3D trips, it can indeed be seen that a bigger difference exists between the s/η → 0 curves than the s/η → ∞ curves.

Large differences between the effects of 2D and 3D trips at small s/η was also observed in the hot-wire signals during the experiments. Within an approximate range of $\bar{R} = 300$ to 550, large laminar disturbances were observed on the oscilloscope for 3D trips at windspeeds slightly below that for transition onset, but only when the hot-wire was close to the trip (< 0.4m). For 2D trips, in both the present tests and the tests of Poll, small isolated disturbances were observed prior to first bursts. However these disturbances were far smaller than the observed disturbances from the 3D trips and they travelled downstream eventually breaking down to form turbulent spots. The disturbances from the 3D trips were much larger, in both amplitude and duration, and were observed decreasing in size as the hot wire was moved from 0.2m downstream of the trip to 0.4m where they were only just detectable. At 0.2m the disturbances were almost as big as a small turbulent spot. However the only apparent connection to the transition process was that they occurred at $\bar{R}$ only slightly less than $\bar{R}_{onset}$, the creation of the turbulent spots both near the trip and far downstream did not appear related to these disturbances. No conclusive explanation for these observations can be offered but the observed disturbances may simply be part of the complex vortex system created by a 3D trip. Further downstream very small isolated disturbances of similar magnitude to those from 2D trips were observed prior to the appearance of turbulent spots.

Finally, intermittency distributions were calculated for a range of trip size/sweep angle combinations resulting in values of d/η for each of the trip regions on the $\bar{R}$ vs d/η graph. These distributions are presented in Fig 5.13. From these graphs it appears that the extent of transition region, $\Delta\bar{R}$, ranges from approximately 50 with small trips to 60 with large trips, a slightly smaller range than obtained with 2D trips (though the positions on the $\bar{R}$ vs d/η graphs for the 2D trip and 3D trip intermittency tests do not correspond exactly).

As mentioned in section 4.5, the intermittency plots show only the increase in $\bar{R}$ and do not account for the increase in d/η. This must be considered when comparing the transition lengths with those from the $\bar{R}$ vs d/η graphs. This goes some way to explaining the apparent difference in the extent of the transition region for the medium sized trip, which appears very small from the intermittency plots. The position of this test configuration on the $\bar{R}$ vs d/η graph is at a point where the increase in $\bar{R}$ between transition onset and transition completion is less significant than the increase in d/η. However, this cannot totally explain the abruptness of the transition region observed in the intermittency tests and no further explanation can be offered.

It was also mentioned, in connection with values of R_{kk}, that the extent of the transition region for fully effective trips on the $\bar{R}$ vs d/η graphs was greater for 3D trips than for 2D trips. This agreed with the limited comparison possible between Poll's 2D trip data and Gregory & Love's 3D trip data from Fig 5.10. However, this disagrees with the intermittency distributions and therefore may suggest possible experimental errors.

However, the differences are not great and despite these problems, in general the intermittency plots support the $\bar{R}$ vs d/η graph and suggest that transition completion was fairly well defined by the hot-wire signal. This conclusion is supported by the good agreement in transition length with the results of Gregory & Love.

As with the 2D trip results, the intermittency distribution for the largest trip and the greatest value of s/η (> 2000) was compared with Stewart's('87) predicted distribution for gross disturbances. Again, a similar shape and extent for the distribution was obtained but due to the slightly higher value of $\bar{R}_{lower}$ for the present model, the actual values of $\bar{R}$ for the experimental and predicted distributions differed by a small constant amount.The intermittency factors were also plotted against the normalised co-ordinates ζ_1 and ζ_2 in Figs 5.14a and 5.14b, together with Narasimha's universal intermittency curves. As with the 2D trips, reasonable agreement with Narasimha's curve is achieved when plotted against ζ_1 but the sensitivity of ζ_2 to $\bar{R}$, for transition onset, makes agreement with this distribution more difficult.

Frequency spectra were also calculated for each of the three tripped regions on the $\bar{R}$ vs d/η graph. However, as stated in section 4.5, any differences in the appearance of the frequency spectra were due to the intermittency or, where first burst conditions were used, the Reynolds number and possibly the measurement height within the boundary layer. No trends, explainable by the different type of trips, were observed, although it is acknowledged that the limited extent of these tests would make any small trends very difficult to spot.

5.6 THE KINK IN THE $\bar{R}$ vs d/η GRAPH

The kink in the $\bar{R}$ vs d/η graph is at the junction between small trips, which introduce small disturbances that subsequently break down at some point downstream, and larger trips, which introduce turbulent spots immediately downstream. Thus a discontinuity exists in the graph at the intersection of the curves for each transition mechanism.

For 2D trips, it was speculated that it is the movement of the transition front from downstream of the reattachment point into the free shear layer and the resulting change in transition mechanisms that causes the discontinuity. There is little evidence, either in the present investigation or in literature, that fully effective 3D trips similarly cause turbulent spots within the short separation region immediately downstream of the trip, although Morkovin('93) did suggest that transition onset may have occurred near the end of the local wake separation due to the instability of the separated vortex sheet over and around the roughness element or due to higher instabilities. Von Doenhoff & Braslow('61) also concluded that the small separated region was involved in the transition process. However,

regardless of the specific location for transition 'at the trip', Morkovin('69) suggested that abrupt changes in transition Reynolds numbers indicate a change in the transition mechanism and Dobbinga('65) stated that a change in the character of the disturbance occurs when the height of the roughness element is increased beyond a critical value. This combined with the fact that the kink occurs as the transition front approaches the trip, does suggest some similar change in transition mechanisms with 3D trips.

From previous investigations of 3D trips on flat plates it had been concluded that the upstream movement of the transition front with increasing Reynolds number was more abrupt than with 2D trips. Evidence from the present tests suggested a similar behaviour for the attachment line boundary layer. One of the factors that supported this conclusion was the reduced severity of the kink in the $\bar{R}$ vs d/η graph, for 3D trips, suggesting that a smaller increase in Reynolds number would be required to advance the transition front from downstream up to the trip itself.

During the experiments, a particular combination of trip size and sweep angle ($d = 0.78$mm and $\Lambda = 71°$) resulted in a value of d/η slightly smaller than the minimum fully effective trip size. A situation therefore existed where turbulent spots were first formed at some distance downstream of the trip but only a small increase in Reynolds number was required to move the transition front up to the trip. It was discovered that, with this situation, slowly increasing the windspeed towards conditions for transition completion revealed the presence of region where the intermittency decreased. It appears that this region is linked to the two curves, on the $\bar{R}$ vs d/η graph, for the two transition mechanisms.

The actual intermittency distribution varied between tests and in some cases was very brief and difficult to detect. In situations where the set-up was not altered between tests a repeatable region was observed. However, if the set-up was altered between tests then the region of decreasing intermittency could occur at different points within the transition region, on either side of the peak in V_{rms}, and vary in the extent of the reduction, although generally the decrease in intermittency resulted in a return to the transition onset signal. It appears that the slight differences were most likely due to the slight changes in sweep producing very small changes in the values of d/η. It therefore proved very difficult to regain identical intermittency distributions from test to test but a generally similar transition region could be observed, and a measured distribution is presented in Fig 5.15. Essentially, it appeared that after the transition region was well developed and numerous turbulent spots could be observed, the number of turbulent spots would start to decrease and the hot-wire signal would return to that associated with transition onset, with only an occasional turbulent spot present. With further increases in windspeed the rate of turbulent spots increased again and the transition region then proceeded as normal. With the sizeable change in Reynolds number from the start of the region, of decreasing intermittency, to the

point of minimum intermittency, the reduction is not a step change but it appears more of a reversal of the transition process.

As mentioned above, the experimental set-up for this observation resulted in a trip which initially introduced laminar disturbances, which subsequently broke down to form turbulent spots, but which only required a small increase in $\bar{R}$ to move the transition front upstream to the trip. It therefore seems likely that the reduction in intermittency is linked to the change in transition mechanism from turbulent spots produced downstream of the trip (by amplification of small disturbances or breakdown of shed eddies) to turbulent spots introduced directly at the trip location (possibly within the free shear immediately downstream of the trip).

If this assumed to be true and $\bar{R}_\epsilon$ is used to define the Reynolds number at which the intermittency factor starts to decrease then a more detailed examination of the transition front movement would show that for $\bar{R} < \bar{R}_\epsilon$ all the turbulent spots originate some distance downstream of the trip. As the Reynolds number increases the point at which the disturbances can breakdown to form the turbulent spots moves upstream towards the trip. However this is only the minimum distance, laminar disturbances will still breakdown to form spots within some range downstream. So for a fixed hot-wire location, an increase in $\bar{R}$ increases the possibility of spots being present at the hot-wire, thus for $\bar{R}$ slightly less than $\bar{R}_\epsilon$ numerous turbulent spots originating at various distances between the trip and the hot-wire should be present. For $\bar{R} = \bar{R}_\epsilon$ conditions are reached where the occasional spot will originate at the trip, due to the different mechanism. Intermittency of these particular spots will be very low. It therefore appears that the introduction of this form of breakdown to turbulent spots in some way prevents the breakdown to spots via laminar disturbances travelling downstream, at least within some range near the turbulent spot originating at the trip. As the number of turbulent spots originating at the trip increases slowly the number of turbulent spots developing downstream reduces quickly until a point is reached where no turbulent spots originate far downstream of the trip. This point probably corresponds to the point at which the overall intermittency, within this region, reaches a minimum. Further increases in $\bar{R}$ increases the intermittency as the number of spots originating at the trip continues to increase.

This behaviour would certainly result in an intermittency distribution similar to that experimentally observed. A factor which supports this theory is that the point at which the reduction in intermittency begins coincides almost exactly with the projected curve for $s/\eta \rightarrow 0$.

The model and instrumentation did not allow a further investigation of this process and the only similar occurrence found in literature concerned the calmed region, downstream of a turbulent spot, observed by Schubauer & Klebanoff('56). This refers to

a region behind a turbulent spot where the laminar boundary layer velocity profile is left in a more stable 'turbulent-like' state. This profile then gradually changes back to the normal laminar velocity profiles at some distance behind the spot. Within the calmed region the normal levels of disturbances observed in a laminar layer are not present and Schubauer & Klebanoff concluded that breakdown to turbulence could not occur within this region. However, these calmed regions have a duration of a fraction of a second and could not by themselves explain the large regions of laminar flow obtained at mid-transition in this present test. It therefore appears that some incompatibility between the two transition mechanisms is the most likely cause, with the mechanism responsible for turbulent spots created at the trip removing, or damping, the disturbances which would otherwise amplify and breakdown to turbulence further downstream.

This region of decreasing intermittency was not observed during 2D trip tests. This is probably due to larger changes in $\bar{R}$ required to move the transition front upstream.

5.7 CONCLUSIONS

It has been shown that the 3D trips have similar effects in both attachment line and flat-plate boundary layers, and also have a similar effect, overall, to 2D trip wires in the attachment line boundary layer. The attachment line and flat-plate boundary layers have similar tolerances to 3D trips, at least for transition onset, which in both cases is considerably greater than that to 2D trips. However, differences between roughness Reynolds numbers for transition completion suggest that, with 3D trips, the extent of the transition region on the attachment line is greater than on the flat plate, despite similar lengths of transition region observed with 2D trips in the two boundary layers. For fully effective trips it also appears that the transition region is longer on the attachment line with 3D trips than with 2D trips. For hot-wire positions further downstream, it was found that the similarity between the attachment line boundary layer behaviour with 2D trips and 3D trips improved as the distance downstream increased.

The other major difference between the effects of 2D and 3D trips is the upstream movement of the transition front with increasing Reynolds number, for small trips. The more rapid movement with 3D trips resulted in a less severe kink in the $\bar{R}$ vs d/η graph, and allowed the observation of a region of decreasing intermittency, possibly due to an incompatibility between different transition mechanisms as the transition front moved up to the trip.

6 - TURBULENCE SPREADING FROM DOWNSTREAM OF ATTACHMENT LINE

It was discussed in the first chapter how a turbulent attachment line boundary layer will result in a turbulent boundary layer over the rest of the wing. Since the turbulence originating from a 3D roughness element will spread out downstream forming a turbulent wedge, the accepted spreading half-angle of which is of the order of 10°, it is apparent that 3D trips located a short distance downstream of the attachment line on either the upper or lower surface of the wing can still cause turbulence at the attachment line. In this case, the turbulence would not then be restricted to a wedge of turbulence on the same surface as the roughness element but would affect the whole of the rest of the wing, beyond the spanwise location at which the turbulence returns to the attachment line, on both wing surfaces.

The turbulence spreading angle, and the effects of Reynolds number on this angle, was therefore examined for trips positioned at various distances downstream of the attachment line. It is recognised that to a certain extent the results for these tests are model dependent. The maximum chordwise distance from the attachment line from which the turbulence spreads back to the attachment line is certainly dependent on the flow divergence and is probably dependent on the pressure gradient, while the conditions for turbulence to originate at the trip also depend on the boundary layer growth downstream of the attachment line. However, the turbulence spreading angle can be obtained relative to the external streamline and, as is discussed later, it is not thought that the cross-flow or flow divergence affects this angle. These tests were therefore considered a worthwhile guide to the turbulence spreading angle, and the influence of Reynolds number, in the vicinity of the attachment line. The tests also defined the limitations of the results obtained for 3D trips positioned on the attachment line.

6.1 PREVIOUS WORK

The turbulent spot was first proposed by Emmons('51) who concluded that the transition phenomenon may be viewed as a process that begins with a series of point breakdowns in the laminar flow. The point breakdowns (or turbulent spots) subsequently develop by spreading longitudinally and laterally until they eventually overlap thereby creating fully turbulent flow.

Most work concerning the turbulent spot and the turbulent wedge has been performed on flat plates at high Reynolds numbers where it appears that a universal turbulent spot is obtained, i.e. constant shape, propagation velocities of leading and trailing edges, and spreading angle. Similar results for all these parameters were obtained by, amongst others, Schubauer & Klebanoff('56), Wygnanski *et al*('75), Narasimha *et al*('84)

and Elder('60). The turbulent spot observed by Schubauer & Klebanoff is presented in Fig 6.1. They considered the effect of Reynolds number on the spreading angle and although the range of Reynolds numbers covered was small and all the values were high, a decrease in spreading angle with smaller Reynolds number was noted. A more complete study of the effect of Reynolds number was performed by De Bruin('89) and his graph of spreading semi-angle against Reynolds number is presented in Fig 6.2. Although De Bruin's model had a small negative pressure gradient, he concluded that this did not affect the turbulence spreading angles. De Bruin obtained a maximum spreading semi-angle of 9.5° at high Reynolds number but at lower Reynolds number the angle decreased to less than 3°. He concluded that a minimum Reynolds number of $R_\theta = 320$ is required for turbulence to spread laterally in a flat-plate boundary layer. This is the value suggested by Preston as a minimum for sustainable fully turbulent flow.

As the turbulent spots grow and the number of them increase, the spots overlap forming a turbulent wedge. Schubauer & Klebanoff observed a similar spreading angle for a wedge as for an individual spot and concluded that a turbulent wedge is essentially a train of turbulent spots. This agreed with Emmon's('51) assumption that the spots grew and overlapped without interacting, although Coles & Savas('79) suggested that there may be some interaction if the spots are very closely packed. The turbulent wedge, presented in Fig 6.3, from Schubauer & Klebanoff, shows that the turbulent wedge does not have a definitive outer edge but consists of a fully turbulent inner core with an intermittent outer region, where the intermittency decreases gradually towards the edges of the wedge.

It has also been observed that the influence of the turbulent spot does not end at its outer edge. Lindberg *et al*('84) demonstrated using linear stability analysis that the flow just to the side of a turbulent spot has reduced stability in comparison with the flow far from the spot. Gad-El-Hak *et al*('79) went one step further and suggested that it is the destabilisation of the already rotational flow outside the edge of the turbulent spots that is responsible for the lateral spreading. This destabilisation induces perturbations which break down forming new turbulence. Matsui('79) agreed with this, suggesting that a longitudinal vortex is induced to the side of an existing vortex, which then shifts away creating lateral growth of the spot. The resulting transverse contamination rates are far greater than the turbulent entrainment rates which lead to longitudinal growth of the turbulent spots. However, as mentioned by Morkovin('93), the actual mechanisms involved in lateral spreading of turbulent spots are not yet clear.

Little previous work concerning turbulence spreading across a three-dimensional boundary layer at low Reynolds numbers could be found. Gregory('60) calculated that for his swept wing, 3D roughness elements positioned at between x/C = 0.003 and x/C = 0.013 downstream of the attachment line could contaminate the attachment line due to lateral spreading. In experiments he found that the range was slightly smaller and may have varied

slightly with the roughness height. Gregory also concluded that the cross-flow, downstream of the attachment line, did not affect the turbulent wedge at all and that the spreading was controlled by conditions in a critical layer within the boundary layer at a certain distance from the surface. Narasimha *et al*('84) also concluded that the turbulence spreading angle relative to the local streamline was independent of streamline divergence, while Arnal & Juillen('88) examined turbulent spots leaving the attachment line and travelling across the wing and concluded that the spots propagate from the attachment line with little modification to their structure. With regards to actual turbulence spreading angles, Poll('83a) observed a turbulent wedge with a local spreading semi-angle of approximately 10° relative to the external streamline direction, originating from a single conical excrescence positioned near the attachment line. However, Pfenninger('65) observed a very small spreading angle close to the attachment line and Poll suggested that in the immediate vicinity of the attachment line where the Reynolds number is low the spreading semi-angle may be lower than 10°. Poll('83b) also considered turbulence spreading, from downstream of the attachment line back onto the attachment line at greater s/η, while developing an equation for intermittency for the attachment line boundary layer subjected to a gross disturbance. However, this merely involved an extension of Emmons' mathematical model using the 'dependence volume' and spot formation rate per unit length. It therefore required assumed turbulence spreading angles.

6.2 PRESENT INVESTIGATION

At the point on the model normally used as the trip position (i.e. s = 0), a line was marked on the model perpendicular to the attachment line. 3D trips were then placed at varying distances downstream of the attachment line, along the marked line. The experimental set-up is sketched in Fig 6.4. Due to the large number of possible variables, the investigation was limited to two hot-wire locations on the attachment line (s = 0.2m and 1.8m), three sweep angles (55°, 60° & 70°) and three trip sizes (0.78mm, 0.98mm & 1.99mm). The investigation was then limited to determining transition onset and completion Reynolds numbers for each trip position. For trips positioned downstream of the attachment line, observation of transition onset refers to conditions for the edge of the turbulent wedge to intersect the attachment line at the hot-wire position, while transition completion refers to conditions for the fully turbulent inner core of the wedge to intersect the attachment line at the hot-wire position. The change in Reynolds number between onset and completion conditions is therefore the increase in Reynolds number required for the spreading angle of the inner fully turbulent core to increase to the initial angle for the outer edge of the wedge.

Although the trips were placed downstream of the attachment line, it is still the attachment line boundary layer and the conditions required for the turbulence from the trip

to reach the attachment line that is of interest. Thus the attachment line Reynolds number $\bar{R}$ continues to be used except for during comparisons with flat plate results. It is also assumed that Reynolds numbers, converted to R_{δ^*}, does not vary much across the limited chordwise extent used for these tests.

The chordwise distance of the trip from the attachment line was measured using a rule. For larger distances from the attachment line the rule was bent to maintain contact with the model's surface. Due to this method and the fact that the attachment line itself is taken to be the marked line, the accuracy of the chordwise distance in the calculations was perhaps optimistically assumed to the nearest 0.5mm. In fact the attachment line itself is probably only marked correctly to within ±0.5mm.

6.3 PRELIMINARY MEASUREMENTS AND CALCULATIONS

Several problems had to be considered before obtaining the final results for turbulence spreading, namely : interpolation of $\bar{R}$ to a given s/η, boundary layer growth downstream of the attachment line, the actual flow divergence angle, pressure gradients and finally the possible influence of cross-flow instabilities.

Since the results were both model and sweep angle dependent it was deemed unnecessary to interpolate values of $\bar{R}$ to a value for a specific s/η. In these tests it is the trends in the turbulence spreading angle and the overall effects of $\bar{R}$ on α, where α is the minimum required turbulence spreading semi-angle for turbulence originating at the trip to intersect the attachment line at the position of the hot-wire, that are of interest, not specific values of $\bar{R}$. However, consideration must be given to changes in the value of s/η between related tests. Any change in $\bar{R}$ will result in a change in s/η and values of $\bar{R}$ for trips placed downstream of the attachment line must be compared with the value of $\bar{R}$ for the trip on the attachment line. This change in s/η may then have an affect on the relative values of $\bar{R}$ for each trip position. The effect of increasing s/η as $\bar{R}$ is increased with increasing x_{trip} was therefore examined.

The two extreme cases where s/η has greatest effect, i.e. smallest and largest d/η, were examined. The two tests conducted for trips on the attachment line with the two hot-wire locations were used to calculate the change in $\bar{R}$ as a function of the change in s/η. This value was then used with the maximum change in s/η for a fixed hot-wire position, as the trip was moved in the chordwise direction, to calculate the maximum change in $\bar{R}$ due solely to the change in s/η. In the worst case the change in $\bar{R}$, due to s/η, was 8. This represented less than 2% of the total change in $\bar{R}$. The effect of changes in s/η, as the trip

is moved further downstream, can therefore be neglected.

Velocity profiles were measured downstream of the attachment line in section 3.4.2. From these profiles, no noticeable boundary layer growth could be detected. It is therefore assumed that, within the limited area used downstream of the attachment line, any boundary layer growth is small. In addition, the increase in Reynolds number as the trip is moved further from the attachment line will result in a decrease in the boundary layer thickness and will certainly dominate over possible boundary layer growth. The decrease in η resulting from the increase in $\bar{R}$ will result in an increase in d/η, however the range of trip sizes required to obtain results for constant d/η would have been prohibitive. Results were therefore obtained for constant trip sizes and the variation in the effective trip sizes was considered in the analysis.

Pressure gradients in the chordwise direction can be read directly from the pressure distribution. Consideration was given to the effects that the pressure gradient may have on the results due to the fact that the trip was lying in a developing 3D boundary layer in a favourable pressure gradient. The turbulent spots created at the trip then had to spread across an effectively adverse pressure gradient while the turbulent spot shape was distorted by the flow divergence and the cross-flow. However, the trips were still relatively close to the attachment line, so the cross-flow was not yet substantial and the pressure gradients were small. In addition it was noted above that Narasimha *et al*('84) observed no effect of streamline divergence on the spreading angle relative to the local external streamline and Gregory('60) observed no affect from the cross-flow on the turbulent wedge. It was therefore expected that the overall effect of these factors was small.

The cross-flow Reynolds number was calculated for the extreme trip positions, with largest x and $\bar{R}$, for both the transition onset and completion Reynolds numbers. The resulting cross-flow Reynolds number were relatively small (due to the small values of x) and were well below the critical value proposed by Owen & Randall('52). It is not, therefore, felt that cross-flow instability influenced the results.

In calculating the turbulence spreading semi-angle, two features must be considered : firstly, the angles between the external streamlines (from $x = 0$ to $x = x_{trip}$) and the attachment line; and secondly, the distances x_{trip} (between trip and attachment line) and s (distance along attachment line to hot-wire location). Obviously both the sweep angle and x will affect the angles of the external streamlines while s, and also x, will affect the required turbulence spreading angle (to the external streamline) for the turbulence to intersect the attachment line at the hot-wire location. A sketch of the external streamlines and turbulence spreading is presented in Fig 6.5 and details of the calculation of the required turbulence

spreading angles for each configuration and varying x are given in appendix F.

6.4 RESULTS

As mentioned above, turbulence spreading from downstream of the attachment line was investigated by determining transition onset and completion conditions at the hot-wire location on the attachment line. For each trip position the transition onset and completion conditions then correspond to conditions for the outer edge of the turbulent wedge and the fully turbulent inner core to intersect the attachment line at the hot-wire. The required turbulence spreading semi-angle with the turbulence assumed to have originated at the trip location was then calculated. The results are presented as graphs of $\bar{R}$ vs α in Figs 6.6 for both isolated spots at the edge of the turbulent wedge and the fully turbulent inner core. It must be noted that the values of α in these graphs are the minimum values which would be required for the turbulence at the hot-wire to have originated at the trip and do not necessarily indicate a true spreading angle at each Reynolds number. Thus at the minimum Reynolds number on each graph, where α is presented as decreasing to zero, the maximum value of α (for $\bar{R} = \bar{R}_{min}$) is the actual turbulence spreading semi-angle. At the maximum Reynolds number the turbulent spots are caused by natural transition and the true spreading semi-angle is the minimum value of α (for $\bar{R} = \bar{R}_{max}$).

As mentioned above, the value of d/η for each trip increases as the trip is moved further downstream and $\bar{R}$ is increased. Therefore, in the graphs of $\bar{R}$ vs α, presented in Figs 6.6, d/η also increases as $\bar{R}$ increases. Curves are plotted for each combination of physical trip size (d), hot-wire location (s), and sweep angles (Λ) as noted in the header on each graph.

The main features of interest from these tests are the turbulence spreading semi-angle, α, and its variation with Reynolds number, and the maximum values of α for $\bar{R} = \bar{R}_{a.l.}$. Each of these features can be determined from the plots of $\bar{R}$ vs α in Figs 6.6.

From these graphs, it is clear that the turbulence spreading semi-angle increases with Reynolds number with values of α varying between approximately 2.5° and 10°.

Two specific values of α were also obtained from these graphs : α_1 = turbulence spreading semi-angle for $\bar{R} = \bar{R}_{a.l.}$ and α_2 = maximum turbulence spreading semi-angle available within the confines of these tests. The positions of α_1 , α_2 and $\bar{R}_{a.l.}$ on the $\bar{R}$ vs α graphs are shown in Fig 6.6. The values of α_1 and α_2 are listed in table 6.1 together with the corresponding values of $\bar{R}$ and d/η, and α_1 is plotted against $\bar{R}$ in Fig 6.8. Differences in the values of α_2 for the two values of s are due to differences in natural transition Reynolds number.

α_1, although equal to the turbulence spreading semi-angle for $\bar{R} = \bar{R}_{a.l.}$, also refers

to the minimum spreading semi-angle for that trip. From Fig 6.8 it can be seen that α_1 varies between 2.5° and 4.5° for the outer edge of the wedge and between 2° and 4° for the fully turbulent inner core. It also appears that the spreading angle for the edge of the wedge and the fully turbulent core increases at similar rates, with increasing Reynolds number.

α_2 was examined simply to determine the largest spreading semi-angle obtained during these tests. It should be noted that α_2 does not essentially refer to the maximum spreading semi-angle, larger spreading angles may be available with further increases in $\bar{R}$ but natural transition on the attachment line would have to be delayed in order to observe this. However Von Doenhoff & Braslow('61) thought that an increase in the stability of a boundary layer may affect the lateral spreading of a turbulent wedge. An attempt to delay natural transition, possibly using suction, could therefore influence the turbulence spreading angle. From table 6.1 it can be seen that the largest value of α_2 is approximately 10° for the edge of the turbulent wedge and 8.5° for the fully turbulent core. These angles were obtained from the tests where the natural transition Reynolds numbers were at a maximum.

Potential errors are greater for these tests than in previous chapters. It has already been mentioned that the chordwise distance was simply measured using a rule and distances were optimistically noted to the nearest 0.5mm. This together with possible small errors in the marked position of the attachment line could introduce errors in x of at least 1mm. In addition to this, restrictions on tunnel access time restricted the number of data points for each graph and thus additional error may be introduced with the application of the line of best fit. This would be especially true for the two limiting values of x, which lead to α_1 and α_2. Errors in x_1 of 1mm would lead to errors in α_1 of less than 0.5°, while similar errors in x_2 would produce smaller errors in α_2.

In comparison to these errors, the errors in the assumed origin of the turbulent wedges are probably small. The spreading angles were calculated assuming that the turbulent wedge originates at the trip. For all the experimental set-ups bar one, the combination of Reynolds number and trip height was sufficient to cause turbulence immediately downstream of the trip. For the single experiment where turbulence first originates downstream of the trip (d=0.78mm, Λ=70°, x=0.0mm) only a small increase in Reynolds number was required to move the transition front up to the trip, so errors should also be small in this case.

In addition, it is doubtful that the slight model vibration which led to lower Reynolds numbers for natural transition at lower sweep angles would have affected the turbulence spreading angle significantly. Any influence it did have would be limited to tests at high windspeeds and low sweep angles.

6.5 DISCUSSION

As mentioned above, the main topics of interest are the turbulence spreading angles and the effect of Reynolds number on this angle. From the graphs presented in Fig 6.6 it is clear that the Reynolds number significantly influences the turbulence spreading angle. For α greater than α_1, the spreading angle increases at first very quickly and then more gradually with increasing $\bar{R}$. The curves for isolated turbulent spots and fully turbulent flow appear quite similar although the values of α_1 are slightly smaller for the fully turbulent flow and the rate of increase of α is slightly greater. On average an increase in $\bar{R}$ of 96 resulted in a 1° increase in the spreading angle of the edge of the turbulent wedge while an increase in $\bar{R}$ of 89 was required for a similar increase in the fully turbulent core spreading angle. This suggests that at higher Reynolds numbers the intermittent outer region decreases in size and the fully turbulent core dominates more of the turbulent spot.

For the outer edge of the turbulent wedge, the overall relation between Reynolds number and spreading semi-angle is plotted in Fig 6.9 together with the data from De Bruin. The lower values of R_{δ^*} for attachment line transition, as discussed in chapters 4 & 5, are again apparent and it would appear that the range of spreading angles are similar. However this graph also shows the considerable variations in α at given Reynolds numbers for the present tests. It appears that this variation is due to a combination of experimental scatter and a small dependence on trip size.

A comparison between graphs for similar sweep angles but different trips suggests that the trip size may influence the spreading angle, with α increasing slightly as the trip size increases. This appears to occur right across the range of Reynolds numbers, even at high Reynolds numbers where the effective trip sizes, in terms of d/η, are very large. A larger trip also results in a smaller initial transition Reynolds number so this trend may alternatively be due to the change in Reynolds number from the initial transition onset value. Certainly this dependence on either trip size or initial transition conditions partly explains the large variation in the turbulent spreading angles obtained at various Reynolds numbers, as shown in Fig 6.9. Schubauer & Klebanoff('56) observed some dependence on the initial conditions at the source of the spots. In particular, one test which produced a larger initial spot also lead to a greater turbulence spreading angle. Gregory('60) also suggested that the turbulence spreading may vary with roughness height although Lindberg *et al*('84) suggested that the characteristics of the spot are independent of the initial disturbance and De Bruin observed little scatter in his graph of R_{δ^*} vs α despite large differences in roughness geometries. It therefore appears that the large variations in α at a given value of R_{δ^*} cannot be totally explained by the variations in trip size.

Careful examination of either Figs 6.6 or table 6.1 shows that, even accounting for the trip size, scatter in the results, in terms of the relation between $\bar{R}$ and α, is considerable. It would therefore appear that the concern expressed over the accuracy of these tests was

justified and experimental errors resulting in scatter in the data contributes significantly to the variations in α.

However, this does not detract from the overall observations that a similar range of turbulence spreading angles, exhibiting a broadly similar dependence on Reynolds number, to De Bruin's flat plate results, was obtained.

It was mentioned in section 6.1 that at high Reynolds numbers a universal turbulent spot is obtained, in flat-plate boundary layers, with a spreading semi-angle of 10°. From tests at lower Reynolds numbers it was also known that this angle is approached asymptotically.

From Figs 6.6 it can be seen that α increases at first quickly and then more gradually as Reynolds number increases. As the Reynolds number approaches the value required for natural transition there appears to be a slight interaction which causes the required spreading angle for the turbulence to have originated at the trip to increase quickly again. If this interaction and the values after natural transition has become dominant are neglected then, overall, the results suggest that an asymptotic value for turbulence spreading angle was being approached at higher Reynolds numbers. However, the lack of sufficient data points at the higher Reynolds number and the intervention of natural attachment line transition means that this can not be conclusively proved. However, the spreading angle apparently being approached asymptotically was of the order of 9° to 12° which is similar to the values for the universal turbulent spot on a flat plate. The maximum spreading semi-angle actually observed during these tests was approximately 10°.

The third feature of interest, mentioned above, is more model dependent but was examined to determine the limitations of the results from chapter 5 for trips on the attachment line. Fig 6.8 shows the turbulence spreading semi-angle for $\bar{R} = \bar{R}_{a.l.}$, α_1. The graphs appear to suggest a value of α_1 of the order of 2.5° to 4.5° for the edge of the turbulent wedge (transition onset) and 2° to 4° for the fully turbulent core (transition completion), with greater values at higher Reynolds number. Again, the scatter is considerable but partly due to differences in trip size. However, the graph clearly shows that, for attachment line transition, the conditions determined in chapter 5, and presented in Fig 5.4 and 5.5, apply to a rather limited chordwise extent for locations of the 3D trips. Of course the trips still cause transition when located beyond this maximum range, but a larger Reynolds number is required for the turbulence to affect the attachment line boundary layer.

In the worst case for the present model and configuration (i.e. $\Lambda = 55°$, $s = 0.2m$) this turbulence spreading angle equates to 5mm downstream of the attachment line. Henke('90) gave 28° as a typical sweep angle for the larger transonic aircraft, while Hardy('88) gave typical values of U_1 for aircraft of approximately 70 compared to 8 for the

present model. For a given point on the wing downstream of the attachment line, an increase in U_1 or a decrease in the sweep angle both result in an increase in the angle between the external streamline and the attachment line. Thus for an actual swept wing the maximum chordwise distance from the attachment line for a 3D trip to cause transition of the attachment line boundary layer at the conditions described in Fig 5.4 will be substantially reduced from the 5mm for the present model.

6.6 CONCLUSIONS

The universal turbulent spot demonstrated in numerous investigations was not realised at the low Reynolds numbers required for attachment line transition in the presence of a 3D trip. In fact, it was revealed that with appropriate conditions for transition onset in the presence of a fully effective 3D trip the turbulent wedge formed downstream of the trip had a spreading semi-angle of the order of just 3°. It is possible that the universal turbulent spot with a turbulence spreading angle of 9° - 12° was being approached at higher Reynolds number. However, for the lower Reynolds numbers associated with attachment line transition, the turbulent spot was a function of Reynolds number and, to a lesser extent, either the trip height or the change in Reynolds number from the initial transition onset value.

As a result the conditions for attachment line transition, obtained in chapter 5, can only be applied to 3D trips within a short chordwise distance from the attachment line. With the trip further downstream, transition may still be caused at the same Reynolds number but only a relatively small spanwise extent downstream of the trip will be affected. A significantly larger Reynolds number is required for the turbulence to affect the attachment line boundary layer, and thus the rest of the wing.

7 - EFFECTS OF FREESTREAM TURBULENCE

Pfenninger & Bacon('69) concluded that atmospheric turbulence has less influence on transition than the micro scale turbulence of low turbulence wind tunnels. However, in some applications, most notably internal flows, freestream turbulence levels can be considerably higher. Gostelow *et al*('94) stated that turbulence levels vary between 2% and 14% in axial flow compressors and can reach 18% in axial flow turbines. The effects of two higher levels of freestream turbulence were therefore examined with both two-dimensional and three-dimensional trips present.

7.1 INTRODUCTION AND PREVIOUS EXPERIMENTAL WORK

The effect of freestream turbulence on transition is broadly similar to that of a trip, although the mechanisms involved are very different. One similarity is that just as the transition process changes with the size of the trip, the transition process also changes as the turbulence intensity increases. The mechanism by which the freestream turbulence influences the boundary layer transition is referred to as receptivity.

For low levels of freestream turbulence, transition occurs due to amplification of Tollmein-Schlichting waves within the boundary layer. The naturally occurring freestream disturbances travel at much higher speeds than the instability waves within the boundary layer. The wavelength of the freestream disturbances at a given frequency are therefore much longer than the TS waves and a wavelength conversion is required to transfer energy from these long waves to the much shorter TS waves. This conversion takes place at locations where the mean flow exhibits rapid changes, which for the present model would be at the leading edge tip or at a roughness element.

For moderate levels of freestream turbulence this process is enhanced and transition occurs at lower Reynolds numbers. For high levels of freestream turbulence the relatively slow amplification of TS waves is bypassed and boundary layer disturbances are introduced more directly.

Due to the increased amplitude of the disturbances in the boundary layer, the effect of a roughness element is enhanced by freestream turbulence. At the same time, roughness induced separation is especially sensitive to freestream disturbances and the rate of amplification, of disturbances, within this region can be significantly increased. Thus trips and freestream turbulence compliment each other in promoting transition.

As with the work on transition tripping with 2D and 3D trips, a majority of the work investigating the effects of freestream turbulence has been performed on flat plates. Fig 7.1

shows a graph of transition Reynolds number against 2D trip size for a range of turbulence levels, from Tani('61). This graph contains data from several tests on flat-plate boundary layers. From the graph it is clear that transition caused by a given roughness occurs earlier in a stream of increased turbulence and that the freestream turbulence has less effect as the trip size increases. In fact for large trips, where $k/\delta > 0.6$, the influence of the freestream turbulence disappears altogether. It also appears that the maximum tolerable 2D trip height increases slightly with turbulence.

The effects of freestream turbulence levels on attachment line transition have not been studied in any great detail. Pfenninger & Bacon('69) briefly examined the effect of freestream turbulence on boundary layer stability. For a clean wind tunnel the attachment line boundary layer did not amplify any disturbance until $\bar{R}$ exceeded 570. When a turbulence screen was introduced ahead of the model, amplification was observed at lower values of $\bar{R}$. However no indication of the levels of freestream turbulence were given.

Morkovin('93) stated that "to expect general quantitative significance in experiments with high turbulent fields characterised by a single u' number at a single point borders on belief in miracles". However, this remains the most common method of defining the general turbulence levels in a wind tunnel. In the present tests graphs of turbulence intensity against windspeed were plotted for two positions in the working section for both moderate and high turbulence configurations. However, in some later graphs involved in the analysis, a single value obtained with a fairly high windspeed at the more central of the two locations is used to define each turbulence level. In the discussion, turbulence levels are referred to as low (from chapters 4 & 5), medium and high where these definitions refer to turbulence intensities of the order of 0.09%, 0.3% and 2.0%, respectively. These definitions agree with those given by Morkovin, from Russian literature, to define broad levels of freestream turbulence, i.e. :

low turbulence	-	$\sigma < 0.1\%$
moderate turbulence	-	$0.1\% < \sigma < 0.7\%$
high turbulence	-	$\sigma > 0.7\%$.

These ranges also refer to the transition processes described above.

7.2 PRESENT INVESTIGATION

7.2.1 8'x4' WIND TUNNEL

The 8'x4' tunnel is a low-speed, closed working section, open return tunnel. The working section is 8ft wide by 4ft high and extends over a length of approximately 10m. The area of the working section used for the present test was towards the downstream end of the working section.

In its clean configuration the freestream turbulence intensity in this tunnel was higher than in the 8'x6' tunnel. In addition, the freestream turbulence intensity could be further increased by inserting a turbulence screen at the start of the working section (approximately 8.5m upstream of model). The screen used in the following high turbulence tests consisted of a large square mesh type screen. The squares were 85mm wide and the wood used to make the mesh was 25mm wide.

The tunnel was carefully calibrated both in its clean configuration and with the turbulence screen inserted. Both the mean and fluctuation velocities were examined across the test section, at several positions along the test section. The mean velocities were obtained using a Pitot-static probe while the fluctuation velocities were obtained using a 1D 'J' shaped (vertical element) TSI hot-wire probe. It was found that the maximum windspeed of the tunnel was 23ms^{-1}. At windspeeds of 10ms^{-1} or greater the windspeed measured using the tunnel static rings was within 3% of that obtained using a Pitot-static probe. The flow uniformity was also examined, it appeared that the mean velocity varied by up to ±2% across the working section. Neither the accuracy of the windspeed measurement or the flow uniformity was affected by the turbulence screen.

For the clean wind tunnel, a graph of freestream turbulence intensity levels, σ, against windspeed was obtained at the centre of the part of the working section used, at two heights. This graph is presented in Fig 7.2. From the overall tunnel calibration the mean turbulence intensity at 15ms^{-1} was 0.3%. For discussion in this chapter, this is referred to as a medium level of turbulence.

A similar graph was obtained for the wind tunnel with the turbulence screen inserted upstream. This graph is presented in Fig 7.3. The mean turbulence intensity at 15ms^{-1} was estimated at 2.0%. For discussion in this chapter, this is referred to as a high level of turbulence.

For measurements of the model pressure distribution, the freestream static pressure was taken from tunnel static rings just upstream of the model (and well downstream of the tunnel contraction). The static pressure gradient, between the measurement position and the model, was therefore very small and of the order of just 0.4% of the freestream dynamic

pressure.

7.2.2 PRELIMINARY MEASUREMENTS

The model was mounted in the 8'x4' tunnel in an identical style to that used in the 8'x6' tunnel. As mentioned in section 3.2.1 the model could be split in order that the shorter span model could be used in the 8'x4' tunnel.

From preliminary tests there was no evidence of model vibration, even at the maximum windspeed, in the 8'x4' wind tunnel. This was as expected since the model is significantly shorter and more steady on the pivot and block, and the maximum windspeed is about half that used in the 8'x6' tunnel. The absence of model vibration was confirmed by the lack of any apparent sweep effects during tests with small 2D and 3D trips (model vibration in the 8'x6' tunnel had resulted in smaller value of $\bar{R}$ at lower sweep angles with zero and small trips).

During the tunnel calibration, the tunnel floor boundary layer thickness was measured to ensure that the model leading edge tip was clear of the boundary layer. At its closest, the leading edge tip is of the order of 210mm above the tunnel floor. The floor boundary layer was found to be of the order of 200mm thick. A larger gap would have been preferable. However, initial tests with the hot-wire near the leading edge tip did not detect any disturbances in the attachment line boundary layer in the leading edge tip area.

It was also noted from preliminary test that the hot-wire signal for both transition onset and completion was more difficult to define in the 8'x4' wind tunnel. This was due to significant fluctuations in the hot-wire signal observed in both fully laminar, just before transition onset, and fully turbulent flows. In a majority of the tests the first bursts were fairly large and easy to distinguish from the laminar fluctuations, however in one or two tests the turbulent spots were only slightly larger and the possibility of some errors exists. The problem with the fully turbulent signal was more severe. Reports had suggested, and observations in the 8'x6' tunnel supported, that a fully turbulent signal from a RMS meter was almost identical to a fully laminar signal. However, this was not the case with the higher levels of freestream turbulence in the 8'x4' tunnel. Continuous small fluctuations were evident throughout the fully turbulent signal. Laminar spots were therefore assumed to be slightly larger fluctuations but this obviously produces probable errors due to the operator's judgement. In addition there was no large decrease in the RMS voltage after mid-transition, only a steady but small decrease.

In several tests involving 3D trips and high turbulence both the RMS and raw hot-wire signal were observed. They showed that the fluctuations, interpreted as laminar spots,

evident in the RMS signal could also be seen as laminar spots in the raw signal.

Prior to starting the investigation of attachment line transition with higher levels of freestream turbulence, the model pressure distribution was measured. This was done primarily to check the effective sweep and blockage correction factor. For this purpose the model pressure distribution was measured at two windspeeds for each of the working sweep angles (i.e. 55°, 60°, 66° and 72°). Appendix C contains the calculations and the results of the corrections for blockage and effective sweep. With these corrections applied the measured pressure distributions matched the theoretical pressure distribution very closely. Thus equations 1.1 for $\bar{R}$ and 1.2 for η can be applied to experimental results from the 8'x4' with similar accuracy as was achieved in the 8'x6' tunnel. Estimated errors in V_e and dU/dx are similar to those from tests in the 8'x6' tunnel, i.e. of the order of 1% at higher windspeeds with a larger error in V_e at lower windspeeds of 3%.

The tests also confirmed the extremely small favourable pressure gradient along the attachment line.

The laminar and turbulent velocity profiles were also briefly re-examined and were found to be a good match with the theoretical profiles and the experimental profiles from the 8'x6' tunnel tests.

7.2.3 TRANSITION EXPERIMENTS

For each trip size / sweep angle combination just two spanwise locations were used for the hot-wire. Results from the 8'x6' tunnel suggested that the hot-wire location played a significant role only with very small and very large trips. With the shortened span of the model in the 8'x4' tunnel, it was decided that two locations would suffice.

The experimental procedure and instrumentation was otherwise identical to that used in the 2D and 3D trip tests in the 8'x6' tunnel. Four sweep angles and the full range of 2D and 3D trips were used with both the medium and high freestream turbulence tunnel configurations.

Sampling of the hot-wire signal for frequency spectra and intermittency distributions was also performed for a number of trip size / sweep angle combinations, one covering each of the regions on the $\bar{R}$ vs d/η graph for both medium and high turbulence tunnel configurations. The sampling for frequency spectra was performed at transition onset conditions with a sample frequency of 14kHz for a duration of 10 seconds. The sampling for intermittency distribution was performed at 5 windspeeds across the transition region with a sample frequency of 2kHz for a duration of 20 seconds. The sampling was more

limited than that in the 8'x6' tunnel due to the large amount of disc space needed to store the data.

7.3 TRANSITION RESULTS

7.3.1 2D TRIPS

Graphs of $\bar{R}$ vs d/η for transition onset and completion are presented in Figs 7.4 and 7.5 for medium freestream turbulence levels and Figs 7.6 and 7.7 for high levels of turbulence. Only the limit on the maximum value of $\bar{R}$, for medium turbulence levels, prevents the curves exhibiting a similar 'z' shape, with the same four regions and a kink, to the low turbulence graphs. However, differences between these graphs and the low turbulence graphs in Figs 4.7 and 4.8 are immediately apparent. For zero and small trips values of $\bar{R}$ are considerably reduced by each increase in freestream turbulence intensity, as are the minimum values of d/η for fully effective tripping. Also evident is the expected reduction in the effects of σ as the trips become large.

It is also noticeable on these graphs that the range of s/η curves is more limited than in the low turbulence graphs of chapter 4. This is due to the shorter span model used in the 8'x4' tunnel. Since only two hot-wire locations were used, linear interpolations were used to obtain values of $\bar{R}$ and d/η at the specified values of s/η. All the graphs show that changes in $\bar{R}$ with s/η are small, so the use of only two hot-wire locations has not resulted in significant errors in interpolated values of $\bar{R}$.

For the curves of best fit, experimental data obtained with the lowest sweep angle, $\Lambda = 56°$, and high turbulence levels have been omitted. Fig 7.8 shows the graph for transition onset together with the results for $\Lambda = 56°$. It is not clear exactly why this sweep angle produces lower transition Reynolds numbers than the larger sweep angles, but similar results were later obtained with 3D trips. Two possible reasons for the difference between the general results and the lowest sweep angle results were examined. The first possibility concerned the tunnel floor boundary layer. It was noted in section 7.2.2 that at $\Lambda = 56°$ the leading edge tip was quite close to outer edge of the floor boundary layer and it cannot be ruled out that the floor boundary layer was influencing the high turbulence tests. However, if the floor boundary layer was influencing conditions at the leading edge tip, it would be more likely to act as a gross disturbance and $\bar{R}$ would then be independent of d/η. Since this is not the case and, additionally, no similar effects were observed during the medium turbulence tests and no disturbances were observed during the initial tests, it seems unlikely that the floor boundary layer is responsible for the observed effects. The second possibility is simply that at lower sweep angles the receptivity to freestream turbulence increases. Against this idea is the difference between the $\Lambda = 56°$ results and the general results at d/η

> 2.0, where the general results for the three turbulence levels suggest that the freestream turbulence as little influence. However the difference does decrease as d/η increases and this would appear to partially support the idea. Due to this uncertainty over the validity of the results obtained at $\Lambda = 56°$ with high turbulence levels, they were omitted from the general results used to consider the effects of turbulence.

For the accepted data, both scatter and repeatability were within acceptable limits. For the medium turbulence results, scatter resulted in experimental data within ±4% of the curves of best fit across both the transition onset and transition completion graphs, a similar value to the low turbulence data. For a majority of the high turbulence results, experimental data was also within ±4% of the curve of best fit. However, a few points resulted in a maximum scatter of ±7%.

In the initial investigation of transition tripping with 2D trips, at low levels of freestream turbulence, three specific values of $\bar{R}$ were examined. $\bar{R}_{lower}$ represented the lower bound on transition tripping. For values of $\bar{R}$ less than $\bar{R}_{lower}$ turbulence introduced by a large trip decayed as it travelled downstream and eventually disappeared. $\bar{R}_{kink}$ referred to the position of the kink in the curves on the $\bar{R}$ vs d/η graph, it represented the value of $\bar{R}$ at which the minimum size for a fully effective trip introduced turbulent spots. Finally, $\bar{R}_{upper}$ was the upper bound on transition tripping and was equal to the linear stability limit. For values of $\bar{R}$ less than $\bar{R}_{upper}$ the boundary layer was stable to the small disturbances present in the freestream. These three values were also investigated for 2D trips with medium and high levels of freestream turbulence. However, limitations in both the tunnel performance and the model size made these values more difficult to estimate than in the low turbulence tests. As a result, potential errors in their values are greater.

Due to the relatively low maximum windspeed of the tunnel, natural transition could not be obtained with medium levels of freestream turbulence. This, in addition to the limited range of s/η in the high turbulence tests, meant that $\bar{R}_{upper}$ and the maximum tolerable roughness could not be accurately estimated for either of the higher turbulence tests. However from the results available it appears that values of $\bar{R}_{upper}$ are of the order of 500 for the medium turbulence levels and 300 for the high turbulence levels, although these values are very approximate. If they are taken as correct then the maximum tolerable roughness for 2D trips with both medium and high levels of freestream turbulence occurs at a trip size of the order $d/\eta = 0.7$. This is slightly lower than the maximum tolerable roughness at low turbulence levels which occurred at $d/\eta = 0.9$.

The difficulty in interpolating values of $\bar{R}$ for $s/\eta \to \infty$ also made estimates of $\bar{R}_{lower}$, for both the medium and high turbulence levels, susceptible to errors. The experimental data obtained with large trips was not therefore plotted as a graph of $\bar{R}$ vs s/η, as in Fig 4.10 for low turbulence levels. Instead, the medium and high turbulence data was compared to the data points from the low turbulence graph. It was observed that the results for both

medium and high turbulence were within the range of curves and had similar gradients to that obtained with low turbulence in Fig 4.10. It therefore appears that the same value for the lower bound can be applied irrespective of the freestream turbulence level. Thus the accepted value for $\bar{R}_{lower}$ is 250 for transition onset for both levels of turbulence. This occurs with a minimum value of $d/\eta = 1.62$ for medium turbulence and $d/\eta = 1.26$ for high turbulence. The corresponding value with low turbulence was $d/\eta = 1.97$.

Although the data available for estimating $\bar{R}_{lower}$ for transition completion was even more limited, a value of approximately 300 does appear appropriate.

Finally, the kink in the $\bar{R}$ vs d/η graph, at the intersection of curves for small trips and curves for fully effective trips, was examined. For transition onset, the kink appears to occur at values of $\bar{R} = 310$ for medium levels of turbulence and $\bar{R} = 285$ for high levels of turbulence. The appropriate values of d/η were 1.29 and 1.03 respectively. From the low turbulence tests the kink occurred at $\bar{R} = 376$ and $d/\eta = 1.67$.

The above values of $\bar{R}$ and the values obtained in chapter 4 for low turbulence, together with the appropriate values of d/η, are listed in table 7.1. Overall, it appears that freestream turbulence intensity levels have no effect on the lower bound for transition and only a slight effect on the maximum tolerable roughness. However the upper bound for transition tripping is greatly reduced with increasing σ, as are both the Reynolds number and the minimum trip size for fully effective tripping.

To enable the effects of σ on $\bar{R}$ and d/η to be seen more clearly, each of the curves of $\bar{R}$ vs d/η for $s/\eta = 2000$, for transition onset and completion, were plotted in Figs 7.9 and 7.10. From these graphs it is clear that the effect of freestream turbulence varies across the four regions of $\bar{R}$ vs d/η graph. With increasing σ, $\bar{R}$ and d/η decrease rapidly for both transition onset and completion in each of the regions of the $\bar{R}$ vs d/η graphs associated with zero, small and medium trips. It is noted, however, that the decrease is more steady for transition onset, while for transition completion the initial rise in turbulence from low to medium levels has a larger effect than the further increase from medium to high levels of turbulence.

With large trips, $\bar{R}$ was not expected to change much with increasing σ, however the graph suggests that $\bar{R}$ decreases slightly for transition completion, and increases and then decreases for transition onset. The apparent decrease in $\bar{R}$ for transition completion cannot be ruled out. However, for transition onset with $\bar{R} < 250$ the large trips should dominate the generation of the turbulent spots and if the freestream turbulence does have an effect on the rate of the decay of the spots then it should probably be to reduce this rate of decay. A reduction in the rate of decay of turbulent spots would lead to a smaller value of $\bar{R}$ at a given d/η and s/η. The curves for different freestream turbulence levels should probably not therefore cross. It therefore appears likely that the observed differences are due to experimental error and may be related to the difference in wind tunnels. Both tunnels

were calibrated using similar methods and errors are certainly greater for the lower windspeeds corresponding to the results with large trips. Flow uniformity may also be poorer at the low windspeeds involved. It is also noted that if this error is due to the windspeed measurement in each wind tunnel and is consistent then the decrease in $\bar{R}$ for transition completion could actually be greater than indicated in Fig 7.10. This suggests that, at least for finite s/η, $\bar{R}$ for transition completion with large trips is indeed slightly reduced by higher levels of freestream turbulence.

For further comparison between results obtained at different levels of σ, projected curves for $s/\eta \rightarrow 0$ for transition onset with each level of freestream turbulence are presented in Fig 7.11, while Fig 7.12 shows the curves for transition completion. As was mentioned above, the projected curves for medium and high turbulence levels are more approximate due to the smaller values of s/η. However the plots clearly show the decrease in transition Reynolds number and fully effective trip sizes, with increasing turbulence.

From the projected curves for $s/\eta \rightarrow 0$, approximate curves represented by constant values of R_{kk}, for transition at the trip, were estimated for transition onset and completion, for both medium and high levels of turbulence. These curves are presented in Figs 7.13 and 7.14. It is apparent that as the freestream turbulence increases, the accuracy by which transition at the trip can be represented by a constant value of R_{kk} decreases. This is due to the changing relation between $\bar{R}$ and d/η, with the rate of decrease in $\bar{R}$ with increasing d/η getting smaller. Nevertheless, critical values of R_{kk} were estimated and, although the agreement was fairly poor, the closest match with curves of $\bar{R}$ vs d/η, for transition at the trip, produced the following values :

$R_{kk} = 275$	transition onset , medium turbulence
$R_{kk} = 350$	transition completion , medium turbulence
$R_{kk} = 200$	transition onset , high turbulence
$R_{kk} = 300$	transition completion , high turbulence

It is apparent that the values of R_{kk} are reduced by increasing σ, as is the range of d/η for which these curves are applicable. The values obtained from the low turbulence level tests were $R_{kk} = 450$ for transition onset and $R_{kk} = 630$ for transition completion.

Similarly, an altered form of Gaster's criterion was attempted to fit these curves but, again, a poor match was obtained and it was not pursued further.

Plots of R_{δ^*} vs R_{kk} for fully effective tripping at each level of turbulence are presented in Fig 7.15 for transition onset and Fig 7.16 for transition completion. The reduction in R_{kk} with increasing turbulence is again apparent in these plots. Also apparent

is the change in R_{kk} with increasing R_{δ^*}, for each curve. This large change reflects the fact that transition at the trip cannot be accurately represented by a single critical value of R_{kk} with medium and high turbulence levels.

Transition in the limit as $s/\eta \rightarrow \infty$ was also studied at low turbulence. However, the range of s/η was too limited to attempt a plot of curves for $s/\eta \rightarrow \infty$ for medium and high turbulence levels.

In the final tunnel session the intermittency distributions for several points on both the $\bar{R}$ vs d/η graphs were briefly examined. This was done for two reasons, firstly to verify the extent of the transition region, as obtained from the investigation of transition onset and completion conditions, and secondly to confirm that Narasimha's universal intermittency distribution is still applicable.

Due to the small number of data points used, the intermittency distribution itself was not well represented. However, the main object of these tests was to confirm the values of $\bar{R}$ for transition completion from the main transition detection tests. This proved rather successful, especially given the concern over the problem of defining transition completion solely from the observation of a hot-wire signal on an oscilloscope, as discussed in section 7.2.2. Differences in $\bar{R}$, from the transition detection tests and the intermittency tests, appeared to range from 0 to approximately 5%. This is considered entirely satisfactory.

There was also sufficient data to examine the general distributions plotted against ζ_1 and ζ_2 with Narasimha's universal intermittency distribution, as presented in Figs 7.17 and 7.18. The distribution plotted against ζ_1 shows good agreement with Narasimha's distribution however the distribution plotted against ζ_2 is too sensitive to the transition onset value and good agreement is difficult to obtain.

Finally, frequency spectra were obtained for a number of test configurations at transition onset conditions for comparison with the frequency spectra obtained during the low turbulence tests. However, as described in chapter 4, the investigation of frequency spectra was too limited to clearly show any effect of different trip types and levels of freestream turbulence intensity. The spectra obtained here appeared to agree with the earlier spectra leading to the conclusion that the differences between plots are due to differences in Reynolds number at the transition conditions and the intermittency. No trends with increasing freestream turbulence were apparent.

7.3.2 3D TRIPS

Results of the investigation into transition tripping with 3D trips are again presented in the form of graphs of $\bar{R}$ vs d/η. These graphs for transition onset and completion are presented in Figs 7.19 and 7.20 for medium freestream turbulence levels and Figs 7.21 and 7.22 for high levels of turbulence. The curves again exhibit the familiar 'z' shape, with the same four regions and the kink. Comparing these graphs to the low turbulence graphs in Figs 5.4 and 5.5, it appears that values of $\bar{R}$ for transition onset with small trips are only slightly reduced by the initial increase in σ to medium turbulence levels but the increase to high levels of turbulence considerably reduces $\bar{R}$. In contrast, for transition completion the initial rise in turbulence, from low to medium levels, causes a greater reduction in $\bar{R}$ than the rise from medium to high levels of turbulence. With bigger trips the effect of σ, as with the 2D trips, is reduced.

Also in common with the 2D trip tests, the experimental data obtained with high level of freestream turbulence and $\Lambda = 56°$ was omitted prior to plotting the curves of best fit. The curve for transition onset at $\Lambda = 56°$ is plotted with the general curves in Fig 7.23. In this case the values of $\bar{R}$ at large d/η agree with the general results. This graph would appear to support the idea that the low values at $\Lambda = 56°$ are due to an increase in receptivity, as discussed in section 7.3.1.

For the experimental data points used in the general curves with medium freestream turbulence levels scatter was within ±2% of the curve of best fit. For high levels of freestream turbulence, scatter is generally within ±6% of the curve of best fit, but a few points have slightly greater errors. Good repeatability for both sets of results was obtained.

The investigation of the three specific values of $\bar{R}$ and d/η was, like the 2D trip tests, hampered by the low maximum speed of the tunnel and the shortened span of the model.

As mentioned in section 7.3.1, values for $\bar{R}_{upper}$ were estimated to be of the order of 500 for transition onset with medium levels of freestream turbulence and 300 for transition onset with high levels of freestream turbulence. With these values, the maximum tolerable roughness for 3D trips is of the order of 1.5 for medium turbulence levels and 1.4 for high turbulence levels. These compare to a maximum tolerable roughness of $d/\eta = 1.33$ with low turbulence levels.

$\bar{R}_{lower}$ was again investigated simply by comparing the experimental results obtained with large trips at medium and high turbulence levels with the curves of $\bar{R}$ vs s/η obtained, for both transition onset and completion, for low turbulence in Fig 5.10. As with the 2D trips, the range of values of $\bar{R}$ were within the range obtained at low turbulence. Thus the accepted value for $\bar{R}_{lower}$ is 250 for transition onset for all levels of σ. This value occurs at a minimum value of $d/\eta = 2.70$ for medium turbulence and $d/\eta = 2.36$ for high turbulence.

For low turbulence the equivalent value was $d/\eta = 2.63$.

It was also determined from the low turbulence tests with 3D trips that $\bar{R}_{lower}$ was approximately 310 for transition completion. However, the accepted general value is 300 and this showed reasonable agreement with the medium and high turbulence results. The accepted value of $\bar{R}_{lower}$ for transition completion is therefore 300.

Finally, for the position of the kink for transition onset, the intersection of curves (of $\bar{R}$ vs d/η) for small trips and curves for fully effective trips appears to occur at values of $\bar{R} = 366$ for medium levels of turbulence and $\bar{R} = 290$ for high levels of turbulence. The appropriate value of d/η were 2.00 and 2.07 respectively. In the low turbulence tests the kink occurred at $\bar{R} = 451$ and $d/\eta = 1.82$.

The above values of $\bar{R}$ and the values obtained in chapter 5 for low turbulence, together with the appropriate values of d/η, are listed in table 7.2. As with the 2D trips, freestream turbulence intensity levels have no effect on the lower bound for transition but result in a large reduction in the upper bound with increasing σ. The effect on the maximum tolerable roughness is unclear but is very small. The effect on the minimum trip size for fully effective tripping is clearer and, in contrast to the 2D trip results, it appears that the minimum fully effective value of d/η increases while the associated Reynolds number is reduced.

To obtain a clearer picture of the effects freestream turbulence on the relation between $\bar{R}$ and d/η each of the curves of $\bar{R}$ vs d/η for $s/\eta = 2000$, for transition onset and completion, were plotted in Figs 7.24 and 7.25. From these graphs it is clear that the effect of freestream turbulence on 3D trips differs from that for 2D trips. The values of $\bar{R}$ in the zero trip region are obviously identical to the 2D trip results and $\bar{R}$ decreases rapidly with increasing σ. However, for small and medium trips turbulence has different effects on transition onset and transition completion. For transition onset, the small increase to medium levels of turbulence only slightly reduces $\bar{R}$ for small trips and does not appear to affect $\bar{R}$ for medium trips while the increase to high levels of turbulence results in a large reduction in $\bar{R}$ for small trips and a fairly large reduction for medium trips. For transition completion it is the increase from low to medium levels of turbulence that has the large effect on $\bar{R}$ and the increase from medium to high levels has only a slight affect.

As with 2D trips, the results for large trips suggest that $\bar{R}$, for transition completion, is reduced slightly by the increase in turbulence while $\bar{R}$, for transition onset, first increases and then decreases. As explained in section 7.3.1 this result for transition onset is most likely due to experimental error and is not a true reflection of the effects of turbulence. However, the possibility that $\bar{R}$ for transition completion is lower for higher levels of freestream turbulence could not be ruled out from the 2D results and is even more evident for the 3D trip results. It is noted though that this particular difference between the 2D trip and 3D trip graphs appears to be due to the difference between values at low

turbulence. Agreement between values of $\bar{R}$ for transition completion with large 2D trips and 3D trips for both medium and high levels of turbulence is quite good.

To further investigate the effects of freestream turbulence on transition with 3D trips, projected curves for $s/\eta \rightarrow 0$ for transition onset and completion were plotted and are presented in Fig 7.26 and Fig 7.27 for each turbulence level. The almost negligible effect of the medium turbulence levels on transition onset with fully effective 3D trips is again apparent, as is the relatively large effect of the initial increase in turbulence on transition completion conditions. As with the similar plots for 2D trips, the projected curves for medium and high turbulence levels are more approximate due to the smaller range of s/η.

From these projected curves for $s/\eta \rightarrow 0$ approximate curves represented by constant values of R_{kk}, for transition at the trip, for transition onset and completion were estimated and are presented in Fig 7.28 for medium levels of turbulence and Fig 7.29 for high levels of turbulence. Unlike the approximate curves for the 2D trips, these curves of constant R_{kk} represent the data fairly well although the modified forms of Gaster's criterion are less representative of the data. The following value were obtained :

$R_{kk} = 650$	transition onset , medium turbulence
$R_{kk} = 750$	transition completion , medium turbulence
$R_{kk} = 550$	transition onset , high turbulence
$R_{kk} = 675$	transition completion , high turbulence

The value for transition onset with medium turbulence is identical to the value in chapter 5 for low turbulence levels. Otherwise, there is a general reduction in the values of R_{kk} with increasing σ. In addition, the ranges of d/η for which these curves are applicable are also reduced. The value of R_{kk} for transition completion with low turbulence levels was 925.

The altered forms of Gaster's criterion provided the following more approximate relations for transition onset :

$(V_e.d/\upsilon) = 61.R_\theta^{1/2}$	medium turbulence
$(V_e.d/\upsilon) = 55.R_\theta^{1/2}$	high turbulence

Plots of R_{kk} against $R_{\delta*}$ for fully effective tripping with each level of turbulence are also presented in Fig 7.30 and 7.31 for transition onset and completion. For each curve, the small change in R_{kk} with variations in $R_{\delta*}$, at least for transition onset, reflect the accurate representation of the results given by the critical values of R_{kk} above. In addition, the differing effects of each freestream turbulence level on transition onset and completion are

again evident.

As with the 2D trips tests a graph for $s/\eta \rightarrow \infty$ was not attempted due to the limited range of s/η.

Also in common with the 2D trip test, the intermittency distributions were examined for several points on both the $\bar{R}$ vs d/η graphs. Similar results were obtained, with $\bar{R}$ for transition completion, from the transition detection tests and the intermittency tests, generally differing by less than 5%. Also, the general distributions were plotted against ζ_1 and ζ_2, and presented in Figs 7.32 and 7.33. The distribution plotted against ζ_1 shows reasonable agreement with Narasimha's universal intermittency distribution. However scatter was too great for the plot against ζ_2 for good agreement to be achieved.

Finally, frequency spectra were obtained for a number of test configurations at transition onset conditions. As with the 2D trips, no trends in the changes in frequency spectra due to increasing freestream turbulence could be detected but the spectra supported the overall observation of the effect of Reynolds number and intermittency, as described in chapter 4.

7.3.3 COMPARISON BETWEEN 2D AND 3D TRIPS

To compare the effects of freestream turbulence intensity levels on attachment line transition tripping by 2D trips and 3D trips, the various specified values (at the upper bound, lower bound and kink) were plotted against σ. Thus a plot of the values of $\bar{R}$, for transition onset with both 2D and 3D trips, is presented in Fig 7.34 and the corresponding values of d/η are presented in Fig 7.35. The critical values of R_{kk}, for transition at the trip, are plotted in Fig 7.36, for both transition onset and completion. In Fig 7.34, $\bar{R}_{kink}$ is omitted to avoid presenting a misleading idea of the effects of freestream turbulence. Since $\bar{R}_{kink}$ refers simply to the Reynolds numbers for transition onset caused by the minimum size of fully effective trip, a decrease in $\bar{R}_{kink}$ does not necessarily indicate a decrease in conditions required for transition at the trip. In the case of 3D trips with low and medium turbulence levels, $\bar{R}_{kink}$ is lower for the medium level. However, the kink has simply moved along the $\bar{R}$ vs d/η curve and, at the kink position for medium turbulence, the same conditions cause transition at the trip for both turbulence levels.

The graphs presented suggest similar effects of freestream turbulence on the critical values of $\bar{R}$ for 2D trips and 3D trips but very different effect on the corresponding critical values of d/η. For 2D trips each of the critical values of d/η appear to decrease with increasing turbulence, while for 3D trips they remain fairly constant with only d/η_{kink} varying

monotonically, increasing slightly with increasing turbulence.

With regards to the critical values of R_{kk}, the effects of turbulence are broadly similar for 2D trips and 3D trips. The major exception is the effect of increasing turbulence from low to medium levels for transition onset, where R_{kk} decreases for 2D trips but remains constant for 3D trips. The subsequent increase from medium to high levels of turbulence results in similar reductions in R_{kk} for 2D and 3D trips. For transition completion, increasing turbulence causes a slightly greater, but overall similar, reduction in R_{kk} for 2D trips than 3D trips.

7.4 DISCUSSION

It is immediately apparent from the results, for 2D and 3D trips with medium and high levels of freestream turbulence, that the effect of σ on $\bar{R}$ is dependent both on d/η and the type of trip and also differs between transition onset and completion.

Observation of the $\bar{R}$ vs d/η graphs shows that the change in transition onset conditions from low to high turbulence is similar for both 2D and 3D trips. The change from low to medium turbulence, however, differs. With 2D trips it appears that only small increases in freestream turbulence creates a large change in transition onset conditions and it may be that for the high turbulence results a lower freestream turbulence level than 2% could have produced the same results. With 3D trips, the small increase in freestream turbulence from the low to medium levels results in only a small change in the transition onset conditions, although the identical zero trip values ensure some similarity between the graphs for 2D and 3D trips results.

For transition completion, changes from low to medium and low to high levels of turbulence appear to have roughly similar effects on results for 2D and 3D trips. However, while the change from low to medium turbulence affects the results to a roughly similar extent as the transition onset results for 2D trips, with 3D trips the initial increase to medium levels of turbulence has a far greater effect on the transition completion conditions than the transition onset conditions.

The differing effects, with 3D trips, of medium levels of freestream turbulence on transition onset and transition completion conditions suggests that the extent of the transition region is affected. This also occurs, though only slightly, with the 2D trips. It appears possible that the initial increase in freestream turbulence affects the extent of the transition region before it affects the onset of the region and this is simply more apparent with 3D trips due to the smaller effect on the transition onset conditions.

A similar occurrence was observed by Gostelow *et al*('94) in tests on a flat plate in flows of varying turbulence intensities. They observed a slight decrease in the transition length as the freestream turbulence level increased. This does provide some support for the

present observations, although in the present tests the increase in freestream turbulence to high levels appears to increase the extent of the transition region again. This increase at higher turbulence levels does not necessarily contradict the decrease at medium turbulence, since it would appear to be due to the diminishing additional effect of elevating turbulence levels on transition completion as the level gets higher.

Another apparent difference between the effects of freestream turbulence on transition onset and completion conditions occurred for both large 2D trips and large 3D trips. It appears that higher levels of freestream turbulence can reduce the transition completion Reynolds numbers, at least at finite s/η, in the presence of a large trip which dominates transition onset.

As well as the general effects on transition onset and completion conditions, the effects of freestream turbulence on values of $\bar{R}$ and d/η for transition onset at the three positions on the $\bar{R}$ vs d/η graph, separating each of the regions described earlier, was examined.

$\bar{R}_{upper}$ refers to zero trip transition (or $d/\eta < d/\eta_{max\ tol.}$), there is therefore no difference between the effects of turbulence on $\bar{R}_{upper}$ obtained during 2D trip and 3D trip tests. In both cases $\bar{R}_{upper}$ decreases with increasing freestream turbulence. The effect of freestream turbulence on the maximum tolerable roughness, associated with $\bar{R}_{upper}$, may well differ for 2D trips and 3D trips. However, as mentioned above, values of $\bar{R}_{upper}$ for medium and high turbulence are very approximate. Therefore the given values of d/η_{upper} represent only estimates of the maximum tolerable roughness. Since the effects of freestream turbulence on the values appear to be very small it is not possible to draw conclusions concerning the effects of the turbulence. Fig 7.1 from Tani('61) suggests that, at the least for a flat plate, the maximum tolerable roughness increases slightly with increasing turbulence.

$\bar{R}_{lower}$ refers to the minimum Reynolds number required for turbulence to be self sustaining. As expected this is independent of the trip type but it also appears to be independent of the freestream turbulence. The corresponding values of d/η generally decreased with increasing turbulence, with the sole exception being the change from low to medium turbulence with 3D trips. For fully effective 3D trips it has been shown above that medium levels of turbulence do not affect the transition onset conditions. It is therefore not surprising that d/η_{lower} is very similar for low and medium turbulence levels. The slight increase is probably just experimental error. As for the general decrease in d/η_{lower}, this was expected since at a given Reynolds number an increase in turbulence normally reduces the trip size required for transition. The decrease in d/η_{lower} was greater for 2D trips than for 3D trips.

So, of the three values of $\bar{R}$ considered, only $\bar{R}_{kink}$ is trip dependent and it has already been mentioned above that decreases in $\bar{R}_{kink}$ alone, with turbulence intensity, does

not necessarily indicate a decrease in conditions required for transition at the trip. The overall results demonstrated that turbulence had a far greater effect on transition onset with 2D trips than with 3D trips. Since the values of $\bar{R}_{kink}$ quoted earlier (and listed in tables 7.1 and 7.2) suggest a fairly similar rate of decrease in $\bar{R}_{kink}$ with increasing turbulence for both 2D trips and 3D trips, it is apparent that the differences in the effects of freestream turbulence must manifest themselves in the values of d/η at the kink.

The minimum fully effective trip height, d/η_{kink}, appears to decrease significantly for 2D trips but increase for 3D trips, with increasing turbulence. For 2D trips, the decrease in both $\bar{R}$ and d/η with increasing turbulence, for small and medium trips, is large and, as can be seen in Fig 7.9, the movement of the kink is clear. Thus an increase in turbulence decreases the conditions, in terms of both Reynolds number and trip size, required for transition at the trip. For 3D trips, it has been established that transition onset conditions for fully effective trips are unaffected by the increase to medium levels of turbulence. However, results with small 3D trips indicate a small decrease in transition onset Reynolds numbers with medium levels of turbulence. For these two observations to be compatible, either the position of the kink must remain unaltered while the gradients of the $\bar{R}$ vs d/η curves are reduced above the kink or the position of the kink must move to lower $\bar{R}$ and higher d/η. The experimental results supported the latter. It therefore appears that for a limited range of smaller fully effective 3D trips, an increase in turbulence from low to medium levels causes turbulent spots to form downstream of the trip at a slightly lower Reynolds number and, with this medium level of turbulence, fully effective tripping for transition onset does not dictate transition onset conditions again until the Reynolds number has decreased and the trip size increased to the new kink position.

It is therefore clear that turbulence has a much smaller effect on the critical trip size for transition onset with 3D trips than with 2D trips. This may be explainable by the difference in the lengths of separation regions downstream of each trip type. In section 7.1 it was mentioned that the free-shear layer downstream of a trip is very sensitive to freestream disturbances. Since this region is significantly greater for 2D trips than for 3D trips, the freestream turbulence is likely to have a greater effect.

It would also have been desirable to examine the effect of freestream turbulence on the influence of s/η, for both amplification of laminar disturbances at high Reynolds numbers and decay of turbulence at low Reynolds numbers. However, this would be very difficult to determine using the present set-up due to the limited s/η and windspeed range available in the 8'x4' tunnel used for the medium and high levels of freestream turbulence tests and the possible errors in windspeed measurement at low $\bar{R}$, as discussed above.

Finally, in chapters 4 and 5 it was determined that the overall behaviour of the attachment line boundary layer and the flat-plate boundary layer when subjected to 2D trips

or 3D trips was similar. For a similar comparison on the effects of freestream turbulence the available data from previous investigations is much more limited. The graph from Tani('61), for 2D trips, presented in Fig 7.1 shows a similar overall effect on transition onset conditions as observed in the present tests. In addition, the small effect of moderate levels of turbulence on critical 3D trip heights has also been observed in previous investigations. Gregory & Walker('50) observed no difference in fully effective trip heights between tests performed with 3D trips on flat plates in two different wind tunnels despite a large difference in turbulence levels between the tunnels and Tani('61) concluded that increasing the freestream turbulence intensity from 0.05% to 0.2% scarcely affected the critical value of R_{kk} for 3D trips. The lack of any effect on R_{kk} for transition onset, with a similar increase in σ, is also evident in the present tests, as shown in Fig 7.36.

7.5 CONCLUSIONS

The limitations of both the model span and the windtunnel's maximum windspeed severely hampered the investigation into the effects of freestream turbulence on attachment line transition. From the result obtained, the most apparent effects were large reductions in the zero trip transition Reynolds number and the reducing effect of σ on $\bar{R}$ as d/η increased. Comparing the different trip types it is clear that smaller levels of freestream turbulence are required to promote transition onset in the presence of small and medium 2D trips than 3D trips. It is also apparent that, with both trip types, increasing turbulence levels initially have a greater effect on transition completion conditions than transition onset conditions and this leads to a initial reduction in the extent of the transition region. The extent of the transition region also appears to be reduced with large trips, where transition onset is no longer influenced by turbulence levels but transition completion conditions are still affected by the freestream turbulence.

Finally, although the comparisons with similar tests on flat plates were very limited, they were sufficient to suggest that the behaviour of the attachment line boundary layer and the flat-plate boundary layer is very similar.

8 - TRIP INTERACTION

As a brief final part to the investigation of attachment line transition tripping, the possibility of interaction between two trips with various streamwise separation distances was examined. The examination of trip interaction was limited to an investigation of the transition onset Reynolds numbers since the expected effects of interaction on Reynolds numbers were small and the slightly greater scatter in results for transition completion would be too large to yield useful results. Thus the main topic of interest is the change in transition onset Reynolds number from the single trip value and the effect on this of the separation distance between the two trips.

Previous investigations of trip interaction is limited but Fig 8.1 shows the graph obtained by Von Doenhoff & Braslow('61) for cylindrical 3D roughness elements. They concluded that the increase in critical roughness height, for closely spaced trips, was due to the rear trip delaying the formation of eddies around the first trip. For greater streamwise spacing the critical Reynolds number reduced to a value below the single trip value, reaching a minimum at a spacing of 5d before gradually increasing again.

For the present tests, the experimental process involved attaching single 2D or 3D trips on the attachment line and examining transition onset conditions. A similar second trip was then placed at various distances downstream of the first trips and the change in the transition onset Reynolds number obtained. Following the trip interaction tests, the single trip transition Reynolds number was re-examined. This was done for a range of 2D and 3D trips. The results from the 3D trip investigation are presented in Fig 8.2a for smaller separation distances and 8.2b for larger separation distances and the results of the 2D trip investigation are presented in Fig 8.3. The results for 2D trips are more limited due to greater difficulty in applying 2D trips, the difficulty in keeping the two trips parallel to each other and perpendicular to the attachment line, the shorter available working span (due to the necessity of placing 2D trips in areas of the model not previously used for 3D work, see page 35) and restricted wind tunnel access time.

The results for the 2D trips and 3D trips were similar and also showed good agreement with trends obtained by Von Doenhoff & Braslow for the flat-boundary layer. In each case, a second trip placed very closely downstream, within the reattachment distance of the separation region downstream of the single trip, results in a small increase in the transition onset Reynolds number. As the separation distance increases, beyond the reattachment distance, the Reynolds number decreases to a value below the single trip value. The more comprehensive examination of 3D trips suggests that this value then remains fairly constant while the separation distance increases slightly but then at considerably larger separation distances, possibly where the second trip is downstream of the recovery position of the first trip, the transition onset Reynolds number returns to the

single trip value. It should be pointed out that the changes in Reynolds number are mostly small and of a similar order to the scatter for single trip tests. However, trends are mostly consistent and the single trip transition onset Reynolds number was examined at the beginning and end of each trip interaction test.

Thus, it would appear that for two trips to interact and produce transition at a lower Reynolds number the separation distance must be between the reattachment distance and the recovery distance for the single trip. For lower separation distances the two trips combine to produce an altered flow which results in an effectively smaller overall trip, while for larger separation distances the flow distortion caused by the trips cannot interact. In addition it appears that small disturbances introduced by the upstream trip will not undergo a secondary amplification at the second trip producing earlier transition, for widely spaced trips. This may be because the disturbances must be either large enough to be amplified and breakdown to turbulence without any input from the second trip or too small to sustain themselves until the second trip.

Trip interaction was also very briefly examined for two trips of different sizes but no interaction was found as the large trip simply dominated the transition region.

Overall, the most significant interaction between two trips occurred when two similar trips were placed very close together resulting in an increase in the transition onset Reynolds number of up to 18%. For separation distances of between the reattachment distance (of the separation region downstream of the single trip) and the recovery distance, reductions in transition onset Reynolds number of up to 8% were observed.

CONCLUSIONS

The initial tests involving 2D trip wires produced a similar overall result to Poll's tests, thus proving both the model's and instrumentation's validity. Poll's and other previous investigations of attachment line transition with 2D trips were very thorough and so most conclusions regarding 2D tripping had already been made. This mostly involved comparison with the flat-plate boundary layer which is less stable and more susceptible to 2D trips. The attachment line boundary layer has a slightly more stable velocity profile, while 2D trips on a flat plate produce a momentum defect equal to the drag of the wire and this results in an artificial increase in R_θ. Any such defect in the attachment line boundary layer would be removed by flow divergence, thus the attachment line boundary layer is less susceptible to 2D trips. Although these conclusions were reached in previous investigations, the present 2D trips tests were useful, not only to check the validity of the model but also to investigate limitations for measurements which had to be applied to later 3D trip tests. In addition, the flow in the vicinity of the trip was also investigated. As on a flat plate, the length of the separation region downstream of a 2D trip varied with Reynolds number and trip size, and also with the separated boundary layer state. With larger trips, and a fully turbulent flow at reattachment, the separation distance tended towards a value of approximately 10 diameters. Although this is a similar value to that for the flat plate, a larger trip size was required to achieve it. This agrees with the relative sizes of 2D trips required to affect the boundary layer stability.

Earlier, very limited, investigations of transition tripping using 3D trips on the attachment line suggested that, like the flat-plate boundary layer, the attachment line boundary layer was less susceptible to 3D trips than to 2D trips. The present investigation verified this. Upper and lower bounds for transition tripping occurred at similar values of $\bar{R}$ for 2D and 3D trips but the maximum tolerable roughness and critical roughness (for transition at the trip) were greater for the 3D trips. As with the 2D trip tests, comparisons were also made with the flat-plate boundary layer for transition tripping with 3D trips. It was observed that, at least for transition onset with fully effective tripping, the two boundary layers could be tripped at similar roughness Reynolds numbers. For transition completion the roughness Reynolds numbers appeared larger on the attachment line, suggesting a greater extent of the transition region. A common feature to both the attachment line boundary layer and the flat-plate boundary layer is the more rapid upstream movement of the transition front, with increasing Reynolds number, for small 3D trips than for small 2D trips. One result of this is that the increase in trip diameter from the maximum tolerable roughness to the minimum size for fully effective tripping is smaller for 3D trips. Another result is a less severe kink in the $\bar{R}$ vs d/η graph. This kink is associated with a change in transition mechanisms from the trip introducing laminar disturbances which amplify as they travel downstream before eventually breaking down to form turbulent spots,

to the trip introducing the turbulent spots immediately downstream, possibly before reattachment of the separation region formed downstream of the trip. The less severe kink for 3D trips allowed the observation of a region of decreasing intermittency that occurred for a trip which initially introduced laminar disturbances but at a slightly greater Reynolds number was able to introduce turbulent spots directly. The relaminarisation occurred midway through the transition region and it appears that the introduction of these directly-produced turbulent spots removed the laminar disturbances, required for breakdown further downstream, over an extensive period and thus prevented several spots from forming downstream. This resulted in the decrease in intermittency. A minimum value for intermittency was apparently reached when all the turbulent spots were introduced directly at the trip and from this point the transition region developed as normal. The mechanisms involved in this relaminarisation region were not investigated and the cause could only be speculated on. However, since the cause appeared to be an incompatibility between transition mechanisms it should certainly be worthy of further attention.

Having obtained transition conditions for 3D trips placed on the attachment line, the trips were moved downstream to examine the turbulence spreading angle and the chordwise extent of the region within which a 3D trip could cause attachment line transition at the same conditions as trips positioned on the attachment line. It was found that at the low Reynolds numbers, required for transition with the trip in the immediate vicinity of the attachment line, turbulence spreading semi-angles were very small and of the order of just 3°, although this value increased slightly with the Reynolds number and, to a lesser extent, the trip size. Thus 3D trips have to be positioned very close to the attachment line in order to cause attachment line transition at the same conditions as for a trip positioned on the attachment line. For the present model, at the minimum sweep, this was equivalent to approximately 5mm in the chordwise direction. Although the extent of this chordwise region refers to causing attachment line transition only a short spanwise distance downstream of the trip, the chordwise region for an aircraft wing, where the sweep angle is lower and the pressure gradient is greater, would likely be smaller still. For trips positioned further from the attachment line, transition may still occur at the same conditions but the turbulence affects only a relatively narrow area downstream of the trip. With an increase in Reynolds number, however, the turbulence spreading angle increases and the trips positioned further downstream can cause attachment line transition. As the Reynolds number increased for the present model, the turbulence spreading semi-angle appeared to be approaching an asymptotic value of approximately 10°. However, the Reynolds number required to reach this asymptotic value was greater than that at which natural transition occurred on the attachment line. Overall, the dependence of the spreading angle on the Reynolds number was similar to that observed by De Bruin on a flat plate. However, considerably more scatter was obtained in the present tests for a plot of R_{δ^*} vs α and this appeared to be partly due to a slight dependence on the initial conditions at which the trip

introduced turbulent spots, via either the trip size or a larger increase in Reynolds number from the initial value for transition onset. It was also suggested that a more stable boundary layer could reduce the turbulence spreading angle. Since boundary layer control work is closely associated with attachment line transition it may be interesting to examine the turbulence spreading angle on a model equipped for boundary layer control via suction.

The effects of higher levels of freestream turbulence on attachment line transition were investigated for both 2D and 3D trips. Again similar behaviour was found to the flat-plate boundary layer, with small increases in freestream turbulence affecting the conditions for transition onset with 2D trips more than with 3D trips. With increasing turbulence both the Reynolds number and trip size, for transition onset and completion with 2D trips, decreased, appearing to approach a minimum at the higher level of freestream turbulence. It also appeared that the initial increase in turbulence had a slightly greater effect on transition completion than on transition onset. With 3D trips however, the initial increase in turbulence had a far greater effect on transition completion than on transition onset resulting in a significant decrease in the extent of the transition region. In fact for transition onset at the trip, the increase in turbulence from low to medium levels had no effect on R_{kk} and critical roughness sizes were only slightly affected, an observation which was similar to previous observations with flat-plate boundary layers. Unfortunately, restrictions in model length and windspeed for the higher turbulence tests made the upper and lower bounds of $\bar{R}$ for transition tripping very difficult to examine. It appeared, though, that while the upper limit was reduced the lower limit remained constant. This restriction in the tunnel size and windspeed severely hampered the present investigation and it would be interesting to re-examine these tests, particularly the 3D trip tests, in a larger faster wind tunnel, preferably with a greater range of turbulence levels. It would also be interesting to investigate further the low values of $\bar{R}$ obtained during the high turbulence tests at the lower sweep angle.

In conclusion, the overall behaviour of the attachment line boundary layer is very similar to that of the flat-plate boundary layer, although values of Reynolds numbers and trip sizes for transition do differ. As for differences in the attachment line boundary layer tripped by 2D trips and 3D trips, Reynolds numbers appear similar but the trip sizes and movement of transition front differ considerably as does the susceptibility to, and effects of, freestream turbulence.

REFERENCES

D. Arnal
J.C. Juillen
1979
Techniques d'analyse conditionnelle d'un signal fil chaud pour l'etude de l'intermittence de transition.
La Recherche Aerospatiale, 1979, no.1. Jan - Feb

D. Arnal
J.C. Juillen
1988
The experimental study of transition and leading edge contamination on swept wings.
DRA/LT - 2197

D. Arnal
J.C. Juillen
G. Casalis
1992
Fundamental studies related to laminar-turbulent transition problems on swept wings.
European forum on laminar technology, Hamburg. March

J.A. Beasley
1973
Calculation of the laminar boundary layer and prediction of transition on a sheared wing.
ARC/R&M - 3787

A. Bertelrud
1983
Experimental and computational investigation of the flow in the leading edge region of a swept wing.
AIAA 83-1762

A.C. de Bruin
1989
The effect of a single cylindrical roughness element on boundary layer transition in a favourable pressure gradient.
Laminar-turbulent transition ; Proceeding of IUTAM symposium , Toulouse , France. Sept. 11 - 15

D. Coles
O. Savas
1979
Interactions for regular patterns of turbulent spots in a laminar boundary layer.
Laminar-Turbulent Transition, IUTAM Symposium, Stuttgart. Sept.

N.A. Cumpsty
M.R. Head
1967
The calculation of three-dimensional turbulent boundary layers. Part II : Attachment line flow on an infinite swept wing.
The Aeronautical Quarterly, Vol.18

N.A. Cumpsty
M.R. Head
1969
The calculation of three-dimensional turbulent boundary layers. Part III : Comparison of attachment line calculations with experiment.
The Aeronautical Quarterly, Vol.20

E. Dobbinga
1965
Boundary-layer disturbance by isolated proturbences of variable height on a cylinder nose.
AGARDograph 97, Vol. 1

A.E. von Doenhoff
A.L. Braslow
1961
The effect of distributed surface roughness on laminar flow.
Boundary layer & flow control. Lachmann Vol.2.

J.W. Elder
1960
An experimental investigation of turbulent spots and breakdown to turbulence.
Journal of Fluid Mechanics, Vol.56, Feb.

A. Elsenaar
1990
The wind tunnel as a tool for laminar flow research.
17th ICAS congress, Stockholm. Vol.1, September 9-14

H.W. Emmons
1951
The laminar-turbulent transition in a boundary layer - Part 1.
Journal of the Aerospace Sciences, Vol.18, No.7, pp490-498, July

J. Flores
E. Tu
B. Anderson
S. Landers
1991
A parametric study of the leading edge attachment line for the F16-XL.
AIAA 91-1621

M Gad-El-Hak
R.F. Blackwelder
J.J. Riley
1979
A visual study of the growth and entrainment of turbulent spots.
Laminar-Turbulent Transition, IUTAM Symposium, Stuttgart. Sept.

M. Gaster
1967
On the flow along swept leading edges.
The Aeronautical Quarterly, Vol.18

J.C. Gibbings
O.T. Goksel
D.J. Hall
1986a

The influence of roughness trips upon boundary layer transition. Part 1 ; Characteristics of wire trips.
The Aeronautical Journal, Vol.90, No.898, Oct.

J.C. Gibbings
O.T. Goskel
D.J. Hall
1986b

The influence of roughness trips upon boundary layer transition. Part 2 ; Characteristics of single spherical trips.
The Aeronautical Journal, Vol.90, No.899, Nov.

J.P. Gostelow
A.R. Blunden
G.J. Walker
1994

Effects of free-stram turbulence and adverse pressure gradients on boundary layer transition.
Journal of Turbomachinery, Vol. 116, No 3. July.

W.E. Gray
1952a

The effect of wing sweep on laminar flow.
RAE TM 255 (ARC 14929)

W.E. Gray
1952b

The nature of the boundary layer flow at the nose of a swept wing.
RAE TM 256 (ARC 15021)

N. Gregory
W.S. Walker
1950

The effect on transition of isolated surface excrescences in the boundary layer.
NPL/R&M/2779 (ARC 13436)

N. Gregory
1960

Transition and the spread of turbulence on a 60° swept-back wing.
Journal of the Royal Aeronautical Society, Vol.64, pp562-564, Sept.

N. Gregory
E.M. Love
1965

Laminar flow on a swept leading edge : Final progress report.
NPL/M/Aero-26 (ARC 27979)

P. Hall
M.R. Malik
D.I.A. Poll
1984

On the stability of an infinite swept attachment line boundary layer.
NASA/CR-172300

P. Hall
S. MacKerrell
1988
Wave interactions in a three-dimensional attachment line boundary layer.
NASA/CR-181653

B.C. Hardy
1988
Experimental investigation of attachment line transition in low-speed, high-lift wind-tunnel testing.
RAE/Tech. Memo/Aero - 2138

R. Henke
F.X. Munch
1990
Laminar flow experiments with a large half model in transonic flow.
17th ICAS congress, Stockholm, vol.1, Sept 9-14

P.S. Klebanoff
G.B. Schubauer
K..D. Tidstrom
1955
Measurement of the effect of 2D and 3D roughness elements on boundary layer transition.
Journal of the Aeronautical Sciences, Vol.22, No.11, Nov.

P.S. Klebanoff
K.D. Tidstrom
1972
Mechanism by which a 2D roughness element induces boundary layer transition. The Physics of Fluids, Vol.15, No.7, July

P.S. Klebanoff
W.G. Cleveland
K.D. Tidstrom
1992
On the evolution of a turbulent boundary layer induced by a three-dimensional roughness element.
Journal of Fluids, Vol.237,

D.G. Lasseigne
T.L. Jackson
F.Q. Hu
1992
Temperature and suction effects on the instability of an infinite swept attachment line.
Physics of Fluids A, Vol.4, No.9, Sept

P. Lindberg
E.M. Fahlgren
P.H. Alfredsson
A.V. Johansson
1984
An experimental study of the structure and spreading of turbulent spots.
2nd IUTAM symposium on laminar-turbulent transition
Novoibirsk, USSR.

F.A. MacMillan
1954
Viscous effects on flattened pitot tubes at low speeds.
ARC 17106

F.A. MacMillan
1956
Experiments on pitot tubes in shear flow.
ARC 18235

T. Matsui
1979
Visualisation of turbulent spots in the boundary layer
along a flat plate in a water flow.
Laminar-Turbulent Transition, IUTAM Symposium, Stuttgart. Sept.

M.V. Morkovin
1969
On the many faces of transition.
Viscous Drag Reduction

M.V. Morkovin
1989
On roughness - induced transition : facts, views and
speculations. Instability and transition, Vol 1. ; Proceeding of the
workshop ; Hampton, VA. May 15 - June 9

M.V. Morkovin
1993
Bypass-transition research : Issues and philosophy.
Instabilities and turbulence in engineering flows. Fluid mechanics
and its applications Vol. 16.

T. Motohashi
K. Ono
T. Tamura
K. Kuwahara
1991
Instabilities around an isolated roughness element.
Boundary layer stability and transition to turbulence ;
Proceedings of the symposium , ASME and JSME joint fluids
engineering conference , 1st , Portland , OR. June 23 - 27

T. Motohashi
K. Ono
T. Tamura
K. Kuwahara
1993
Instability around an isolated roughness in the boundary
layer.
Near-Wall turbulent flows : Proceedings of the
international conference on near-wall turbulent flows ;
Tempe, Arizona. Mar. 15 - 17

R. Narasimha
1957
On the distribution of intermittency in the transition
region of a boundary layer.
Journal of Aeronautical Sciences, Vol.24, pp711-712

R. Narasimha
C. Subramanian
M.A. Badri Narayanan
1984
Turbulent spot growth in favourable pressure gradients.
AIAA Journal, Vol.22, No.6, June

P.R. Owen
D.G. Randall
1952
Boundary layer transition on a swept back wing.
RAE TM 277 (ARC 15022)

P.R. Owen
D.G. Randall
1953
Boundary layer transition on a swept back wing: a further investigation.
RAE TM 330

W. Pfenninger
J.W. Bacon Jnr.
1961a
About the development of swept laminar suction wings with full chord laminar flow.
Boundary layer & flow control. Lachmann Vol.2.

W. Pfenninger
E. Groth
1961b
Low drag boundary layer suction experiments in flight on a wing glove of an F-94A airplane with suction through a large number of fine slots.
Boundary layer & flow control. Lachmann Vol.2.

W. Pfenninger
1965
Some results from the X-21 program. Part 1.
Flow phenomena at the leading edge of swept wings.
Recent development in boundary layer research - part IV.
AGARDograph 97

W. Pfenninger
J.W. Bacon
1969
Amplified laminar boundary layer oscillations and transition at the front attachment line of a 45° swept flat-nosed wing with and without boundary layer suction.
Viscous Drag Reduction, pp85-105

D.I.A. Poll
1978
Some aspects of the flow near a swept attachment line with particular reference to boundary layer transition.
CIT/CoA - 7805

D.I.A. Poll
1983a
Transition description and prediction in three-dimensional flows.
CIT/CoA - 8332

D.I.A. Poll
1983b
The development of intermittent turbulence on a swept attachment line including the effects of compressibility.
Aeronautical Quarterly, Vol.34

D.I.A. Poll
D.J. Paisley
1985
On the effect of wing taper and sweep direction on leading edge transition.
The Aeronautical Journal, Vol.89, No.883, March

D.I.A. Poll
1989
The effect of isolated roughness elements on transition in attachment line flows.
Laminar-turbulent transition ; proceedings of IUTAM symposium, Toulouse. Sept 11-15

D.I.A. Poll
M. Danks
A.J. Davies
1992
The effect of surface suction near the leading edge of a swept-back wing.
European forum on laminar technology, Hamburg. March.

W.H. Rae Jr.
A. Pope
1984
Low-Speed Wind Tunnel Testing. 2nd Edition

Rosenhead
1963
Laminar boundary layers.

S.P. Schneider
1995
Improved methods for measuring laminar-turbulent intermittency in boundary layers.
Experiments in Fluids, No.18, Vol.5

G.B. Schubauer
P.S. Klebanoff
1956
Contributions on the mechanics of boundary layer transition.
NACA Report 1289

I.R. Stewart
1987
A model for transition by attachment line contamination and an examination of crossflow instability in three-dimensional boundary layers.
CIT/CoA - PhD thesis

I. Tani
1961
Effect of two-dimensional and isolated roughness on laminar flow.
Boundary layer & flow control. Lachmann Vol.2.

I. Wygnanski
M. Sokolov
D. Friedman
1975

On a turbulent spot in a laminar boundary layer.
Journal of Fluid Mechanics, Vol.78, Nov.

D.H. Zhang
Y.T. Chew
S.H. Winoto
1995

A proposed intermittency measurement method for transitional boundary layer flows.
Experiments in Fluids, Vol.19, No.6, Pg426, Oct.

APPENDIX A - CALCULATION OF η

The characteristic length used in attachment line work is η. This parameter is the divergence rate of the flow off the attachment line and is represented, in general, by the equation:

$$\eta = \left(\frac{\nu_e}{(dU_e/dx)_{x=0}}\right)^{1/2}$$

For a swept cylinder this can be greatly simplified to the following:

$$\eta = \sqrt{\frac{\nu r}{2 Q_\infty \cos\Lambda}}$$

This equation is obtained as follows:

For a swept cylinder $C_p = \cos^2\Lambda\,(1 - 4\sin^2\phi)$

where $C_p = (p_{local} - p_\infty) / q_\infty$

and ϕ represents the position on the model relative to the attachment line

So, considering the change in pressure between the attachment line and a point at ϕ

$$\begin{aligned} p_{a.l.} - p_\phi &= (p_{a.l.} - p_\infty) - (p_\phi - p_\infty) \\ &= q_\infty C_{p_{a.l.}} - q_\infty C_{p_\phi} \\ &= q_\infty \cos^2\Lambda - q_\infty \cos^2\Lambda\,(1 - 4\sin^2\phi) \\ &= 4\, q_\infty \cos^2\Lambda \sin^2\phi \end{aligned}$$

For a cylinder

$$\phi\ (\text{rad}) \approx x / r \qquad \text{for small } \phi$$

Thus

$$p_{a.l.} - p_\phi \approx 4\, q_\infty \cos^2\Lambda \sin^2(x/r) \qquad \text{for small } x$$

Applying Bernouilli's equation between the attachment line and ϕ
Where

$$V_e = \text{const} \quad \text{and} \quad U_\phi = U_e(\phi) = k\, x(\phi)$$

The following is obtained :

$$p_{a.l.} + \tfrac{1}{2}\rho V_e^2 = p_\phi + \tfrac{1}{2}\rho(V_e^2 + U_\phi^2)$$

i.e.

$$p_{a.l.} - p_\phi = \tfrac{1}{2}\rho U_\phi^2$$

Thus

$$\tfrac{1}{2}\rho U_\phi^2 = 4\, q_\infty \cos^2\Lambda \sin^2(x/r) \qquad \text{as } x \to 0$$

Which leads to

$$U_\phi = 2\, Q_\infty \cos\Lambda \sin(x/r) \qquad \text{as } x \to 0$$

Thus, at ϕ

$$dU_e / dx = 2\, Q_\infty \cos\Lambda \cos(x/r) / r$$

which for $x \to 0$, becomes

$$dU_e / dx = 2\, Q_\infty \cos\Lambda / r$$

and so

$$\eta = \sqrt{\frac{\nu r}{2 Q_\infty \cos\Lambda}}$$

Alternatively, since

$$Q_\infty \cos\Lambda = U_\infty$$

this equation can be expressed as

$$\eta = \left[\frac{\nu . r}{2 . U_\infty}\right]^{1/2}$$

APPENDIX B - CALCULATION OF INTERMITTENCY FACTOR

During transition detection tests the raw (uncalibrated) hot-wire signal was sampled for the purpose of calculating the intermittency factor. At several windspeeds, from transition onset up to fully turbulent conditions, data was sampled at 2kHz for a period of 20 seconds. This was done for several experimental configurations covering the $\bar{R}$ vs d/η graph for each set of tests. Having obtained the sampled data and stored it in CSV files, a short computer program was written which read in each of these files, calculated a criterion function for each data point and, using a specified limiting value for this function, calculated the intermittency factor. The criterion function and the calculations used to obtain the intermittency factor are described below.

Several methods for calculating the intermittency were considered, namely those reported in Schneider('95), Zhang *et al*('95) and Arnal & Juillen('79). In the end it was decided that the method of Arnal was the most suitable for the uncalibrated (unlinearised) hot-wire signal sampled.

The method is based on the calculation of the second derivative of the hot-wire output voltage with respect to time. A limiting value of this derivative is then used to define the point as laminar or turbulent. The total number of turbulent points divided by the total number of sampled points then gives the intermittency factor.

So assuming that $u(t_i)$ is the hot-wire output at time t_i then the derivative can be estimated from :

$$\frac{\partial^2 U}{\partial t^2}(t_i) = \frac{[u(t_{i+1}) - 2u(t_i) + u(t_{i-1})]}{\Delta t^2}$$

The maximum value of this derivative in laminar flow was calculated for each test configuration used. In each case the maximum was found to be slightly less than 32000. This value was therefore used as the specified limiting value. For derivatives smaller than this value the point t_i is laminar, for derivatives greater it is turbulent.

To remove freak spikes in the signal in a laminar region the derivative used for the point t_i was actually the average of four points around it,

i.e.

$$D(t_i) = \frac{[|\frac{\partial^2 U}{\partial t^2}(t_i-2)| + |\frac{\partial^2 U}{\partial t^2}(t_i-1)| + |\frac{\partial^2 U}{\partial t^2}(t_i)| + |\frac{\partial^2 U}{\partial t^2}(t_i+1)|]}{4}$$

Thus, using the above equation and the specified limit, the program appointed either a zero (for laminar flow) or a one (for turbulent flow) to each point of the sample file. The intermittency factor was then simply the sum of the appointed values divided by the number of points in the data file.

APPENDIX C - EFFECTIVE SWEEP AND BLOCKAGE CORRECTION

The measured static pressure distribution did not, at first, exactly match the theoretical pressured distribution. The most likely cause for this (assuming that the pressure distribution should in fact match) was errors in estimated value of freestream velocity and effective sweep angle. It was assumed that the tunnel calibration for windspeed and static pressure gradient was satisfactory. The error in windspeed must therefore have appeared via the blockage correction factor.

The assumption that the pressure distribution should, in fact, match the theoretical distribution was checked first. It was assumed that if the model pressure distribution had been measured accurately then, when the distribution at each sweep was translated to zero sweep, all the measured distributions should match. If, however, an error existed in the effective sweep then translating to zero sweep would introduce an error, which was greater for greater sweep angles, and the distributions would not match.

To translate the pressure distribution to zero sweep, the Cp was divided by $\cos^2\Lambda$. So if, for example, there was a 1° error in the flow angle then $\cos^2\Lambda_{eff}/\cos^2\Lambda_{meas}$ would be 0.91 for $\Lambda = 70°$ and 0.94 for $\Lambda = 60°$ and thus a bigger error would be introduced in the 70° translation.

It was found that each pressure distribution, translated to 0°, did not match exactly. To quantify the difference a factor was introduced. This factor represented the value by which Cp_{theory} was multiplied in order for the pressure gradients to match. The following values were obtained by averaging the factor for each sweep angle from all the tests performed.

Λ	55°	60°	65°	70°
Factor	0.92	0.94	0.87	0.89

There is a definite trend that the error increases with sweep angle and the values are similar to the error estimated for a 1° error in flow angle. It therefore appears that the model pressure distribution should match the theoretical distribution but an error exists in the effective sweep angle.

So having concluded that there was an error in the effective sweep angle, this error was estimated. Comparing the measured pressure distributions with the theoretical distribution it appeared that the gradient for the measured distribution was too shallow. Thus the effective sweep must be greater than the measured sweep. With the blockage correction factor (which was also known to contain an error) reduced to zero, the change in sweep required to get the pressure distribution from each test to match the theoretical

gradients, between ±20°, was examined. The value appeared relatively constant and did not vary significantly with model sweep or windspeed. The average value was calculated as 1° in the 8'x6' wind tunnel (or 1.5° in the 8'x4' wind tunnel) and thus all sweep angles must be corrected as follows :

$$Sweep_{eff} = Sweep_{mea} + 1°$$

Having obtained a pressure gradient, which matched the theoretical value, the error in actual values of Cp was examined. This was assumed to be due to the other source of error, namely the freestream velocity. Since the empty tunnel calibration was taken to be accurate, the error in freestream velocity was assumed to be in the blockage correction.

Decreasing the blockage correction decreases Q_∞ but increase p_∞. However, the effect on p_∞ is relatively small and the overall effect on Cp is a reduction without significantly altering the gradient. So for each test performed, the blockage correction was re-evaluated not by getting the Cp values to directly match the theoretical values but by applying Bernoulli's equation between the far upstream freestream and the model taps to obtain V_e. Q'_∞ (the value corrected for blockage) was then calculated from V_e / sinΛ and the blockage correction was calculated by comparing this value with that obtained from the tunnel static rings.

So applying Bernoulli's equation between far upstream (i.e. before blockage correction) and the static pressure at the attachment line, assuming :

p_∞ = freestream static pressure
p'_∞ = freestream static pressure corrected for blockage
p_1 = static pressure upstream of working section

Then

$$p_\infty + q_\infty = p'_\infty + q'_\infty = p_{a.l.} + \tfrac{1}{2}\rho V_e^2$$

and

$$(p_\infty - p_1) + q_\infty = (p_{a.l.} - p_1) + \tfrac{1}{2}\rho V_e^2$$

where $(p_\infty - p_1)$ is from empty tunnel static pressure gradient calibration
q_∞ is from empty tunnel dynamic pressure calibration
$(p_{a.l.} - p_1)$ is from the model pressure distribution measurement

So V_e is calculated without using blockage corrections.

V_e can also be estimated from the freestream dynamic pressure with blockage corrections.

$$V_e = Q'_{\infty} \sin \Lambda$$

where

$$q'_{\infty} = \tfrac{1}{2}\rho Q'^{2}_{\infty}$$

The following values for blockage correction were obtained by averaging the values at each sweep angle.

Λ	55°	60°	65°	70°
ϵ	0.022	0.027	0.0275	0.033

It is immediately obvious that the blockage correction factor is increasing with sweep angle. Calculations from Rae & Pope('84) suggested the opposite. However, further consideration of the model suggest some defects with the Rae & Pope values. The biggest factor should be that the model does not extend from the floor to the ceiling. There will therefore be additional base drag, leading to greater wake blockage, at higher sweeps due to the top and bottom bases of the model. The values from Rae & Pope were also greater than those given above. With all the uncertainty, it was decided to use a single constant value of blockage correction factor for all tests performed in the 8'x6' tunnel.

Different values were obtained from similar tests in the 8'x4' tunnel. The final accepted value for each tunnel were :

8'x6' Tunnel:

$$\Lambda \rightarrow \Lambda + 1°$$
$$\epsilon = 0.03$$

8'x4' Tunnel:

$$\Lambda \rightarrow \Lambda + 1\tfrac{1}{2}°$$
$$\epsilon = 0.05$$

The blockage correction factor is applied to measured dynamic and static pressures as follows :

$$q = q_{measured}\,(1 + 2\epsilon)$$
$$p = p_{measured} - 2\epsilon q_{measured}$$

These blockage corrections gave excellent agreement between the measured pressure distribution and the theoretical distribution (see Fig 3.3), and also gave good agreement for V_e during the velocity profile tests where V_e was also measured with the Pitot

probe.

Comparisons between values of V_e obtained using the Pitot probe and those obtained using the tunnel static rings, showed a maximum variation of approximately 2% at higher windspeeds.

It is noted that V_e can also be obtained more directly by measuring the undisturbed freestream static and dynamics pressures (far upstream of the model) and the static pressure at the attachment line during the actual tests. Bernouilli's equation is then applied, as above. However, since this requires the measurements of the model static pressure throughout the tests, the blockage correction approach was adopted.

APPENDIX D - CORRECTIONS FOR FLATTENED PITOT TUBE

Results obtained using the traversable Pitot probe, i.e. velocity profile measurements, had to be corrected for various effects. These included viscous and near wall effects on the measured total pressure and wall deflection effects on the effective measuring height. The corrections used were obtained from MacMillan('54&'56).

Corrections for viscous effects were given in terms of a Cp where:

$$Cp = \frac{P - p_\infty}{q_\infty}$$

To apply this to results obtained with the probe the following equations were considered:

$$P_{meas} = p_\infty + q_\infty Cp$$

and

$$P_{correct} = p_\infty + q_\infty$$

So, equating q_∞

$$(P - p_\infty)_{correct} = \frac{(P - p_\infty)_{measured}}{Cp}$$

The value of Cp varies with Reynolds number, based on velocity at the probe position and the external thickness of the probe. The velocity at the probe position, k from the surface, was calculated from the ratio V_k/V_e from Rosenhead's('63) theoretical profile. V_e was found using the tunnel static rings, as usual.

A range of values covering the range of Reynolds number used in the tests were taken from the graph in MacMillan, for a flattened probe with width / height = 7, and are presented in the following table.

R_k	30	40	50	60	70	80	90
Cp	0.994	0.988	0.985	0.983	0.984	0.985	0.986

R_k	100	200	300	400	500	600	700
Cp	0.987	0.988	0.990	0.991	0.992	0.993	0.994

Corrections for near wall effects were expressed as a correction to the measured velocity. It was given as a function of measured velocity and was independent of Reynolds number. The value varied only with the probe height. The following values were used:

Height (mm)	0.00	0.15	0.30
v / V	0.0150	0.0034	0.0006

Where

$$V_{cor} = V_{meas} \cdot (1 + v / V)$$

Correction for wall deflection (or shear) effects were given as a displacement of the effective centre of the probe (or measurement height). The value was a constant, independent of Reynolds number and was applied across the boundary layer. The displacement was given in terms of the external probe height (or thickness) as:

$$\Delta z = 0.15 \cdot \text{height}$$

APPENDIX E - VELOCITY PROFILES BEHIND TRIPS

Tests were performed to estimate the velocity profiles behind trips and the static pressure gradient around trips. The two sets of tests were performed separately but the velocity profiles require data from the static pressure tests. In each set of tests a pressure difference was measured at a range of windspeeds. The two pressures measured were :

$$\Delta p_{12} = p_{downstream} - p_{upstream}$$

measured using the model static taps at 1° from rows 1 and 2
and

$$q = P_{total} - p_{upstream}$$

measured using the flattened Pitot probe and the upstream model static tap positioned just off the attachment line (at 1°).

In each case the trip was positioned between the upstream and downstream pressure taps.

For the static pressure gradient:

$$Cp = (p - p_\infty) / q_\infty$$

where in this case $p = p_{downstream}$

So, we require ΔCp where

$$\Delta Cp = \frac{p - p_\infty}{q_\infty}\Big|_{trip} - \frac{p - p_\infty}{q_\infty}\Big|_{notrip}$$

Since $p_{upstream}$ is not changed by the trip, we can add $(p_{upstream} - p_\infty) / q_\infty$ to the both the trip and no trip parts of the right hand side of the equation. Simplification of the resulting equation leaves:

$$\Delta Cp = \frac{\Delta p_{12}}{q_\infty}\Big|_{trip} - \frac{\Delta p_{12}}{q_\infty}\Big|_{notrip}$$

And so ΔCp can easily be obtained from the measured values since $\Delta p_{12}|_{no\ trip}$ is also measured during the tests.

For the velocity profiles the following value was measured at each probe height:

$$q \quad = \quad P_{total} - p_{upstream}$$

Thus the static pressure must be corrected to the position behind the trip. This is done using the values of $\Delta p_{12}|_{trip}$ obtained during the static pressure gradient tests. Following the correction to the static pressure, the total pressure must be corrected for viscous and near wall effects (see Appendix D).

So prior to MacMillan's('54&'56) corrections, have :

$$\frac{q_{uncorrected}}{q_\infty} = \frac{q_{measured}}{q_\infty} - \frac{\Delta p_{12}}{q_\infty}\Big|_{trip}$$

This however assumes that dp/dz is negligible and since the boundary layer is separated this may not be true. There is no apparent easy way to estimate, or measure, this gradient but it seems likely that the static pressure gradient will be small and can be neglected.

Assuming that dp/dz is negligible then $q_{correct}$ is obtained from $q_{uncorrected}$ simply by applying MacMillan's correction, i.e.:

$$q_{correct} = q_{uncorrected} \cdot (1 + (v/V)_{correction})^2 / Cp_{MacMillan}$$

and

$$z = z + 0.15H$$

Thus the local velocity can be obtained from the measured pressure differences from:

$$V = \frac{[1 + (\frac{v}{V})_{correction}]}{\sqrt{\frac{1}{2}.\rho.Cp_{MacMillan}}} \cdot [q_{measured} - q_\infty \frac{\Delta P_{12}}{q_\infty}|_{trip}]^{\frac{1}{2}}$$

To normalise the calculated velocity V_e is used where V_e is calculated from the freestream dynamic pressure.

Thus, during the tests the total pressure distribution at several distances downstream

of a trip was measured by traversing the flattened Pitot probe across the boundary layer. The wall static pressure was measured at an undisturbed location upstream of the trip and was then corrected to the wall static pressure at the probe position. This was done using results from measurements of the static pressure gradient around the trips. The static pressure gradient across the boundary layer was considered negligible, a source of error which is likely to be small in comparison with other errors. A far more significant error was probably introduced via probe intrusion.

In a normal attached flow it was decided that the probe intrusion effects were insignificant, however with a separation bubble present the probe was, in effect, upstream in the re-circulating flow. The flow was therefore forced around and under the probe, between it and the wall. In addition, where the probe was close to the surface and in an upstream flowing region, a base pressure rather than a total pressure was measured.

The 'ski' legs may also intrude in cases where the reattachment point is downstream of them, though this did not appear to happen (i.e. reattachment points were quite close to the trips).

Finally, no corrections were applied for possible errors in the initial, or reference, height of the probe.

In conclusion, the accuracy of measured profiles behind the trips is poor. However, the profiles should be of sufficient quality to demonstrate the general flow field downstream of the trip.

APPENDIX F - CALCULATION OF TURBULENCE SPREADING ANGLE

For the examination of turbulence spreading from downstream of the attachment line it was necessary to estimate a turbulence spreading angle from given values of x (for trip positioned downstream of attachment line) and s (for hot-wire positioned along attachment line). This spreading angle was required relative to the external streamline at the trip. This problem was approached in reverse, i.e. a range of turbulence spreading angles were chosen and for a given hot-wire position, x was calculated for turbulent spots at each spreading angle to intersect the attachment line at the hot-wire location. Since the angle between the external streamline and the attachment line increases with x, this calculation involved an iterative procedure for which a computer program was written.

So, put ψ = angle between the external streamline and the attachment line then

$$\tan\psi = \frac{U_e(x)}{V_e}$$

Since the areas of interest are still fairly close to the attachment line, it is possible to write:

$$U_e = kx = U_\infty \frac{2x}{r} \qquad V_e = V_\infty$$

since

$$k = \frac{dU_e}{dx}\Big|_{x=0} = \frac{2U_\infty}{r}$$

(see Appendix A)

so

$$\tan\psi = \frac{U_\infty}{V_\infty}\frac{2x}{r} = \frac{2x}{r\tan\Lambda}$$

since

$$U_\infty = Q_\infty \cos\Lambda \qquad V_\infty = Q_\infty \sin\Lambda$$

So for each sweep angle and hot-wire position used in the tests a range of turbulence spreading angles from 1° to 20° was assumed and the x-position of the trip (for the turbulent spot to intersect the attachment line at the hot-wire location) was calculated for each configuration.

With the assumed values of α, Λ and s, $x_{i=0}$ is set to zero. For each step in the procedure, the computer program increases x by 0.05mm, i.e.

$$x_i = x_{i-1} + 0.05$$

ψ_i is then calculated from the equation :

$$\tan\psi_i = \frac{2x_i}{r\tan\Lambda}$$

Next an intermediate distance s_i is calculated from :

$$s_i = \frac{\Delta x}{\tan(\alpha-\psi_i)}$$

This loop is repeated while a running total of s is kept.
So after j steps then the total value of s_j is given by:

$$s_j = \sum_{i=1,j} s_i$$

When s_j reaches a value equal to the hot-wire distance then x_j is noted. This value of x represents the point from which turbulence spreading at angle α reaches the attachment line at the hot-wire.

From the table of data created a quadratic equation relating α with x was obtained for each hot-wire location / sweep angle configuration, allowing the turbulence spreading angle to be calculated for each experimental setup.

APPENDIX G

EXPERIMENTAL DATA

2D TRIPS - LOW TURBULENCE LEVELS

			TRANSITION ONSET			TRANSITION COMPLTN		
d	Swp	s	$\bar{R}$	d/n	s/n	$\bar{R}$	d/n	s/n
mm	deg	m						
.00	56.05	.70	553.9	.00	3071			
.00	56.00	.70	552.8	.00	3070			
.00	56.05	2.30	532.4	.00	9698			
.00	56.05	2.30	525.7	.00	9576			
.00	60.83	.70	591.5	.00	2719			
.00	60.83	.70	601.6	.00	2765			
.00	60.83	.70	604.7	.00	2780			
.00	60.88	.70	612.5	.00	2810			
.00	60.85	.70	621.1	.00	2853			
.00	60.85	.70	616.1	.00	2830			
.00	60.77	1.50	541.6	.00	5348			
.00	60.85	1.50	562.8	.00	5540	636.2	.00	6262
.00	60.80	1.50	596.5	.00	5883			
.00	60.83	2.30	554.2	.00	8371	631.9	.00	9544
.00	60.77	2.30	567.7	.00	8596	632.6	.00	9578
.00	60.73	2.30	576.0	.00	8735			
.00	60.77	2.30	571.2	.00	8649			
.00	60.90	2.30	581.7	.00	8761	636.1	.00	9581
.00	60.88	2.30	585.6	.00	8828			
.00	65.92	.70	690.1	.00	2540			
.00	66.13	.70	695.8	.00	2536			
.00	65.77	1.50	660.7	.00	5247			
.00	65.90	1.50	647.7	.00	5113	715.9	.00	5652
.00	66.00	1.50	664.3	.00	5219			
.00	65.77	2.30	637.8	.00	7766			
.00	66.08	2.30	635.3	.00	7625	685.5	.00	8227
.00	66.73	2.30	641.1	.00	7460	706.8	.00	8225
.00	66.80	2.30	646.0	.00	7492	721.4	.00	8366
.00	66.80	2.30	650.7	.00	7547			
.00	71.06	.70	785.3	.00	2219			
.00	70.98	.70	800.5	.00	2272			
.00	71.15	.70	802.8	.00	2257			
.00	70.82	.70	809.2	.00	2318			
.00	70.82	.70	808.0	.00	2314			
.00	70.98	1.50	714.3	.00	4345	787.1	.00	4788
.00	70.98	1.50	722.5	.00	4395			
.00	71.17	1.50	717.2	.00	4316			
.00	70.87	2.30	648.6	.00	6088	690.7	.00	6483
.00	71.06	2.30	647.9	.00	6016	713.2	.00	6622
.00	70.83	2.30	670.7	.00	6309	737.4	.00	6937
.00	71.15	2.30	682.3	.00	6303	755.1	.00	6976
.00	70.77	2.30	675.2	.00	6373	718.5	.00	6782
.00	70.77	2.30	675.5	.00	6376	725.8	.00	6850
.00	70.77	2.30	681.3	.00	6430			
.28	56.28	.10	480.7	1.06	374			
.28	56.28	1.00	469.6	1.03	3687	544.1	1.20	4272
.28	56.25	1.80	465.6	1.02	6588	542.8	1.19	7681
.28	60.83	.10	526.6	.97	342			

.28	60.87	1.00	526.2	.97	3450	603.6	1.11	3957
.28	60.93	1.80	526.4	.96	6197	599.8	1.10	7061
.28	65.95	.10	598.0	.88	311			
.28	66.22	1.00	595.7	.86	3088	669.7	.97	3472
.28	65.77	1.80	595.0	.88	5671	650.1	.96	6196
.28	70.72	.10	720.4	.83	294			
.28	71.00	.20	665.2	.75	539	775.6	.88	628
.28	70.67	1.00	639.7	.74	2640	725.9	.84	2996
.28	71.00	1.50	628.8	.71	3821	695.3	.79	4225
.28	70.72	1.80	627.0	.72	4645	680.5	.78	5041
.49	56.08	.10	402.2	1.56	309	432.6	1.68	332
.49	56.27	1.00	384.6	1.48	3021	430.2	1.66	3379
.49	56.13	1.80	379.8	1.47	5398	420.4	1.63	5976
.49	60.82	.10	445.9	1.44	284	485.7	1.56	310
.49	61.00	1.00	420.3	1.34	2741	482.8	1.54	3149
.49	60.77	1.80	418.3	1.35	4957	470.7	1.52	5578
.49	65.87	.10	498.4	1.29	255	567.6	1.47	290
.49	65.87	1.00	472.3	1.22	2489	530.8	1.37	2797
.49	65.75	1.80	456.4	1.19	4354	513.8	1.33	4901
.49	71.07	.10	575.2	1.14	225	658.2	1.30	258
.49	71.32	1.00	541.5	1.06	2154	613.4	1.20	2440
.49	70.78	1.80	530.2	1.07	3914	594.3	1.19	4388
.75	56.00	.20	302.8	1.80	481	336.9	2.01	535
.75	56.30	1.00	305.1	1.80	2394	342.4	2.01	2686
.75	56.37	1.80	309.1	1.81	4354	338.3	1.99	4765
.75	60.92	.20	352.2	1.73	461	383.6	1.88	502
.75	60.90	1.00	350.3	1.72	2294	382.8	1.88	2507
.75	60.88	1.80	353.6	1.74	4171	376.6	1.85	4443
.75	65.92	.20	414.6	1.63	436	444.0	1.75	467
.75	66.03	1.00	399.8	1.57	2091	439.5	1.72	2299
.75	66.22	1.80	407.8	1.59	3806	438.7	1.71	4094
.75	70.83	.20	425.5	1.31	348	507.7	1.56	415
.75	70.83	.20	434.0	1.33	355	508.4	1.57	418
.75	70.75	.20	453.9	1.40	373	513.7	1.58	420
.75	70.75	1.00	437.7	1.35	1798	504.9	1.56	2074
.75	70.83	1.50	432.1	1.33	2651	505.4	1.55	3101
.75	70.83	1.50	426.8	1.31	2618	498.0	1.53	3055
.75	70.78	1.80	442.7	1.36	3269	507.0	1.56	3743
1.04	56.42	.20	235.1	1.91	367	314.4	2.55	491
1.04	56.33	1.00	240.5	1.96	1885	320.5	2.61	2512
1.04	56.42	1.80	243.1	1.97	3417	311.8	2.53	4384
1.04	60.78	.20	269.3	1.84	354	338.3	2.31	445
1.04	60.83	1.00	275.7	1.88	1810	348.0	2.38	2285
1.04	60.92	1.80	266.1	1.81	3134	342.8	2.33	4037
1.02	65.83	.20	301.4	1.62	318	391.6	2.11	414
1.02	65.83	.20	299.5	1.61	316	389.1	2.10	411
1.04	65.92	.20	332.3	1.82	349	389.2	2.13	409
1.04	66.03	1.00	311.3	1.69	1628	391.8	2.13	2049
1.02	65.83	1.50	297.2	1.60	2354	390.1	2.10	3089
1.02	65.83	1.50	301.4	1.62	2387	394.7	2.13	3126
1.04	66.03	1.80	311.1	1.69	2929	387.8	2.11	3651
1.04	70.75	.20	394.3	1.68	324	444.0	1.90	365
1.04	70.75	1.00	390.7	1.67	1605	442.0	1.89	1816
1.04	71.20	1.80	361.8	1.51	2608	442.2	1.84	3188
1.53	56.17	.20	195.8	2.36	309	287.3	3.53	455
1.55	56.05	.20	195.9	2.41	310	268.8	3.24	424
1.55	56.15	1.00	229.7	2.81	1812	298.0	3.64	2351
1.53	56.17	1.50	239.9	2.89	2837	295.6	3.57	3496

1.55	55.72	1.80	238.4	2.96	3441			
1.55	60.87	.20	213.7	2.17	280	327.2	3.32	429
1.55	60.87	1.00	227.4	2.31	1491	329.1	3.34	2157
1.55	60.80	1.80	244.6	2.49	2895			
1.55	65.83	.20	243.5	1.99	257	372.9	3.05	394
1.55	65.67	1.00	242.2	2.00	1288	344.0	2.84	1830
1.55	66.10	1.80	245.5	1.98	2304			
1.55	70.73	.20	294.7	1.88	242			
1.55	71.32	1.00	295.2	1.82	1174	433.0	2.67	1722
1.55	70.73	1.80	275.6	1.76	2041	430.0	2.74	3184
1.96	56.27	.20	165.5	2.55	260	265.5	4.09	417
1.96	56.27	1.00	220.1	3.39	1729	290.7	4.48	2283
1.96	56.20	1.80	239.4	3.70	3394	298.0	4.60	4224
1.96	60.75	.20	185.5	2.40	244	300.4	3.88	396
1.96	60.83	1.00	224.0	2.88	1471	313.3	4.03	2057
1.96	60.83	1.80	236.0	3.04	2790	326.6	4.20	3860
1.96	66.20	.20	220.5	2.24	229	348.2	3.54	361
1.96	66.07	1.00	239.9	2.45	1252	347.1	3.55	1812
1.96	65.58	1.80	250.2	2.62	2406	345.2	3.61	3320
1.96	71.03	.20	260.7	2.07	211	391.7	3.10	317
1.96	71.67	1.00	264.9	2.02	1033	381.5	2.91	1487
1.96	71.03	1.80	260.6	2.07	1897	381.6	3.02	2778

3D TRIPS - LOW TURBULENCE LEVELS

			TRANSITION ONSET			TRANSITION COMPLTN		
d	Swp	s	$\bar{R}$	d/n	s/n	$\bar{R}$	d/n	s/n
mm	deg	m						
.38	56.03	.10	467.8	1.41	375	496.2	1.49	397
.38	56.03	1.00	463.6	1.40	3675	481.7	1.45	3818
.38	56.13	1.80	465.7	1.40	6620	481.5	1.44	6844
.38	60.87	.10	531.4	1.32	352	555.2	1.38	368
.38	60.83	.20	551.3	1.38	724	582.2	1.45	765
.38	60.83	1.00	527.1	1.32	3461	544.3	1.36	3574
.38	60.98	1.80	526.5	1.31	6185	544.0	1.35	6391
.38	65.77	.10	613.7	1.23	328	633.1	1.27	339
.38	66.03	.20	652.5	1.30	683	679.6	1.35	711
.38	66.02	1.00	613.9	1.22	3212	626.5	1.25	3278
.38	65.92	1.00	640.9	1.28	3369	671.6	1.34	3531
.38	65.82	1.80	611.6	1.23	5815	624.7	1.25	5940
.38	65.92	1.80	628.2	1.26	5946	652.9	1.30	6179
.38	71.00	.10	725.3	1.12	297	749.4	1.15	307
.38	70.92	.20	747.0	1.16	608	770.4	1.19	627
.38	70.88	.20	769.2	1.19	627	799.2	1.24	652
.38	71.10	.30	774.9	1.19	936	820.6	1.26	992
.38	70.88	1.00	675.6	1.05	2755	747.6	1.16	3049
.38	70.70	1.00	709.4	1.11	2923	733.7	1.15	3023
.38	70.78	1.80	650.8	1.01	4804	697.7	1.09	5151
.38	71.10	1.80	666.2	1.02	4830	774.7	1.19	5617
.38	71.00	1.80	682.6	1.05	4978	719.8	1.11	5249
.38	70.92	1.80	688.4	1.06	5042	735.4	1.14	5386
.78	56.05	.20	339.6	2.10	538	357.6	2.21	567
.78	56.05	1.80	337.1	2.08	4806	353.7	2.19	5043
.78	60.90	.20	381.1	1.95	499	409.2	2.09	536
.78	60.80	.20	381.6	1.96	502	411.5	2.11	541
.78	60.83	.20	385.3	1.97	506	404.8	2.07	532
.78	60.83	1.00	380.9	1.95	2502	409.7	2.10	2690
.78	60.90	1.00	382.2	1.95	2503	403.0	2.06	2639
.78	60.87	1.80	380.7	1.95	4493	404.6	2.07	4775
.78	60.88	1.80	381.4	1.95	4500	401.9	2.05	4741
.78	60.88	1.80	385.5	1.97	4547	407.1	2.08	4802
.78	60.88	1.80	385.5	1.97	4547	407.1	2.08	4802
.78	60.90	1.80	383.8	1.96	4524			
.78	65.93	.20	448.3	1.84	471	514.0	2.11	540
.78	65.97	.20	458.8	1.88	481	507.0	2.07	532
.78	65.97	1.00	446.3	1.83	2341	500.7	2.05	2626
.78	65.90	1.00	441.1	1.81	2321	502.1	2.06	2643
.78	65.97	1.80	446.3	1.83	4214	499.1	2.04	4712
.78	66.03	1.80	445.0	1.82	4190	504.3	2.06	4748
.78	66.73	1.80	454.3	1.79	4137	516.0	2.04	4699
.78	70.93	.20	495.1	1.57	403	562.1	1.78	457
.78	70.93	.20	495.0	1.57	403	564.1	1.79	459
.78	70.97	.20	503.6	1.59	409	568.9	1.80	462
.78	70.97	.20	517.4	1.64	420	601.1	1.90	488
.78	70.83	.20	517.6	1.65	423	600.4	1.92	491
.78	71.10	.30	504.1	1.58	609	585.9	1.84	708
.78	71.10	.30	506.3	1.59	612	582.3	1.83	2346
.78	70.90	1.00	513.5	1.63	2092	572.0	1.82	2330
.78	70.77	1.00	518.7	1.66	2129	585.1	1.87	2401
.78	71.10	1.00	524.3	1.65	2112	571.0	1.79	2530
.78	71.10	1.10	525.1	1.65	2327			

.78	70.93	1.80	518.5	1.64	3796	561.5	1.78	4111
.78	70.77	1.80	513.1	1.64	3790	563.7	1.80	4164
.78	70.97	1.80	519.5	1.64	3795	562.6	1.78	4109
.78	70.82	1.80	517.0	1.65	3809	579.5	1.85	4268
.78	70.82	1.80	515.8	1.65	3799	580.3	1.85	4274
.78	70.97	1.80	521.2	1.65	3807	581.5	1.84	4247
.78	70.82	1.80	518.0	1.65	3815	580.7	1.85	4277
.78	70.82	1.80	518.0	1.65	3815	585.1	1.87	4310
.78	70.77	1.80	513.1	1.64	3790	563.7	1.80	4164
.99	56.12	.20	291.5	2.28	461	339.8	2.66	537
.99	56.12	1.00	292.4	2.29	2310	337.3	2.64	2665
.99	56.28	1.80	293.1	2.28	4143	337.3	2.62	4767
.98	60.87	.20	327.2	2.10	429	369.3	2.37	484
.99	60.78	.20	327.5	2.13	431	386.3	2.52	508
.98	60.87	1.00	328.3	2.11	2152	380.6	2.45	2495
.99	60.83	1.00	327.8	2.13	2153	381.4	2.48	2505
.98	60.73	1.80	323.9	2.09	3845	371.7	2.40	4412
.99	60.83	1.80	328.4	2.14	3882	366.9	2.39	4337
.98	60.95	1.80	325.7	2.09	3831	355.8	2.28	4186
.98	65.98	.20	375.4	1.93	394	422.3	2.17	443
.98	66.20	.20	380.1	1.93	394	427.5	2.17	444
.98	65.82	.20	375.1	1.94	396	402.4	2.08	425
.99	65.83	.20	377.4	1.97	398	441.7	2.31	466
.98	66.20	.20	380.3	1.93	395	436.1	2.22	453
.98	66.00	.30	379.2	1.95	596	425.2	2.18	668
.98	65.95	1.00	377.4	1.94	1982	438.7	2.26	2303
.99	65.93	1.00	378.3	1.97	1988	441.3	2.30	2319
.99	66.12	1.80	378.9	1.95	3553	449.9	2.32	4218
.98	65.97	1.80	377.7	1.94	3566	421.4	2.17	3979
.98	65.82	1.80	376.1	1.95	3576	407.9	2.11	3878
.98	66.20	1.80	384.0	1.95	3586	411.4	2.09	3842
.98	66.67	1.80	384.6	1.91	3513	428.5	2.13	3914
.98	71.03	.20	440.4	1.75	356	505.2	2.00	409
.99	70.83	.20	460.9	1.87	377	517.5	2.10	423
.98	70.77	1.00	445.8	1.79	1830	511.3	2.06	2098
.99	71.03	1.00	463.7	1.86	1875	517.8	2.07	2094
.98	71.03	1.80	448.2	1.78	3263	504.3	2.00	3671
.99	70.83	1.80	452.7	1.83	3333	516.9	2.09	3805
.98	70.97	1.80	446.3	1.77	3260	491.7	1.96	3591
1.58	56.08	.20	227.8	2.85	360	314.9	3.94	498
1.58	56.25	1.00	239.7	2.98	1884	316.1	3.93	2485
1.58	56.08	1.80	245.3	3.07	3493	320.0	4.00	4557
1.58	60.83	.20	249.5	2.59	328	333.6	3.46	438
1.57	61.22	.20	250.9	2.55	324	329.1	3.34	425
1.57	60.78	.20	247.3	2.56	325	300.9	3.11	396
1.57	60.78	.20	252.6	2.61	332	324.2	3.35	427
1.58	60.83	1.00	254.1	2.64	1669	340.3	3.53	2234
1.57	60.78	1.80	248.6	2.57	2945	302.5	3.13	3584
1.58	60.87	1.80	252.2	2.61	2976	347.2	3.60	4097
1.57	60.78	1.80	250.4	2.59	2966	319.9	3.31	3790
1.57	61.22	1.80	253.3	2.57	2946	329.1	3.34	3828
1.57	60.88	1.80	251.9	2.59	2971	330.5	3.40	3898
1.57	60.93	1.80	257.6	2.64	3032	344.5	3.54	4055
1.58	66.03	.20	285.9	2.36	299	381.0	3.15	399
1.58	65.98	1.00	285.5	2.37	1497	385.1	3.19	2019
1.58	65.75	1.80	283.9	2.38	2708	396.5	3.32	3782
1.57	66.83	1.80	292.6	2.31	2652	398.6	3.15	3613
1.58	71.25	.20	333.1	2.10	266	441.2	2.78	352

1.58	71.25	1.00	336.3	2.12	1343	446.6	2.82	1784
1.58	71.10	1.80	331.7	2.11	2405	457.3	2.91	3316
1.57	71.05	1.80	330.7	2.10	2404	443.3	2.81	3224
1.57	70.97	1.80	339.4	2.16	2479	455.2	2.90	3325
1.99	56.03	.20	198.4	3.13	315	304.3	4.80	482
1.99	56.25	1.00	220.2	3.45	1731	297.3	4.65	2337
1.99	56.03	1.80	241.0	3.80	3438	309.8	4.89	4420
1.99	60.78	.20	222.8	2.92	293	290.4	3.80	382
1.99	61.22	.20	228.9	2.94	296	316.7	4.07	409
1.99	60.78	.20	225.6	2.95	297	312.2	4.09	411
1.99	60.78	.20	225.6	2.95	297	328.6	4.30	432
1.99	60.92	.20	228.6	2.98	299	321.1	4.18	420
1.99	60.85	.20	220.4	2.88	289	325.4	4.25	427
1.99	60.80	1.00	236.2	3.09	1553	314.5	4.12	2068
1.99	60.78	1.80	234.6	3.07	2779	295.8	3.87	3503
1.99	60.78	1.80	234.5	3.07	2777	295.5	3.87	3500
1.99	61.22	1.80	240.6	3.09	2799	315.5	4.06	3670
1.99	60.78	1.80	240.0	3.14	2842	337.5	4.42	3998
1.99	60.75	1.80	240.7	3.16	2855	333.8	4.38	3958
1.99	65.83	.20	251.2	2.64	265	365.9	3.84	386
1.99	65.75	1.00	262.3	2.77	1390	353.9	3.73	1876
1.99	66.03	1.80	260.1	2.71	2449	378.8	3.94	3566
1.99	70.92	.20	286.6	2.32	233	389.2	3.15	317
1.99	71.00	.20	291.7	2.35	236	420.1	3.39	340
1.99	70.92	1.00	296.4	2.40	1206	406.2	3.29	1653
1.99	71.02	1.80	292.1	2.35	2127	423.9	3.41	3087

3D TRIPS PLACED OFF THE ATTACHMENT LINE
LOW TURBULENCE LEVELS

Sweep = 56.05 deg
s = 0.2m

d	x	alpha	TRANSITION ONSET $\bar{R}$	d/n	s/n	TRANSITION COMPLTN $\bar{R}$	d/n	s/n
mm	mm							
.00	0		553.9	.00	3071			
.00	0		552.8	.00	3070			
.78	0	.00	339.6	2.10	1883	357.6	2.21	1983
.78	4	2.36	345.4	2.14	1919	370.1	2.29	2056
.78	8.5	4.99	377.9	2.34	2099	460.3	2.85	2557
.78	10.5	6.15	454.2	2.81	2523			
.78	12.5	7.31	548.9	3.40	3049			
.78	14.5	8.47	560.5	3.47	3114			
.99	0	.00	291.5	2.28	1612	339.8	2.66	1879
.98	8.5	4.99	336.2	2.61	1868	434.7	3.38	2415
.98	10.5	6.15	421.1	3.27	2339	548.9	4.27	3049
.98	12.5	7.31	547.0	4.25	3039			
.98	14.5	8.47	561.0	4.36	3116			
1.99	0	.00	198.4	3.13	1101	304.3	4.80	1688
1.99	8.5	4.99	240.7	3.80	1337	328.9	5.19	1827
1.99	12.5	7.31	393.2	6.21	2184	508.5	8.03	2824
1.99	14.5	8.47	468.0	7.39	2600			
1.99	16	9.34	548.6	8.66	3048			
1.99	17.5	10.20	562.1	8.88	3122			

Sweep = 56.05 deg
s = 1.8m

d	x	alpha	TRANSITION ONSET $\bar{R}$	d/n	s/n	TRANSITION COMPLTN $\bar{R}$	d/n	s/n
mm	mm							
.00	0		532.4	.00	9698			
.00	0		525.7	.00	9576			
.78	0	.00	337.1	2.08	6141	353.7	2.19	6444
.78	4	1.87	339.9	2.10	6193	354.7	2.19	6462
.78	8	3.78	351.7	2.17	6407	392.0	2.42	7141
.78	12	5.67	428.2	2.65	7800	555.4	3.43	10118
.78	14	6.60	521.6	3.22	9502			
.78	15.5	7.30	530.1	3.27	9657			
.99	0	.00	293.1	2.28	5294	337.3	2.62	6091
.98	8.5	4.02	302.6	2.35	5512	361.3	2.80	6581
.98	12.5	5.90	413.4	3.21	7530	559.3	4.34	10189
.98	14	6.60	498.9	3.87	9088			
.98	16	7.53	530.0	4.11	9655			
1.99	0	.00	241.0	3.80	4393	309.8	4.89	5647
1.99	12.5	5.90	329.3	5.19	5999	439.5	6.93	8007
1.99	16	7.53	445.1	7.01	8108			
1.99	18.5	8.69	526.5	8.30	9591			
1.99	20	9.37	527.5	8.31	9609			

Sweep = 60.88 deg
s = 0.2m

d	x	alpha	TRANSITION ONSET $\bar{R}$	d/n	s/n	TRANSITION COMPLTN $\bar{R}$	d/n	s/n
mm	mm							
.00	0		612.5	.00	2810			
.00	0		621.1	.00	2853			
.00	0		616.1	.00	2830			
.78	0	.00	385.3	1.97	1771	404.8	2.07	1861

.78	8	4.22	416.4	2.13	1912	523.2	2.68	2403
.78	12	6.31	498.8	2.55	2291	639.2	3.27	2936
.78	14	7.35	610.0	3.12	2802			
.78	16	8.39	617.4	3.16	2836			
.99	0	.00	327.5	2.13	1509	386.3	2.52	1779
.98	8.5	4.48	374.1	2.41	1718	521.8	3.36	2397
.98	12	6.31	465.5	2.99	2138	608.6	3.91	2795
.98	14.5	7.61	607.5	3.91	2790			
.98	16	8.39	616.9	3.97	2834			
1.99	0	.00	220.4	2.88	1012	325.4	4.25	1495
1.99	8.5	4.48	241.2	3.15	1108	370.0	4.83	1700
1.99	12	6.31	326.9	4.27	1501	543.3	7.09	2495
1.99	14	7.35	458.0	5.98	2103	586.0	7.65	2692
1.99	16	8.39	573.5	7.49	2634			
1.99	18	9.43	607.6	7.93	2791			
1.99	20	10.46	614.8	8.03	2824			

Sweep = 60.88 deg

s = 1.8m

			TRANSITION ONSET			TRANSITION COMPLTN		
d	x	alpha	$\bar{R}$	d/n	s/n	$\bar{R}$	d/n	s/n
mm	mm							
.00	0		585.6	.00	8828	636.1	.00	9966
.00	0		581.7	.00	8761	640.7	.00	10018
.00	0		567.7	.00	8596			
.00	0		571.2	.00	8649	407.1	2.14	4936
.78	0	.00	385.5	1.97	5810			
.78	0	.00	385.5	1.97	5810	402.5	2.15	4960
.78	0	.00	383.8	1.96	5781			
.78	3	1.15	394.5	2.02	5942	413.3	2.19	5056
.78	6	2.34	380.5	1.94	5735	392.7	2.08	4805
.78	12.5	4.88	410.8	2.10	6187	447.9	2.37	5479
.78	15	5.84	445.5	2.28	6709	548.6	2.89	6680
.78	18	6.99	533.9	2.73	8041	614.0	3.30	7605
.78	20	7.76	574.9	2.95	8704			
.78	21.5	8.33	575.2	2.94	8662	633.0	3.38	7797
.78	24	9.28	577.7	2.95	8700	635.7	3.37	7784
.99	0	.00	328.4	2.14	4960	366.9	2.42	4396
.98	0	.00	325.7	2.09	4895	355.8	2.38	4365
.98	8.5	3.32	328.2	2.10	4933	366.1	2.46	4520
.98	12	4.68	349.5	2.24	5253	393.7	2.65	4862
.98	16.5	6.42	446.1	2.86	6705	582.4	3.90	7166
.98	20	7.76	573.5	3.70	8683	630.7	4.29	7874
.98	20.5	7.95	569.3	3.65	8557	624.1	4.19	7694
.98	24.5	9.46	571.0	3.66	8599			
1.99	0	.00	240.7	3.16	3648	333.8	4.49	4064
1.99	9	3.51	244.0	3.19	3687	334.8	4.46	4038
1.99	12.5	4.88	270.1	3.53	4081	370.1	4.94	4465
1.99	16	6.23	351.2	4.59	5307	478.6	6.38	5773
1.99	20	7.76	533.5	6.99	8078	637.8	8.55	7732
1.99	24	9.28	565.7	7.41	8565			
1.99	24.5	9.46	576.8	7.53	8704			

Sweep = 70.83 deg

s = 0.2m

			TRANSITION ONSET			TRANSITION COMPLTN		
d	x	alpha	$\bar{R}$	d/n	s/n	$\bar{R}$	d/n	s/n
mm	mm							
.00	0		800.5	.00	2272			
.00	0		809.2	.00	2318			

.00	0		808.0	.00	2314			
.78	0	.00	517.6	1.65	1482	600.4	1.96	503
.78	9	3.85	520.6	1.66	1491	613.0	2.00	514
.78	12	5.13	560.9	1.79	1607	790.1	2.58	662
.78	16	6.83	635.5	2.03	1820			
.78	20	8.53	798.1	2.55	2286			
.78	24	10.21	802.5	2.56	2299			
.99	0	.00	460.9	1.87	1319	517.5	2.13	431
.98	12.5	5.35	497.2	1.99	1424	755.8	3.10	634
.98	16	6.83	560.3	2.25	1605	807.9	3.33	679
.98	20	8.53	779.7	3.13	2234			
.98	24	10.21	812.2	3.26	2327			
1.99	0	.00	286.6	2.32	816	389.2	3.23	325
1.99	12.5	5.35	338.9	2.76	971	596.6	4.98	500
1.99	16.5	7.05	403.0	3.28	1154	807.6	6.78	681
1.99	20	8.53	629.6	5.13	1804	820.8	6.97	700
1.99	22	9.37	720.4	5.87	2064			
1.99	24	10.21	804.8	6.55	2305			

Sweep = 70.82 deg

s = 1.8m

			TRANSITION ONSET			TRANSITION COMPLTN		
d	x	alpha	$\bar{R}$	d/n	s/n	$\bar{R}$	d/n	s/n
mm	mm							
.00	0		670.7	.00	6309	733.0	.00	7098
.00	0		681.3	.00	6430	727.6	.00	7119
.00	0		675.2	.00	6373	725.8	.00	7201
.00	0		675.5	.00	6376			
.78	0	.00	513.1	1.64	4843	563.7	1.85	4277
.78	0	.00	513.1	1.64	4843	563.7	1.85	4277
.78	3	.71	507.8	1.61	4740	534.5	1.76	4052
.78	6	1.46	515.9	1.63	4815	544.8	1.79	4130
.78	12.5	3.08	507.0	1.62	4769	528.2	1.75	4048
.78	24	5.90	524.6	1.67	4935	613.7	2.04	4703
.78	27	6.62	586.1	1.86	5470	668.3	2.20	5072
.78	30	7.35	618.0	1.96	5784	659.6	2.19	5062
.78	33	8.07	625.3	1.98	5836	670.8	2.21	5107
.78	36.5	8.91	631.3	2.00	5892	679.7	2.25	5190
.78	41	9.98	661.9	2.12	6247	713.8	2.40	5542
.78	48	11.62	675.0	2.14	6300	725.9	2.41	5562
.99	0	.00	452.7	1.83	4259	516.9	2.13	3868
.98	0	.00	446.3	1.77	4165	491.7	2.04	3745
.98	16.5	4.06	444.2	1.77	4162	486.7	2.03	3736
.98	20.5	5.04	460.3	1.81	4252	515.8	2.13	3906
.98	24.5	6.02	488.5	1.95	4577	591.8	2.47	4543
.98	28.5	6.99	519.3	2.07	4858	671.3	2.75	5047
.98	32	7.83	615.7	2.45	5759	663.5	2.72	4988
.98	35.5	8.67	631.1	2.51	5890	677.2	2.77	5095
.98	41	9.98	659.4	2.65	6224	707.8	2.99	5496
.98	48	11.62	678.9	2.70	6336	731.8	3.00	5501
.98	52	12.56	676.7	2.69	6316	733.6	3.01	5531
1.99	0	.00	292.1	2.35	2718	423.9	3.50	3170
1.99	9	2.21	295.7	2.37	2735	437.4	3.57	3229
1.99	16	3.94	301.4	2.42	2801	421.8	3.46	3128
1.99	24.5	6.02	374.0	3.01	3480	522.5	4.26	3855
1.99	32	7.83	568.3	4.58	5289	676.6	5.52	4993
1.99	40.5	9.86	635.4	5.11	5910	682.9	5.65	5113
1.99	41	9.98	643.2	5.25	6071	689.9	5.92	5357
1.99	47.5	11.51	669.5	5.39	6228	733.0	6.09	5504

2D TRIPS - MEDIUM TURBULENCE LEVELS

			TRANSITION ONSET			TRANSITION COMPLTN		
d	Swp	S	$\bar{R}$	d/n	s/n	$\bar{R}$	d/n	s/n
mm	deg	m						
.00	73.35	1.30	607.0	.00	2776			
.28	73.17	.90	606.6	.60	1943			
.48	56.63	.20	314.6	1.17	488	349.8	1.30	542
.48	56.53	.90	306.3	1.14	2144	341.1	1.27	2388
.48	61.92	.20	354.8	1.07	445	389.9	1.17	489
.48	61.88	.90	347.3	1.05	1965	377.2	1.14	2134
.48	67.80	.20	417.4	.96	401	449.7	1.04	432
.48	67.73	.90	412.4	.95	1788	441.7	1.02	1915
.48	73.52	.20	504.6	.84	351	542.4	.91	378
.48	73.67	.90	499.3	.83	1549	539.0	.89	1672
.75	56.62	.20	263.9	1.53	409	290.7	1.69	451
.75	56.62	.90	266.7	1.55	1860	293.5	1.71	2047
.75	61.87	.20	292.0	1.38	367	326.9	1.54	411
.75	61.90	.90	288.7	1.36	1632	325.6	1.53	1841
.75	67.78	.20	334.7	1.21	322	378.0	1.36	363
.75	67.80	.90	325.0	1.17	1404	364.2	1.31	1573
.75	73.57	.20	397.8	1.04	276	446.1	1.16	310
.75	73.37	.90	391.3	1.03	1237	433.0	1.14	1369
1.04	56.60	.20	220.5	1.78	342	292.1	2.36	453
1.04	56.67	.90	243.3	1.96	1694	291.7	2.35	2031
1.04	61.95	.20	247.7	1.61	311	308.9	2.01	387
1.04	61.88	.90	255.9	1.67	1448	302.7	1.98	1713
1.04	67.88	.20	282.5	1.40	270	339.9	1.69	325
1.04	67.78	.90	278.7	1.39	1206	329.1	1.65	1424
1.04	73.42	.20	331.6	1.21	232	394.3	1.44	276
1.04	73.42	.90	326.2	1.19	1028	388.6	1.42	1225
1.55	56.60	.20	190.5	2.29	296	262.9	3.16	408
1.55	56.67	.90	234.6	2.81	1634	285.4	3.42	1987
1.55	61.90	.20	207.1	2.02	260	276.6	2.69	347
1.55	61.90	.90	234.3	2.28	1325	292.9	2.85	1656
1.55	67.68	.20	234.4	1.75	226	311.4	2.33	301
1.55	67.78	.90	243.6	1.81	1054	321.9	2.40	1392
1.55	73.53	.20	277.2	1.49	193	371.1	2.00	258
1.55	73.42	.90	277.7	1.51	875	381.8	2.07	1204
1.96	56.83	.20	172.1	2.59	265	257.8	3.89	396
1.96	56.65	.90	231.3	3.51	1612	287.7	4.37	2005
1.96	62.00	.20	189.4	2.32	237	284.2	3.48	356
1.96	61.92	.90	226.0	2.78	1276	305.2	3.75	1724
1.96	67.73	.20	218.9	2.07	211	331.7	3.13	320
1.96	67.70	.90	225.1	2.13	978	339.5	3.21	1474
1.96	73.27	.20	240.3	1.67	170	370.1	2.57	262
1.96	73.17	.90	243.8	1.70	781	371.7	2.59	1190

2D TRIPS - HIGH TURBULENCE LEVELS

			TRANSITION ONSET			TRANSITION COMPLTN		
d	Swp	S	$\bar{R}$	d/n	s/n	$\bar{R}$	d/n	s/n
mm	deg	m						
.00	61.85	.60	312.6	.00	1181			
.00	61.82	1.30	280.7	.00	2300			
.00	61.95	.60	326.6	.00	1229			
.00	61.87	1.30	288.9	.00	2362	441.4	.00	3609
.00	67.72	.60	321.4	.00	930			
.00	67.63	1.30	308.7	.00	1943			
.00	67.72	.60	330.3	.00	955	520.8	.00	1506
.00	67.72	1.30	313.0	.00	1961	497.4	.00	3117
.00	73.45	.60	330.7	.00	694			
.00	73.45	1.30	325.7	.00	1480			
.00	73.35	.60	337.0	.00	711	527.5	.00	1114
.00	73.00	1.30	323.1	.00	1511	516.8	.00	2416
.28	56.63	.20	290.6	.63	450			
.28	56.53	.90	257.5	.56	1802	377.2	.82	2641
.28	61.95	.20	322.6	.57	404			
.28	61.92	.90	288.9	.51	1632	427.7	.75	2416
.28	67.83	.20	318.0	.43	305	517.2	.69	496
.28	67.78	.90	315.3	.42	1364	483.7	.65	2092
.28	73.47	.20	333.7	.33	233	525.8	.51	367
.28	73.67	.90	321.9	.31	999	503.8	.49	1563
.48	56.63	.20	271.0	1.01	420	324.3	1.21	503
.48	56.55	.90	207.0	.77	1448	318.6	1.19	2229
.48	61.92	.20	292.5	.88	367	365.2	1.10	458
.48	61.90	.90	281.9	.85	1593	355.6	1.07	2011
.48	67.77	.20	327.0	.75	315	423.8	.98	408
.48	67.78	.90	313.8	.72	1357	402.9	.93	1743
.48	73.62	.20	312.8	.52	216	496.5	.82	343
.48	73.67	.90	306.0	.51	949	471.6	.78	1463
.75	56.62	.20	226.6	1.32	351	276.2	1.61	428
.75	56.52	.90	219.8	1.28	1539	282.9	1.65	1981
.75	61.92	.20	254.0	1.20	319	304.5	1.43	382
.75	61.90	.90	258.8	1.22	1463	301.6	1.42	1705
.75	67.77	.20	294.7	1.06	283	350.5	1.26	337
.75	67.73	.90	285.2	1.03	1237	332.9	1.20	1443
.75	73.47	.20	323.8	.85	226	410.7	1.08	287
.75	73.47	.90	320.5	.84	1007	385.9	1.01	1213
1.04	56.60	.20	194.3	1.57	301	260.1	2.10	403
1.04	56.77	.90	184.8	1.48	1282	272.4	2.18	1889
1.04	61.88	.20	218.5	1.43	275	279.4	1.83	351
1.04	61.80	.90	231.4	1.52	1314	294.6	1.93	1673
1.04	67.77	.20	247.8	1.24	238	312.7	1.56	301
1.04	67.72	.90	250.1	1.25	1085	312.1	1.56	1354
1.04	73.48	.20	285.2	1.03	199	369.3	1.34	258
1.04	73.48	.90	281.4	1.02	884	362.1	1.31	1137
1.55	56.58	.20	174.5	2.10	271	259.0	3.12	402
1.55	56.60	.90	190.4	2.29	1330	278.4	3.35	1944
1.55	61.97	.20	192.6	1.87	241	271.3	2.63	340
1.55	61.87	.90	214.9	2.10	1217	281.9	2.75	1596
1.55	67.78	.20	219.8	1.64	211	299.5	2.23	288
1.55	67.78	.90	227.2	1.69	983	305.1	2.27	1320
1.55	73.48	.20	251.2	1.36	175	350.3	1.89	244
1.55	73.48	.90	250.2	1.35	786	357.6	1.93	1123
1.96	56.83	.20	150.2	2.26	231	254.0	3.83	391

1.96	56.90	.90	182.5	2.74	1260	277.5	4.17	1916
1.96	61.92	.20	162.8	2.00	204	266.6	3.28	335
1.96	61.90	.90	204.9	2.52	1159	283.9	3.50	1605
1.96	67.73	.20	187.0	1.77	180	292.7	2.76	282
1.96	67.73	.90	208.8	1.97	906	299.4	2.83	1298
1.96	73.17	.20	208.4	1.45	148	336.8	2.35	240
1.96	73.17	.90	216.9	1.51	695	345.8	2.41	1108

3D TRIPS - MEDIUM TURBULENCE LEVELS

			TRANSITION ONSET			TRANSITION COMPLTN		
d	Swp	s	$\bar{R}$	d/n	s/n	$\bar{R}$	d/n	s/n
mm	deg	m						
.39	73.50	.20	637.9	.87	445			
.39	73.50	.90	616.8	.84	1935			
.78	56.47	.20	338.8	2.06	528	359.6	2.19	561
.78	56.37	.90	335.3	2.05	2362	346.6	2.12	2441
.78	61.80	.20	386.1	1.90	487	411.0	2.02	519
.78	61.83	.90	385.1	1.89	2184	397.9	1.96	2256
.78	67.65	.20	454.0	1.71	439	480.5	1.81	465
.78	67.68	.90	451.1	1.70	1961	465.8	1.75	2025
.78	73.63	.20	553.5	1.49	383	601.0	1.62	415
.78	73.63	.90	547.1	1.47	1702	569.6	1.54	1772
.98	56.30	.20	297.1	2.28	466	306.4	2.36	481
.98	56.35	.90	294.8	2.26	2078	303.6	2.33	2140
.98	61.78	.20	338.8	2.10	428	346.6	2.14	438
.98	61.80	.90	336.5	2.08	1910	343.2	2.12	1949
.98	67.68	.20	399.7	1.89	386	413.0	1.96	399
.98	67.63	.90	395.6	1.88	1724	406.6	1.93	1772
.98	73.42	.20	481.5	1.65	337	508.5	1.75	356
.98	73.47	.90	479.5	1.64	1507	494.5	1.69	1554
1.57	56.47	.20	237.0	2.90	370	248.6	3.04	388
1.57	56.47	.90	245.7	3.01	1724	269.8	3.30	1893
1.57	61.80	.20	261.1	2.59	329	275.2	2.73	347
1.57	61.82	.90	262.2	2.59	1487	277.5	2.75	1574
1.57	67.67	.20	302.6	2.30	292	318.5	2.42	308
1.57	67.70	.90	300.6	2.28	1305	314.0	2.38	1364
1.57	73.58	.20	366.6	2.00	254	389.3	2.12	270
1.57	73.58	.90	365.2	1.99	1140	381.8	2.08	1191
1.99	56.48	.20	211.1	3.27	329	228.6	3.54	356
1.99	56.47	.90	244.6	3.79	1716	269.3	4.18	1890
1.99	61.77	.20	233.5	2.93	295	254.9	3.20	322
1.99	61.80	.90	244.5	3.07	1388	277.0	3.48	1573
1.99	67.68	.20	265.5	2.55	256	304.6	2.93	294
1.99	67.68	.90	267.0	2.57	1160	287.8	2.77	1251
1.99	73.48	.20	320.7	2.23	224	343.5	2.39	240
1.99	73.48	.90	318.8	2.21	1001	333.6	2.32	1048

3D TRIPS - HIGH TURBULENCE LEVELS

			TRANSITION ONSET			TRANSITION COMPLTN		
d	Swp	s	$\bar{R}$	d/n	s/n	$\bar{R}$	d/n	s/n
mm	deg	m						
.39	61.72	.20	314.5	.78	398			
.39	61.83	.90	281.6	.69	1597	420.3	1.03	2383
.39	67.67	.20	318.2	.60	307			
.39	67.68	.90	315.9	.60	1373	483.8	.91	2103
.39	73.37	.20	330.2	.45	232	542.1	.74	381
.39	73.33	.90	326.6	.45	1036	505.9	.70	1604
.78	56.27	.20	286.1	1.75	449	344.5	2.11	541
.78	56.40	.90	261.3	1.59	1838	335.6	2.05	2361
.78	61.80	.20	309.6	1.52	391	390.4	1.92	493
.78	61.80	.90	277.9	1.37	1578	380.6	1.87	2161
.78	67.65	.20	314.0	1.18	304	460.1	1.74	445
.78	67.63	.90	289.1	1.09	1260	443.3	1.67	1932
.78	73.52	.20	328.3	.89	229	540.6	1.47	376
.78	73.30	.90	322.0	.89	1023	499.6	1.38	1587
.98	56.40	.20	272.9	2.09	427	305.5	2.34	478
.98	56.47	.90	239.3	1.83	1679	299.1	2.29	2099
.98	61.77	.20	298.6	1.85	377	344.4	2.13	435
.98	61.83	.90	275.7	1.70	1563	337.9	2.09	1916
.98	67.65	.20	317.1	1.50	307	405.8	1.92	393
.98	67.68	.90	322.3	1.53	1401	395.8	1.87	1721
.98	73.50	.20	324.5	1.11	226	491.8	1.68	343
.98	73.50	.90	302.3	1.03	948	477.7	1.63	1498
1.57	56.47	.20	211.8	2.59	330	241.0	2.95	376
1.57	56.47	.90	228.6	2.80	1604	278.1	3.40	1952
1.57	61.82	.20	243.6	2.41	307	282.2	2.79	356
1.57	61.80	.90	247.2	2.45	1403	285.7	2.83	1622
1.57	67.68	.20	282.6	2.14	273	318.6	2.42	308
1.57	67.65	.90	282.3	2.14	1229	314.1	2.39	1367
1.57	73.65	.20	319.4	1.73	220	384.8	2.09	266
1.57	73.37	.90	305.0	1.68	964	369.7	2.04	1169
1.99	56.48	.20	188.8	2.93	294	219.1	3.40	341
1.99	56.47	.90	223.1	3.46	1566	257.5	4.00	1807
1.99	61.77	.20	209.0	2.63	264	247.1	3.11	312
1.99	61.83	.90	229.0	2.87	1298	266.5	3.34	1511
1.99	67.65	.20	246.2	2.37	238	283.8	2.73	275
1.99	67.70	.90	254.6	2.44	1105	287.8	2.76	1250
1.99	73.40	.20	293.3	2.05	206	340.1	2.37	239
1.99	73.40	.90	287.4	2.01	907	329.0	2.30	1038

INTERACTION BETWEEN TWO 2D TRIPS
TRANSITION ONSET ; LOW TURBULENCE LEVELS

d1 = 0.28mm Sweep = 71.00deg

d2 mm	S12 mm	Shw mm	$\bar{R}$	d/n	S12/n	Shw/n
.00	.00	200	665.21	.75	.00	539
.00	.00	1500	628.83	.71	.00	3821
.28	2.80	200	704.98	.80	8.00	571
.28	2.80	1500	639.06	.72	7.25	3883
.28	5.50	200	666.71	.76	14.85	540
.28	5.50	1500	630.59	.72	14.05	3832
.28	200	200	610.37	.69	495	495
.28	200	1300	598.95	.68	485	3154

d1 = 0.75mm Sweep = 70.83deg

d2 mm	S12 mm	Shw mm	$\bar{R}$	d/n	S12/n	Shw/n
.00	.00	200	425.51	1.31	.00	348
.00	.00	200	434.00	1.33	.00	355
.00	.00	1500	432.08	1.33	.00	2651
.00	.00	1500	426.80	1.31	.00	2618
.75	4.00	200	493.12	1.51	8.07	403
.75	4.00	1500	484.69	1.49	7.93	2974
.76	7.50	200	454.12	1.39	13.93	371
.76	7.50	1500	452.93	1.39	13.89	2779
.76	15.10	200	419.64	1.29	25.92	343
.76	15.10	1500	408.73	1.25	25.24	2508
.75	200	200	405.31	1.24	332	332
.75	200	1300	394.95	1.21	323	2100
.75	200	1300	398.50	1.22	326	2119

d1 = 1.02mm Sweep = 65.83deg

d2 mm	S12 mm	Shw mm	$\bar{R}$	d/n	S12/n	Shw/n
.00	.00	200	301.43	1.62	.00	318
.00	.00	200	299.48	1.61	.00	316
.00	.00	1500	301.43	1.62	.00	2387
.00	.00	1500	297.19	1.60	.00	2354
1.04	5.30	200	356.15	1.92	9.97	376
1.04	5.30	1500	354.79	1.91	9.93	2810
1.04	10.10	200	322.05	1.73	17.17	340
1.04	10.10	1500	322.05	1.73	17.17	2551
1.03	19.80	200	283.99	1.53	29.69	300
1.03	19.80	1500	283.99	1.53	29.69	2249
1.04	200	200	299.63	1.61	316	316
1.04	200	1300	299.63	1.61	316	2057

d1 = 1.53mm Sweep = 56.17deg

d2 mm	S12 mm	Shw mm	$\bar{R}$	d/n	S12/n	Shw/n
.00	.00	200	195.85	2.36	.00	309
.00	.00	1500	239.86	2.89	.00	2837
1.55	8.00	200	216.81	2.62	13.68	342
1.55	8.00	1500	246.35	2.97	15.54	2914
1.55	15.80	200	195.85	2.36	24.40	309
1.55	15.80	1500	239.86	2.89	29.88	2837

1.55	30.00	200	178.33	2.15	42.18	281
1.55	30.00	1500	239.86	2.89	56.74	2837
1.55	200	200	185.94	2.24	293	293
1.55	200	1300	239.86	2.89	378	2459

INTERACTION BETWEEN TWO 3D TRIPS
TRANSITION ONSET - LOW TURBULENCE LEVELS

d1 = 0.38mm Sweep = 70.92

d2 mm	S12 mm	Shw mm	$\bar{R}$	d/n	S12/n	Shw/n
.00	n/a	200	746.96	1.16	.00	608
.00	n/a	1800	666.15	1.02	.00	4830
.00	n/a	1800	688.39	1.06	.00	5042
.38	.80	200	773.18	1.20	2.52	629
.38	.80	1800	682.19	1.05	2.22	4997
.38	2.00	200	721.09	1.12	5.92	592
.38	1.90	1800	658.69	1.03	5.14	4866
.38	3.70	200	718.98	1.12	10.92	590
.38	3.80	1800	663.56	1.03	10.35	4902
.38	4.00	1800	663.05	1.03	10.88	4898
.38	7.60	200	709.26	1.11	22.12	582
.38	7.40	1800	660.70	1.03	20.06	4880
.38	11.70	200	706.27	1.10	33.91	580
.38	100	200	720.41	1.10	290	580
.38	100	1000	704.20	1.08	284	2836
.38	200	200	760.14	1.16	612	612
.38	200	1000	699.63	1.07	564	2818
.38	800	200	709.51	1.09	2286	572
.38	800	1000	668.36	1.02	2154	2692

d1 = 0.78mm Sweep = 70.93deg

d2 mm	S12 mm	Shw mm	$\bar{R}$	d1/n	S12/n	Shw/n
.00	n/a	200	495.13	1.57	.00	403
.00	n/a	200	494.98	1.57	.00	403
.00	n/a	1800	515.76	1.65	.00	3799
.00	n/a	1800	517.97	1.65	.00	3815
.78	1.70	200	555.13	1.76	3.84	452
.78	1.70	1800	550.33	1.75	3.80	4029
.78	4.30	200	484.70	1.55	8.53	397
.78	4.00	1800	488.22	1.56	7.99	3596
.78	7.70	200	481.81	1.54	15.18	394
.78	7.40	1800	488.22	1.56	14.78	3596
.78	15.40	200	471.79	1.51	29.73	386
.78	15.60	1800	474.13	1.51	30.27	3493
.78	100	200	477.39	1.50	192	385
.78	100	1000	495.55	1.56	200	1996
.78	200	200	480.05	1.51	387	387
.78	200	1000	501.07	1.57	404	2018
.78	800	200	501.73	1.58	1617	404
.78	800	1000	511.05	1.61	1647	2059

d1 = 0.98mm Sweep = 66.10deg

d2 mm	S12 mm	Shw mm	$\bar{R}$	d1/n	S12/n	Shw/n
.00	n/a	200	380.08	1.93	.00	394
.00	n/a	200	380.31	1.93	.00	395
.00	n/a	1800	383.96	1.95	.00	3586
.00	n/a	1800	376.12	1.95	.00	3576
.98	2.10	200	408.00	2.11	4.53	431
.98	2.10	1800	438.91	2.27	4.87	4173

.98	5.10	200	349.84	1.78	9.26	363
.98	4.90	1800	356.26	1.81	9.06	3327
.98	10.10	200	351.34	1.79	18.41	365
.98	10.10	1800	354.84	1.80	18.60	3314
.98	20.90	200	348.32	1.77	37.77	361
.98	20.00	1800	348.97	1.77	36.22	3259
.98	100	200	367.67	1.89	193	385
.98	100	1000	371.25	1.91	194	1945
.98	200	200	363.22	1.86	381	381
.98	200	1000	369.28	1.90	387	1934
.98	800	200	352.83	1.81	1478	370
.98	800	1000	377.30	1.94	1581	1976

d1 = 1.57mm Sweep = 60.78

d2 mm	S12 mm	Shw mm	$\bar{R}$	d1/n	S12/n	Shw/n
.00	n/a	200	247.31	2.56	.00	325
.00	n/a	200	252.57	2.61	.00	332
.00	n/a	1800	248.64	2.57	.00	2945
.00	n/a	1800	250.37	2.59	.00	2966
1.57	4.00	200	289.35	2.94	7.48	374
1.57	4.00	1800	289.35	2.94	7.48	3366
1.57	8.10	200	232.19	2.40	12.38	306
1.57	8.20	1800	240.53	2.48	12.98	2849
1.57	16.10	200	232.19	2.40	24.60	306
1.57	16.10	1800	240.53	2.48	25.48	2849
1.57	31.50	200	232.19	2.40	48.13	306
1.57	31.60	1800	243.10	2.51	50.55	2879
1.57	100	200	239.93	2.48	158	316
1.57	100	1000	245.67	2.54	162	1617
1.57	200	200	244.90	2.53	322	322
1.57	200	1000	247.31	2.56	325	1627
1.57	800	200	240.29	2.48	1265	316
1.57	800	1000	255.81	2.64	1347	1683

d1 = 1.99mm Sweep = 60.78

d2 mm	S12 mm	Shw mm	$\bar{R}$	d1/n	S12/n	Shw/n
.00	n/a	200	225.59	2.95	.00	297
.00	n/a	200	225.59	2.95	.00	297
.00	n/a	1800	239.97	3.14	.00	2842
.00	n/a	1800	240.07	3.10	.00	2803
1.99	5.00	200	250.31	3.23	8.12	325
1.99	5.00	1800	250.31	3.23	8.12	2923
1.99	9.70	200	219.05	2.87	13.98	288
1.99	10.50	1800	234.57	3.07	16.21	2778
1.99	20.00	200	215.54	2.82	28.37	284
1.99	20.00	1800	234.57	3.07	30.87	2778
1.99	39.70	200	219.05	2.87	57.22	288
1.99	39.90	1800	234.57	3.07	61.59	2778
1.99	100	200	219.12	2.87	144	288
1.99	100	1000	225.18	2.95	148	1482
1.99	200	200	222.47	2.91	293	293
1.99	200	1000	229.16	3.00	302	1508
1.99	800	200	219.45	2.87	1155	289
1.99	800	1000	233.98	3.06	1232	1540

TABLE 6.1

3D TRIP POSITIONED DOWNSTREAM OF ATTACHMENT LINE - LIMITING VALUES FOR ISOLATED SPOTS

Λ	d (mm)	s (m)	x_1 (mm)	α_1 (deg)	$\bar{R}$ d/η	x_2 (mm)	α_2 (deg)	$\bar{R}$ d/η
56°	0.78	0.2	4.5	2.6	344 2.10	12.5	7.3	549 3.40
		1.8	5	2.6	344 2.08	14	6.6	521 3.22
	0.98	0.2	4.5	2.5	295 2.28	14	7.3	547 4.25
		1.8	6.5	2.5	295 2.28	19.5	7.5	530 4.11
	1.99	0.2	6	2.5	201 3.08	22	9.3	548 8.66
		1.8	12	2.9	244 3.80	35.5	8.7	526 8.30
61°	0.78	0.2	5	3.0	391 1.97	12.5	7.3	610 3.12
		1.8	6.5	3.1	388 1.96	17	7.8	575 2.95
	0.98	0.2	3	2.7	333 2.13	14.5	7.6	607 3.91
		1.8	7	2.7	330 2.11	20	7.8	570 3.65
	1.99	0.2	6	2.5	221 2.08	22.5	9.4	607 7.93
		1.8	12	2.9	244 3.16	35	8.5	550 7.20

71°	0.78	0.2	7	4.1	522 1.65	14.5	8.5	798 2.55
		1.8	9.5	4.4	517 1.64	19	8.9	631 2.00
	0.98	0.2	7	3.6	465 1.87	16	8.5	780 3.13
		1.8	10.5	4.1	454 1.80	26	10.0	659 2.65
	1.99	0.2	7	3.0	290 2.32	24	10.2	804 6.55
		1.8	12	3.0	295 2.35	36.5	8.8	600 4.84

TABLE 7.1

LIMITING VALUES OF $\bar{R}$ AND d/η FOR 2D TRIPS VARIOUS LEVELS OF FREESTREAM TURBULENCE

σ	$\bar{R}_{upper}$	d/η_{upper}	$\bar{R}_{kink}$	d/η_{kink}	$\bar{R}_{lower}$	d/η_{lower}
low	600	0.90	376	1.67	250	1.97
medium	500*	0.7*	310	1.29	250	1.62
high	300	0.7	285	1.03	250	1.26

TABLE 7.2

LIMITING VALUES OF $\bar{R}$ AND d/η FOR 3D TRIPS VARIOUS LEVELS OF FREESTREAM TURBULENCE

σ	$\bar{R}_{upper}$	d/η_{upper}	$\bar{R}_{kink}$	d/η_{kink}	$\bar{R}_{lower}$	d/η_{lower}
low	600	1.33	451	1.82	250	2.63
medium	500*	1.5*	366	2.00	250	2.70
high	300	1.4	290	2.07	250	2.36

* - Estimated value

FIG 1.1
ATTACHMENT LINE BOUNDARY LAYER
FROM POLL'83b

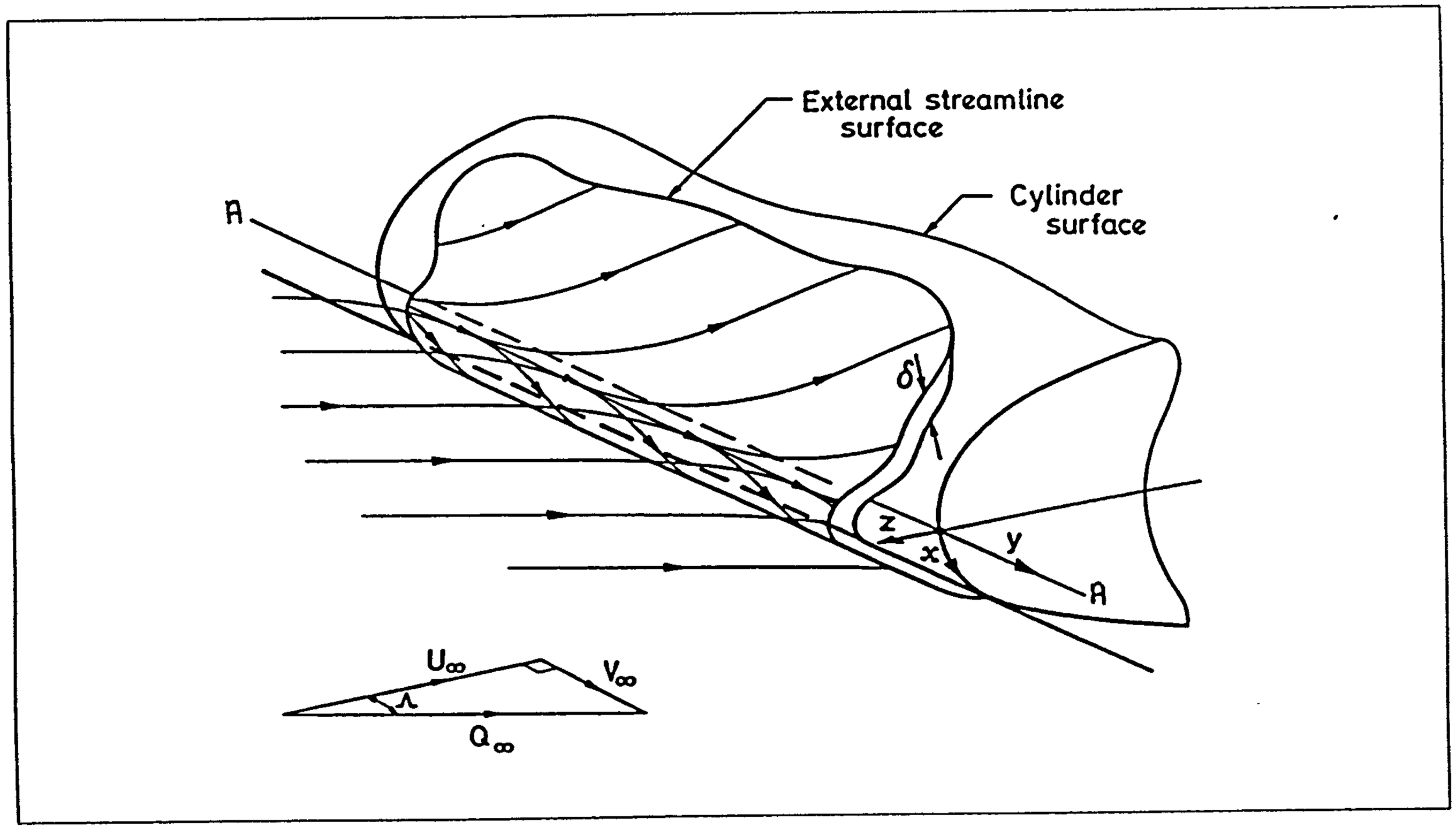

FIG 1.2
LAMINAR VELOCITY PROFILES

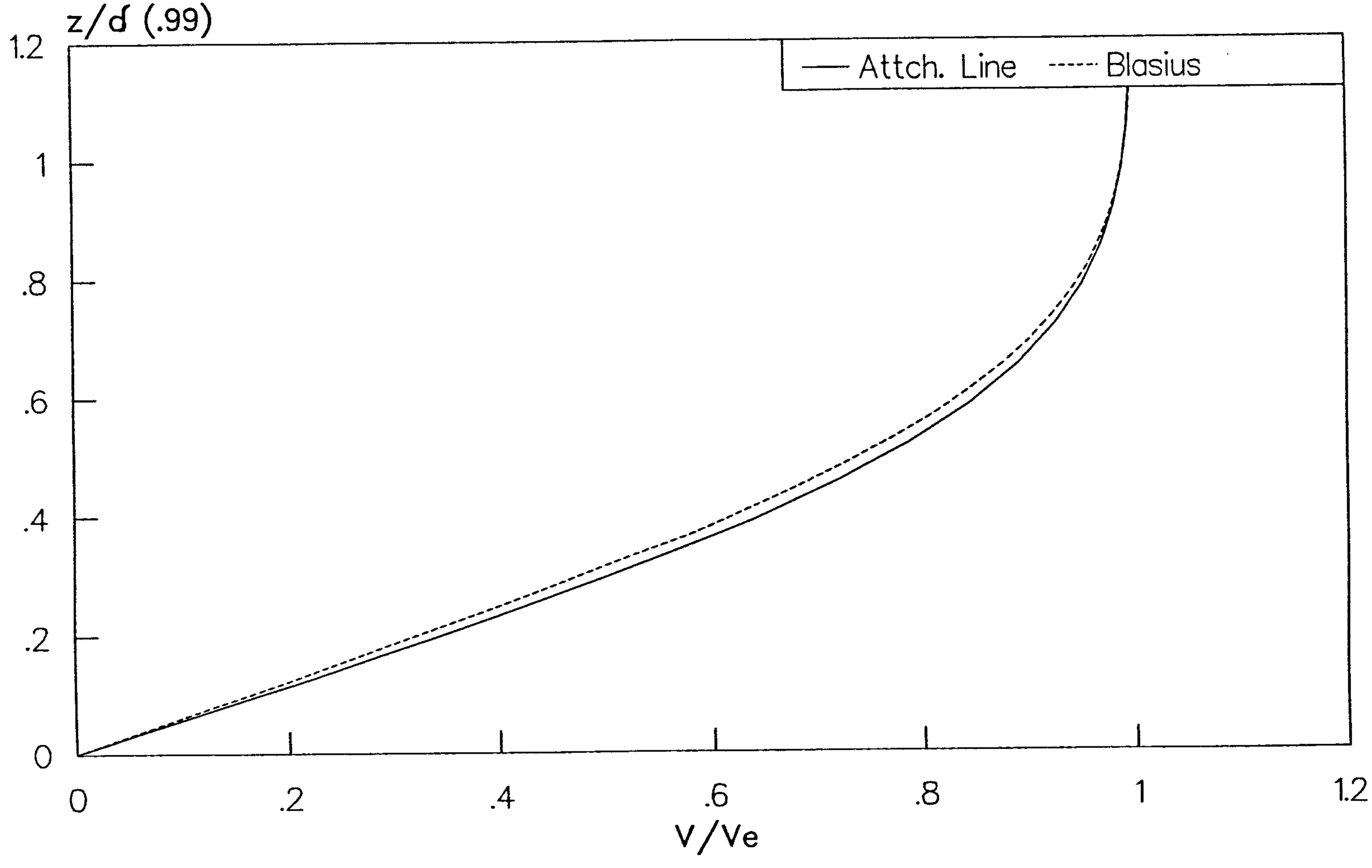

FIG 3.1
8'x6' WIND TUNNEL

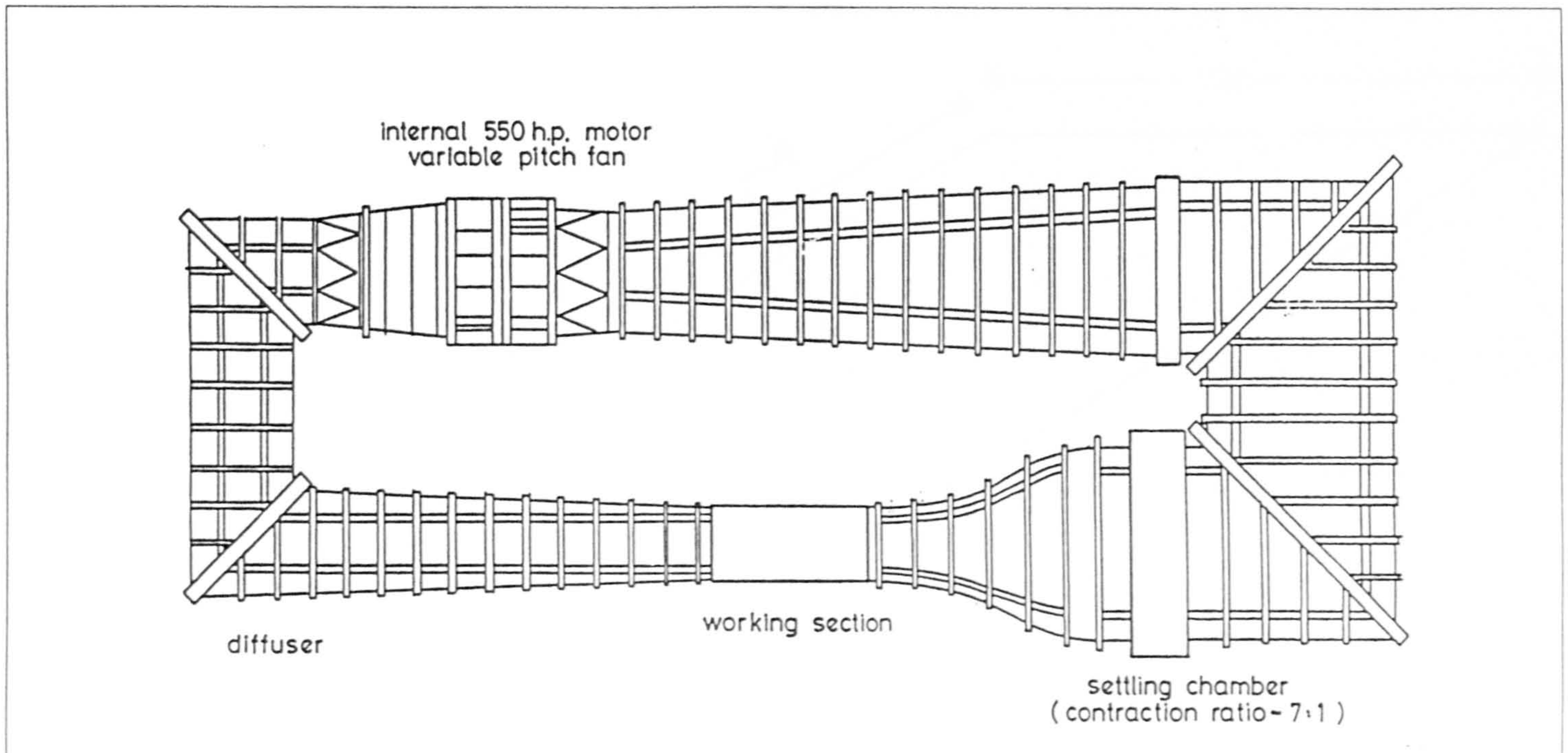

FIG 3.2
SWEPT CYLINDER MODEL

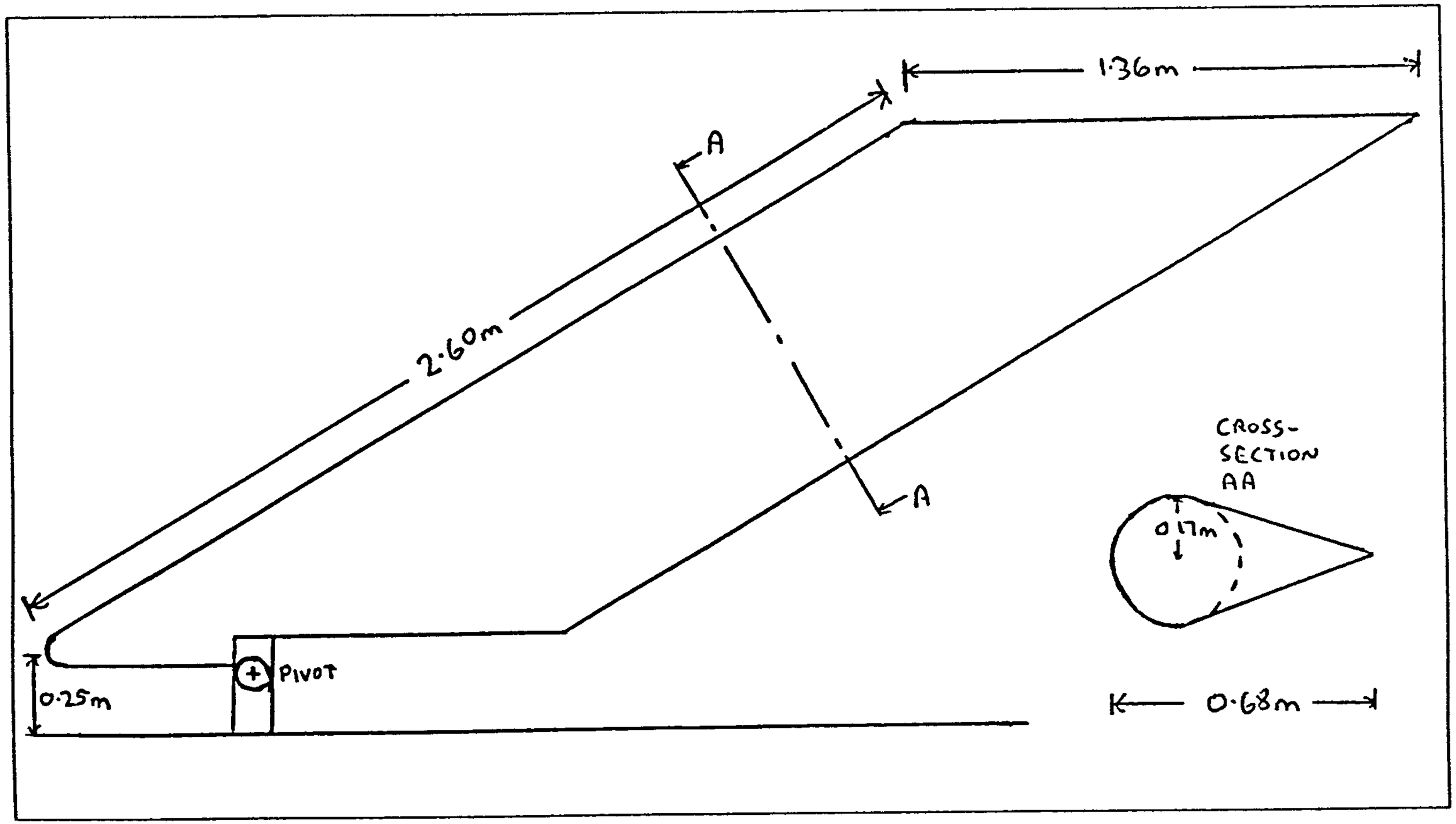

FIG 3.3
MODEL PRESSURE DISTRIBUTION
Sweep = 56, 61 and 71 deg

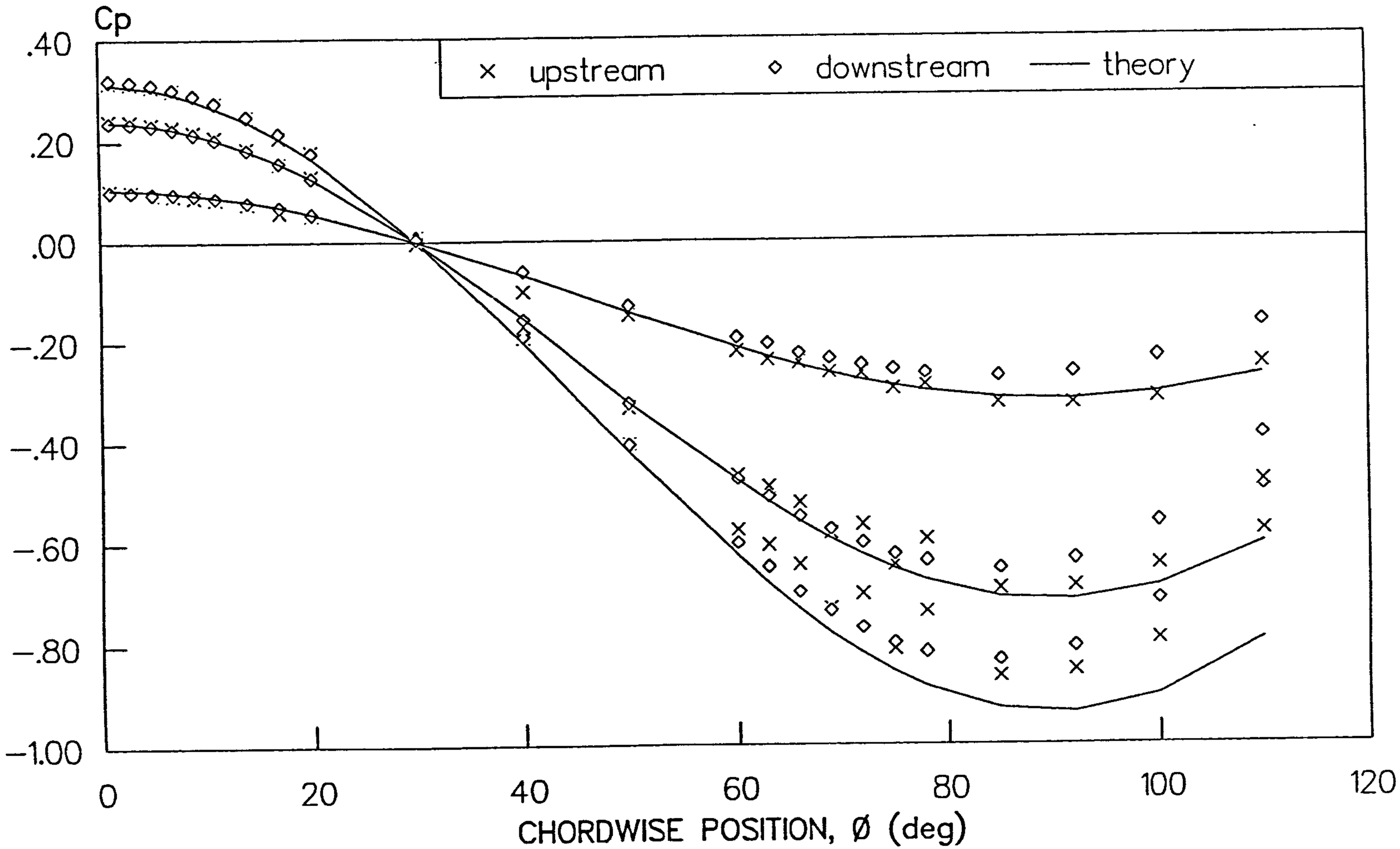

FIG 3.4
ATTACHMENT LINE BOUNDARY LAYER
LAMINAR VELOCITY PROFILES

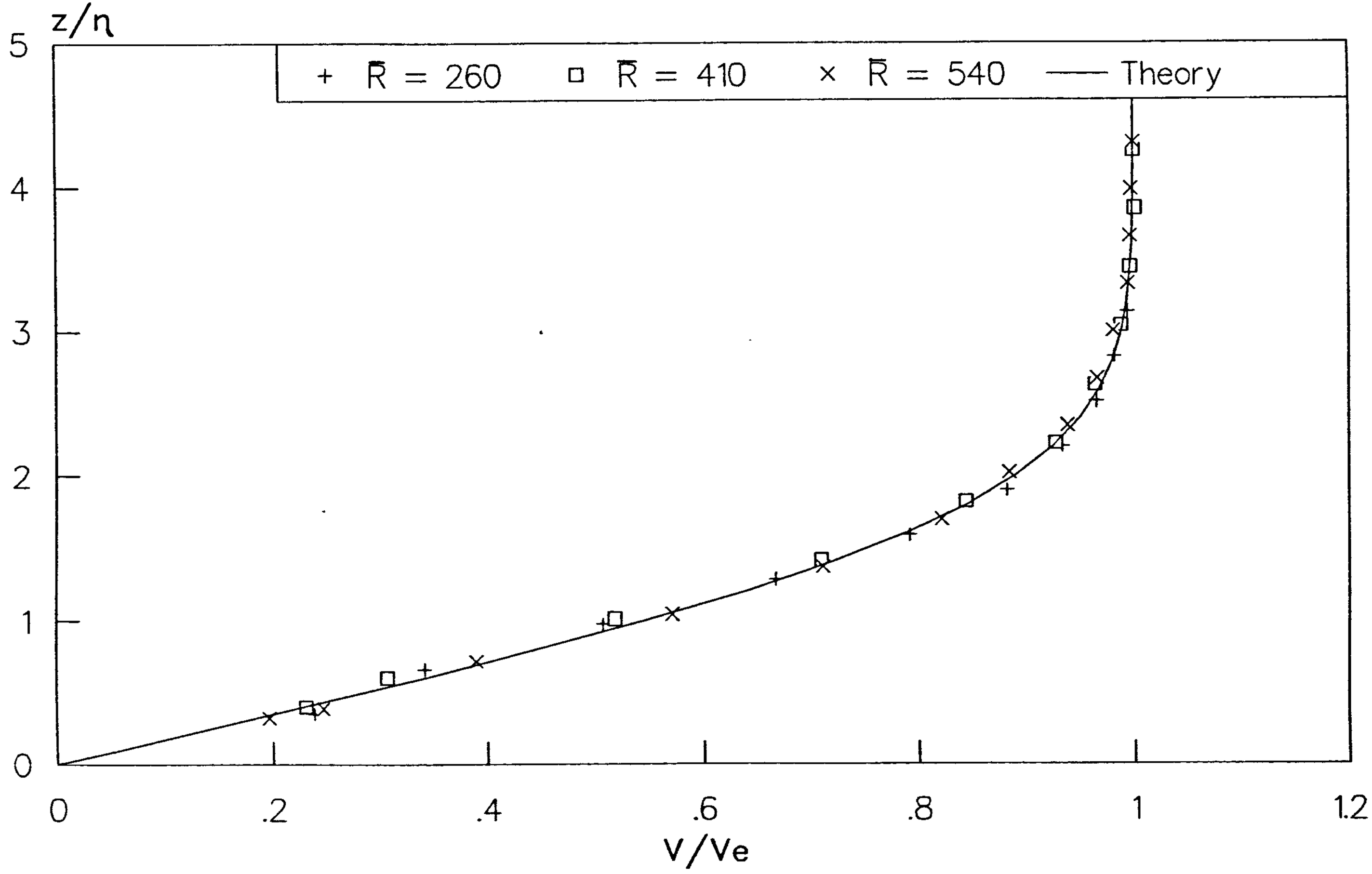

FIG 3.5
DOWNSTREAM OF ATTACHMENT LINE
LAMINAR VELOCITY PROFILES, PARALLEL TO A.L.

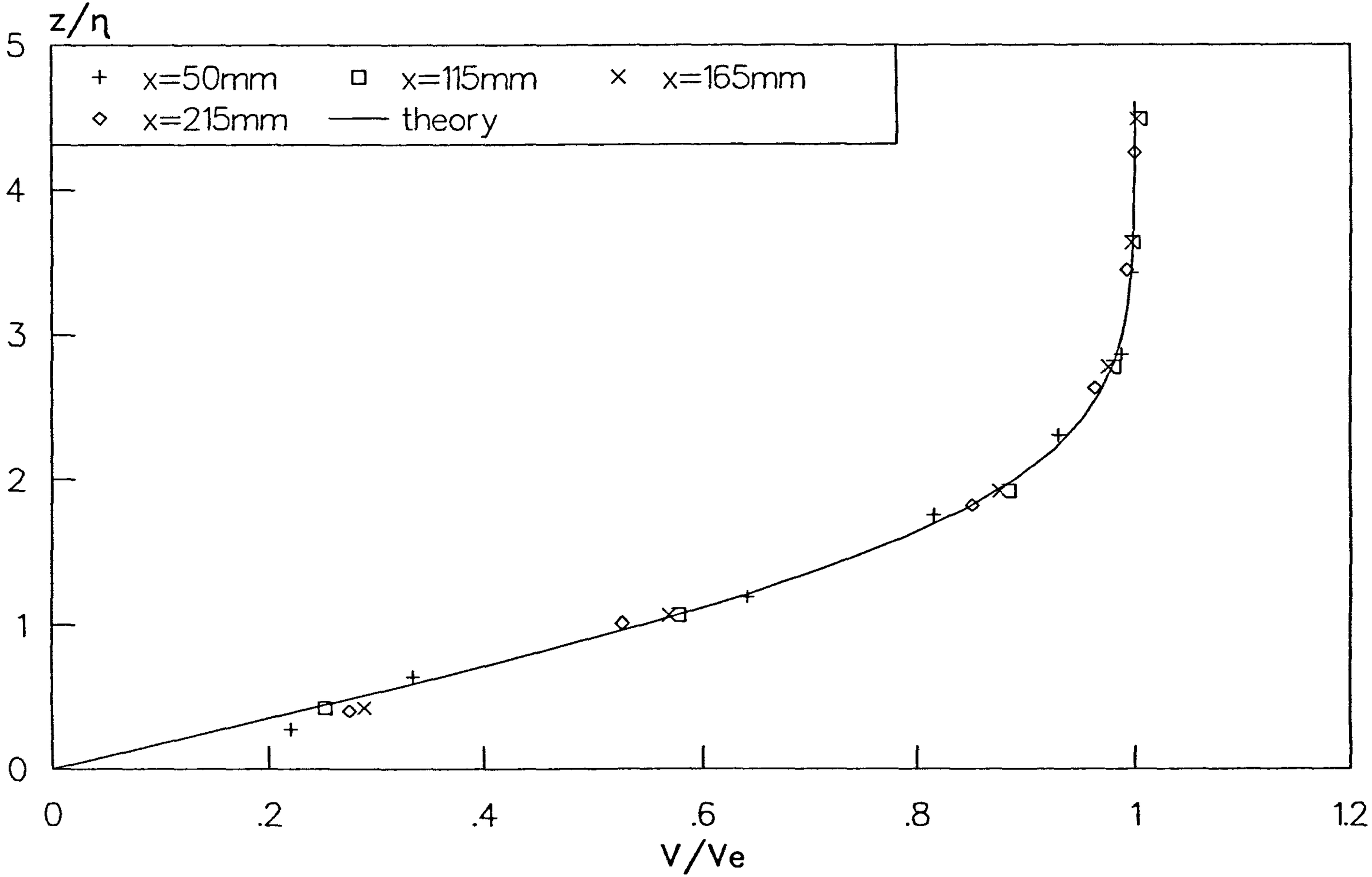

FIG 3.6
ATTACHMENT LINE BOUNDARY LAYER
TURBULENT VELOCITY PROFILES

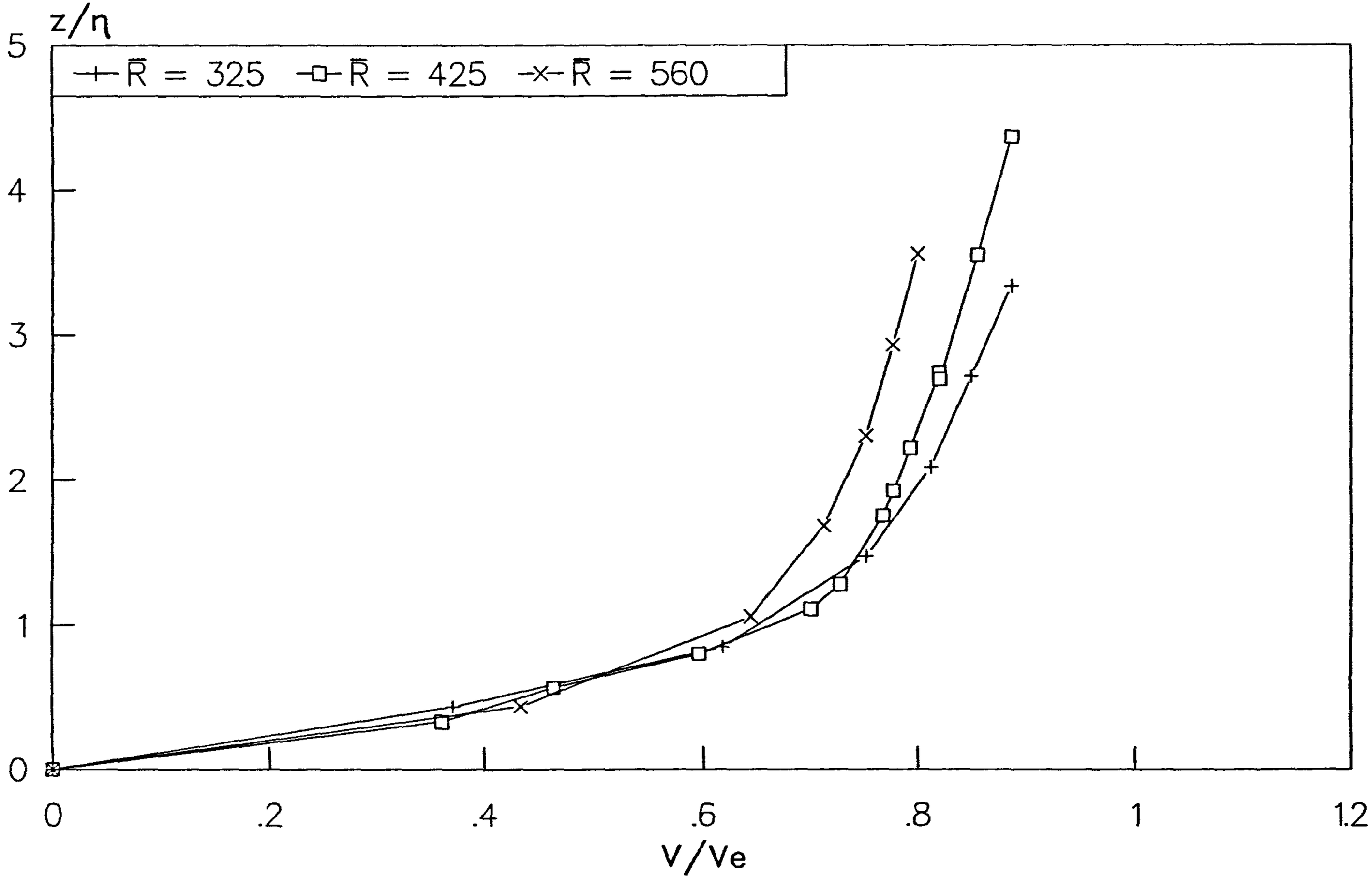

FIG 4.1
2D TRIPS; TRANSITION ONSET & COMPLETION
POLL'S RESULTS (Poll'78)

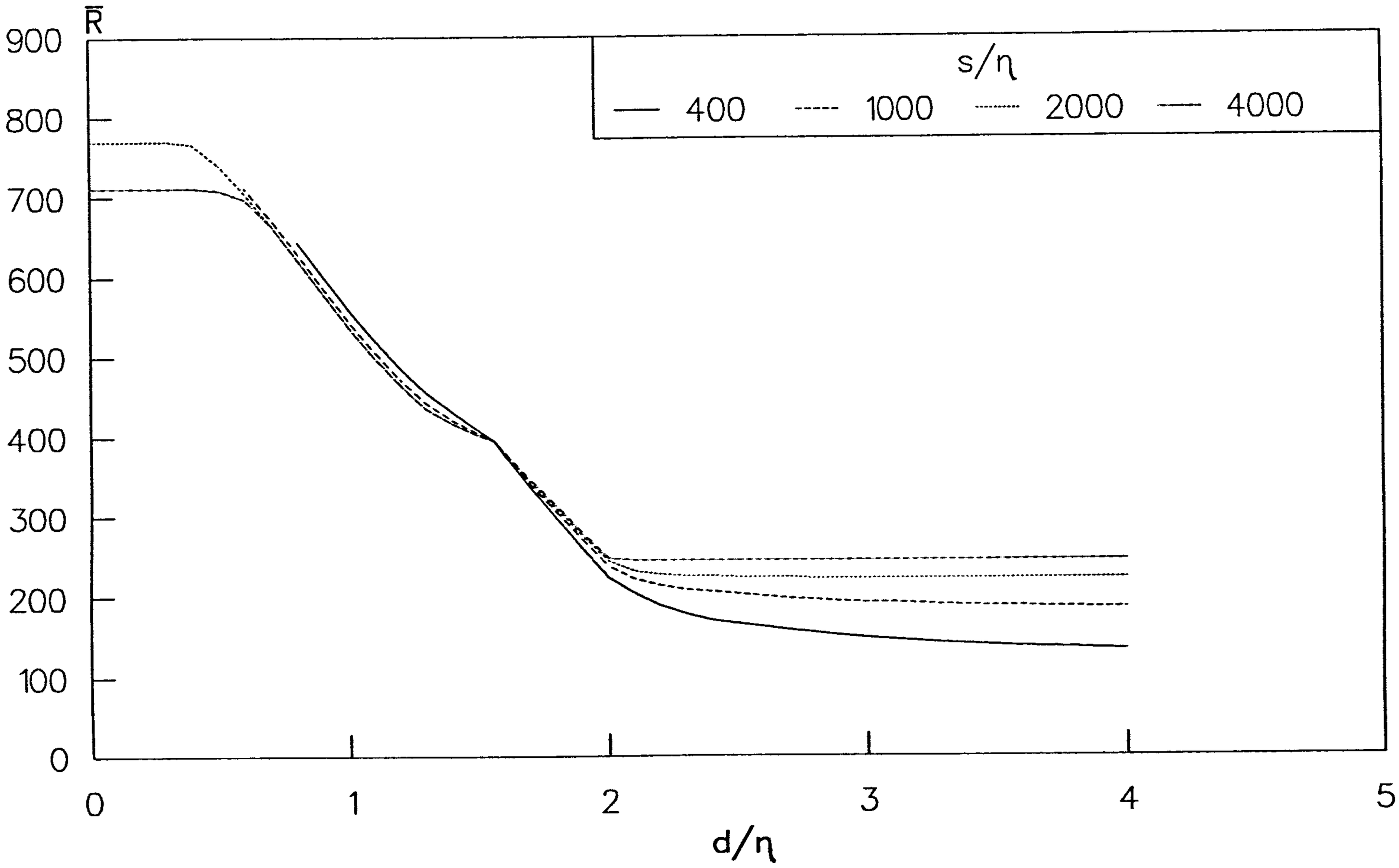

FIG 4.2
2D TRIPS; TRANSITION COMPLETION
POLL'S RESULTS (Poll'78)

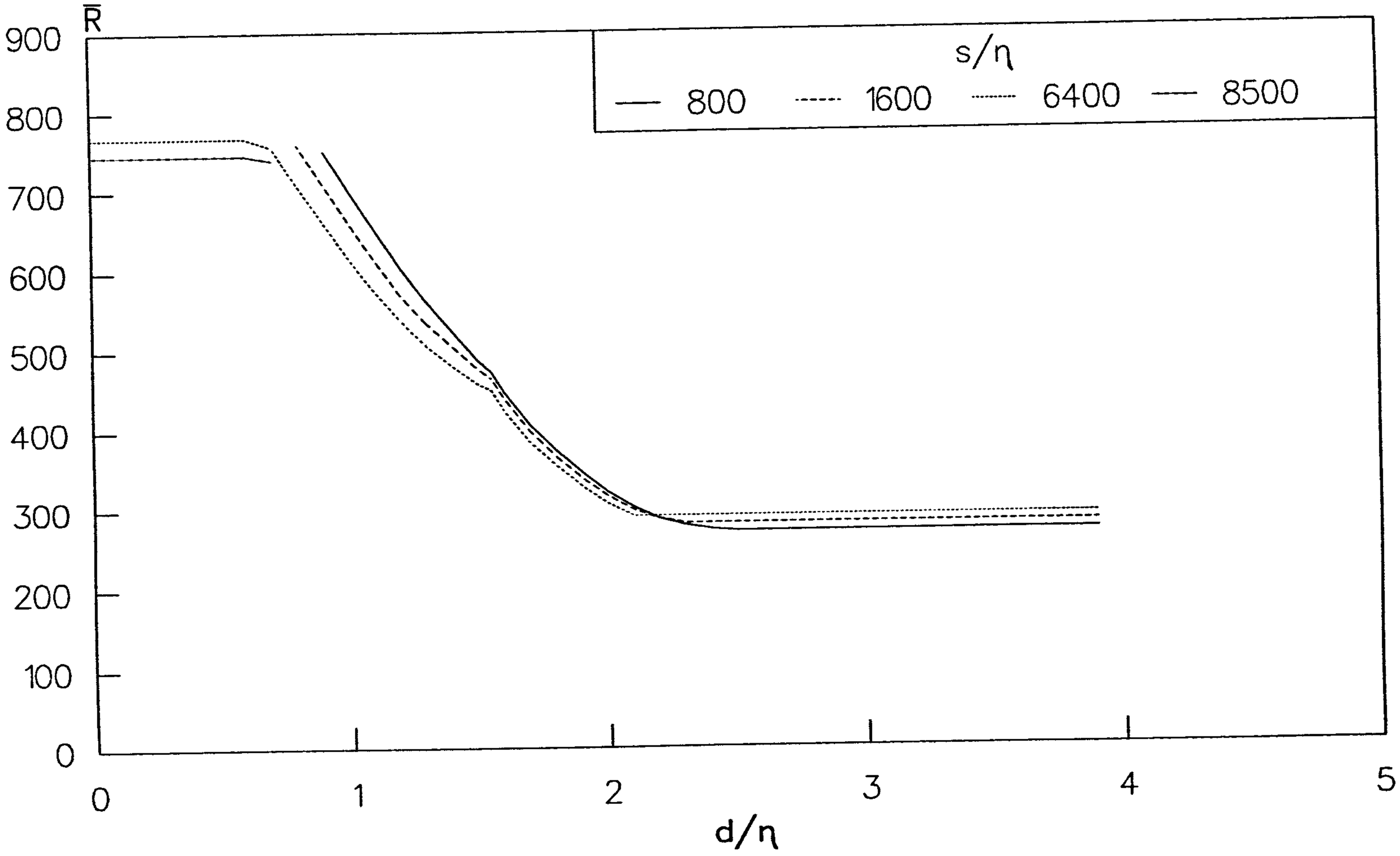

FIG 4.3
PREVIOUS INVESTIGATIONS, FROM POLL('89)
TRANSITION ONSET & COMPLETION AT TRIP

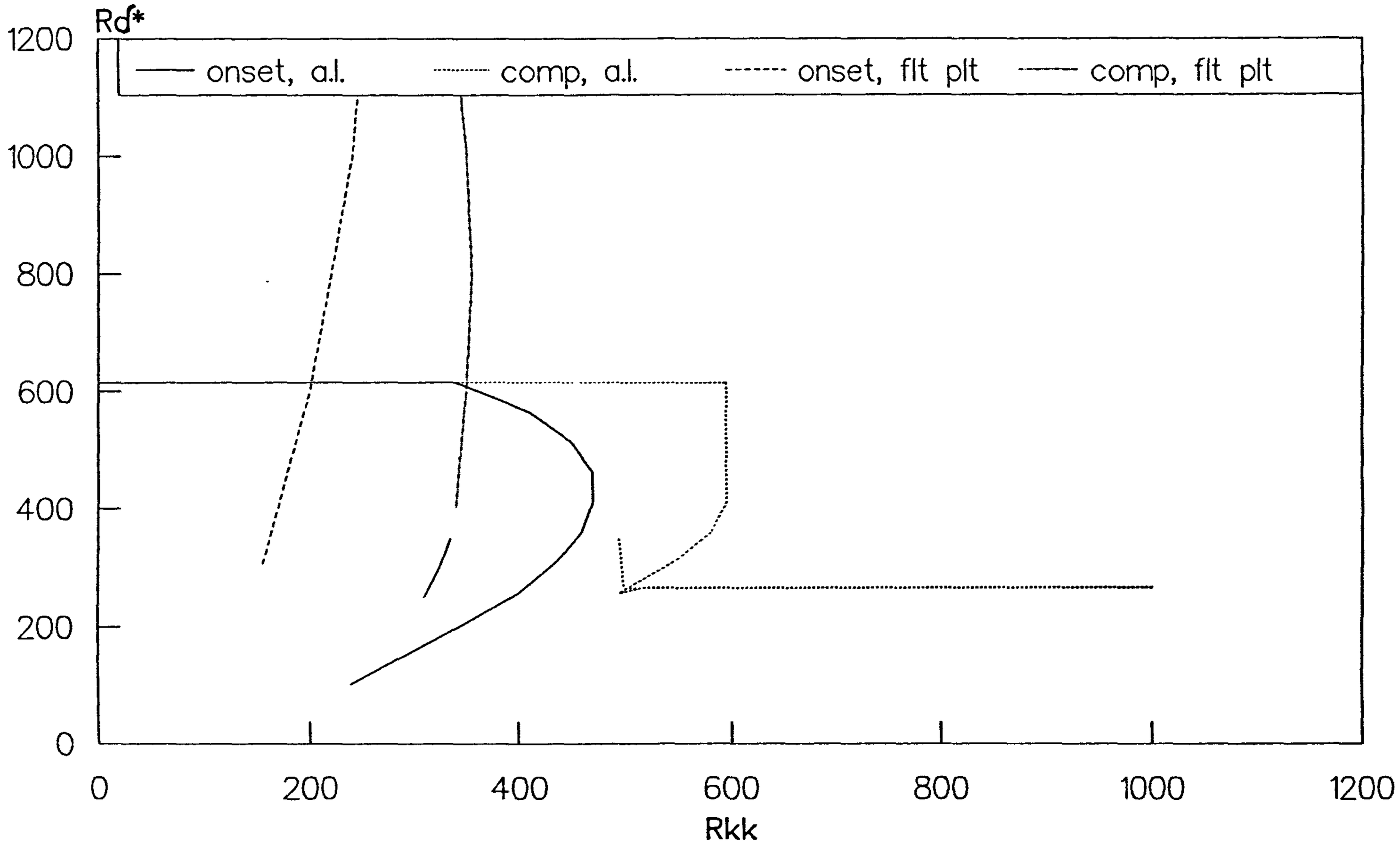

FIG 4.4
CHANGE IN ATTACHMENT LINE STATIC PRESSURE
DUE TO PRESENCE OF LARGE 2D TRIP

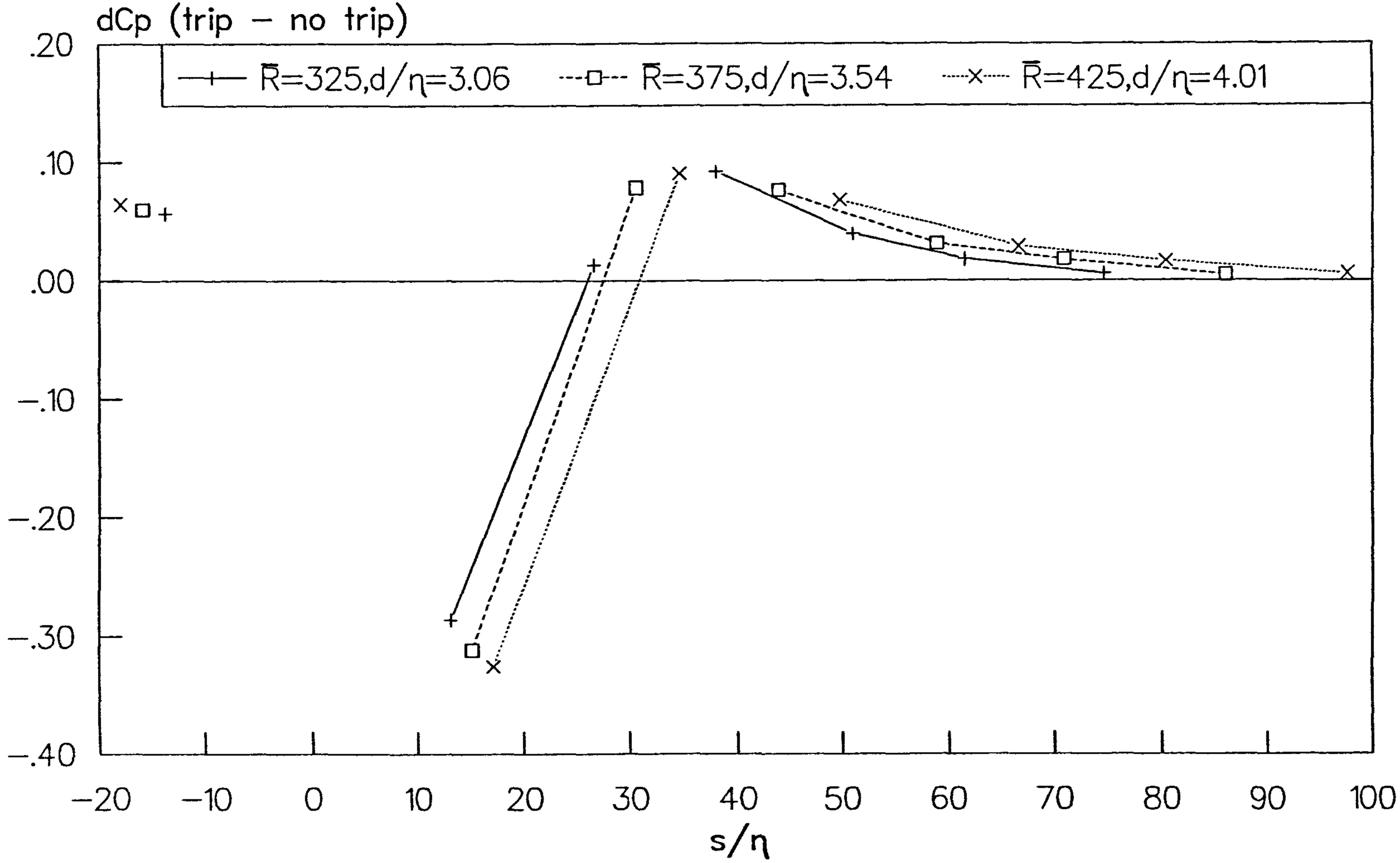

FIG 4.5
REATTACHMENT DISTANCE DOWNSTREAM OF 2D TRIP
Rd* IN RANGE 333 TO 575

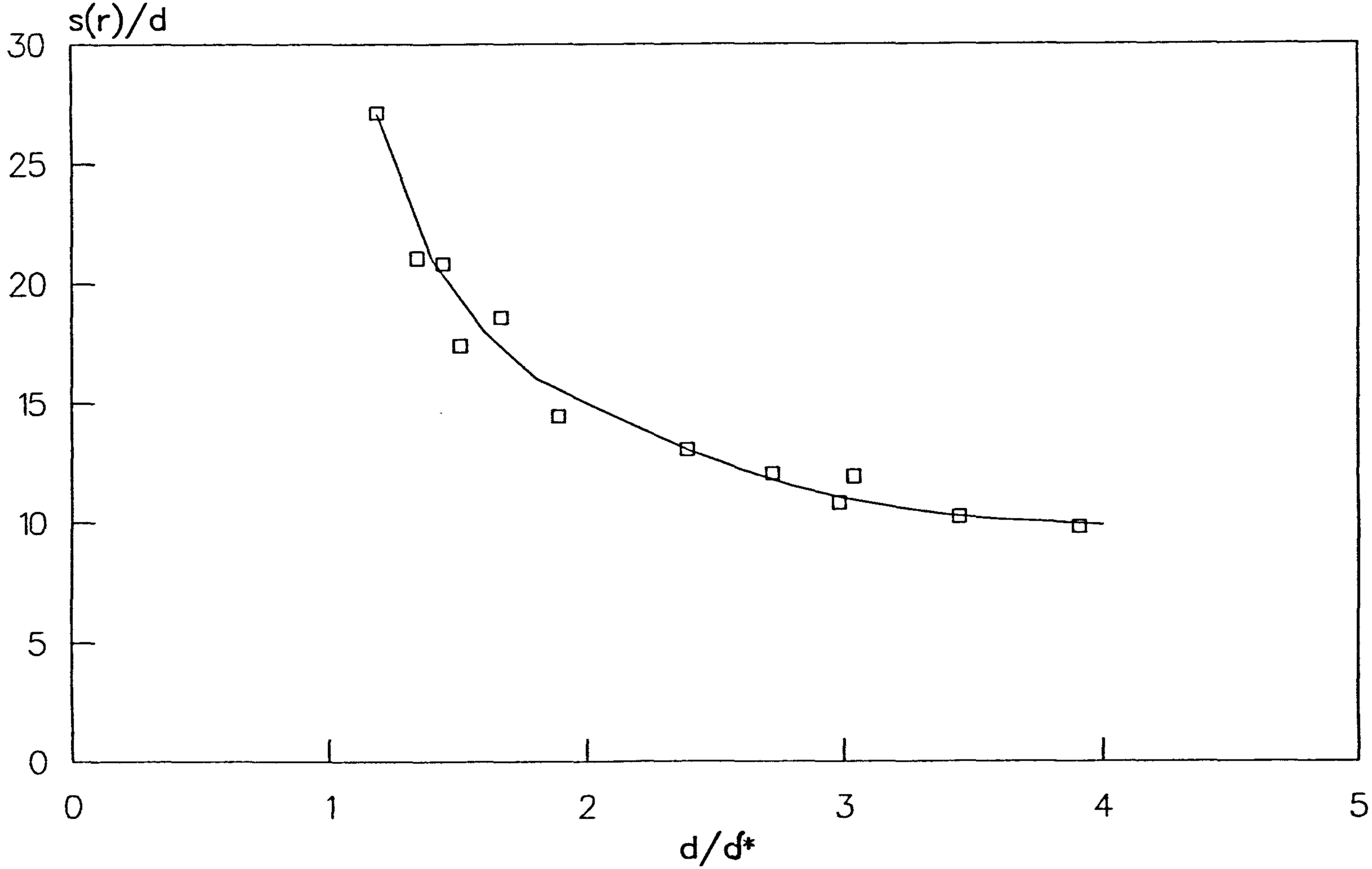

FIG 4.6
REATTACHMENT DISTANCE DOWNSTREAM OF 2D TRIP
FLAT PLATE, FROM GIBBINGS '86a

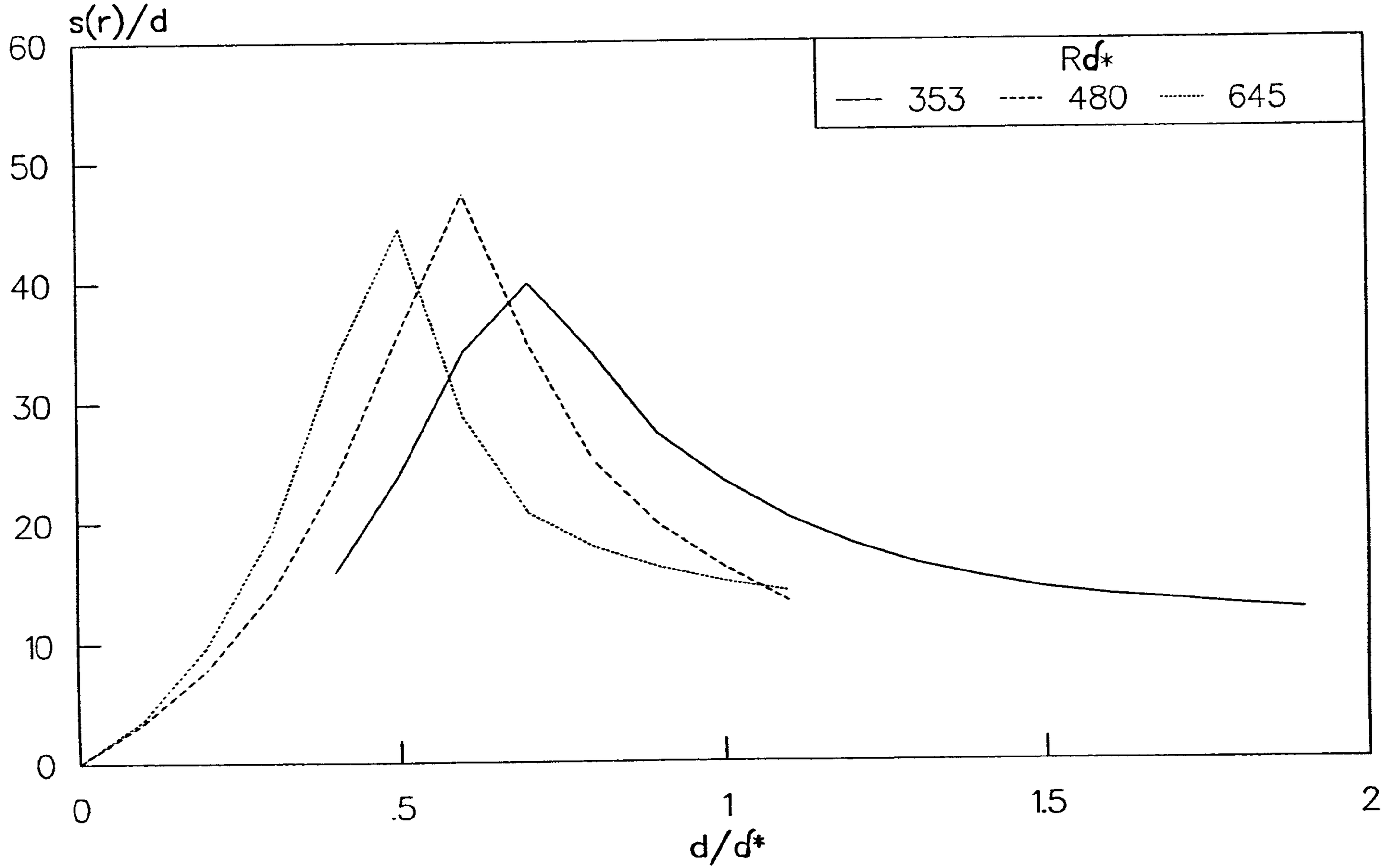

FIG 4.7
APPROX. VELOCITY PROFILES DOWNSTREAM OF 2D TRIP
$\bar{R} = 560$, $d/\eta = 3.12$

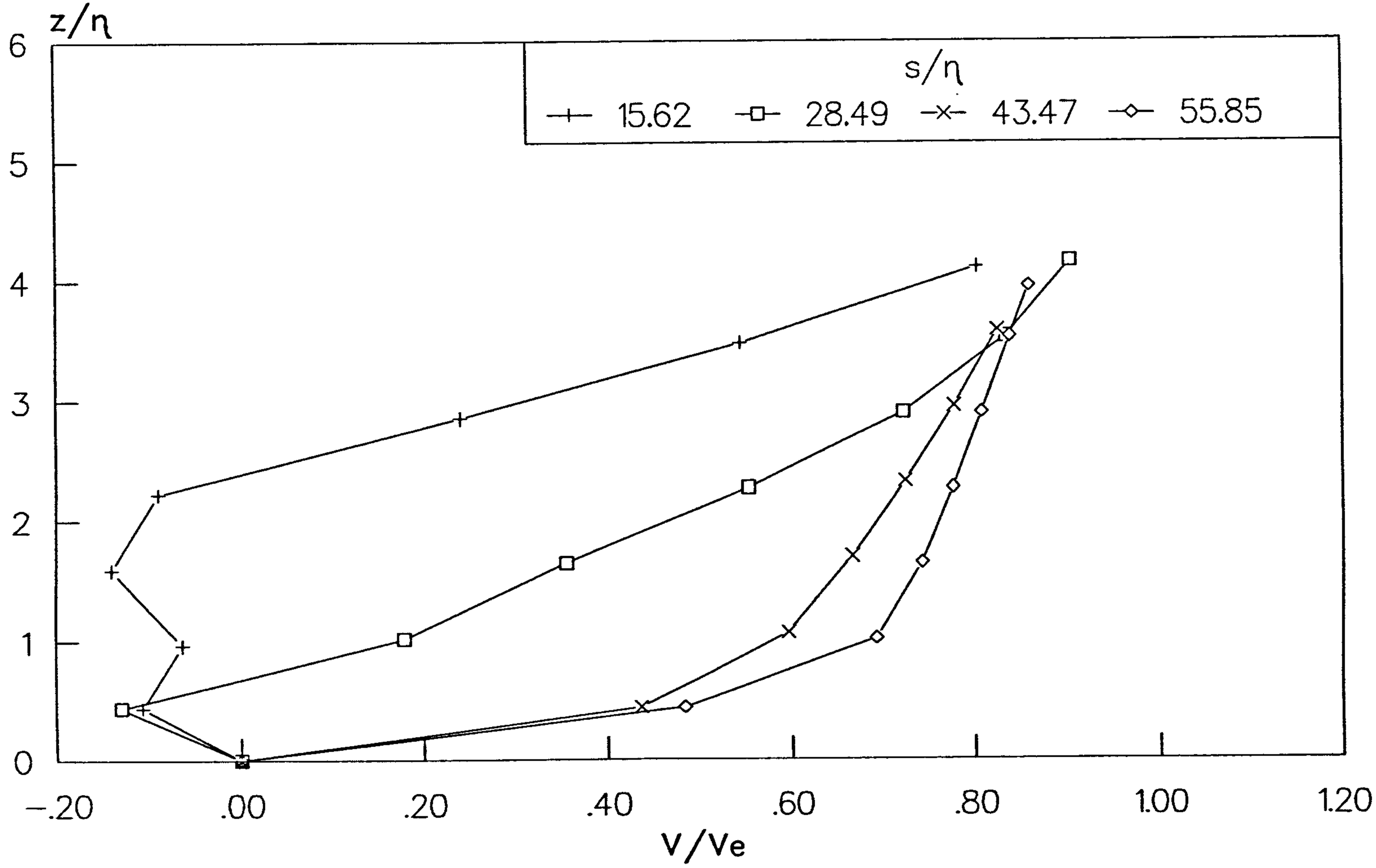

FIG 4.8
2D TRIPS
TRANSITION ONSET

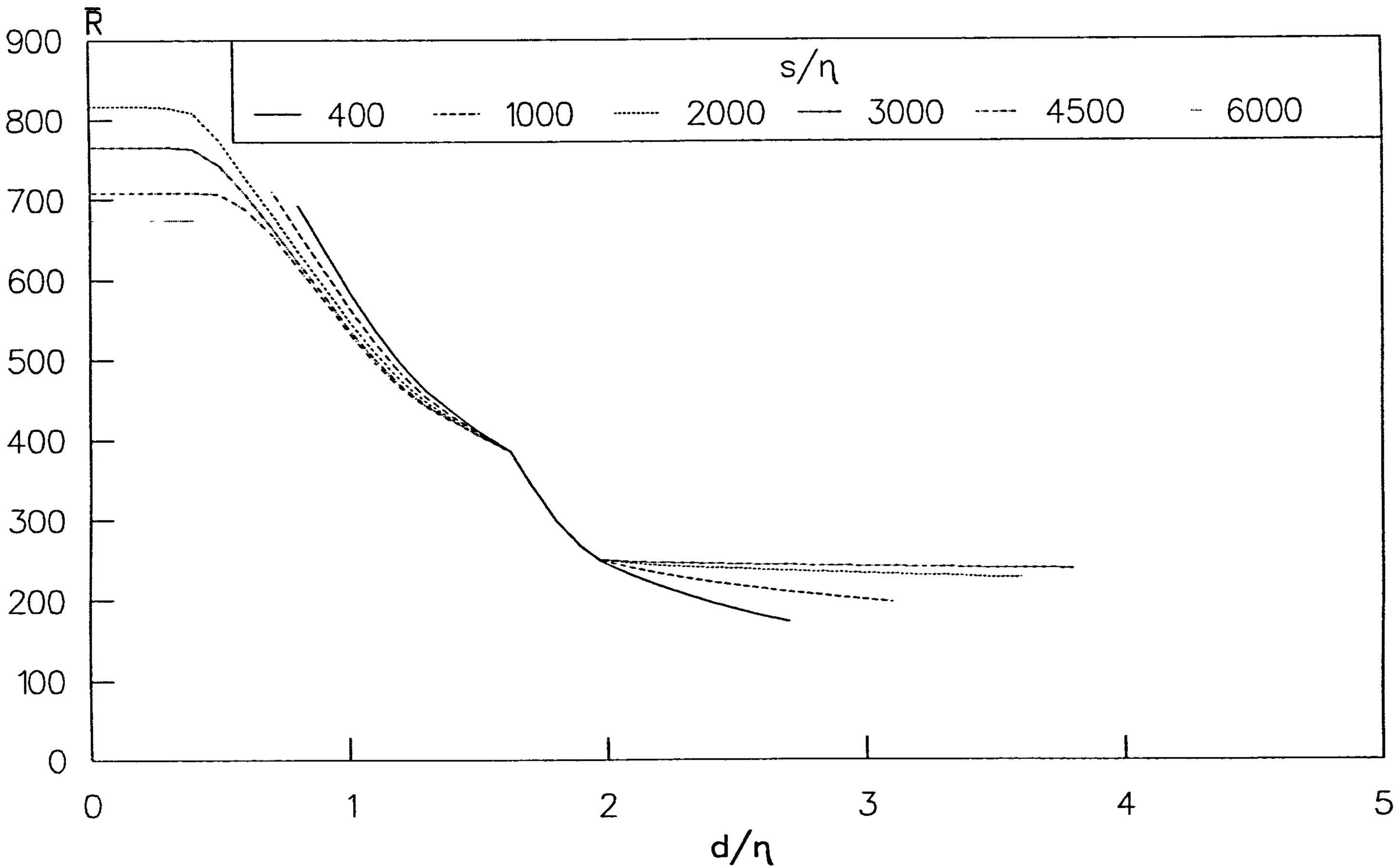

FIG 4.9
2D TRIPS
TRANSITION COMPLETION

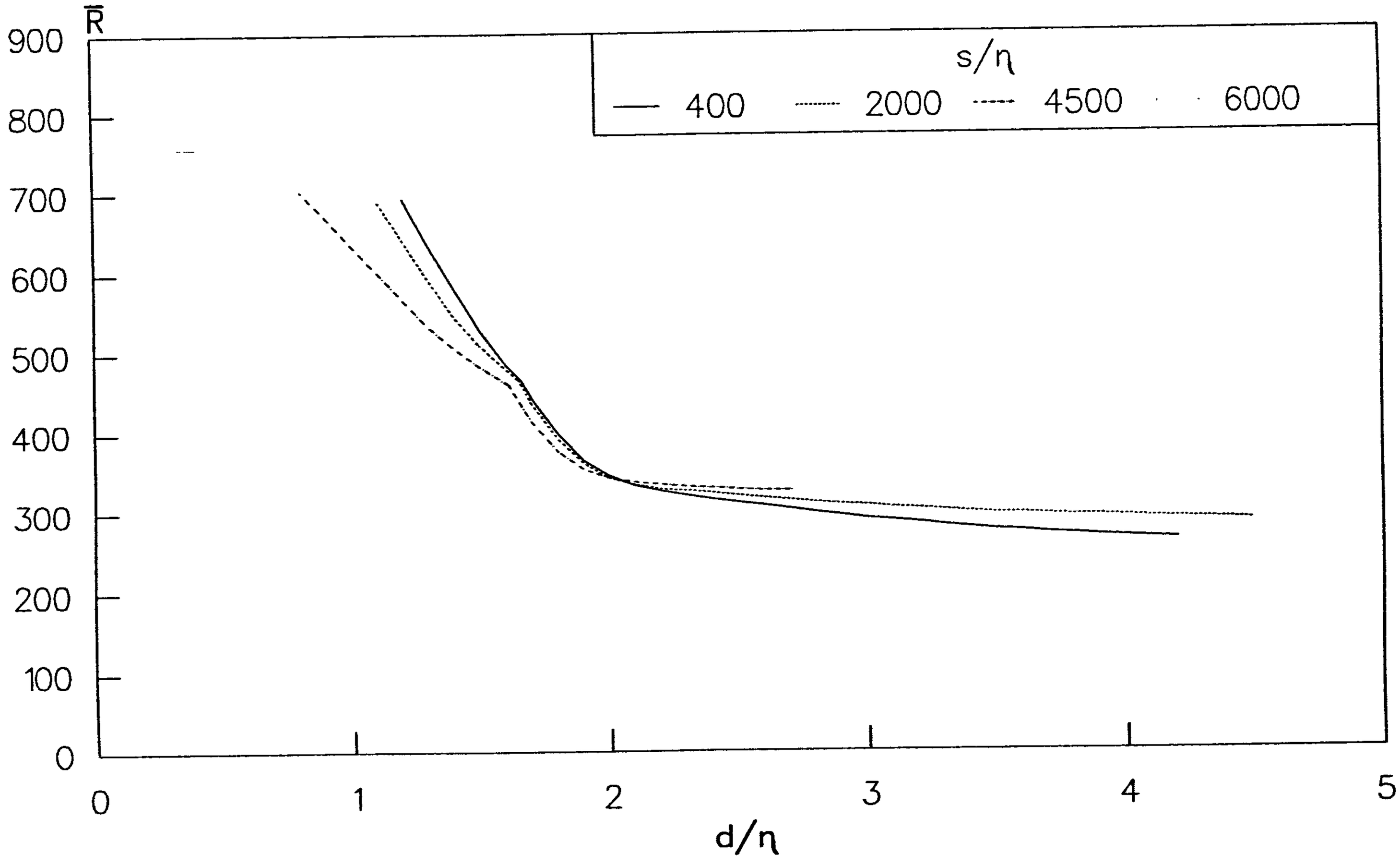

FIG 4.10
INTERPOLATED DATA POINTS, $s/\eta = 2000$
TRANSITION COMPLETION

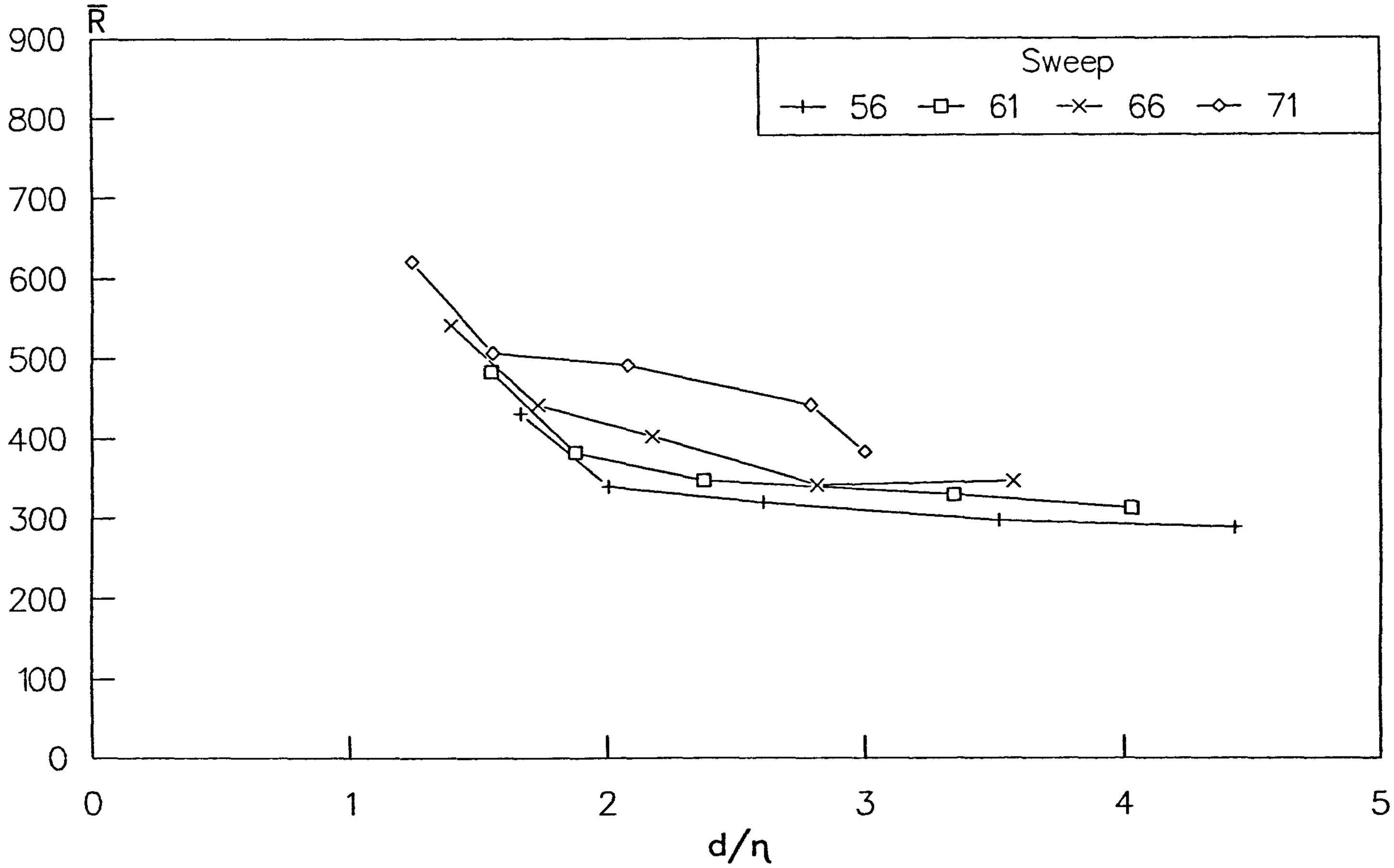

FIG 4.11
TRANSITION IN PRESENCE OF LARGE TRIP
LOWER BOUND FOR TRANSITION TRIPPING

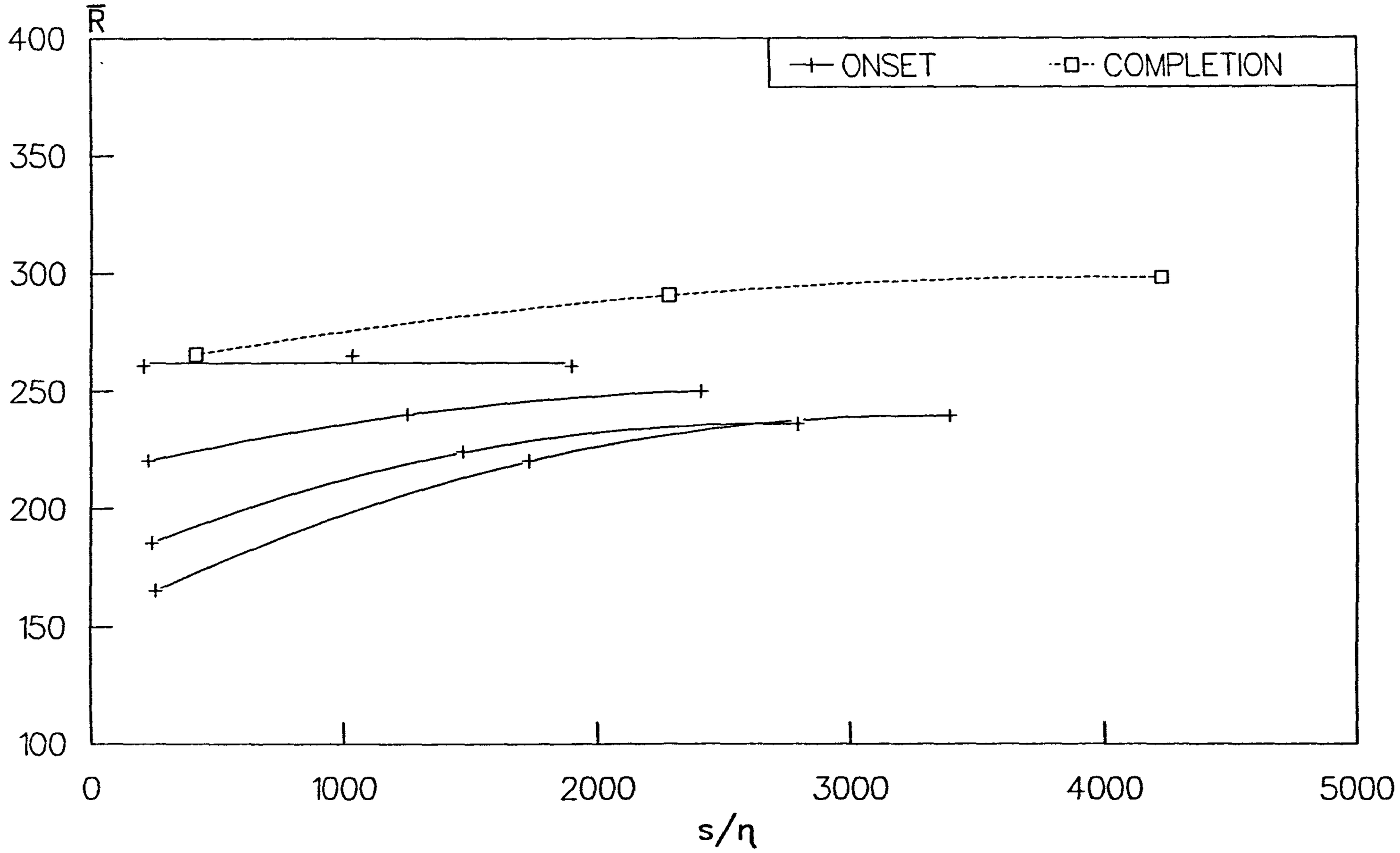

FIG 4.12
TRANSITION IN ABSENCE OF TRIP
UPPER BOUND FOR TRANSITION TRIPPING

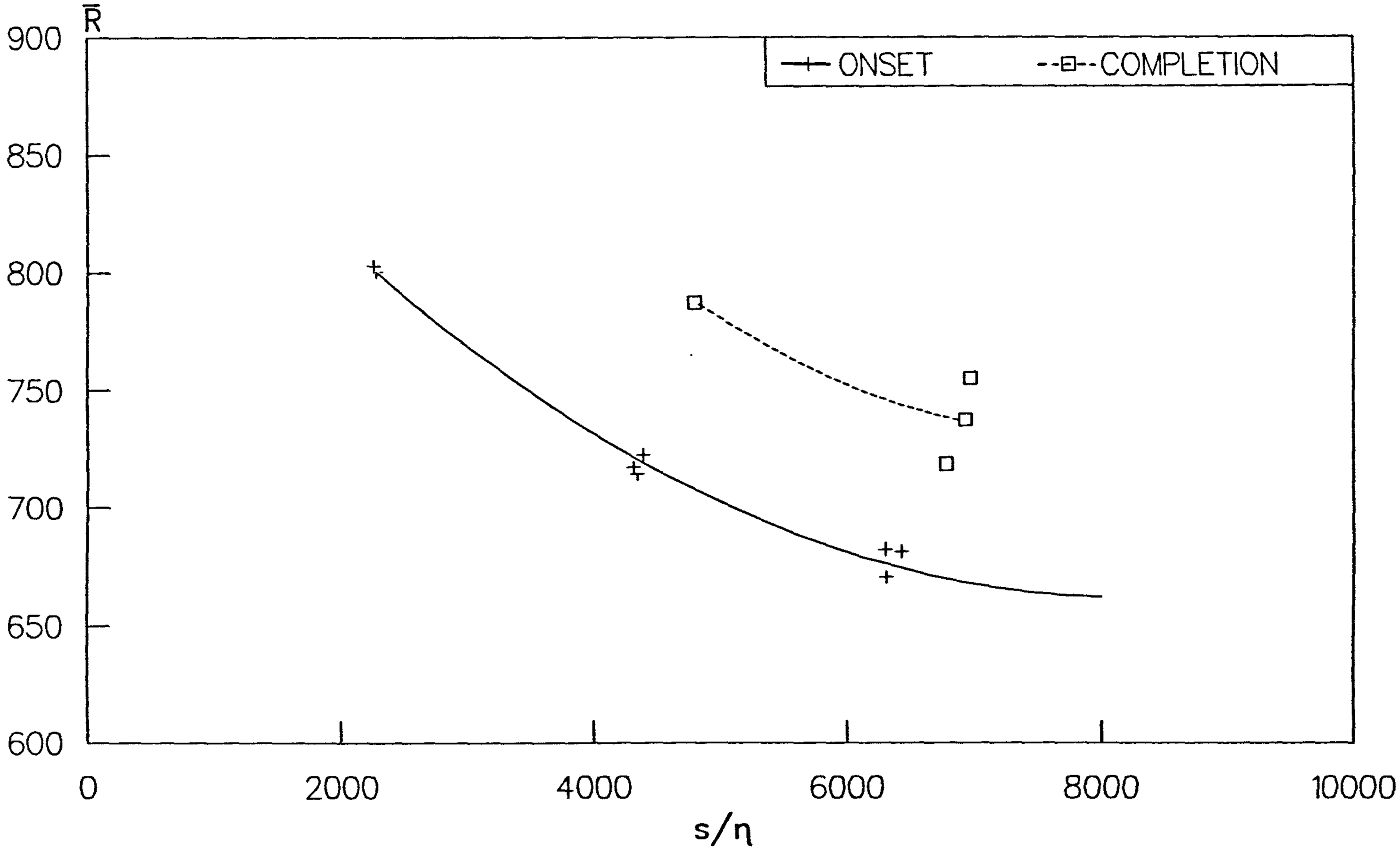

FIG 4.13
TRANSITION IN LIMIT AS s/η TENDS TO ZERO
2D TRIPS

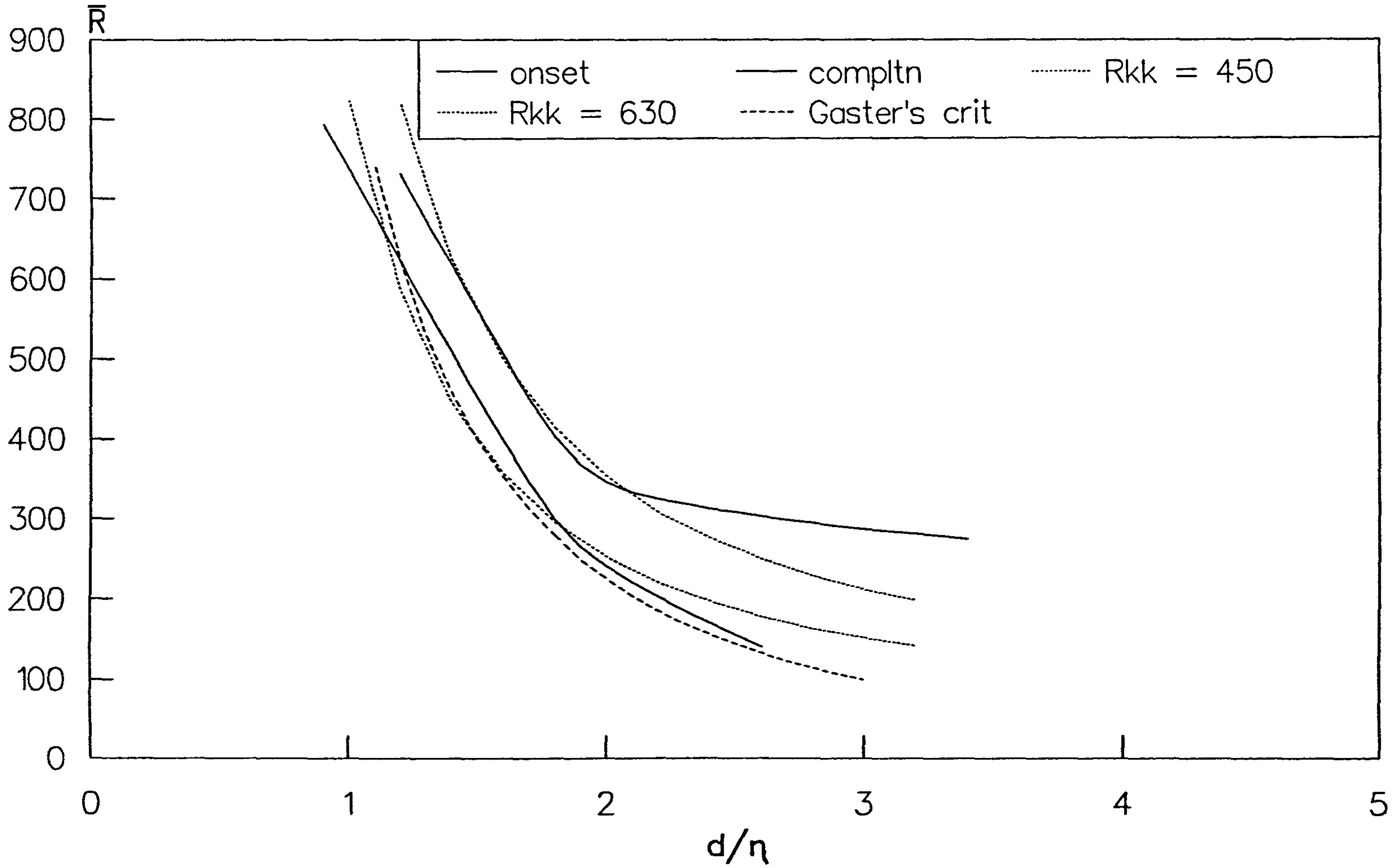

FIG 4.14
TRANSITION IN LIMIT AS s/η TENDS TO INFINITY
2D TRIPS

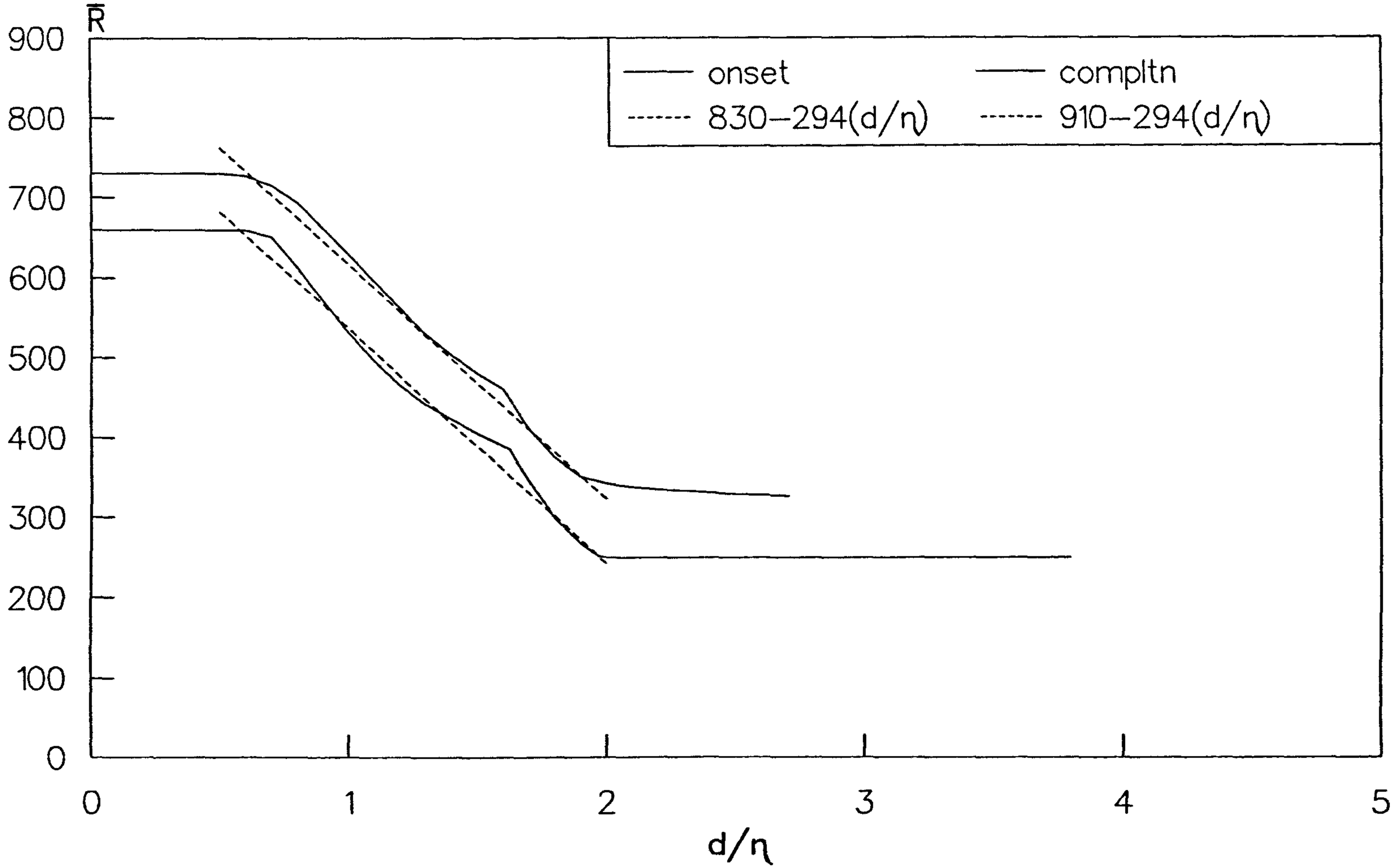

FIG 4.15
2D TRIPS; TRANSITION ONSET & COMPLETION
COMPARISON BETWEEN PRESENT AND POLL'S RESULTS

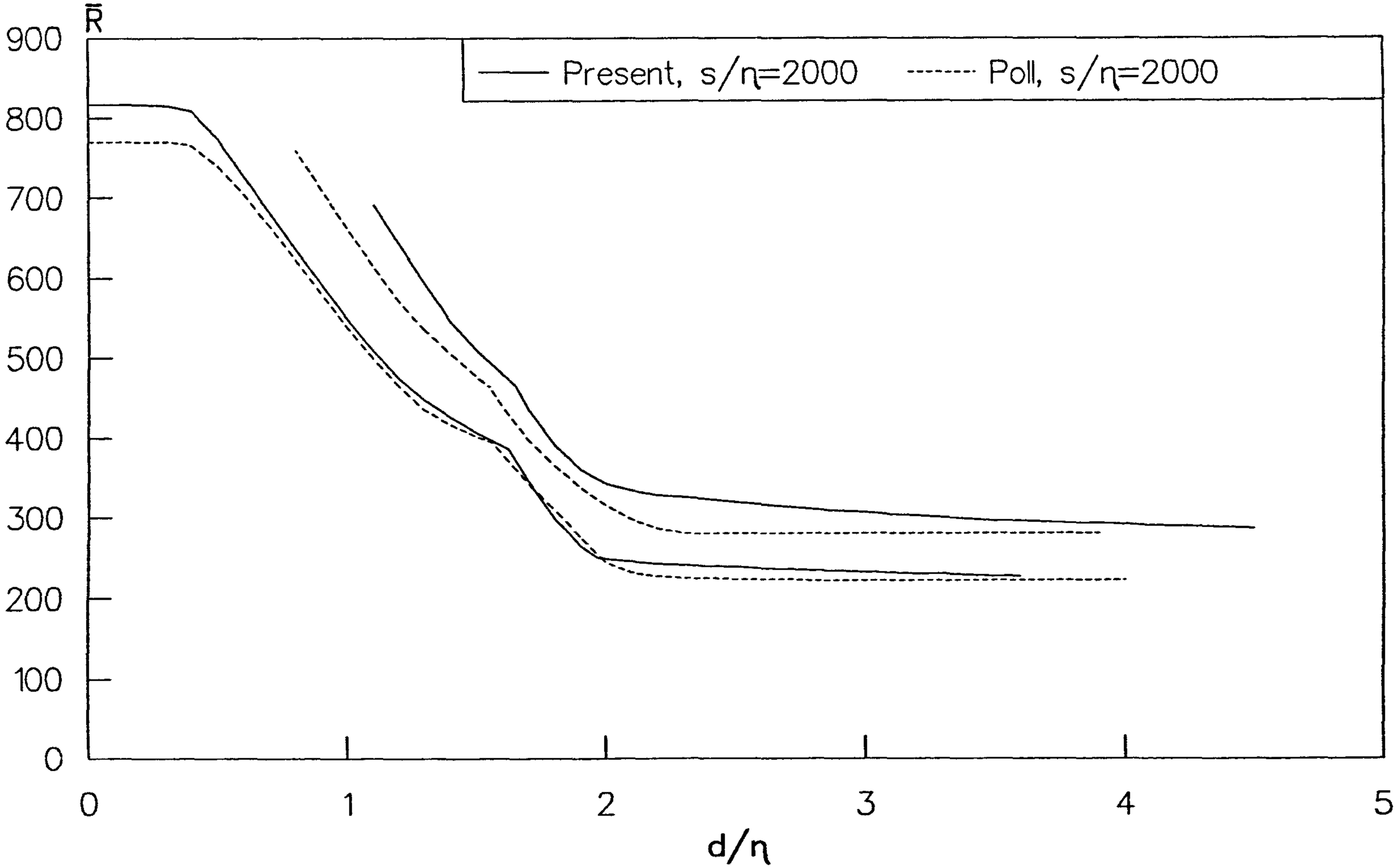

FIG 4.16
PRESENT & PREVIOUS INVESTIGATIONS
TRANSITION ONSET AT TRIP

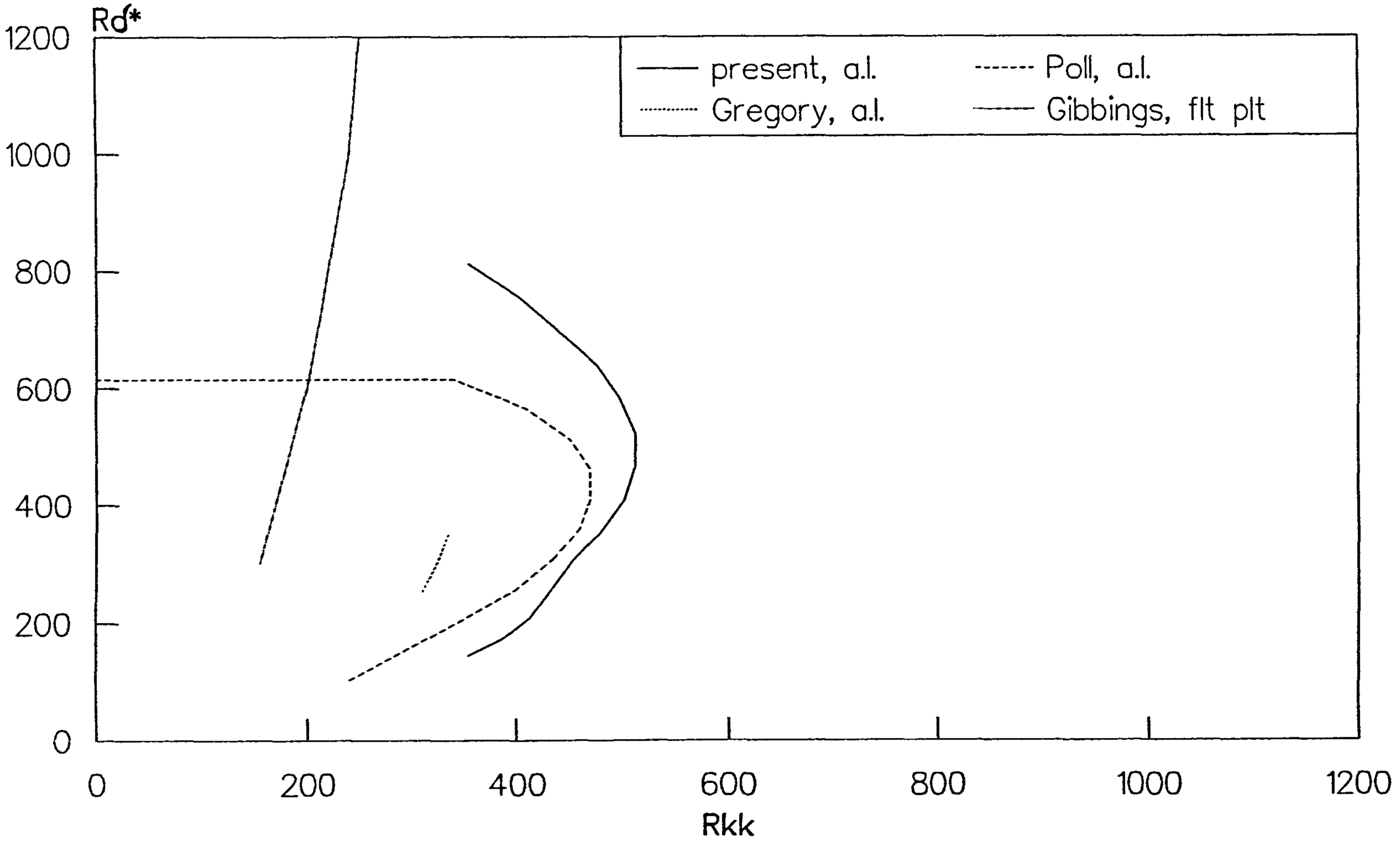

FIG 4.17
PRESENT & PREVIOUS INVESTIGATIONS
TRANSITION COMPLETION AT TRIP

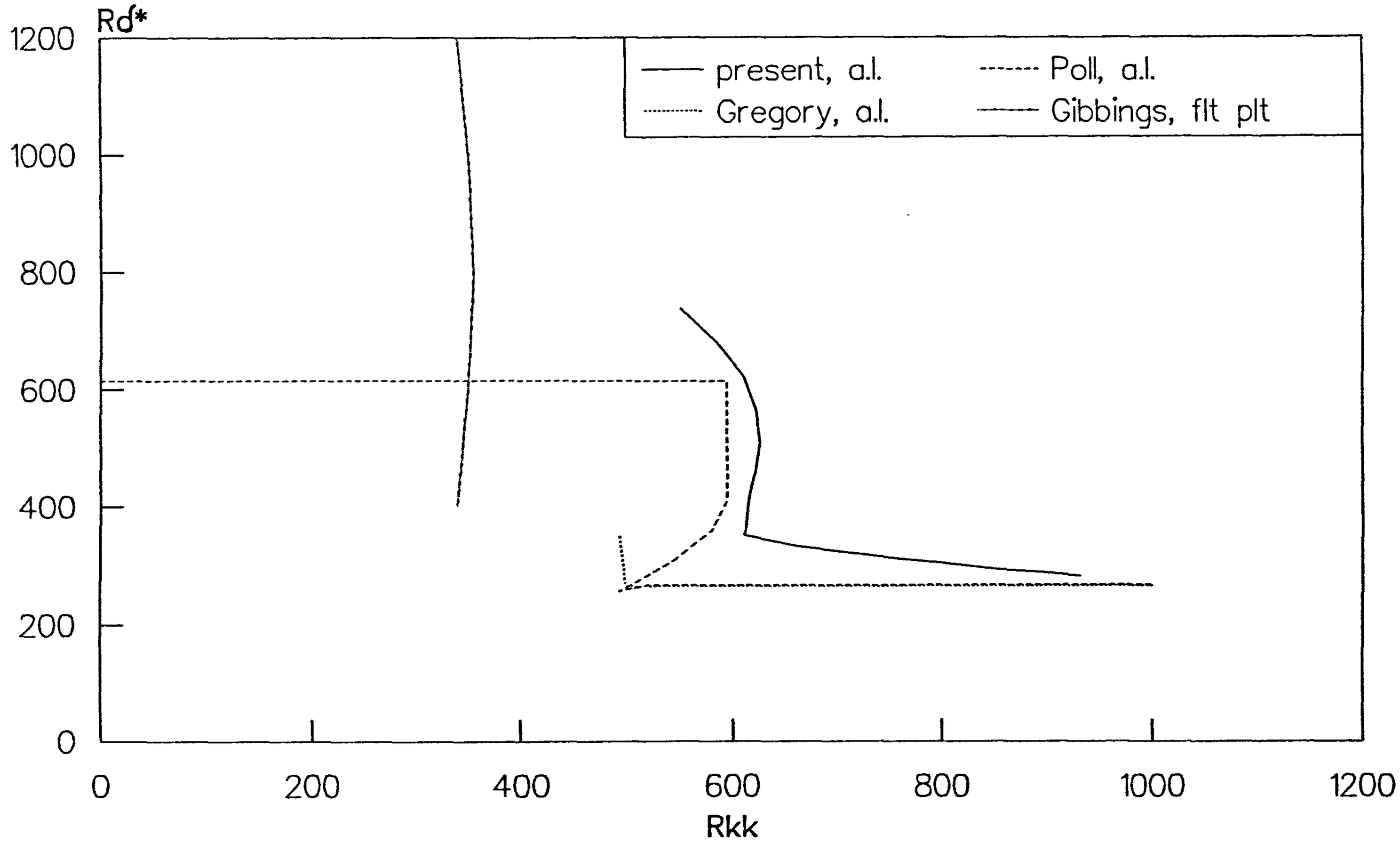

FIG 4.18a
INTERMITTENCY DISTRIBUTION
NATURAL TRANSITION ; s = 1.8m

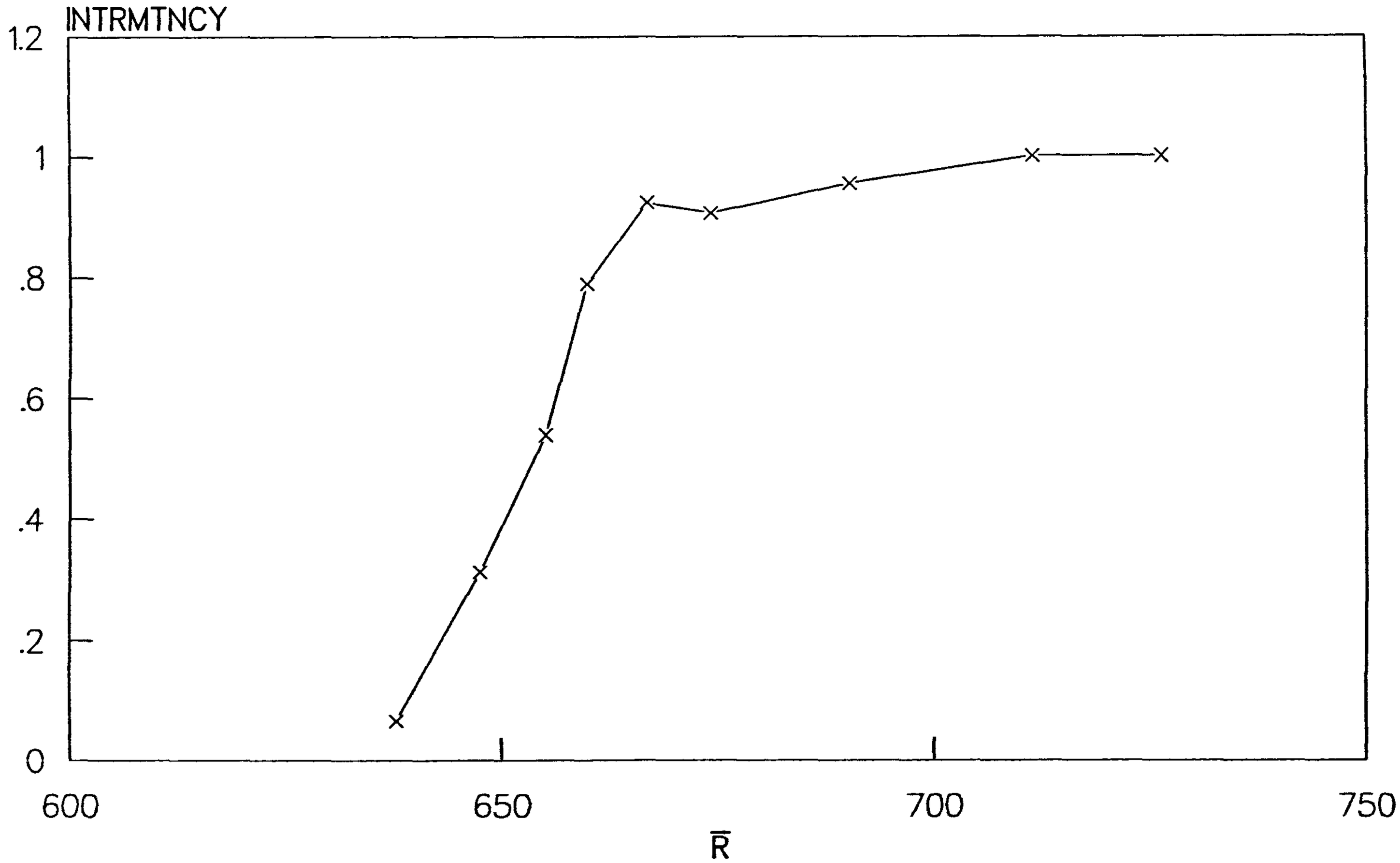

FIG 4:18b
INTERMITTENCY DISTRIBUTIONS
2D TRIPS

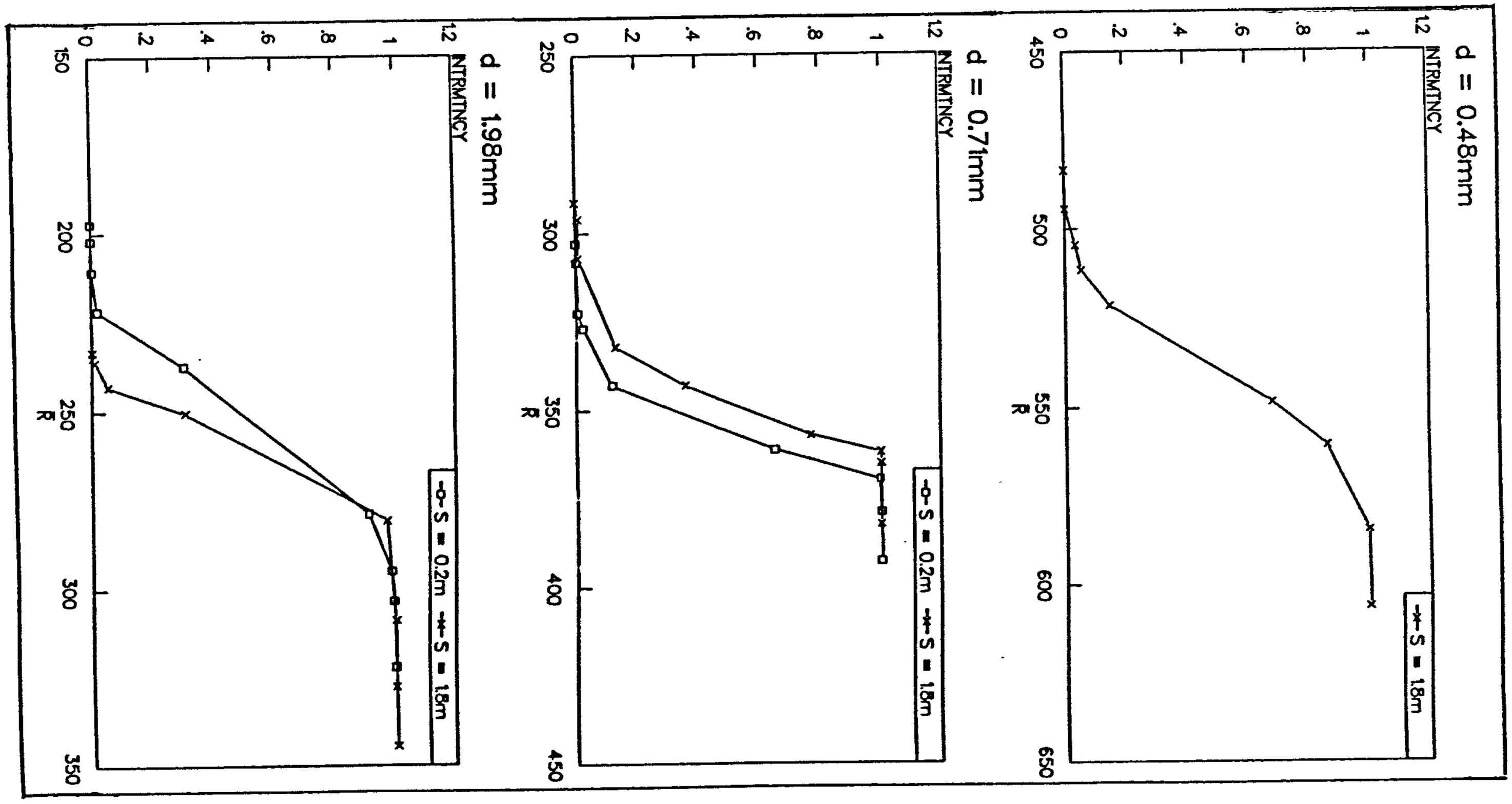

FIG 4.19a
GENERAL INTERMITTENCY DISTRIBUTION
2D TRIPS

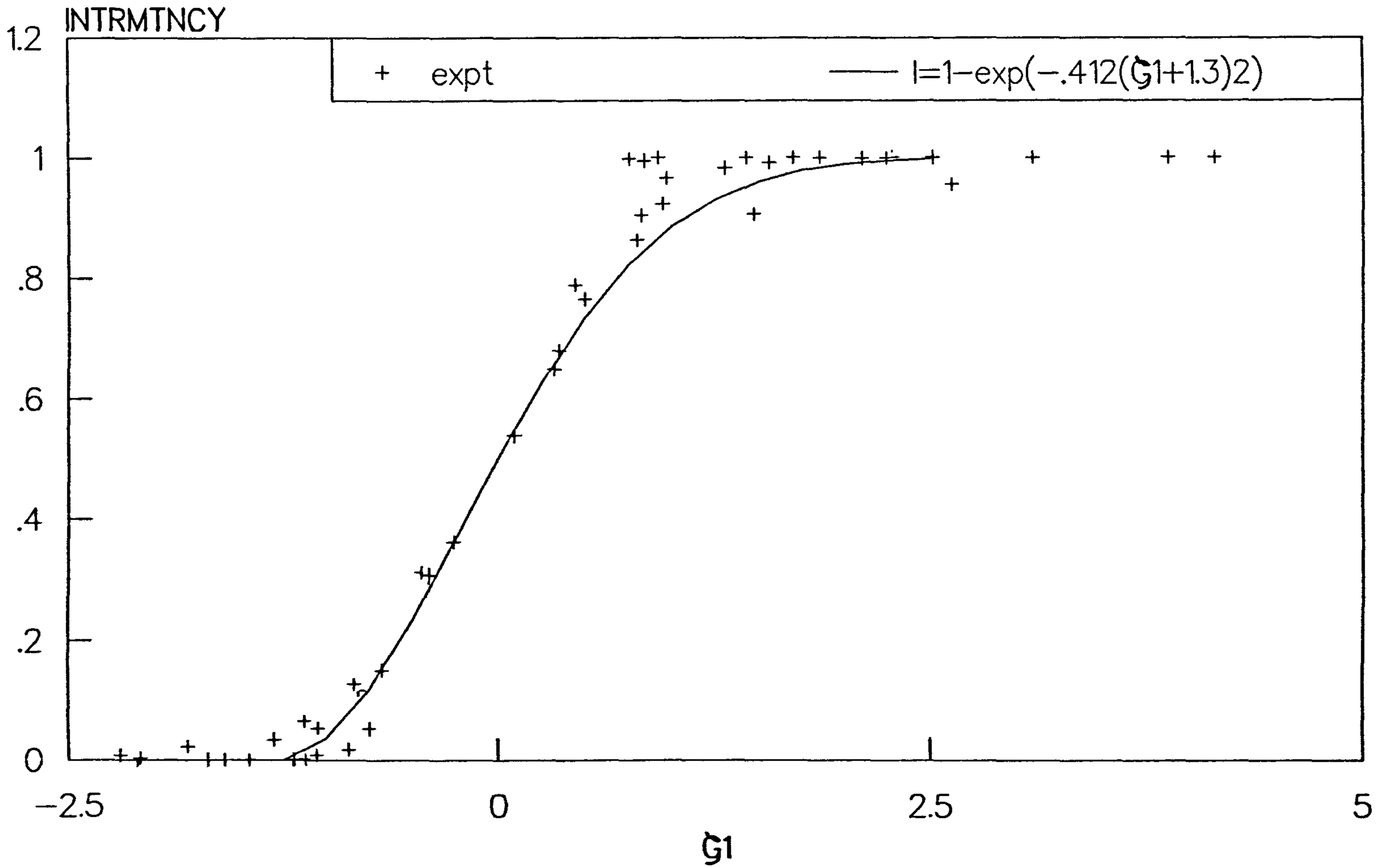

FIG 4.19b
GENERAL INTERMITTENCY DISTRIBUTION
2D TRIPS

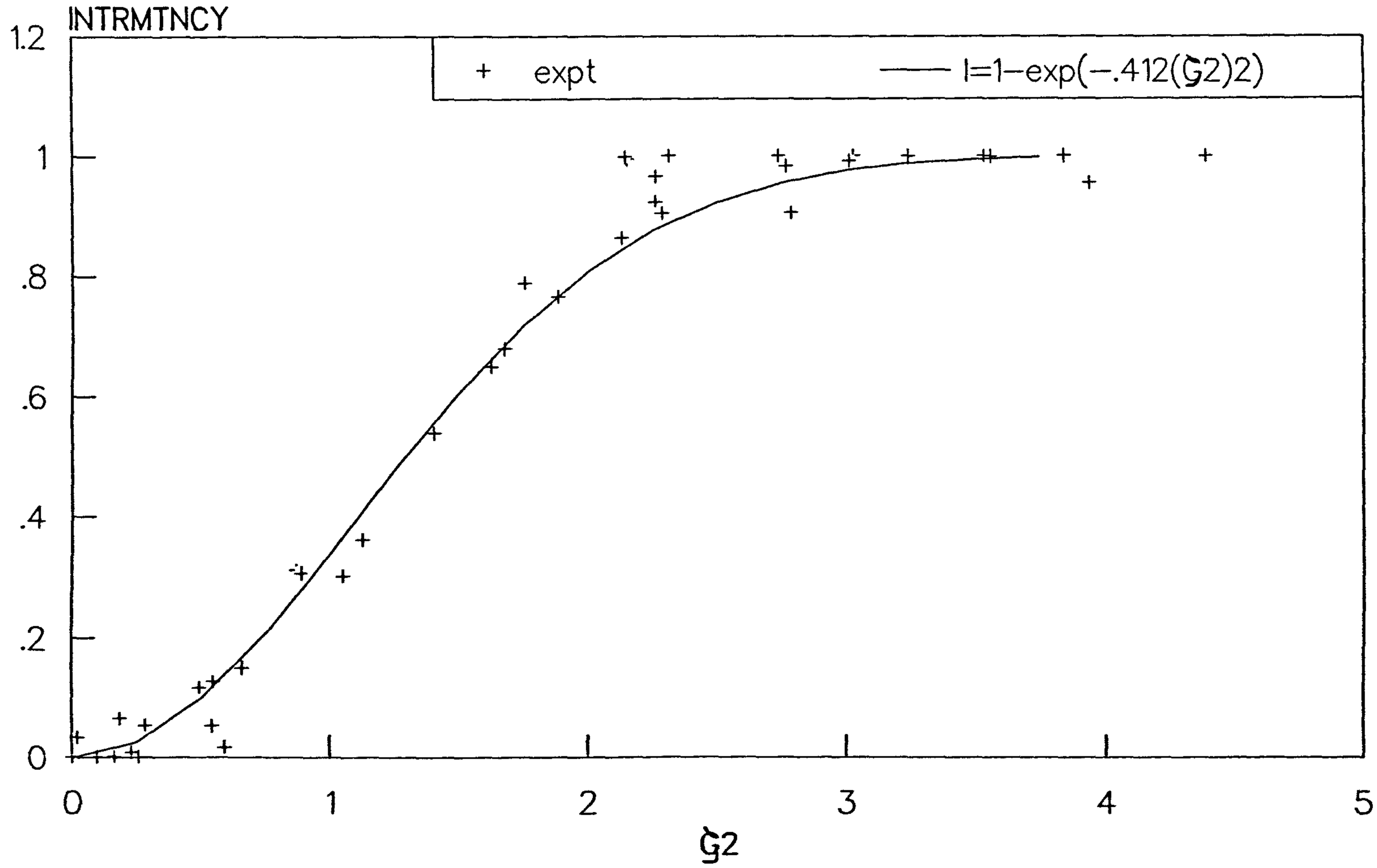

FIG 4.20
INTERMITTENCY DISTRIBUTIONS FOR GROSS DISTURBANCES
STEWART'S EQUATION AND MEASURED DATA
$s/\eta > 2000$

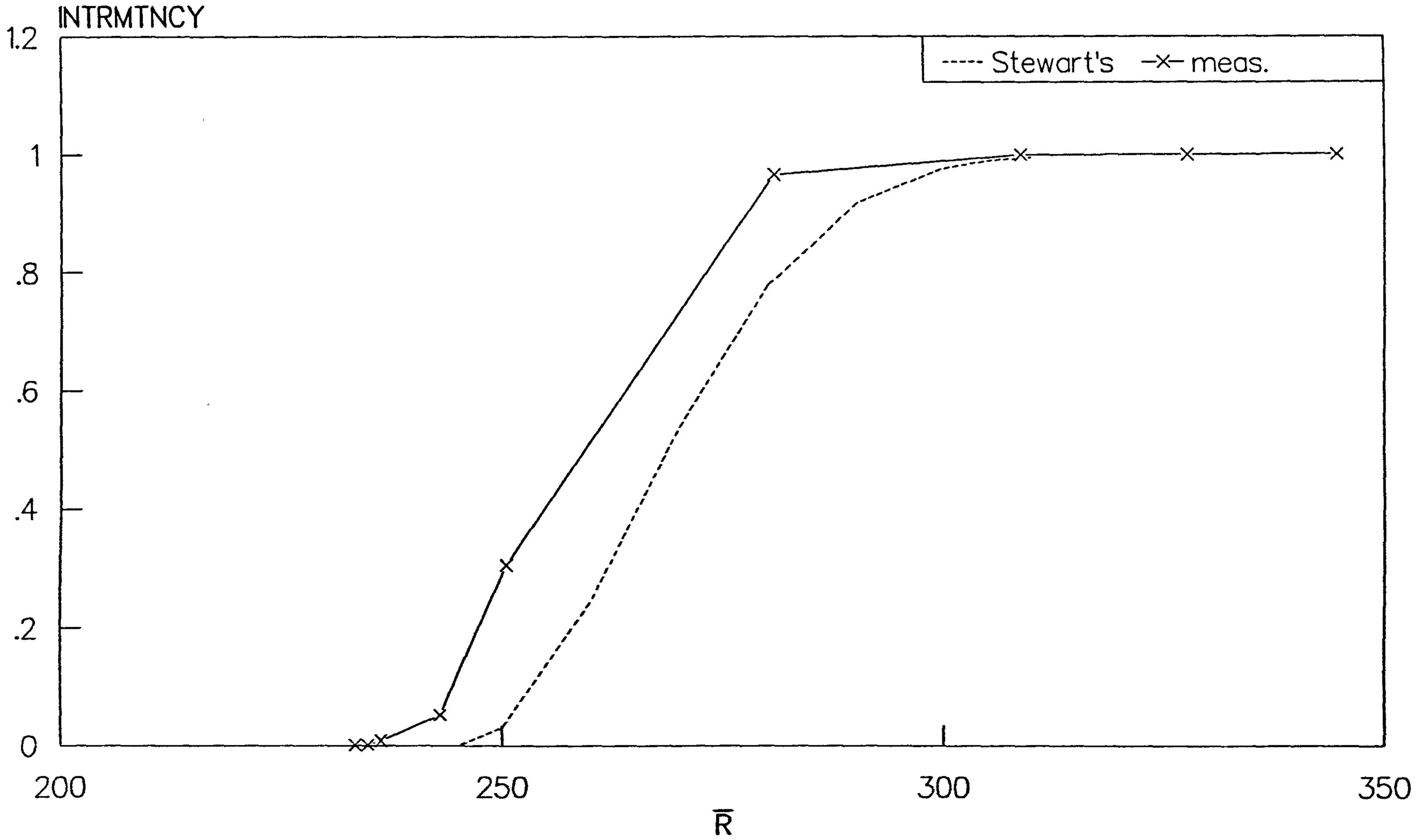

FIG 4.21a
FREQUENCY SPECTRA
TRANSITION ONSET

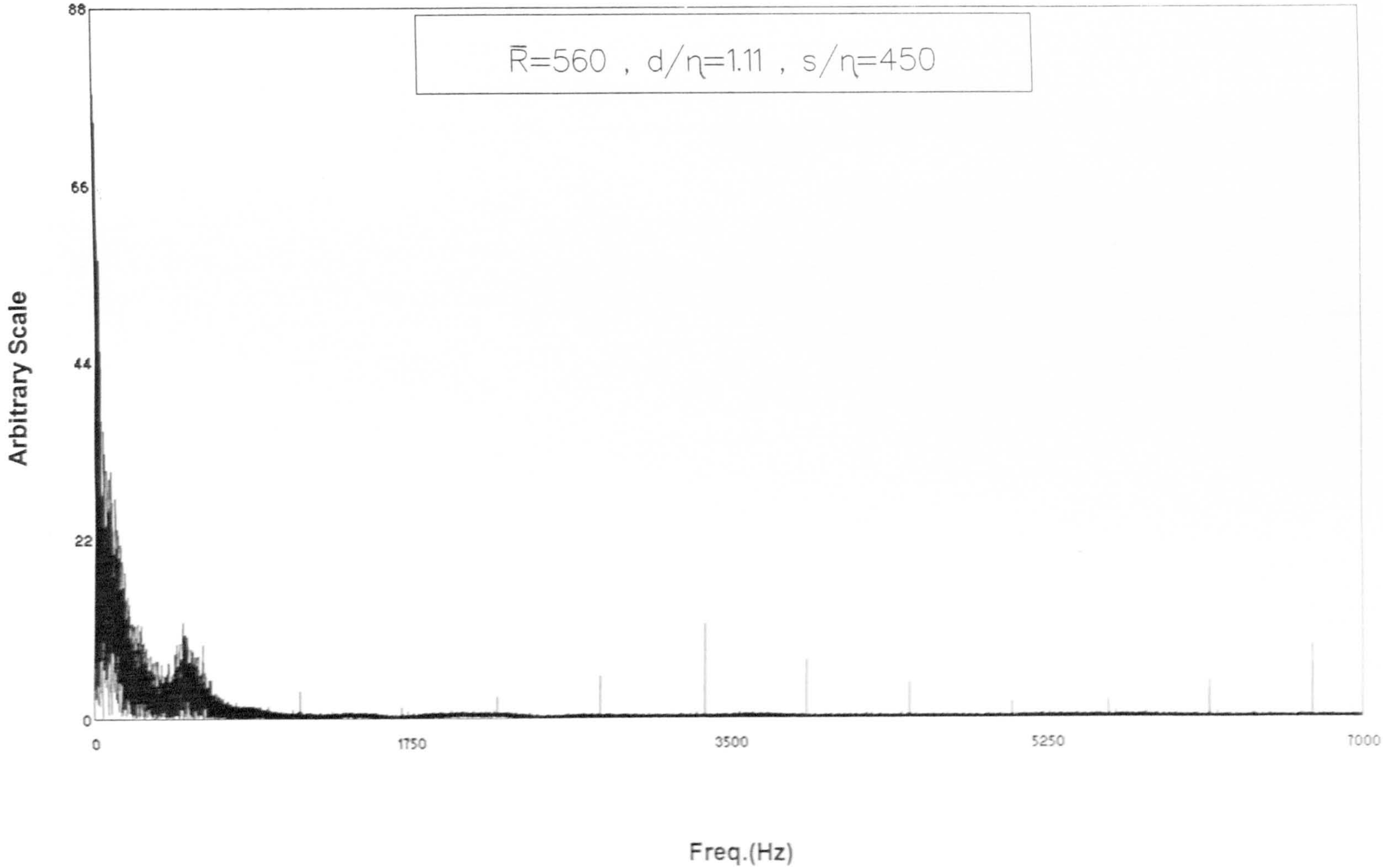

FIG 4.21b
FREQUENCY SPECTRA
TRANSITION ONSET

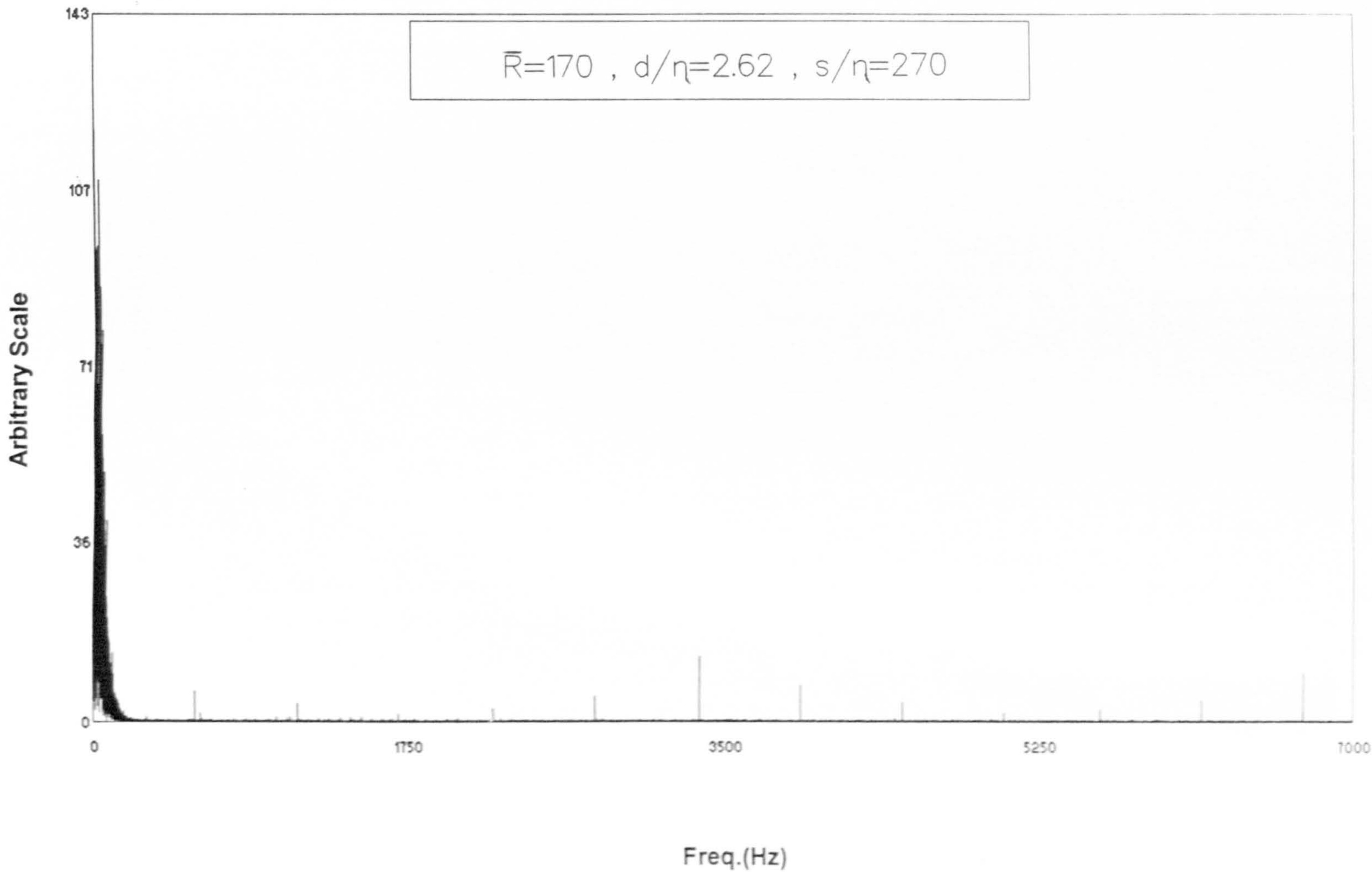

FIG 4.21c
FREQUENCY SPECTRA
FULLY TURBULENT

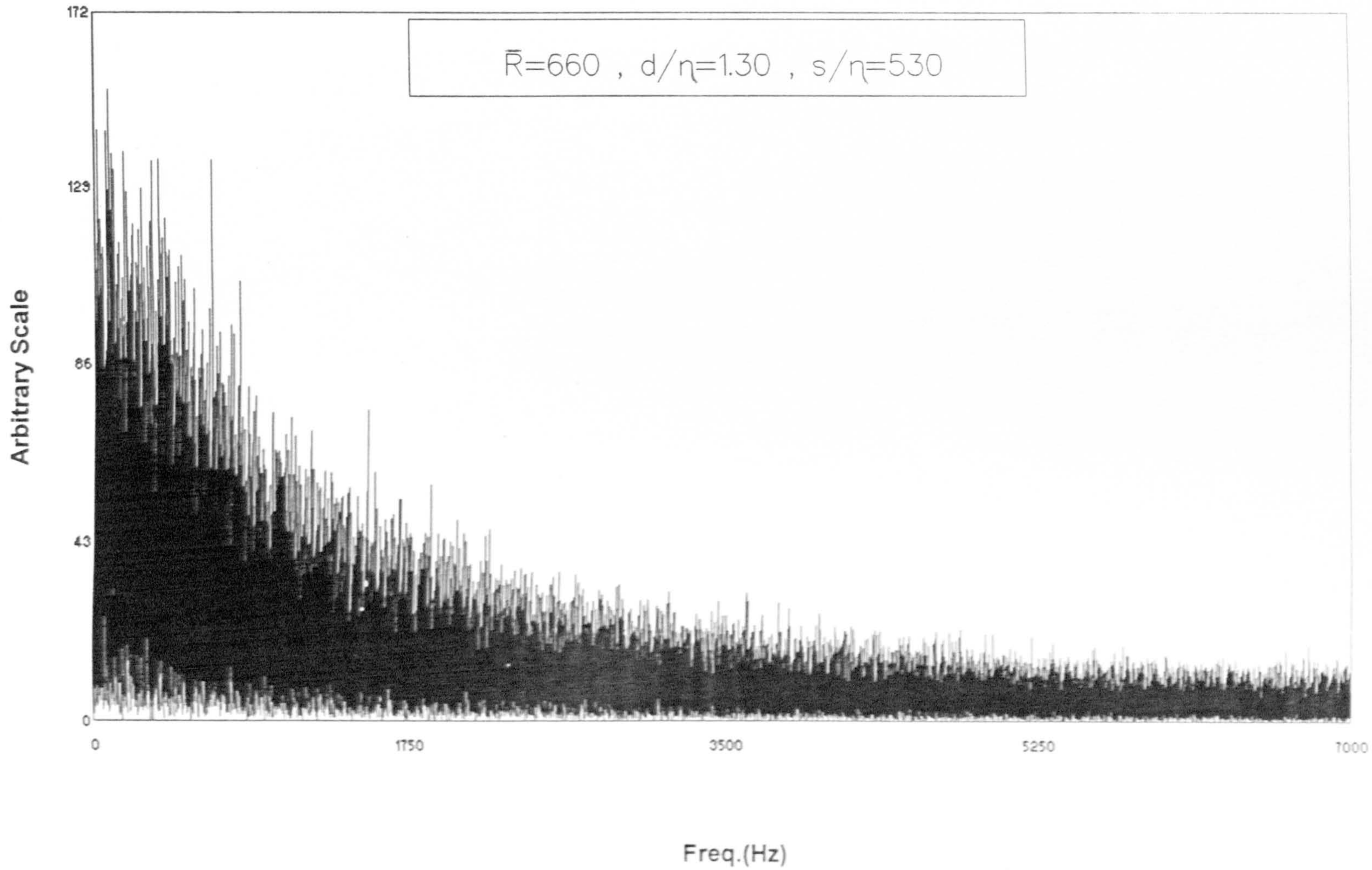

FIG 5.1a
PREVIOUS INVESTIGATIONS, FROM POLL('89)
TRANSITION ONSET AT TRIP

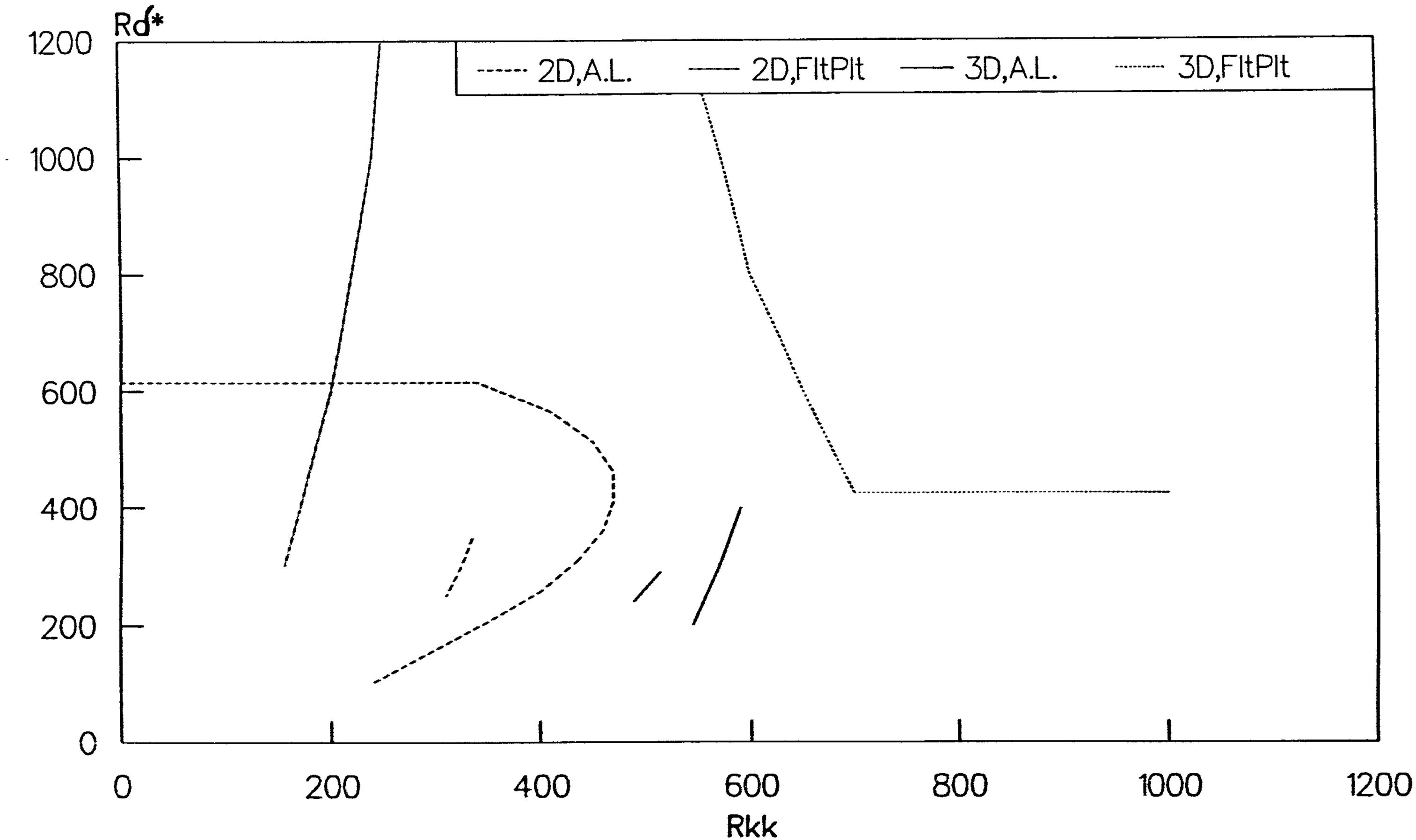

FIG 5.1b
PREVIOUS INVESTIGATIONS, FROM POLL('89)
TRANSITION COMPLETION AT TRIP

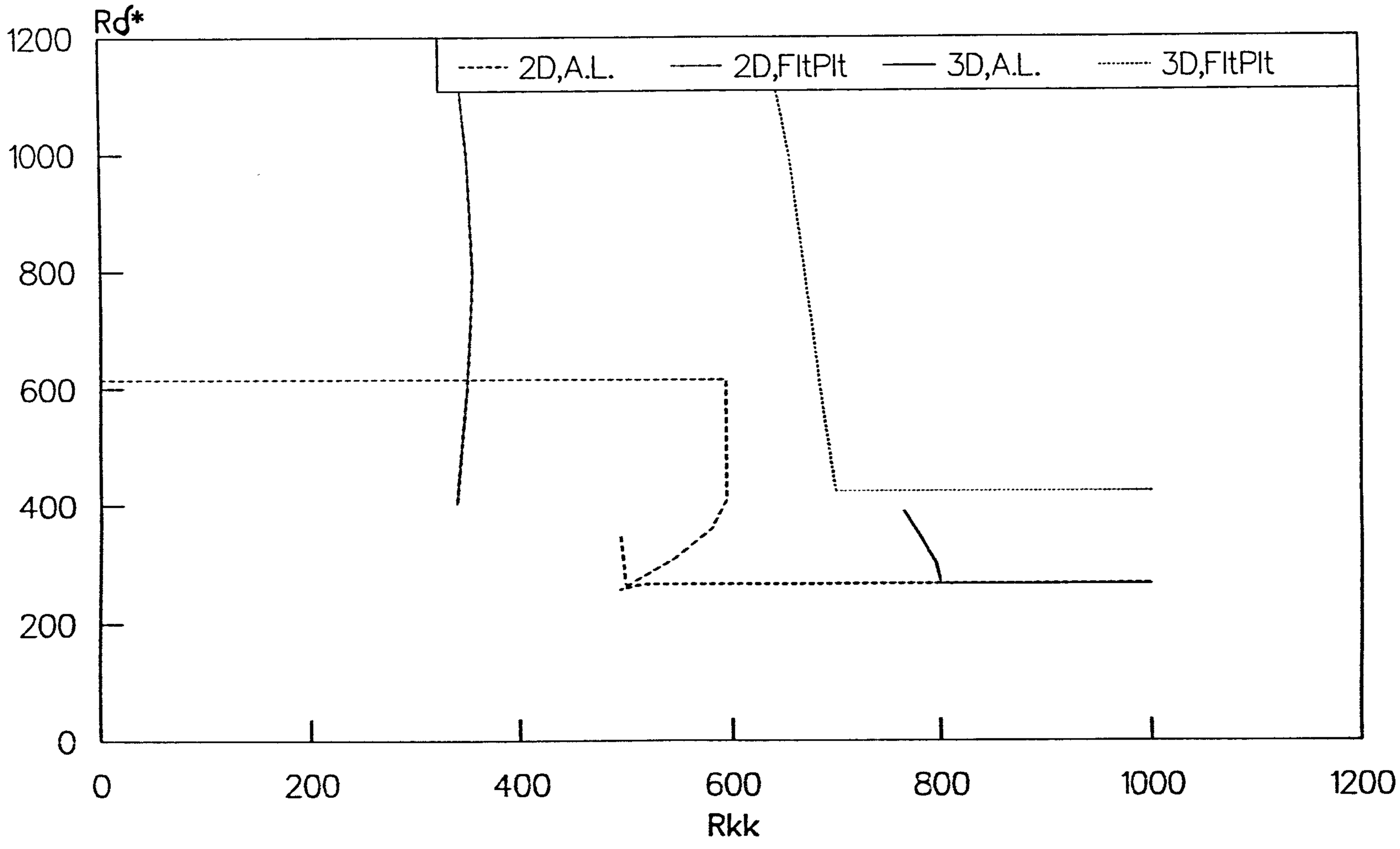

FIG 5.2
CHANGE IN ATTACHMENT LINE STATIC PRESSURE
DUE TO PRESENCE OF LARGE 3D TRIP

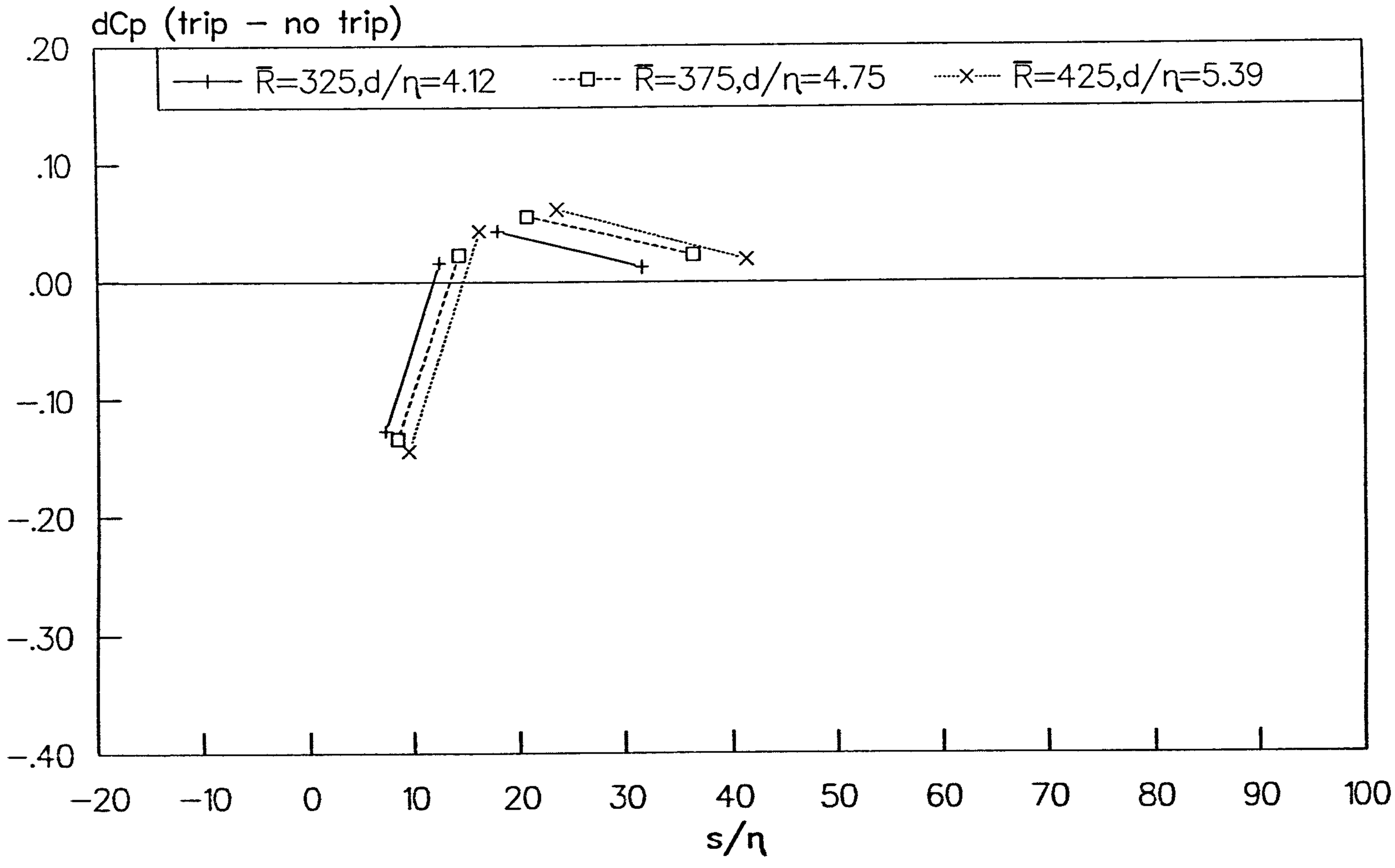

FIG 5.3a
APPROX. VELOCITY PROFILE DOWNSTREAM OF 3D TRIP
$\bar{R} = 425$, $d/\eta = 5.39$

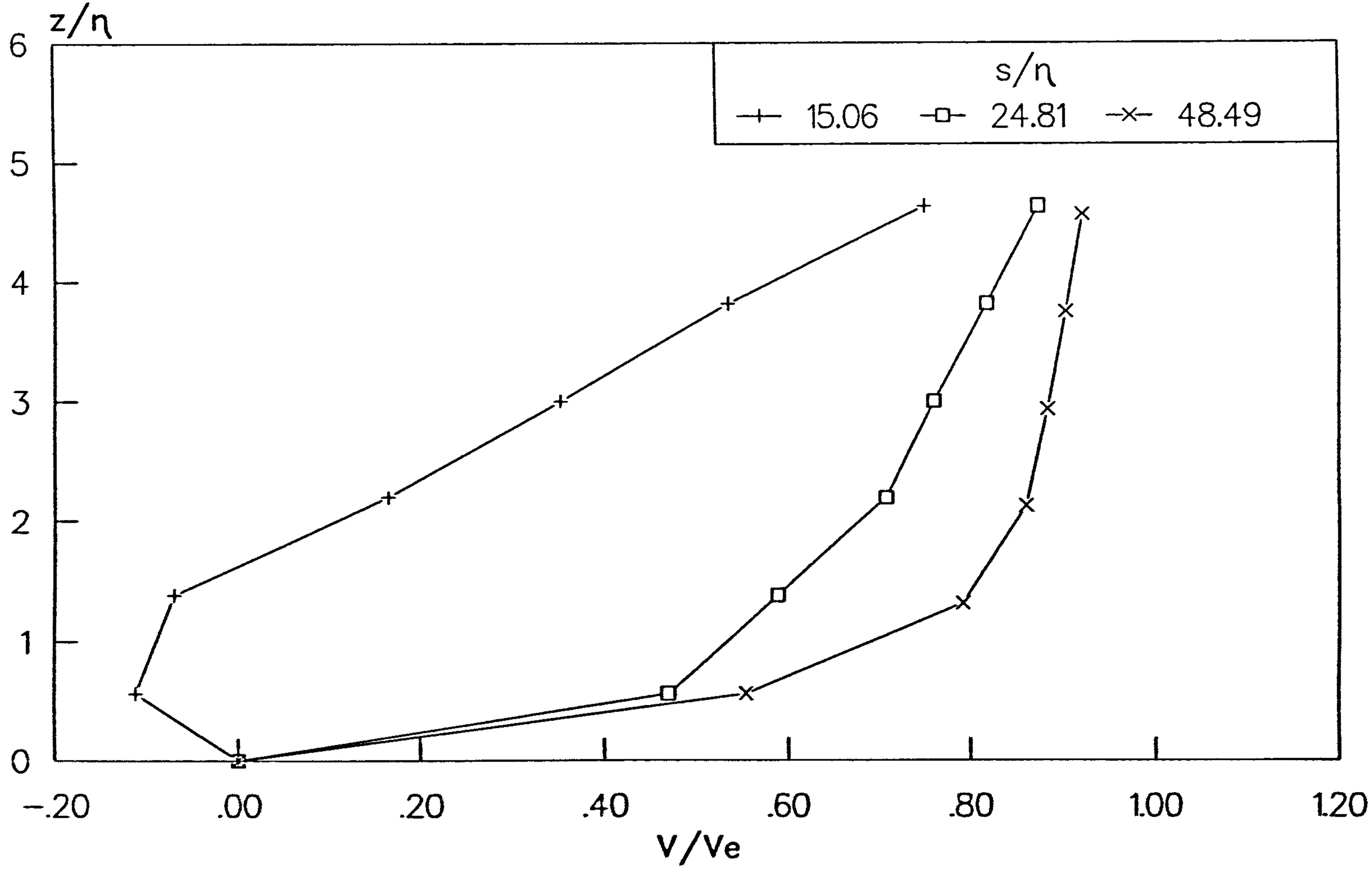

FIG 5.3b
APPROX. VELOCITY PROFILES DOWNSTREAM OF 3D TRIP
$\bar{R} = 375$, $d/\eta = 2.34$

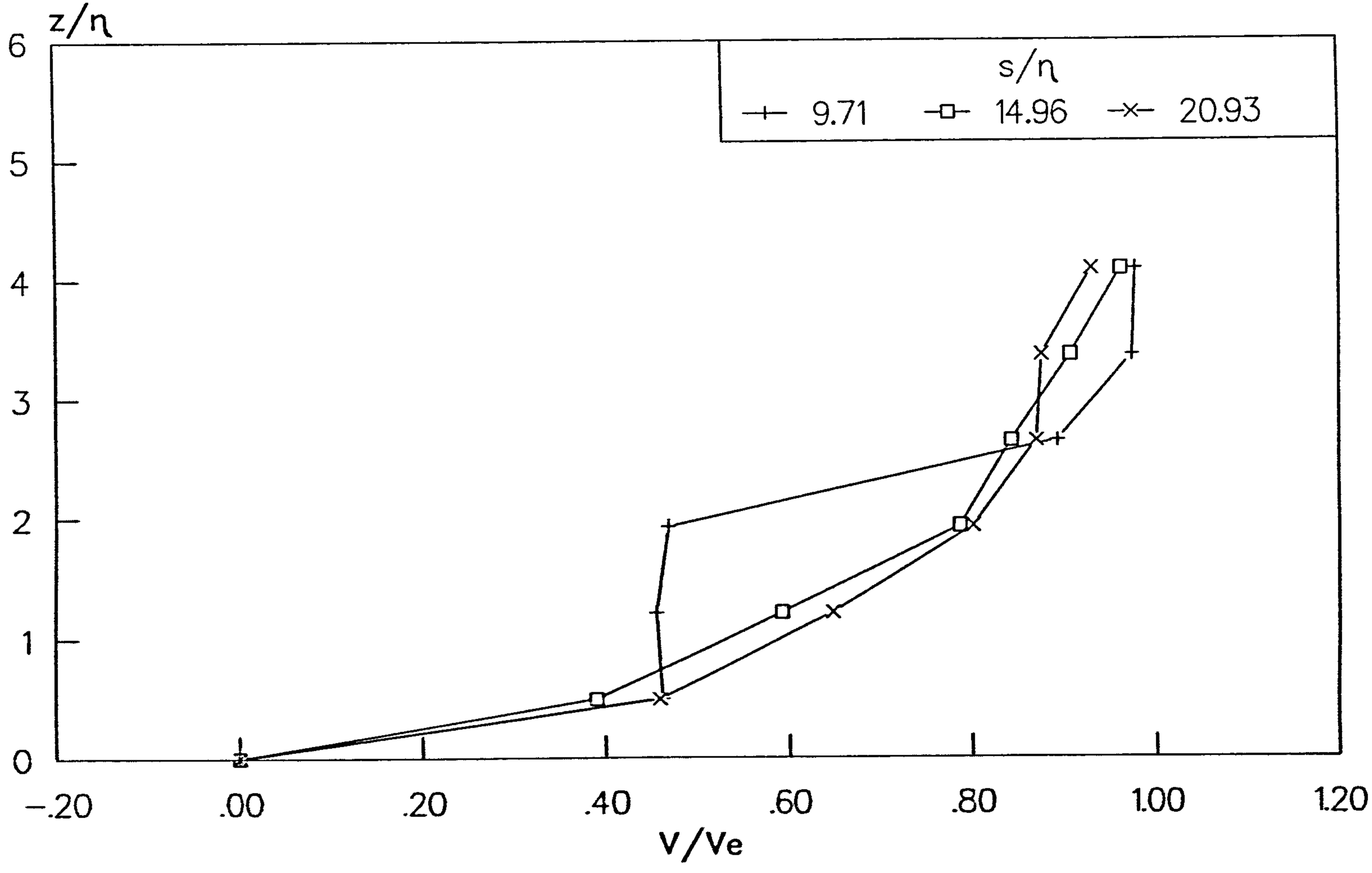

FIG 5.4
3D TRIPS
TRANSITION ONSET

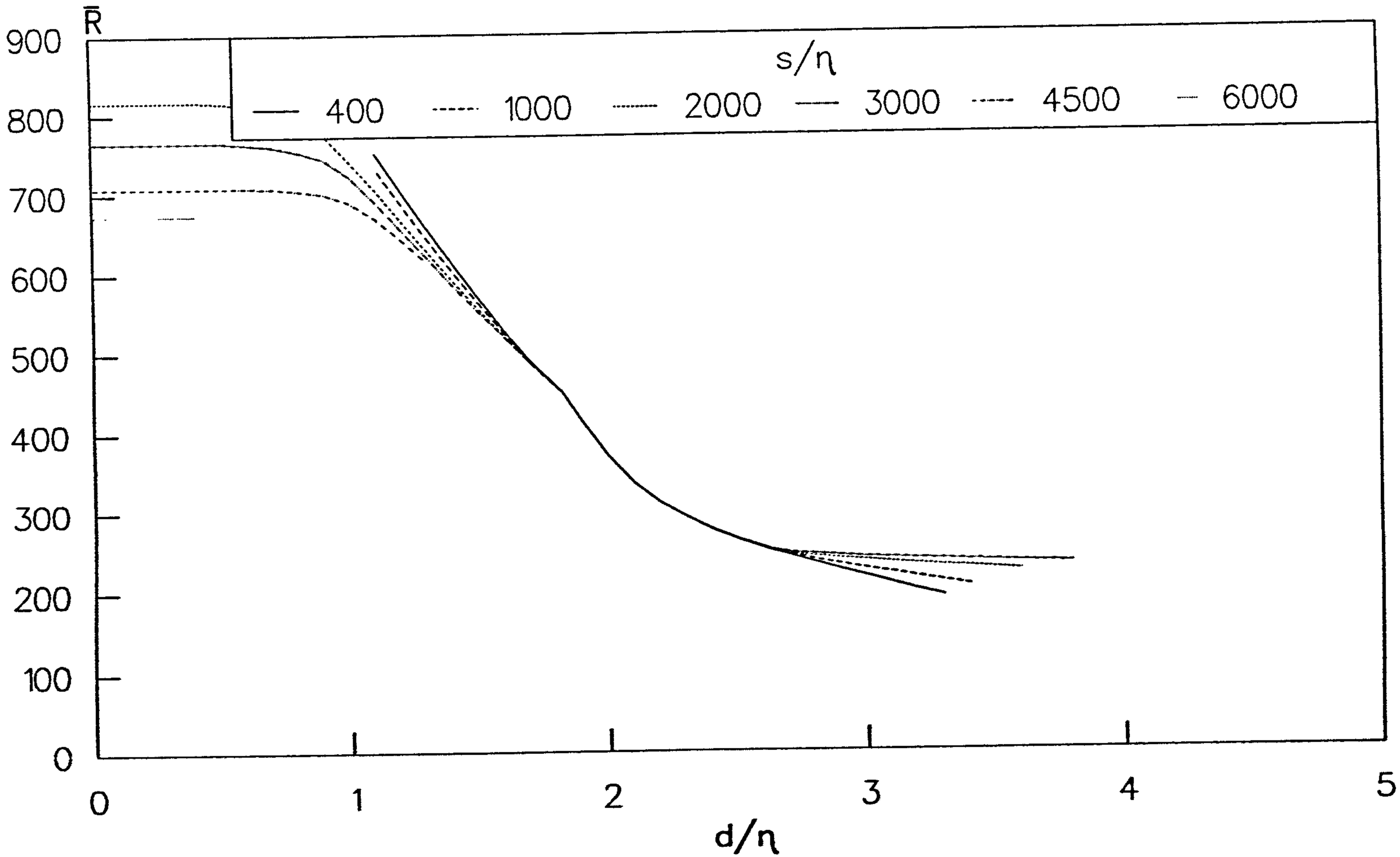

FIG 5.5
3D TRIPS
TRANSITION COMPLETION

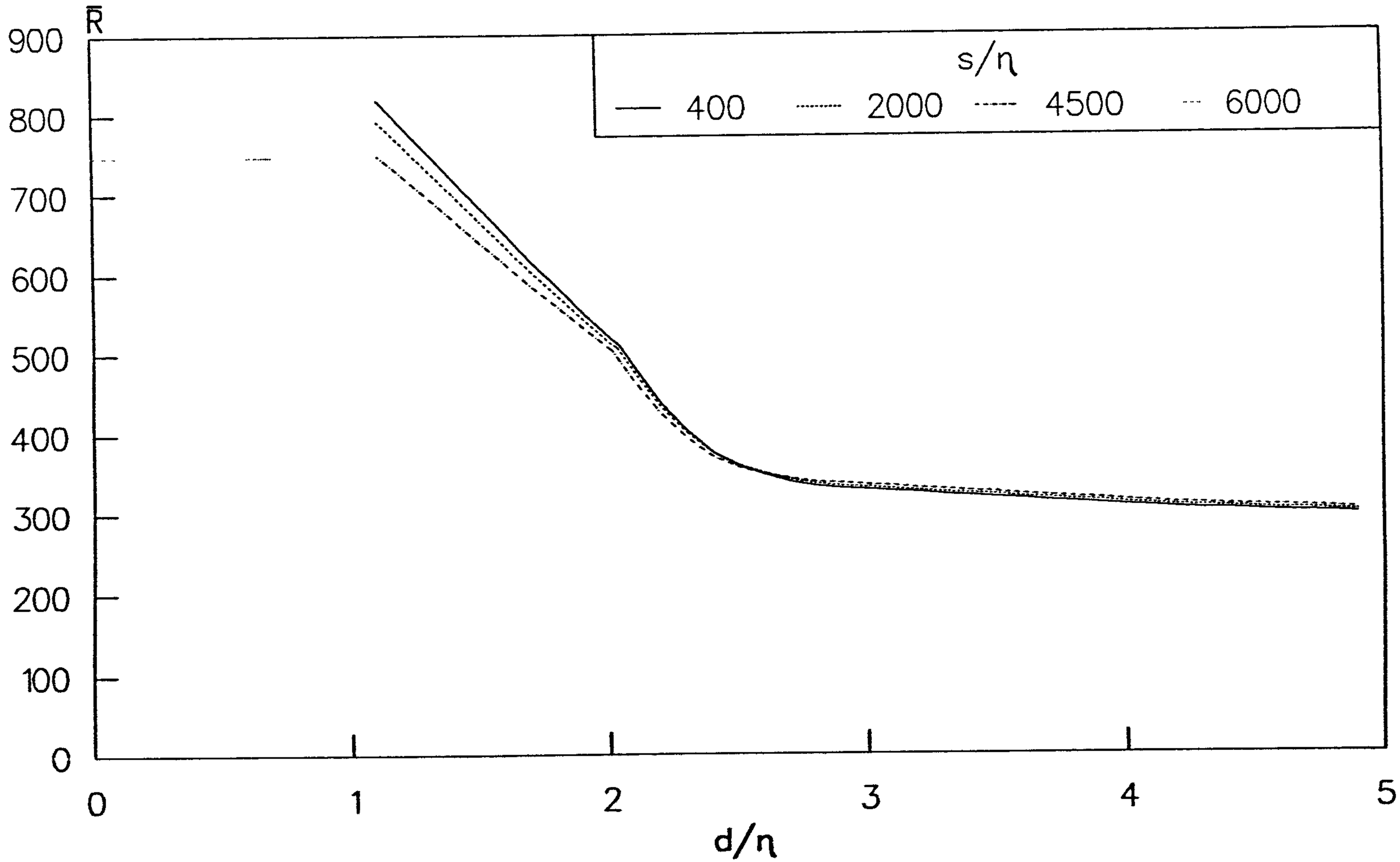

FIG 5.6
TRANSITION IN PRESENCE OF LARGE TRIP
LOWER BOUND FOR TRANSITION TRIPPING

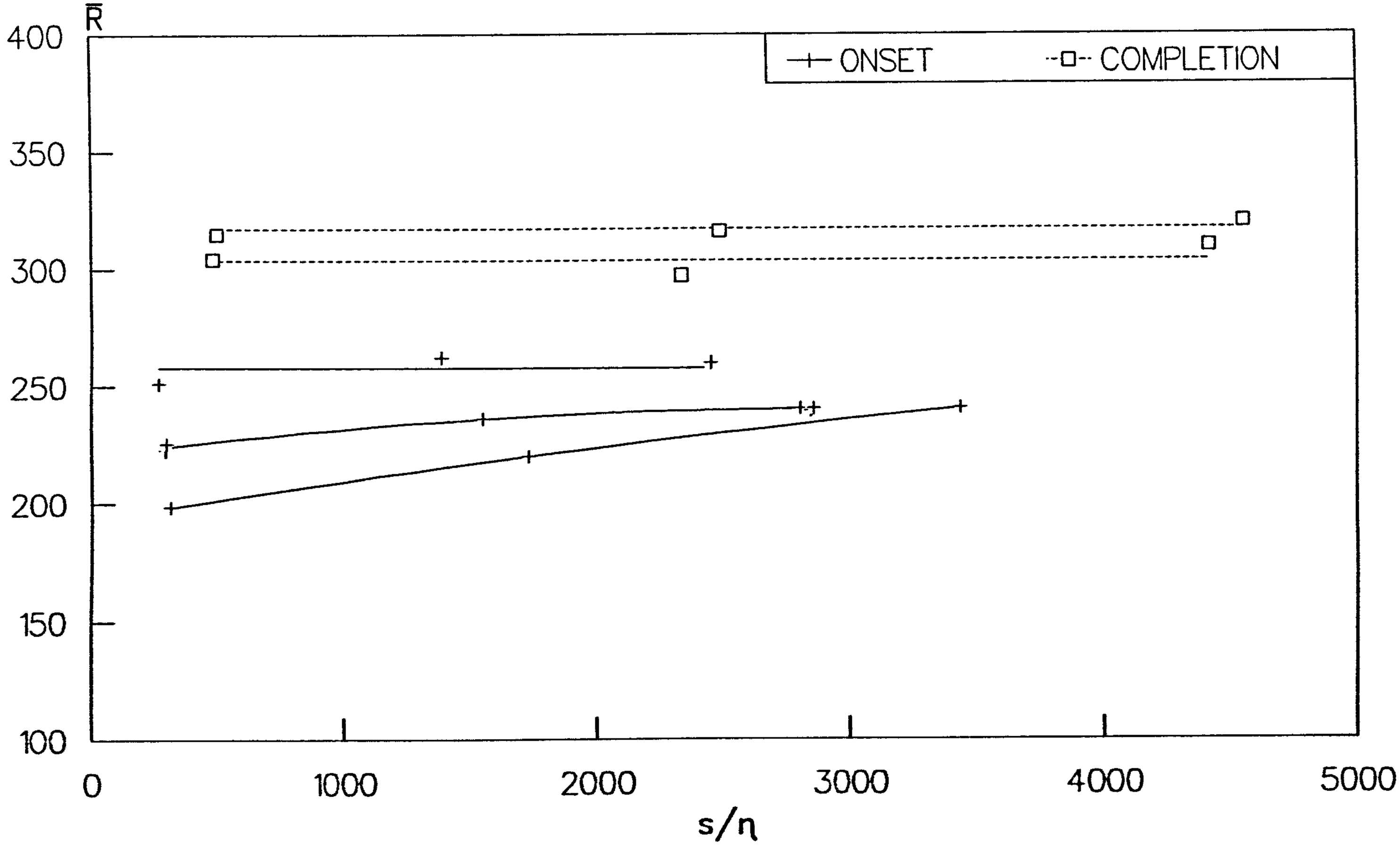

FIG 5.7
TRANSITION IN LIMIT AS s/η TENDS TO ZERO
3D TRIPS

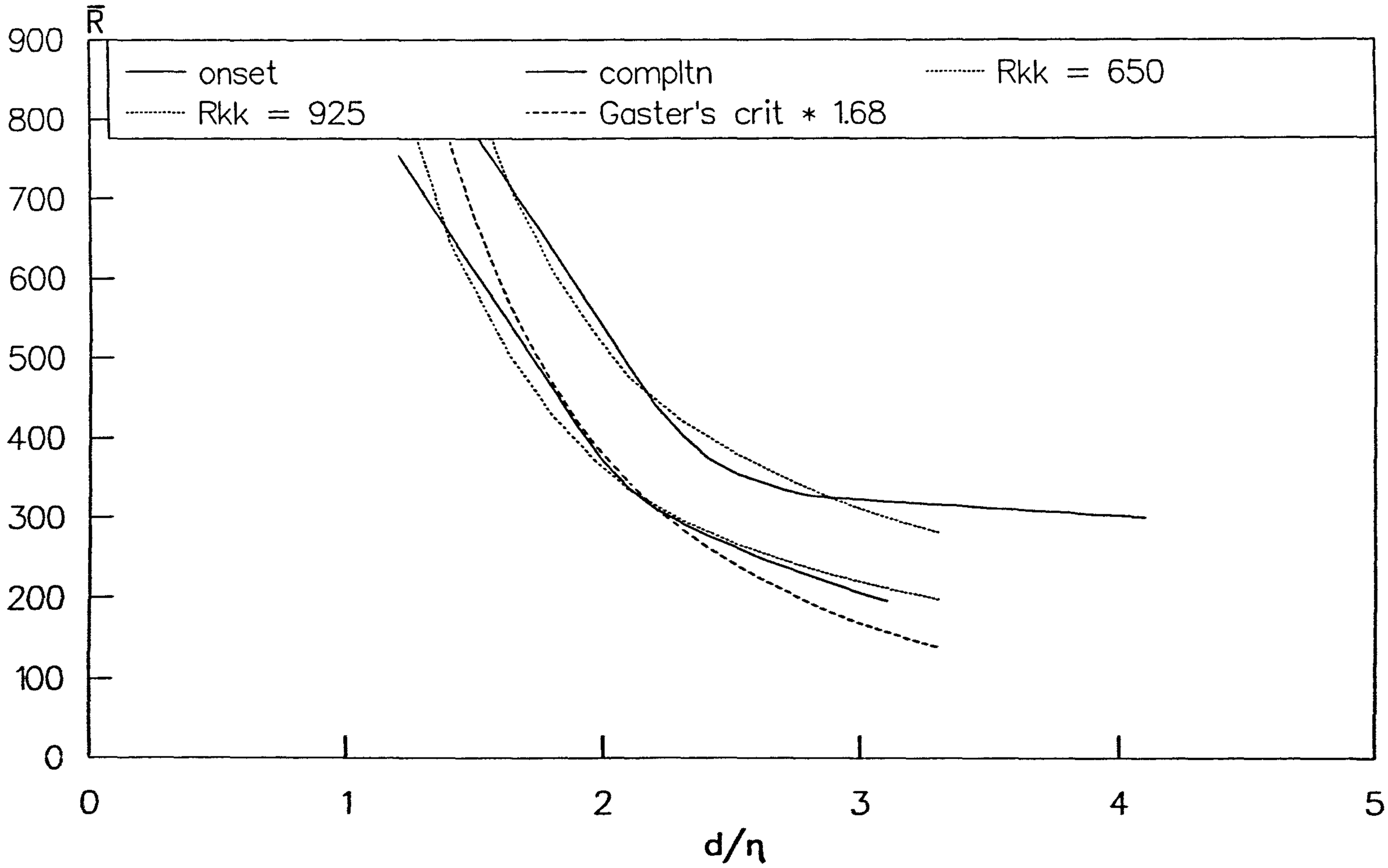

FIG 5.8
TRANSITION IN LIMIT AS s/η TENDS TO INFINITY
3D TRIPS

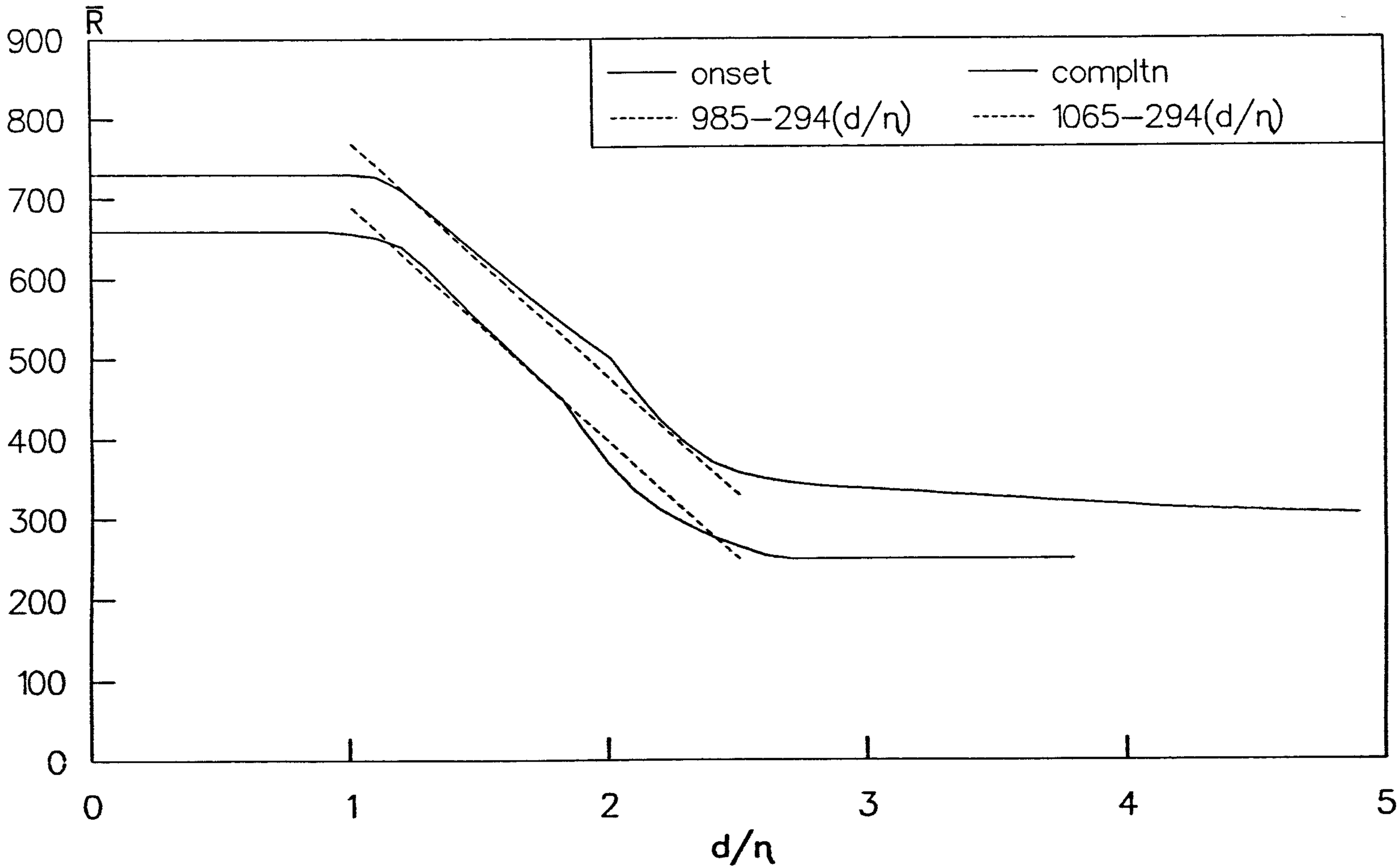

FIG 5.9
COMPARISON BETWEEN 2D AND 3D TRIPS
$s/\eta = 2000$

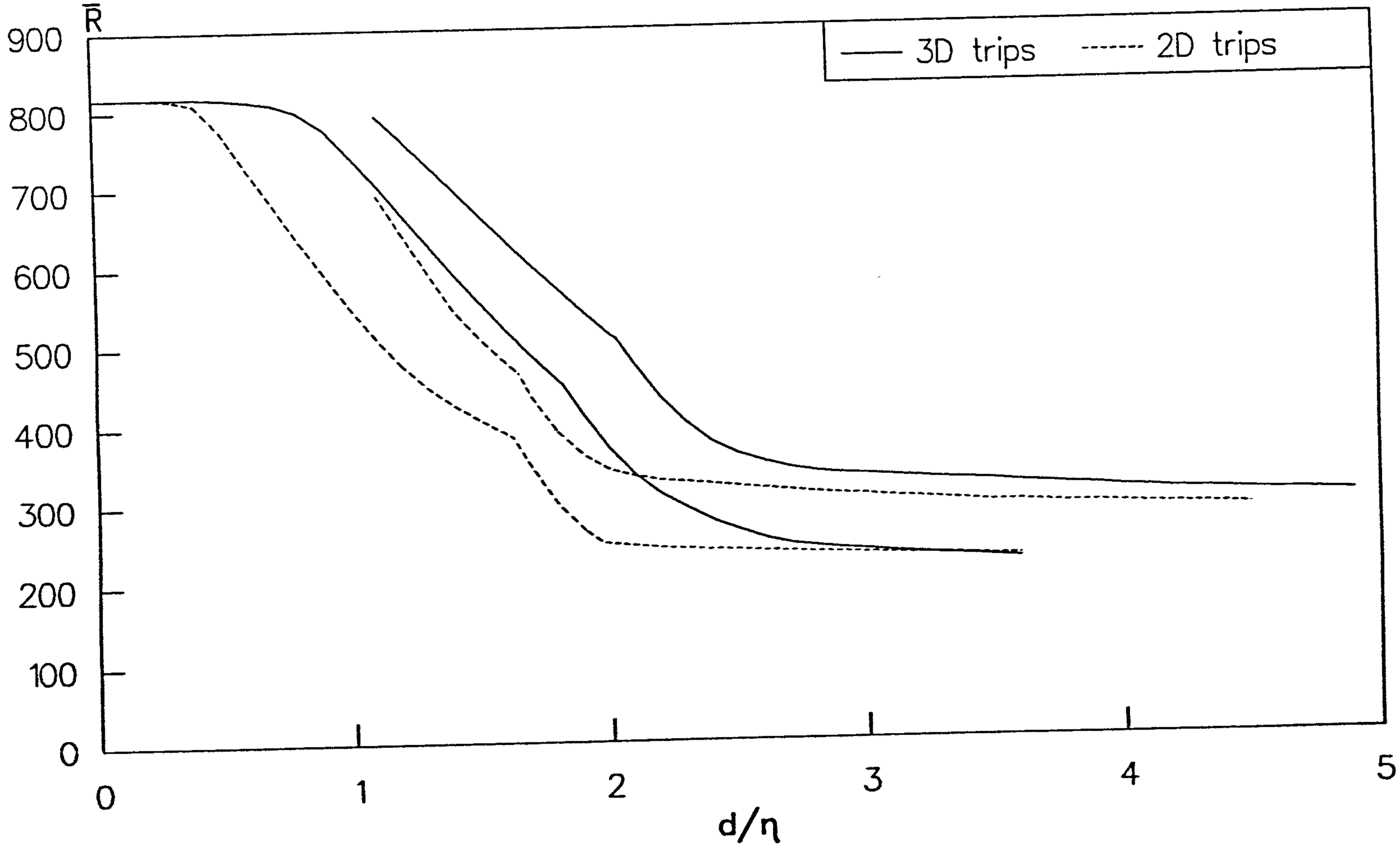

FIG 5.10
PRESENT & PREVIOUS INVESTIGATIONS, 3D TRIPS
TRANSITION ONSET & COMPLETION AT TRIP

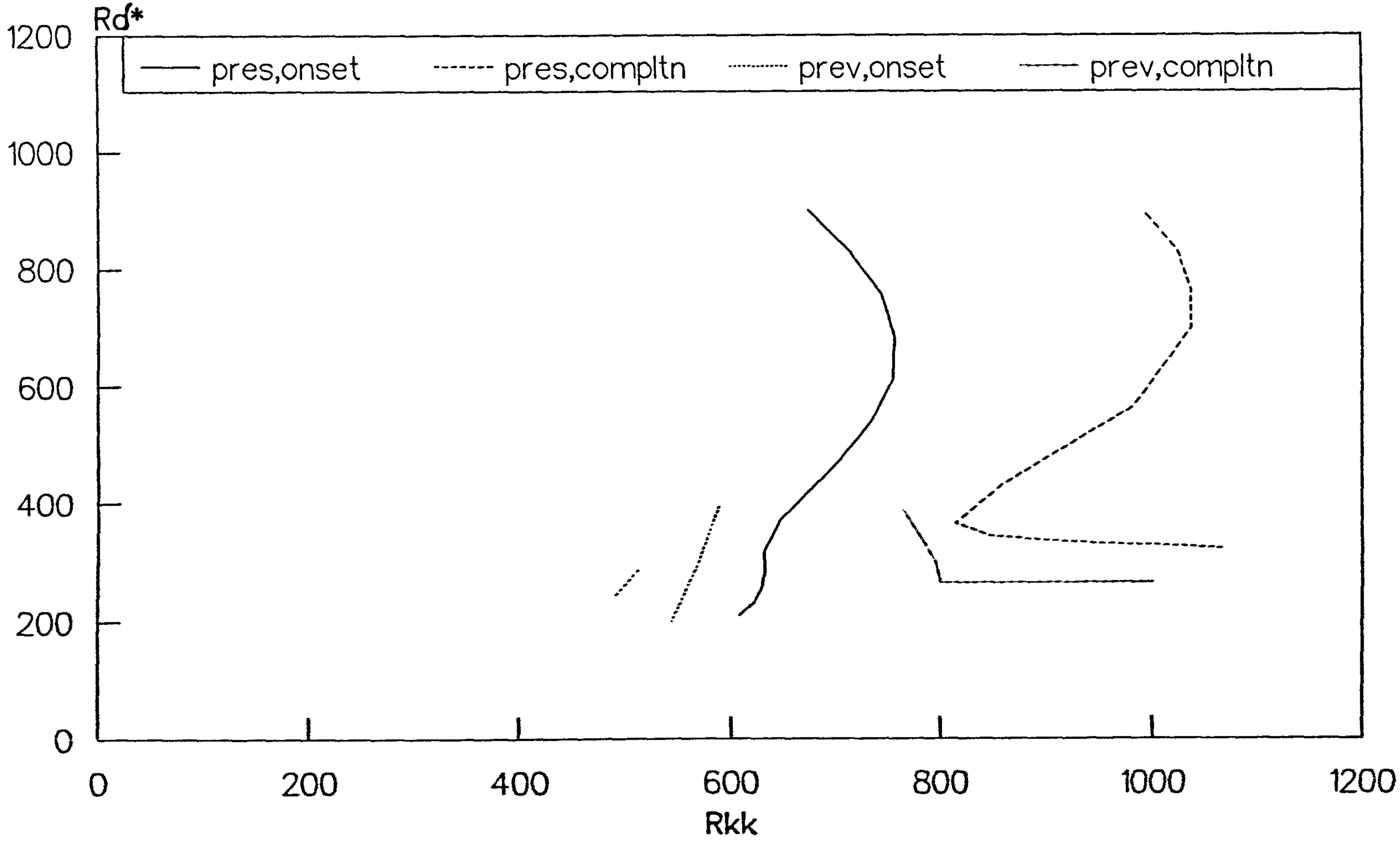

FIG 5.11
COMPARSION BETWEEN 2D & 3D TRIPS
TRANSITION ONSET AT TRIP

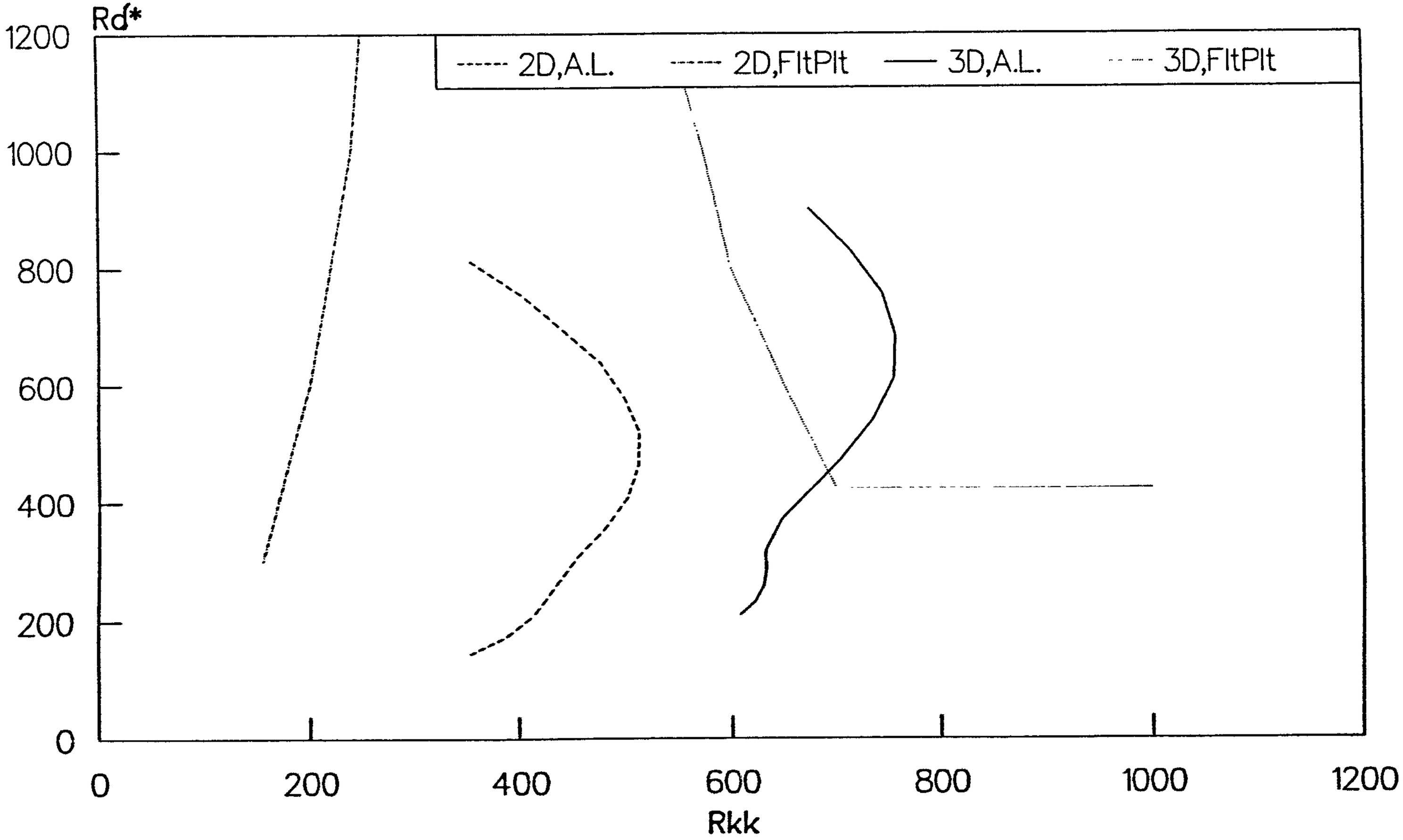

FIG 5.12
COMPARSION BETWEEN 2D & 3D TRIPS
TRANSITION COMPLETION AT TRIP

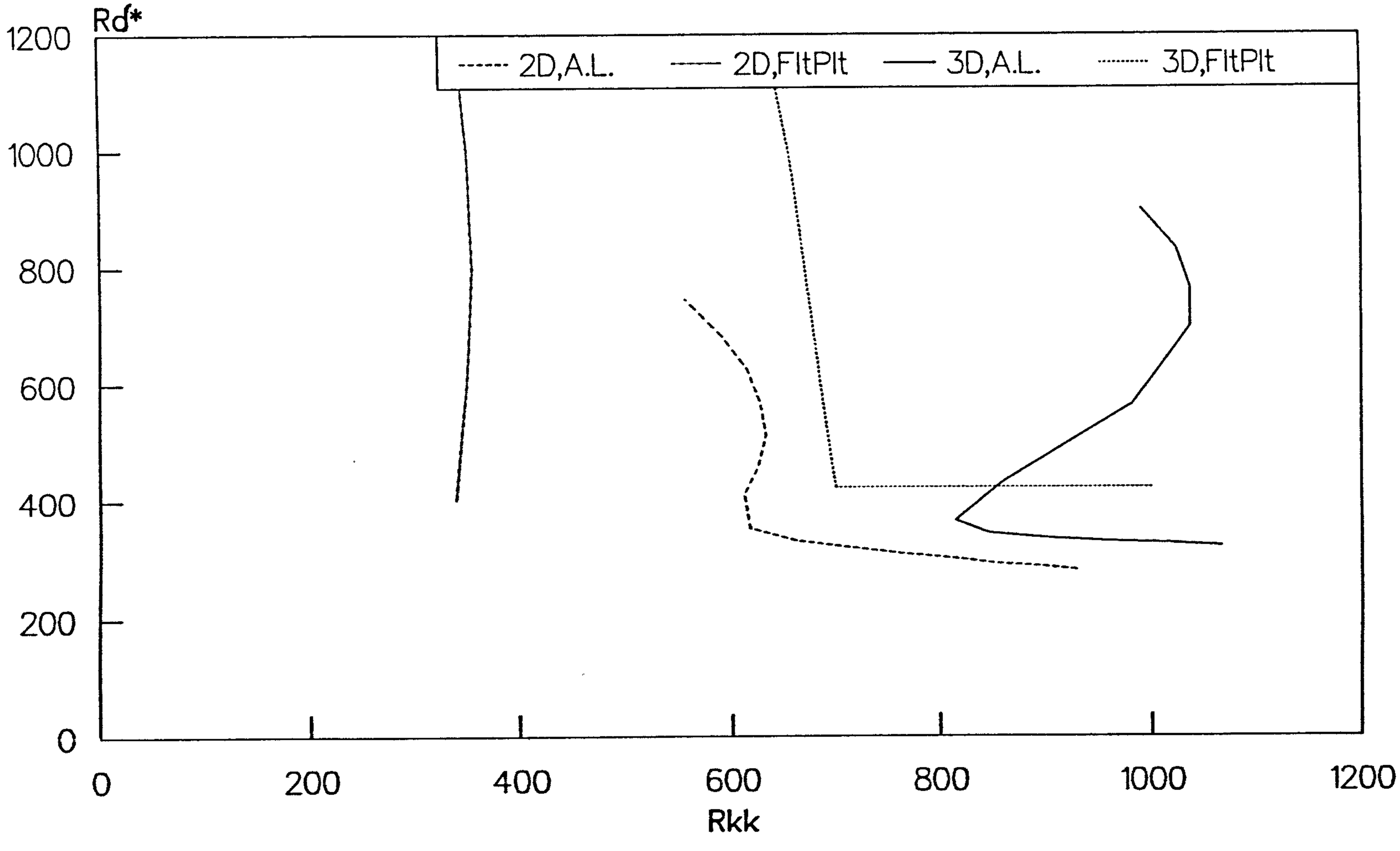

FIG 5.13
INTERMITTENCY DISTRIBUTIONS
3D TRIPS

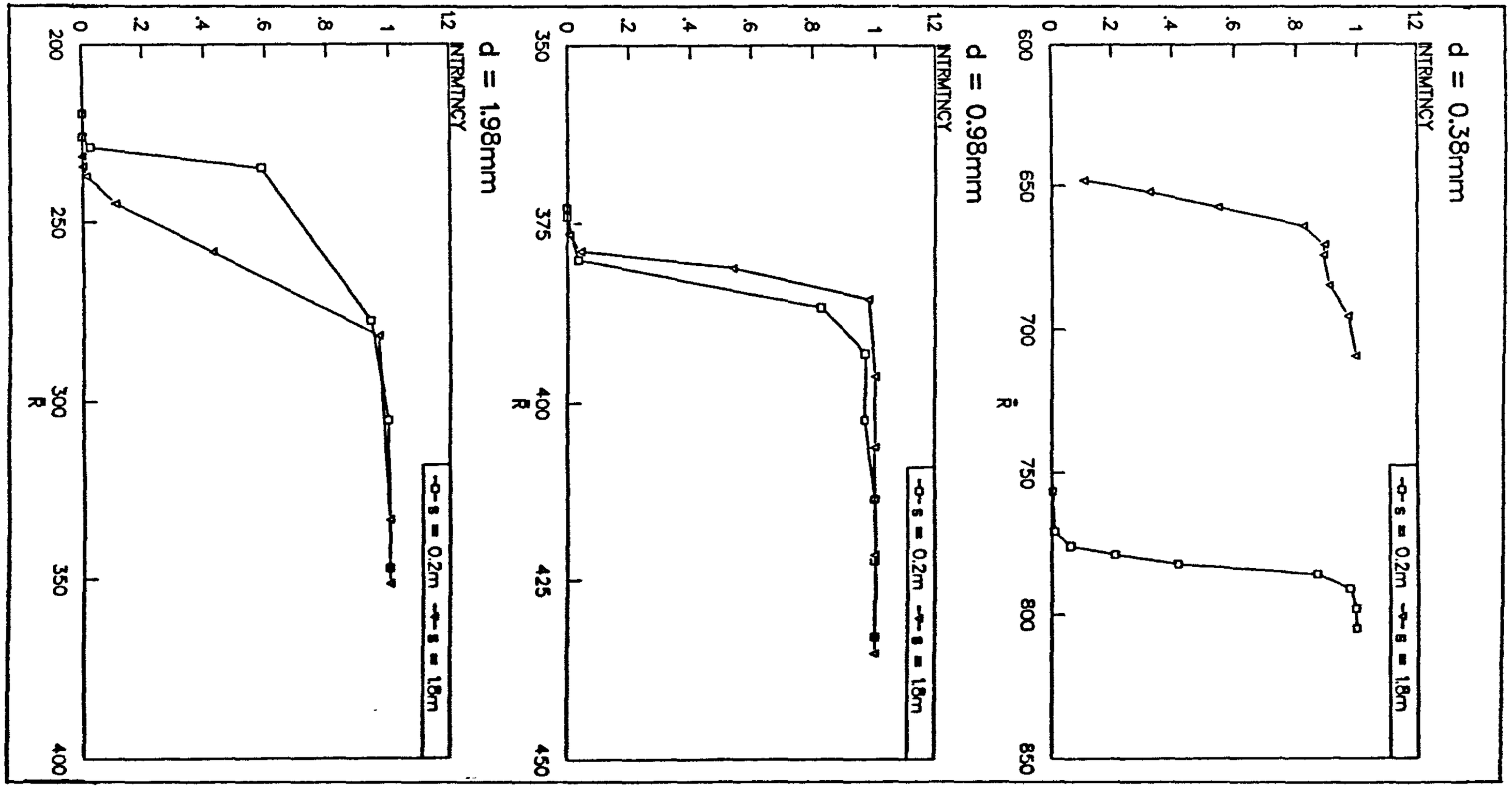

FIG 5.14a
INTERMITTENCY DISTRIBUTION
3D TRIPS

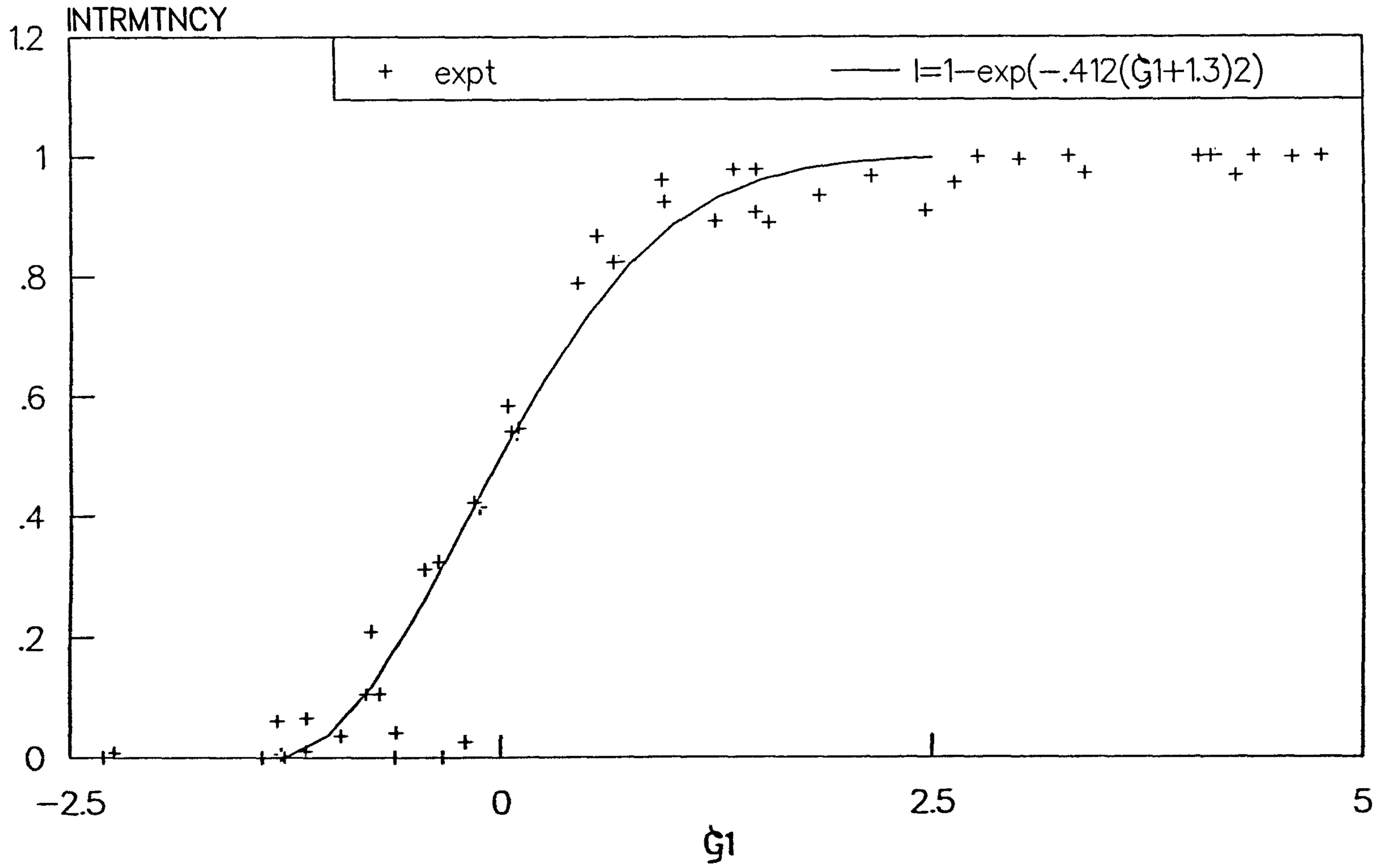

FIG 5.14b
INTERMITTENCY DISTRIBUTION
3D TRIPS

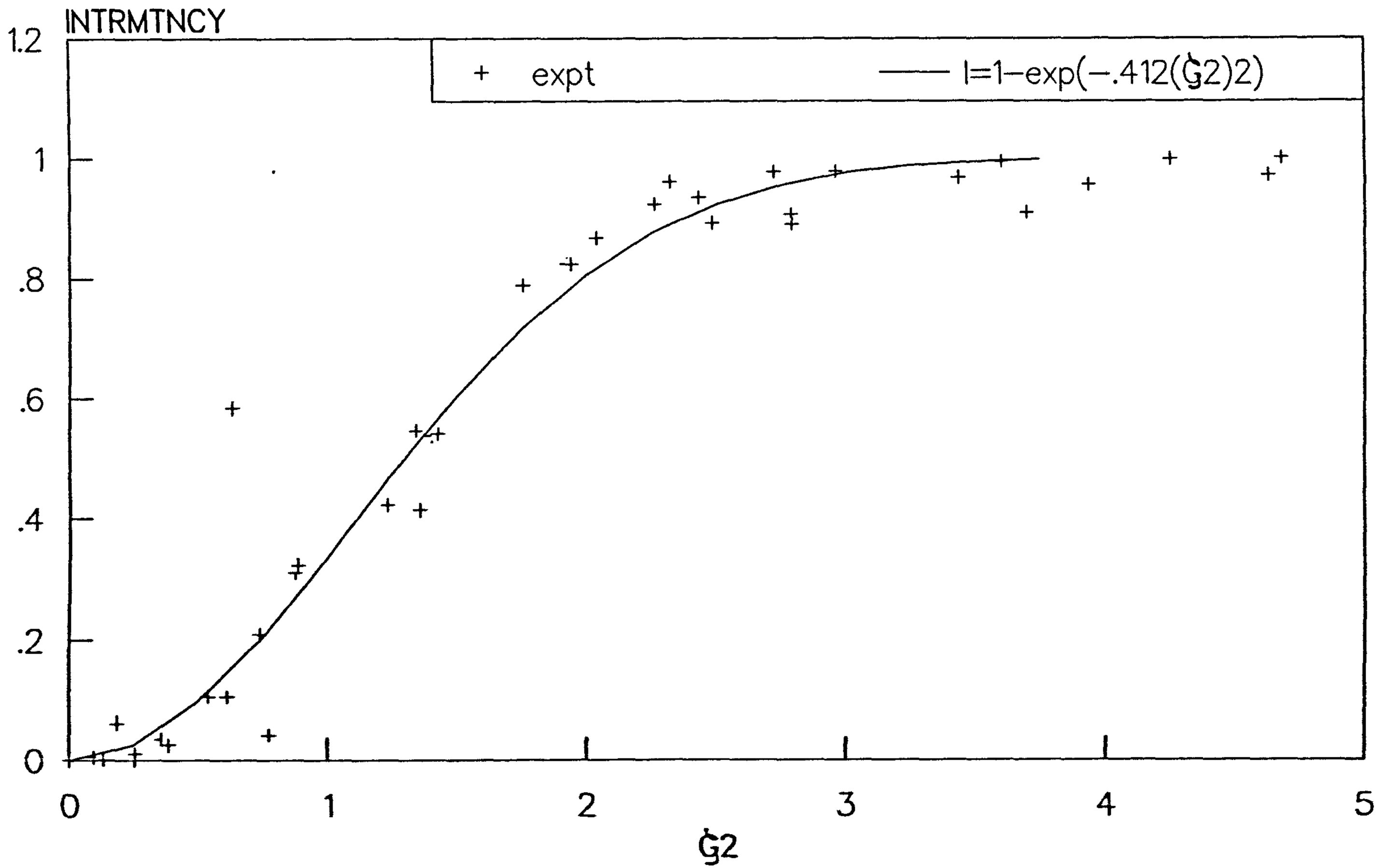

FIG 5.15
INTERMITTENCY DISTRIBUTION
3D TRIP ; d = 0.78mm

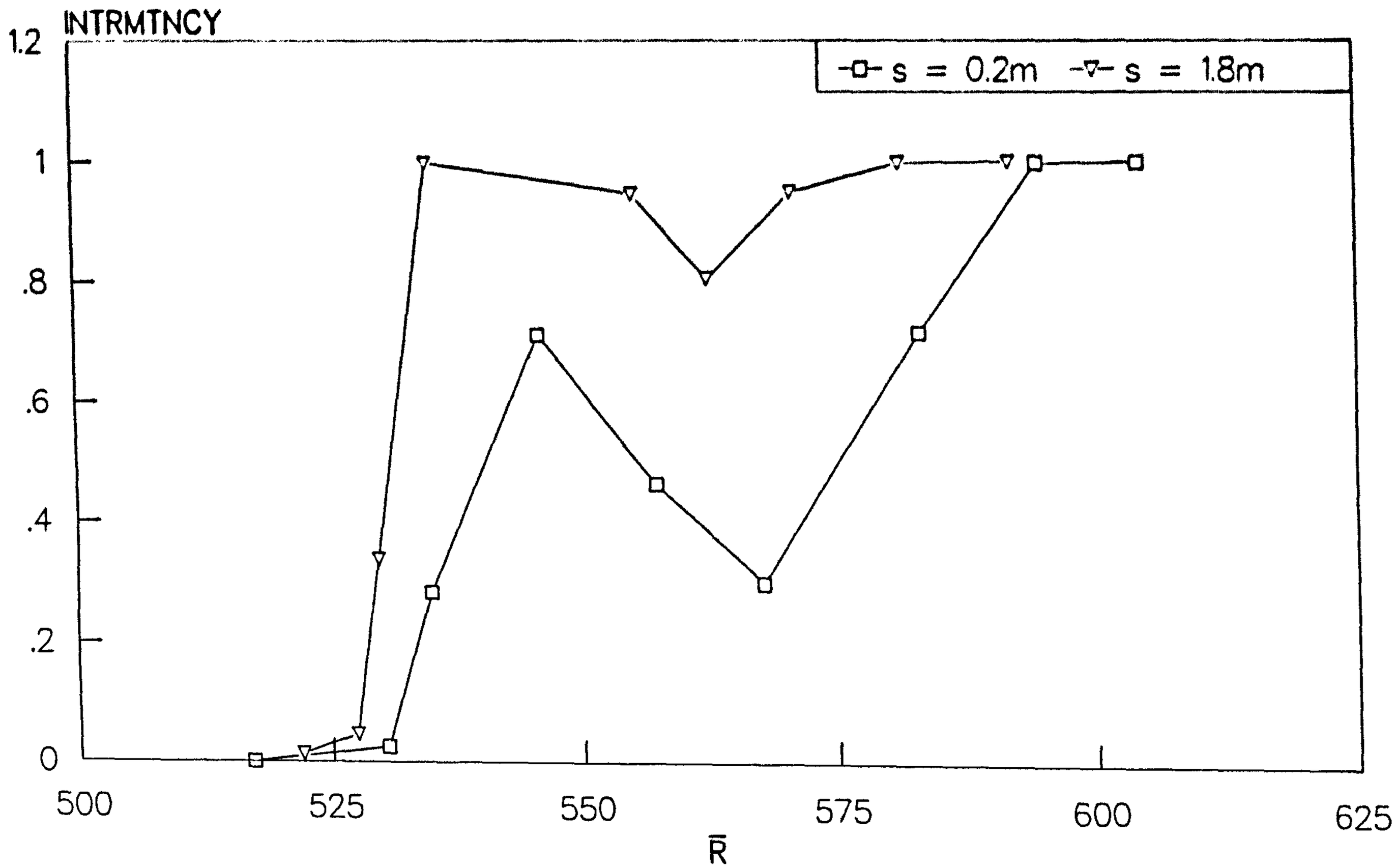

FIG 6.1
TURBULENT SPOT ON FLAT PLATE
FROM SCHUBAUER'56

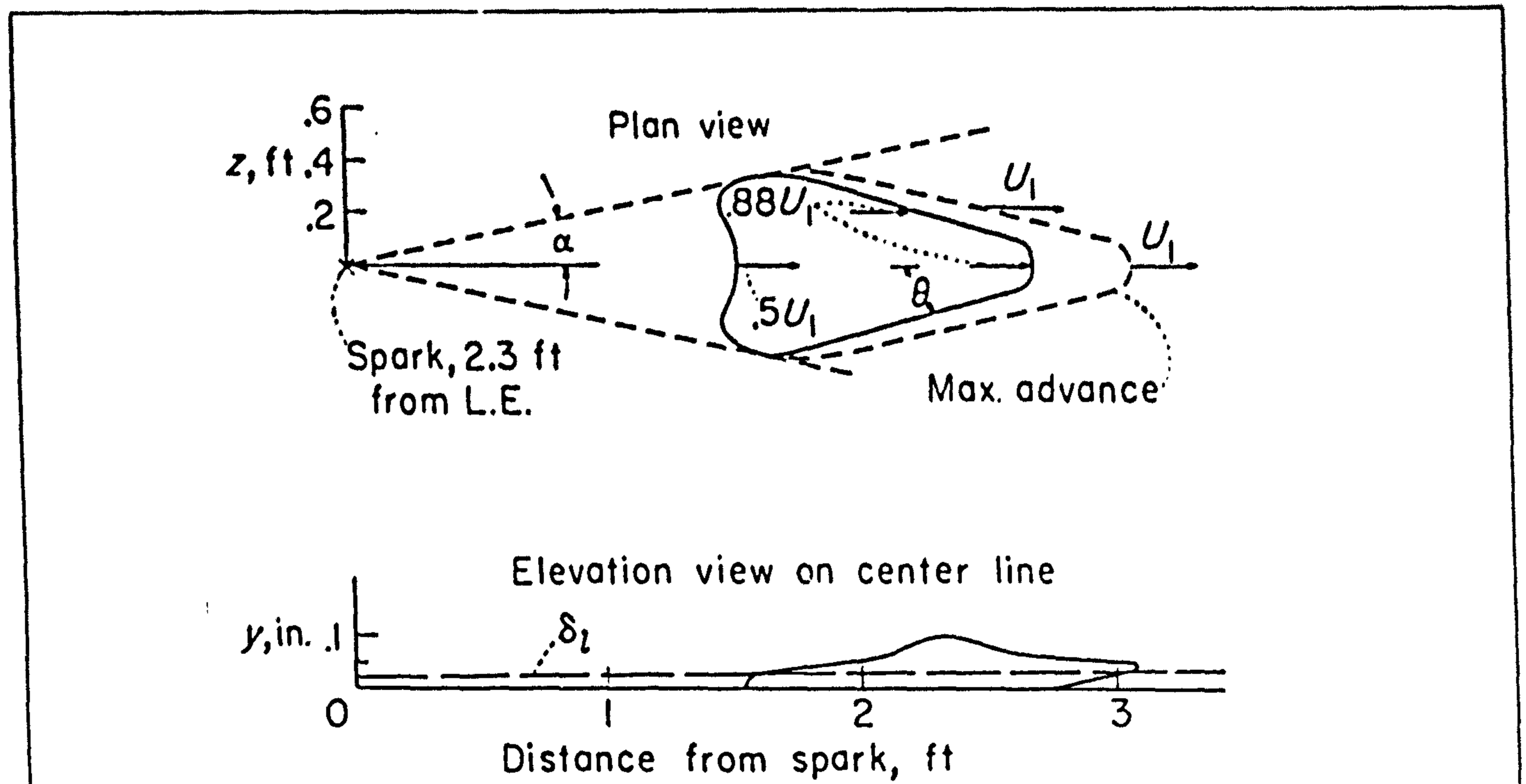

FIG 6.2
TURBULENCE SPREADING ANGLE
FLAT PLATE, FROM De BRUIN('89)

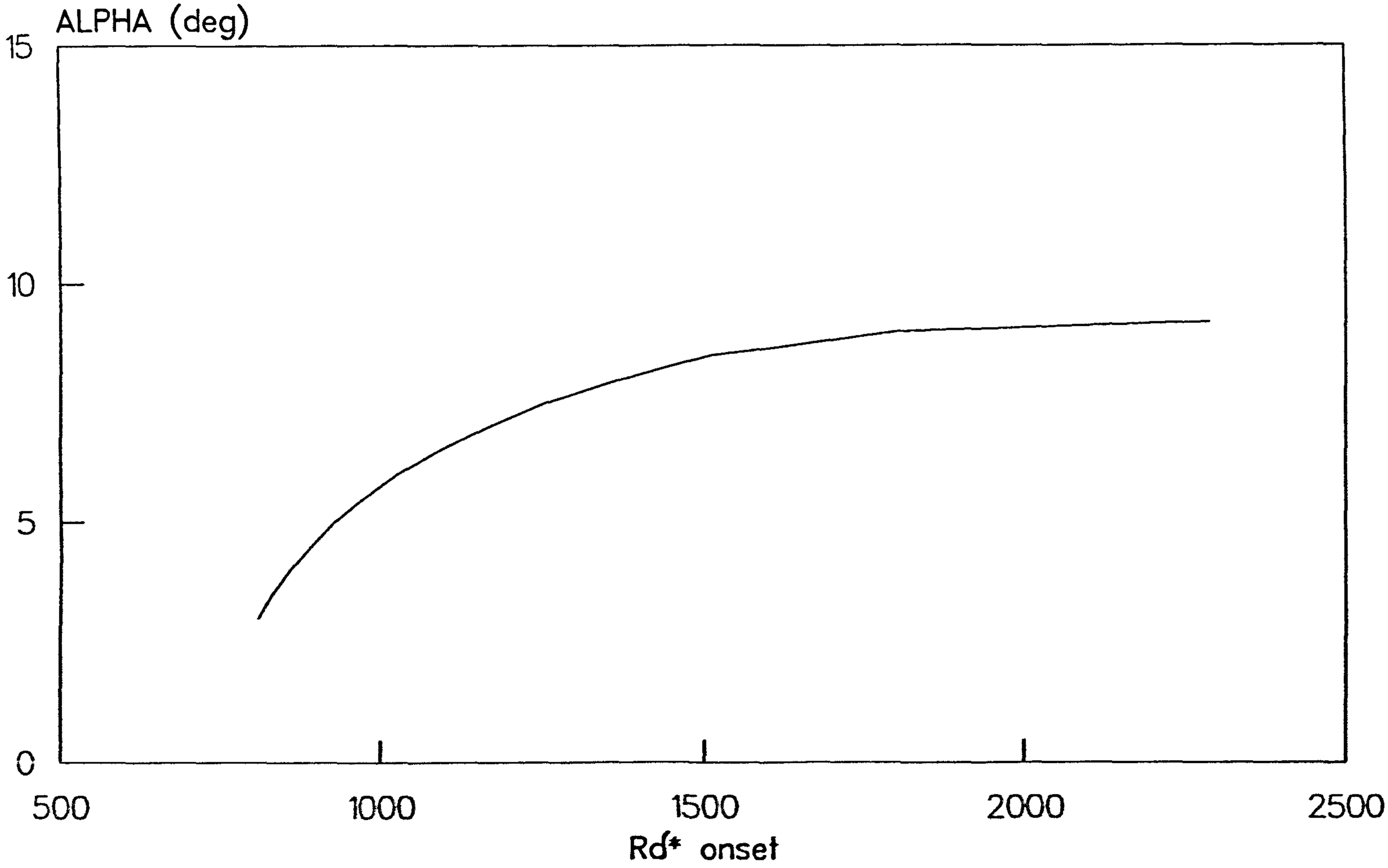

FIG 6.3
TURBULENT WEDGE ON FLAT PLATE
FROM SCHUBAUER'56

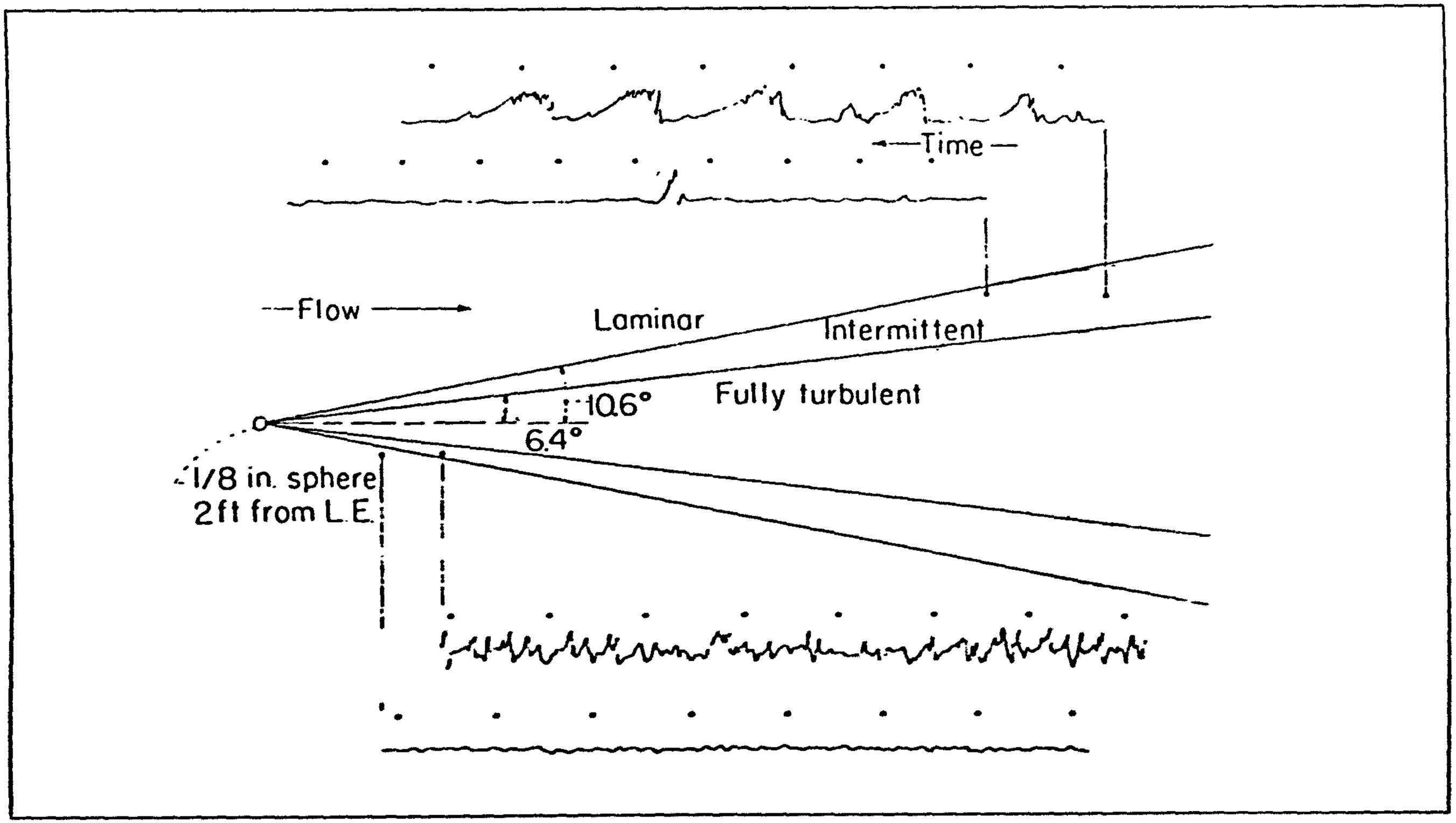

FIG 6.4
EXPERIMENTAL SET-UP FOR 3D TRIPS
PLACED DOWNSTREAM OF ATTACHMENT LINE

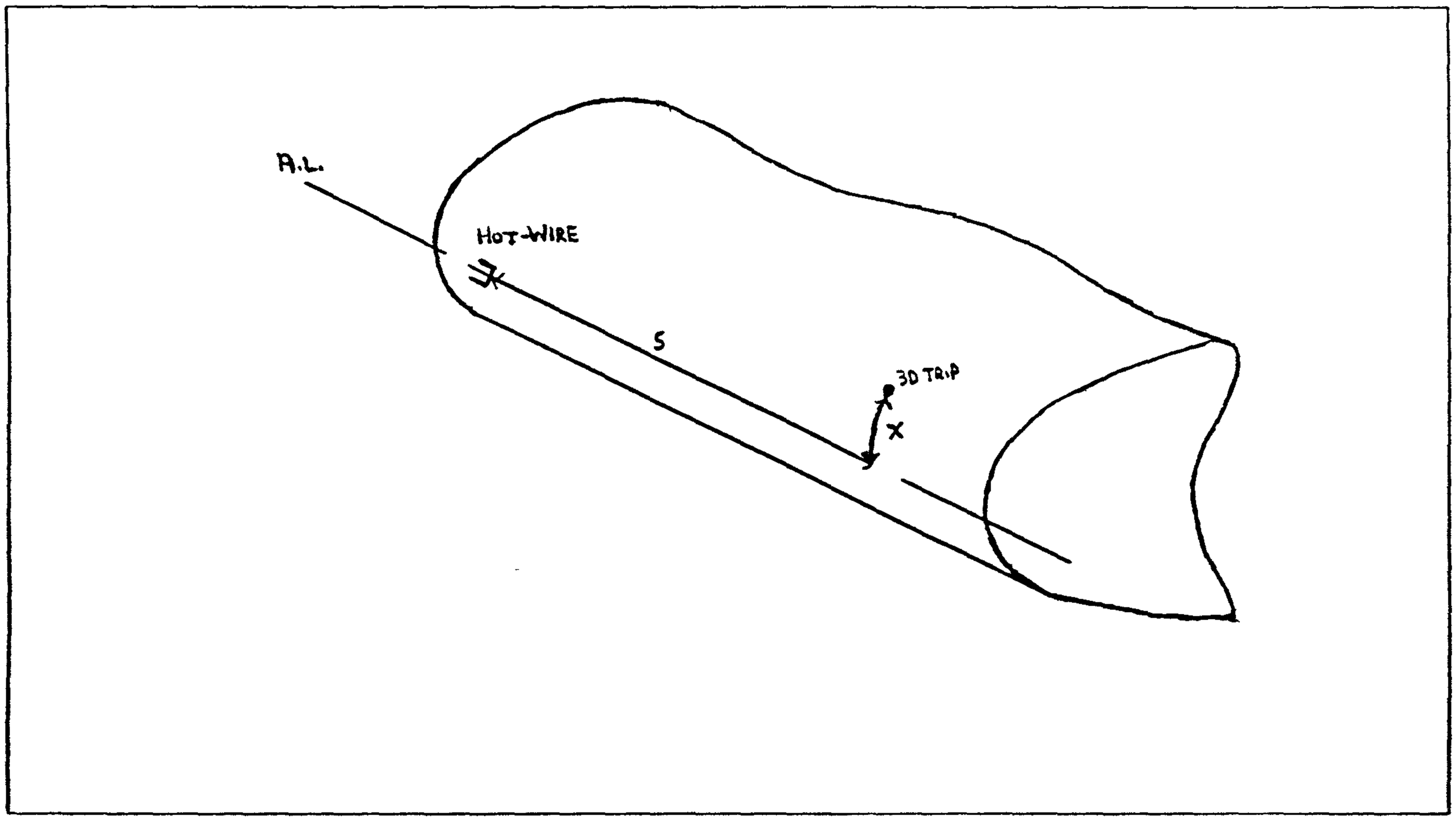

FIG 6.5
EXTERNAL STREAMLINES
IN VICINITY OF ATTACHMENT LINE

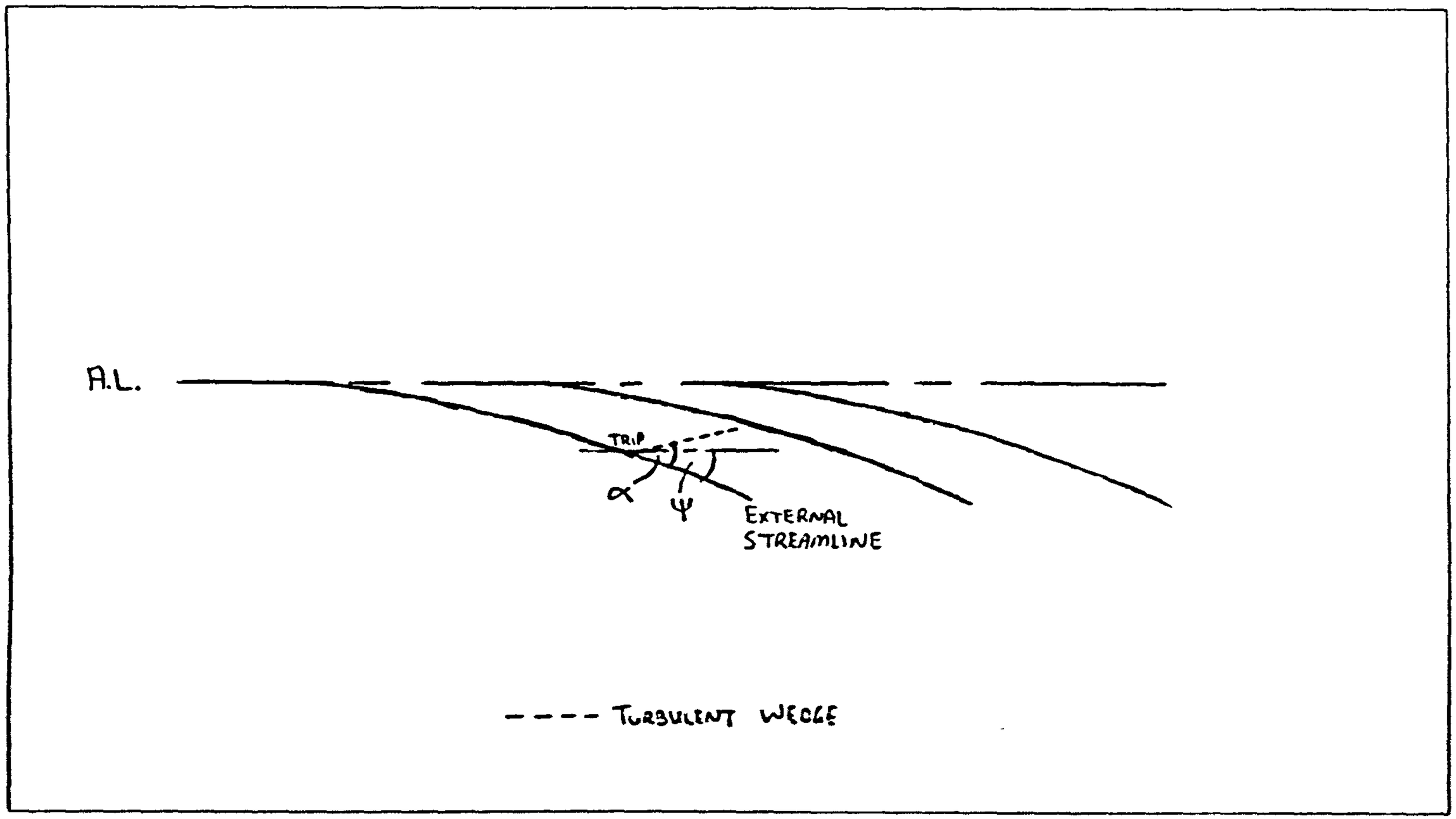

FIG 6.6a
3D TRIPS DOWNSTREAM OF ATTACHMENT LINE
TURBULENCE SPREADING ANGLES
d = 0.78mm

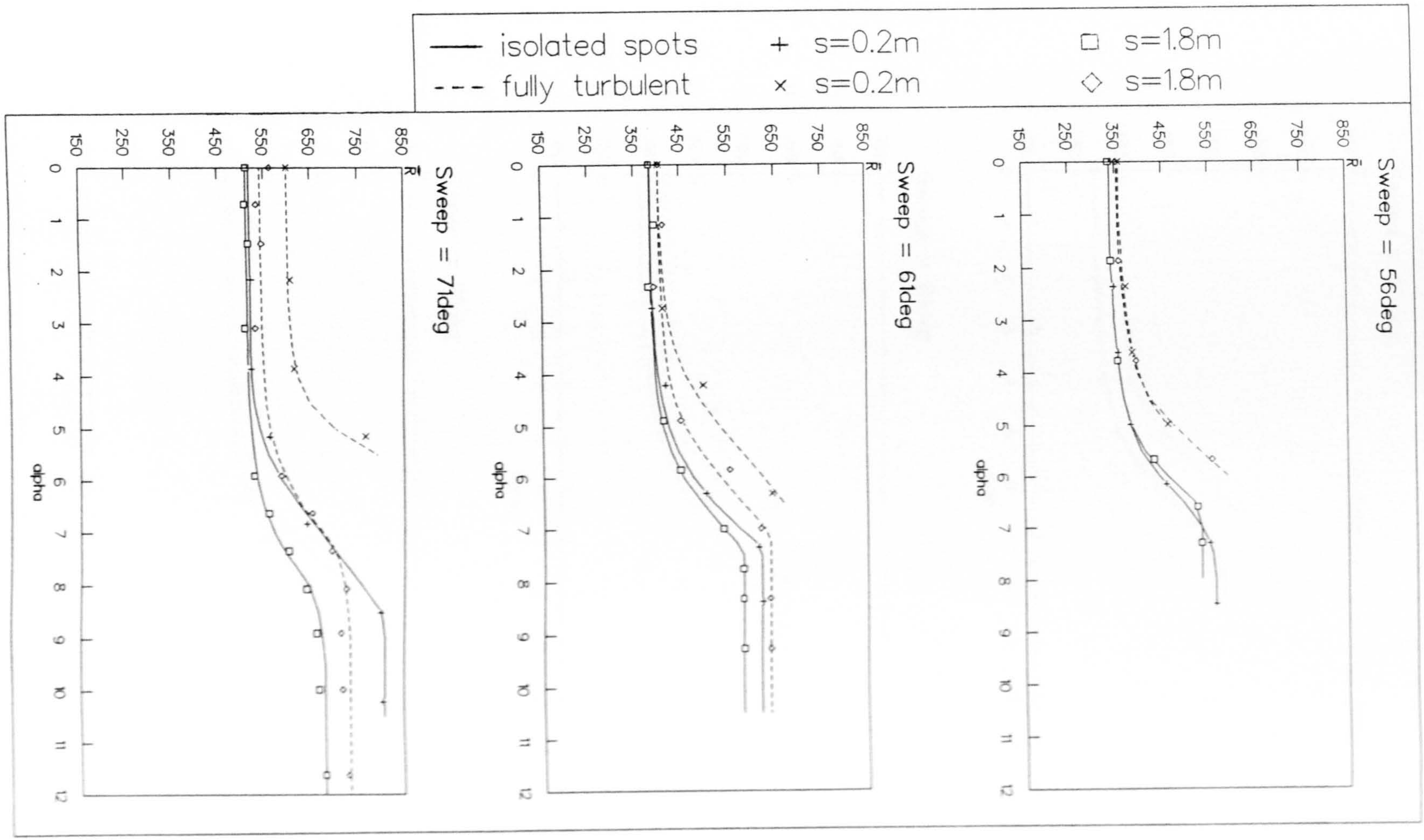

FIG 6.6b
3D TRIPS DOWNSTREAM OF ATTACHMENT LINE
TURBULENCE SPREADING ANGLES
d = 0.98mm

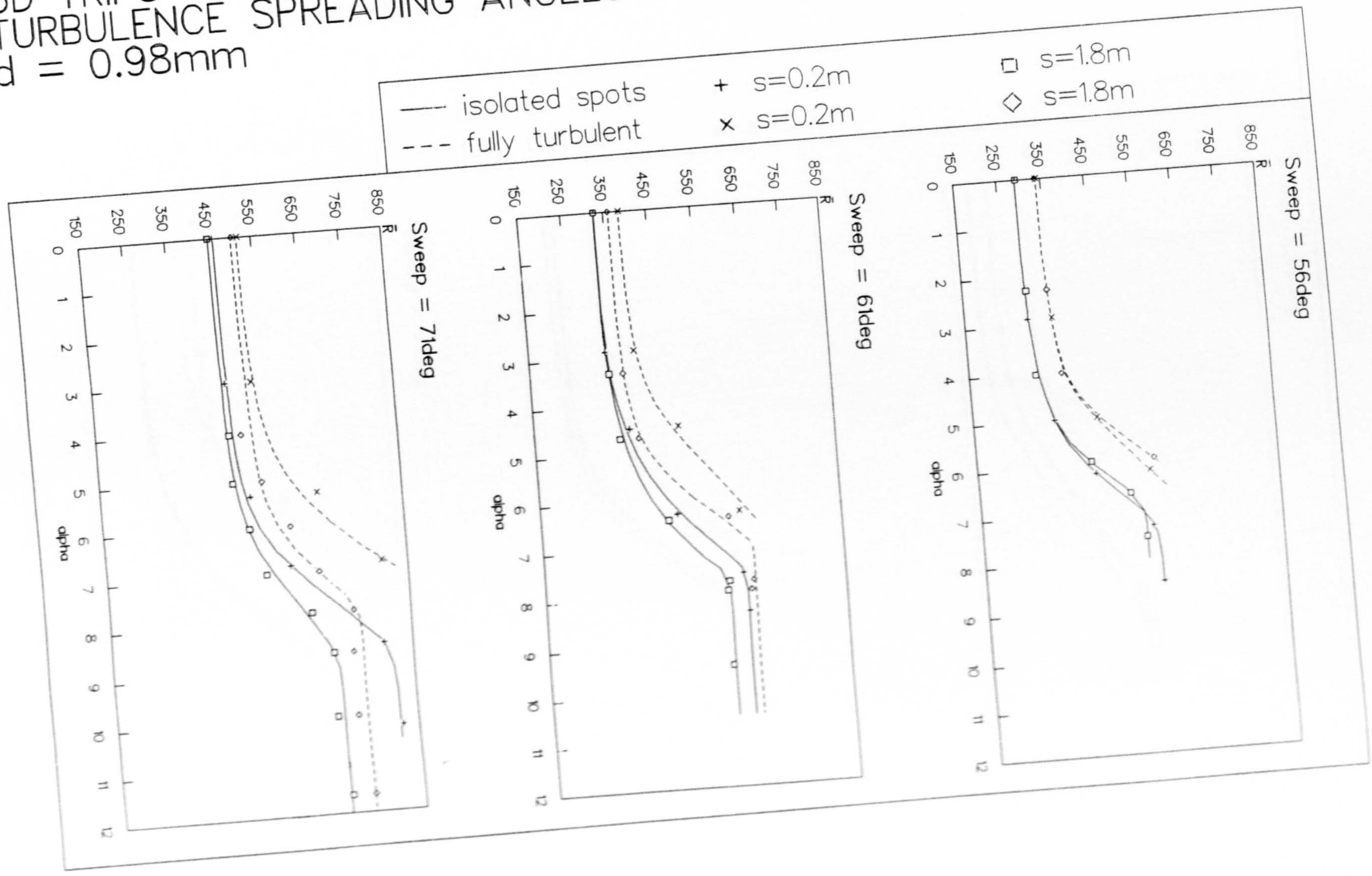

FIG 6.6c
3D TRIPS DOWNSTREAM OF ATTACHMENT LINE
TURBULENCE SPREADING ANGLES
d = 1.99mm

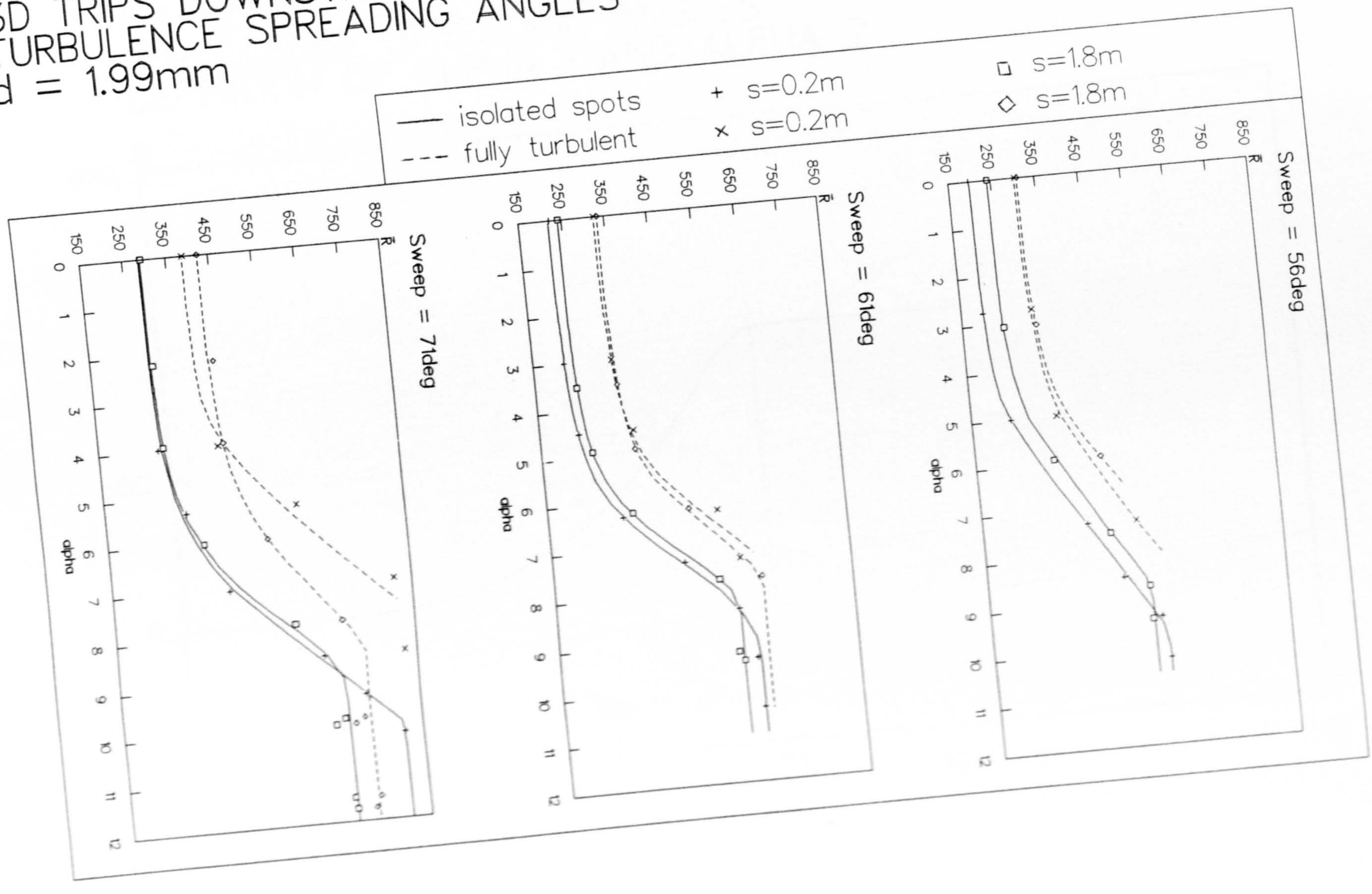

FIG 6.7
TURBULENCE SPREADING ANGLES
DEFINITION OF ALPHA 1 AND ALPHA 2

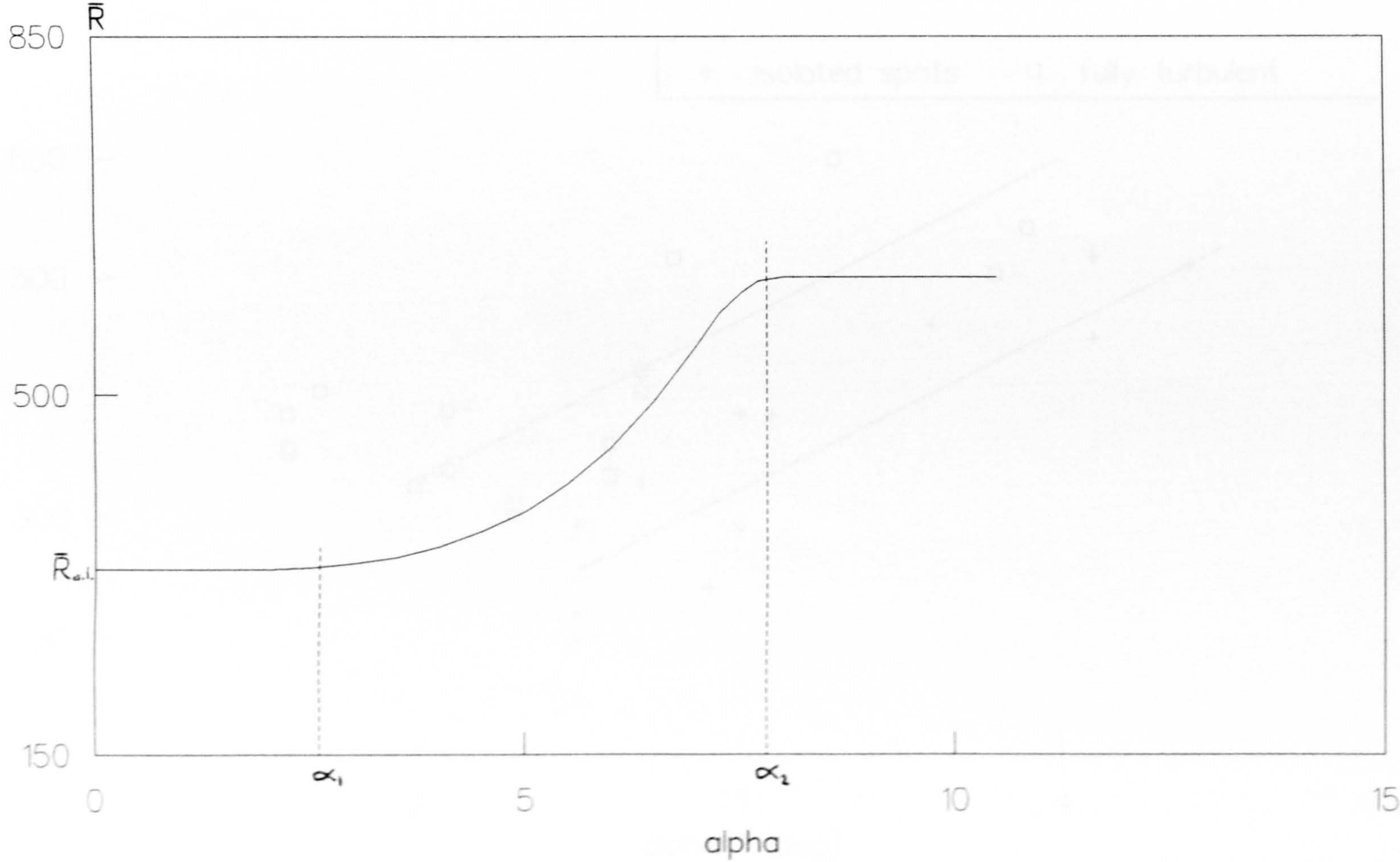

FIG 6.8
TURBULENCE SPREADING ANGLES
ALPHA 1

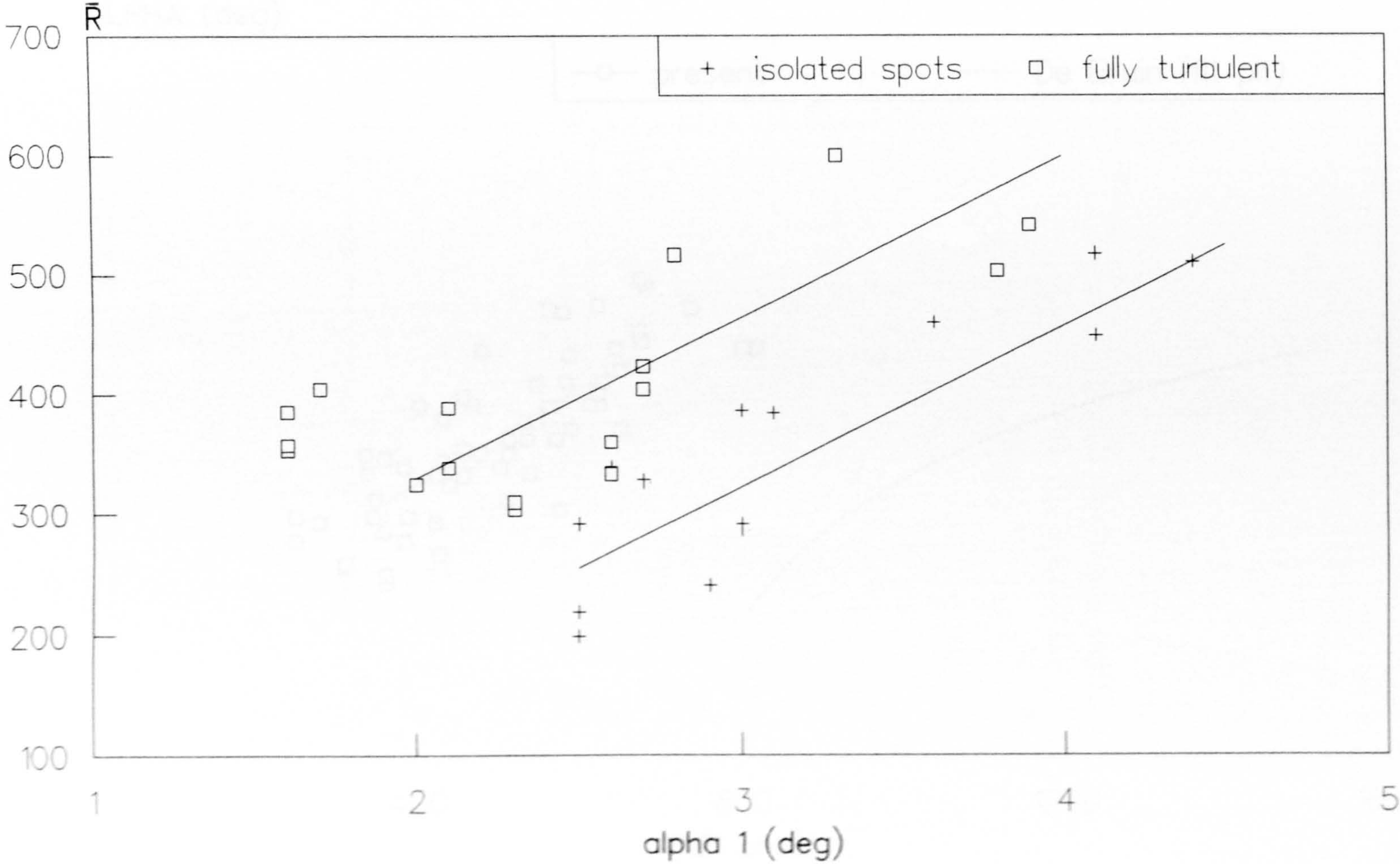

FIG 6.9
3D TRIPS DOWNSTREAM OF ATTACHMENT LINE
TURBULENCE SPREADING ANGLES ; ISOLATED SPOTS

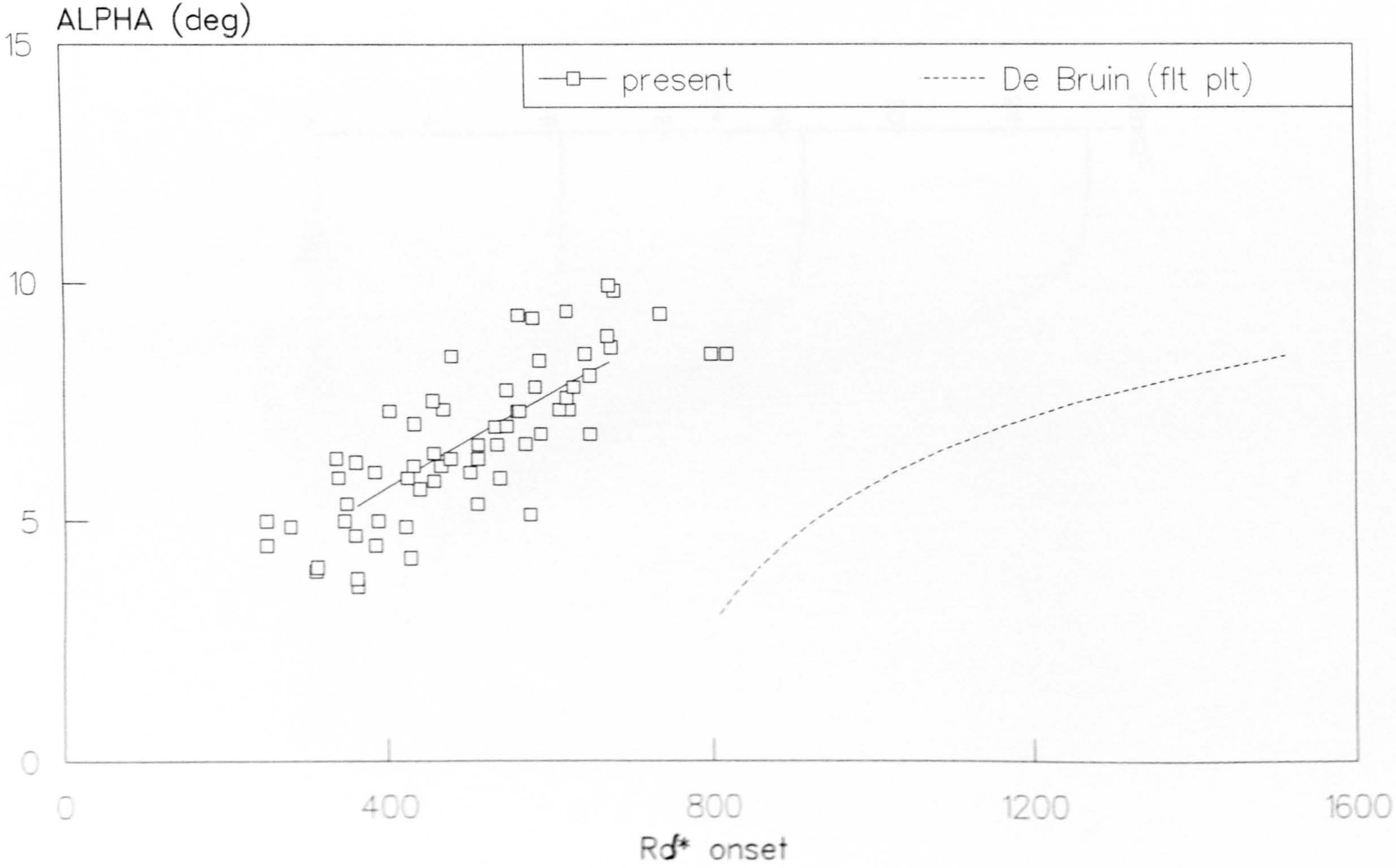

FIG 7.1
EFFECT OF FREESTREAM TURBULENCE ON
FLAT PLATE BOUNDARY LAYER WITH 2D TRIP
FROM TANI'61

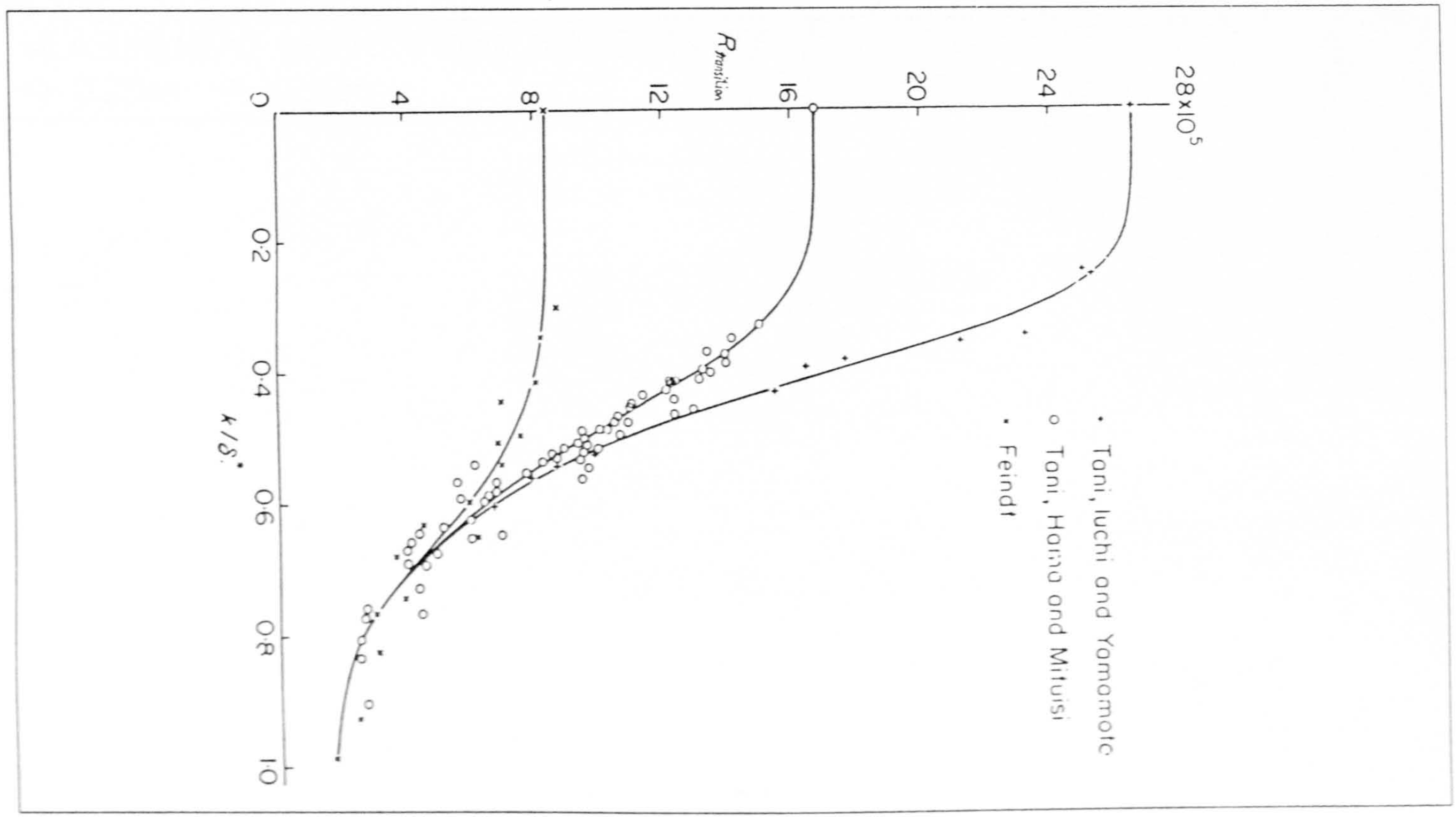

FIG 7.2
FREESTREAM TURBULENCE INTENSITY
'MEDIUM' LEVELS

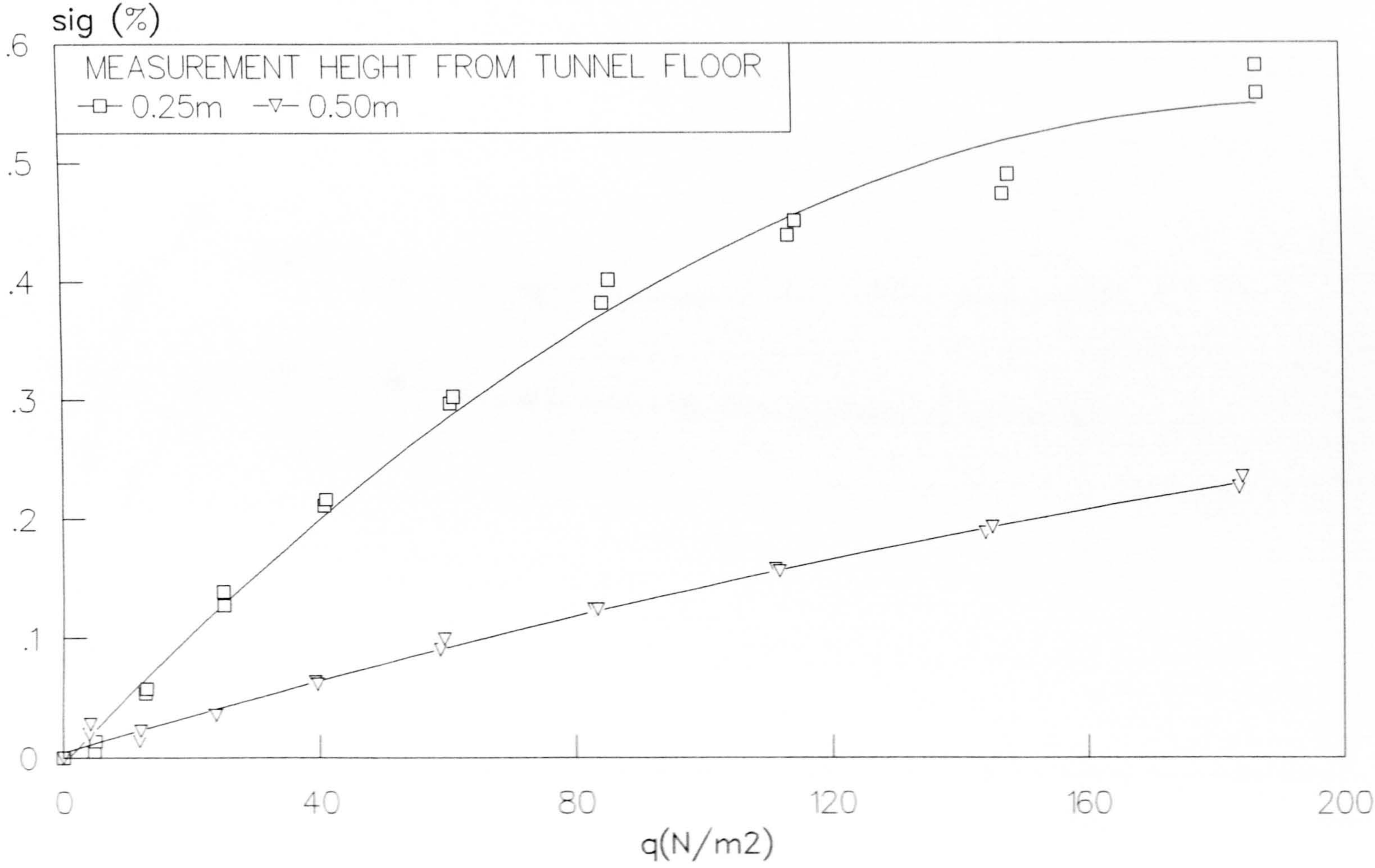

FIG 7.3
FREESTREAM TURBULENCE INTENSITY
'HIGH' LEVELS

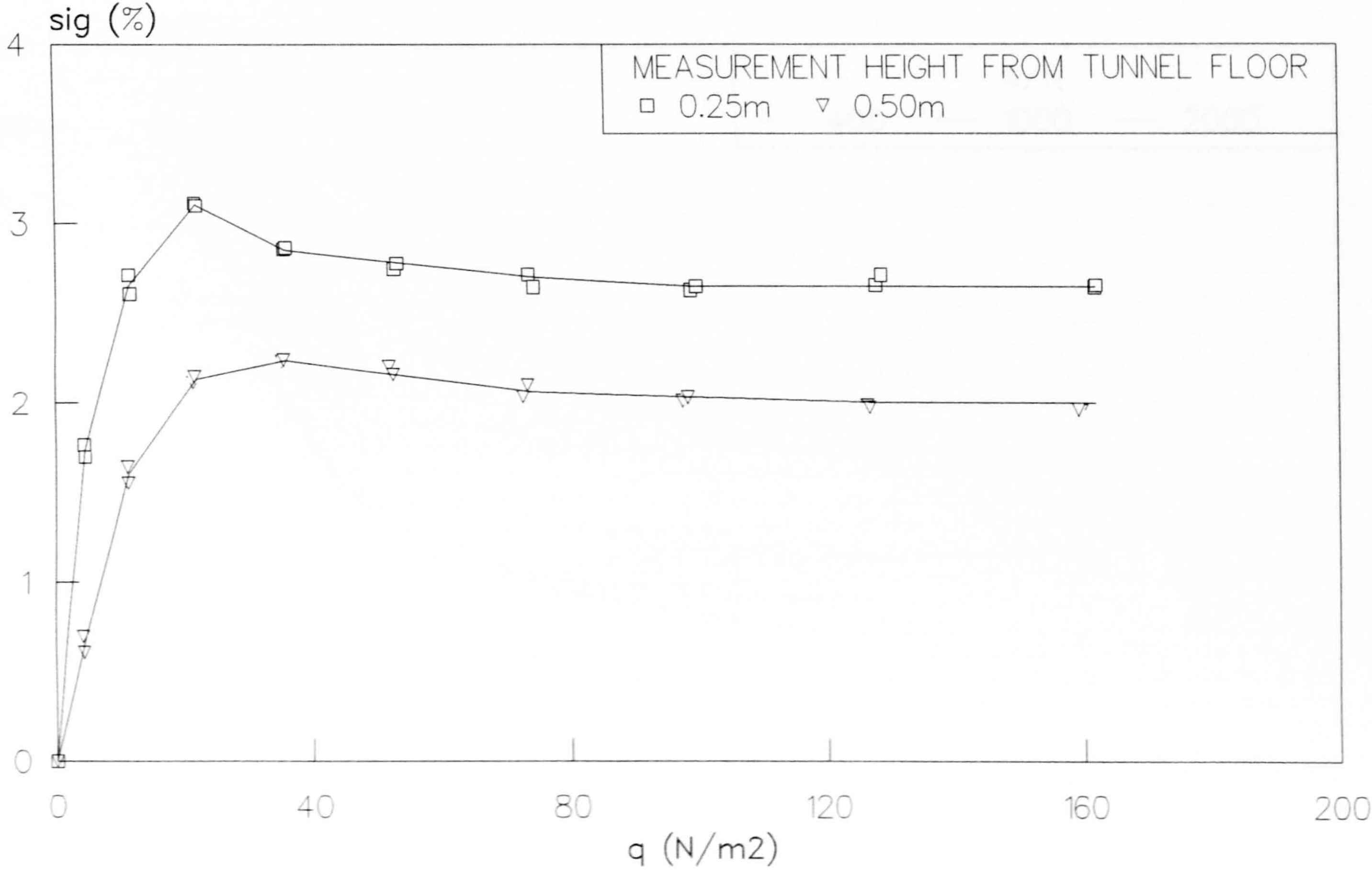

FIG 7.4
2D TRIPS, MEDIUM LEVELS OF FREESTREAM TURBULENCE
TRANSITION ONSET

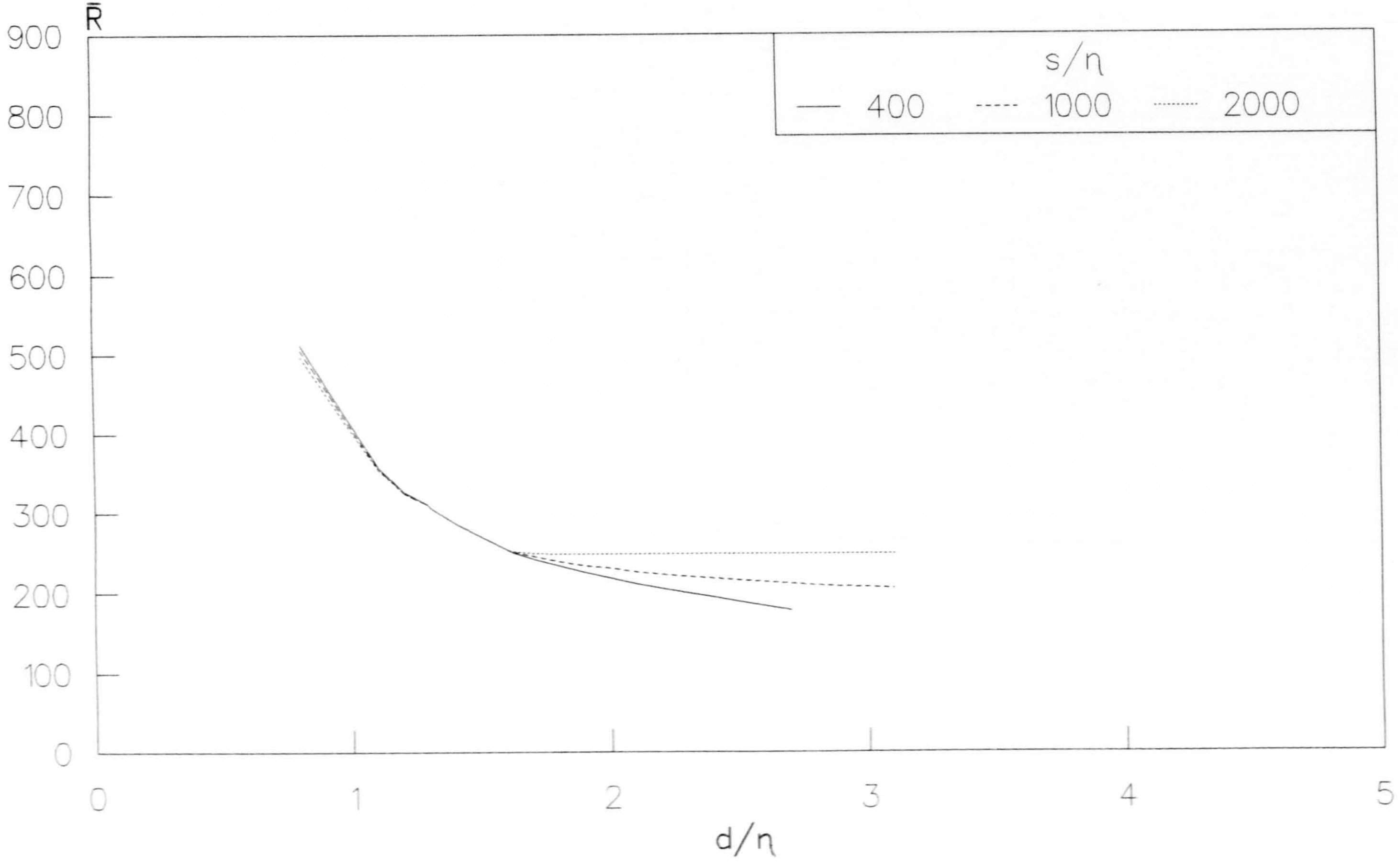

FIG 7.5
2D TRIPS, MEDIUM LEVELS OF FREESTREAM TURBULENCE
TRANSITION COMPLETION

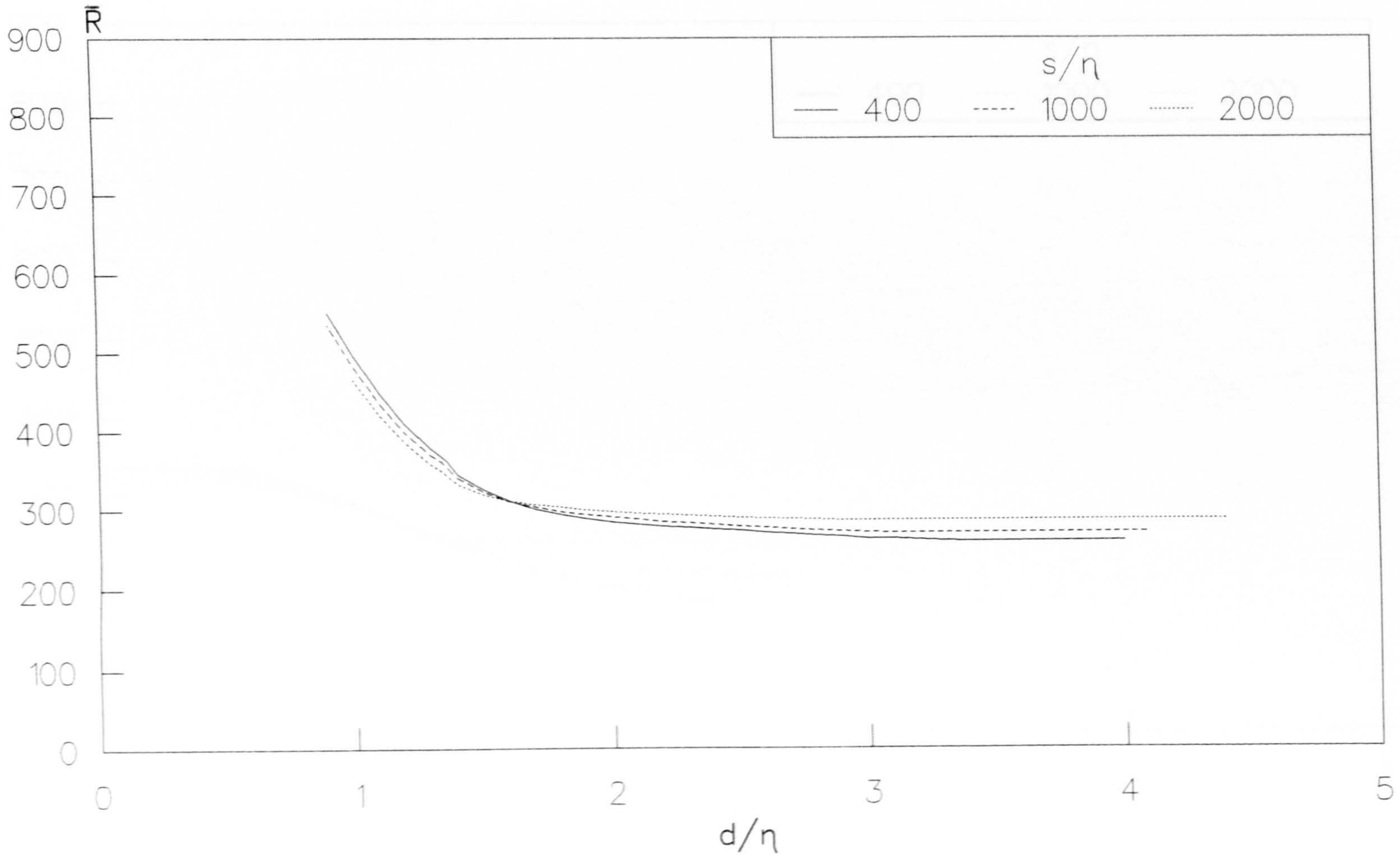

FIG 7.6
2D TRIPS, HIGH LEVELS OF FREESTREAM TURBULENCE
TRANSITION ONSET

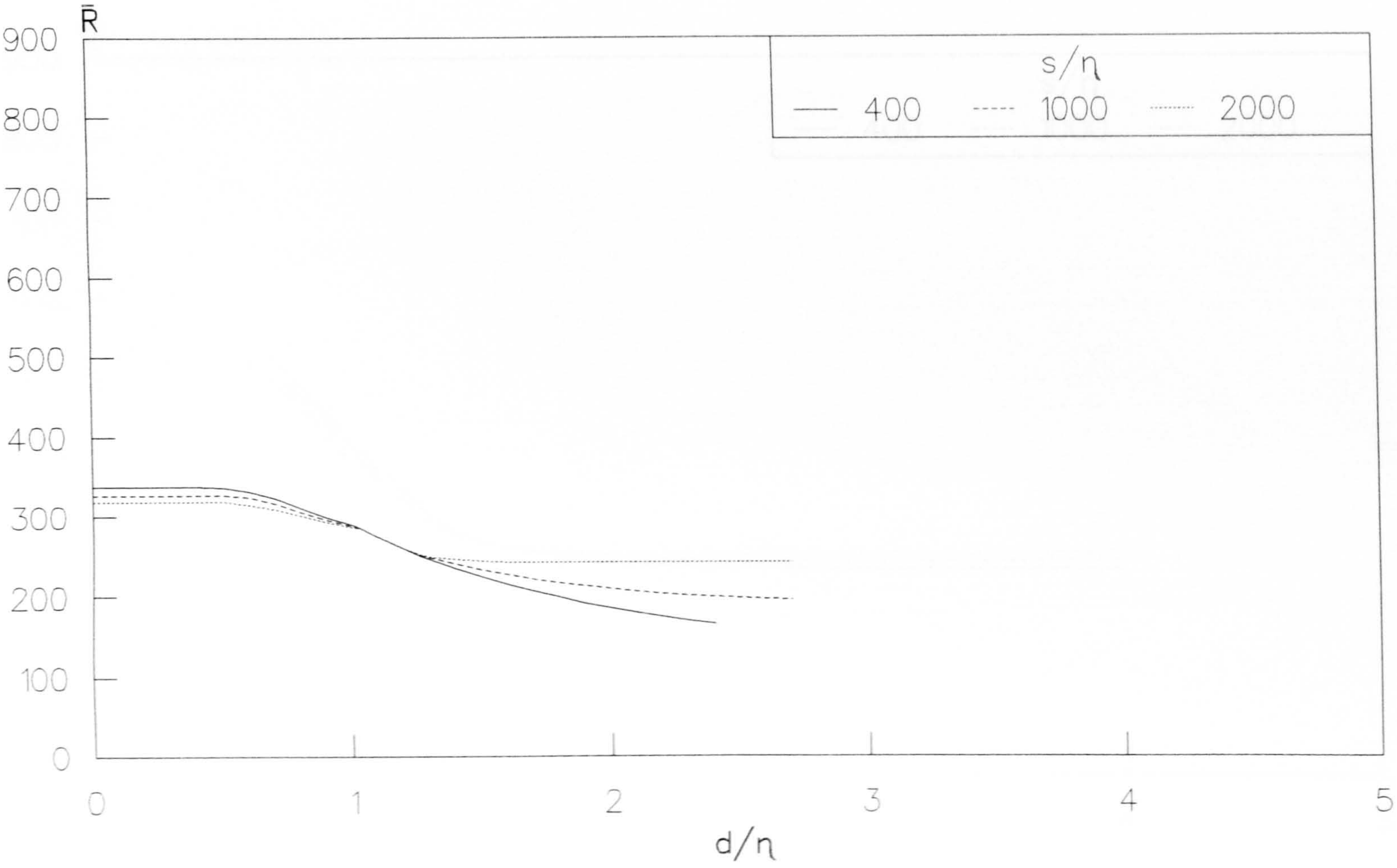

FIG 7.7
2D TRIPS, HIGH LEVELS OF FREESTREAM TURBULENCE
TRANSITION COMPLETION

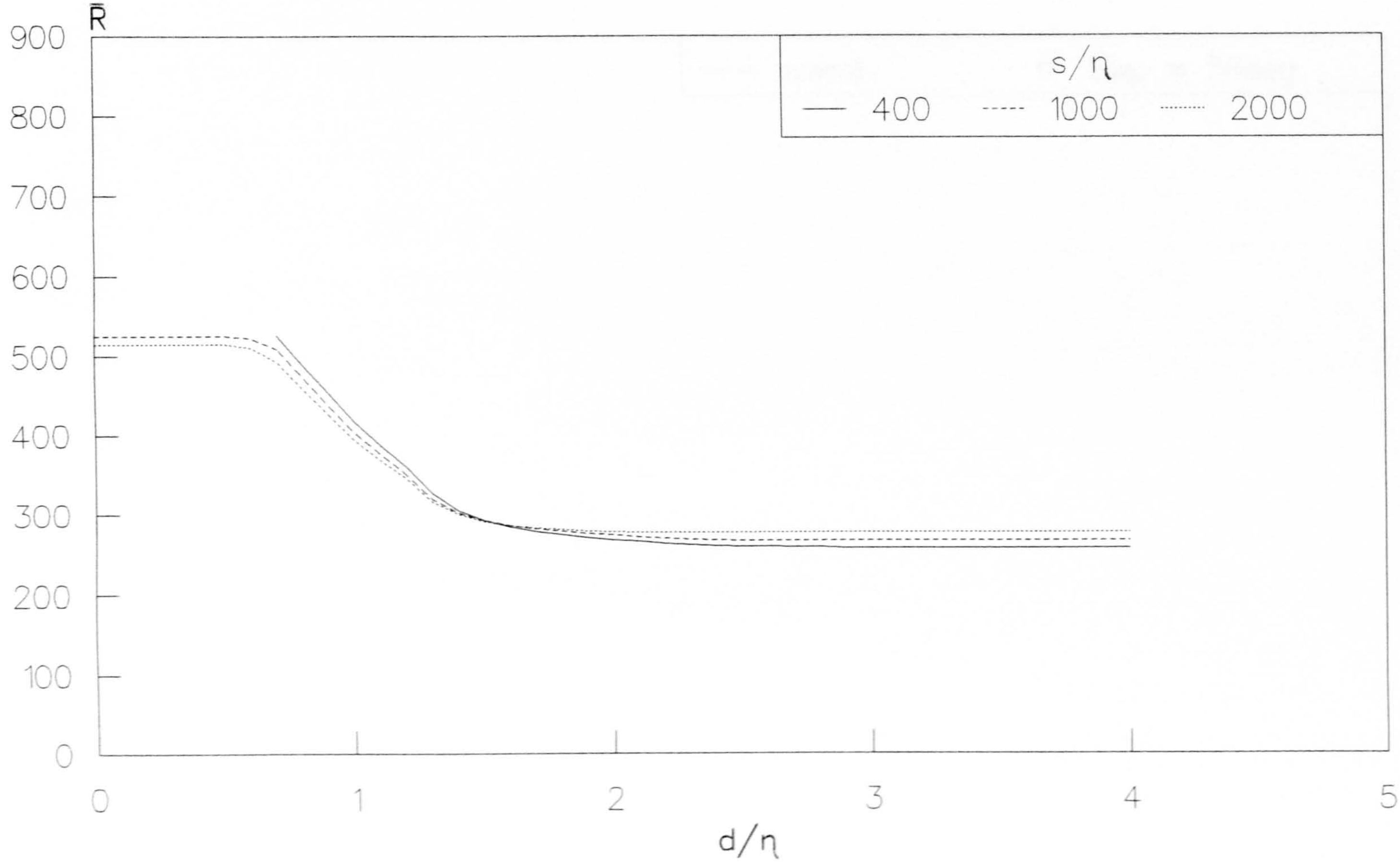

FIG 7.8
2D TRIPS, HIGH LEVELS OF FREESTREAM TURBULENCE
TRANSITION ONSET ; $s/\eta = 1000$

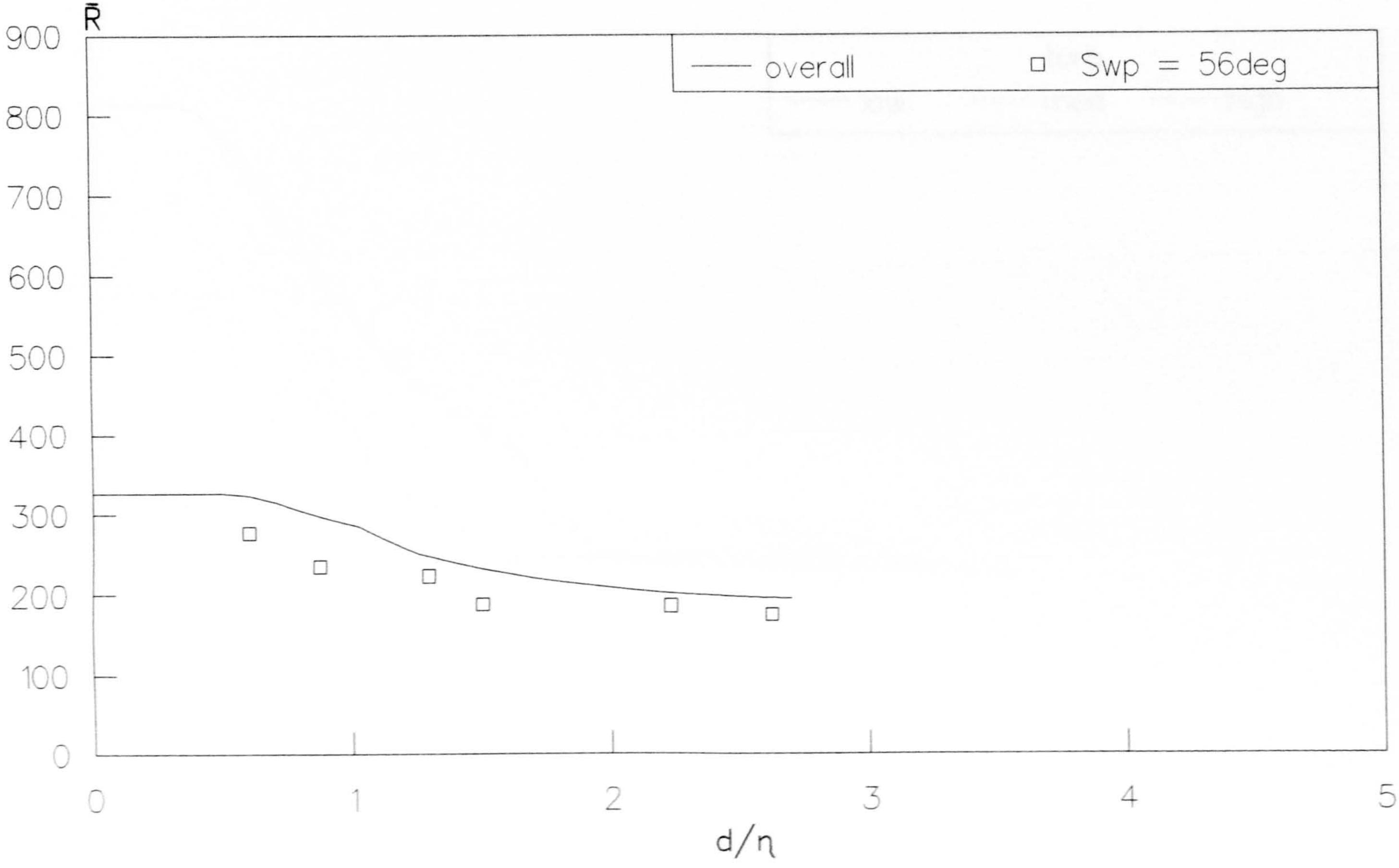

FIG 7.9
TRANSITION ONSET, $s/\eta = 2000$
2D TRIPS ; VARIOUS LEVELS OF FREESTREAM TURBULENCE

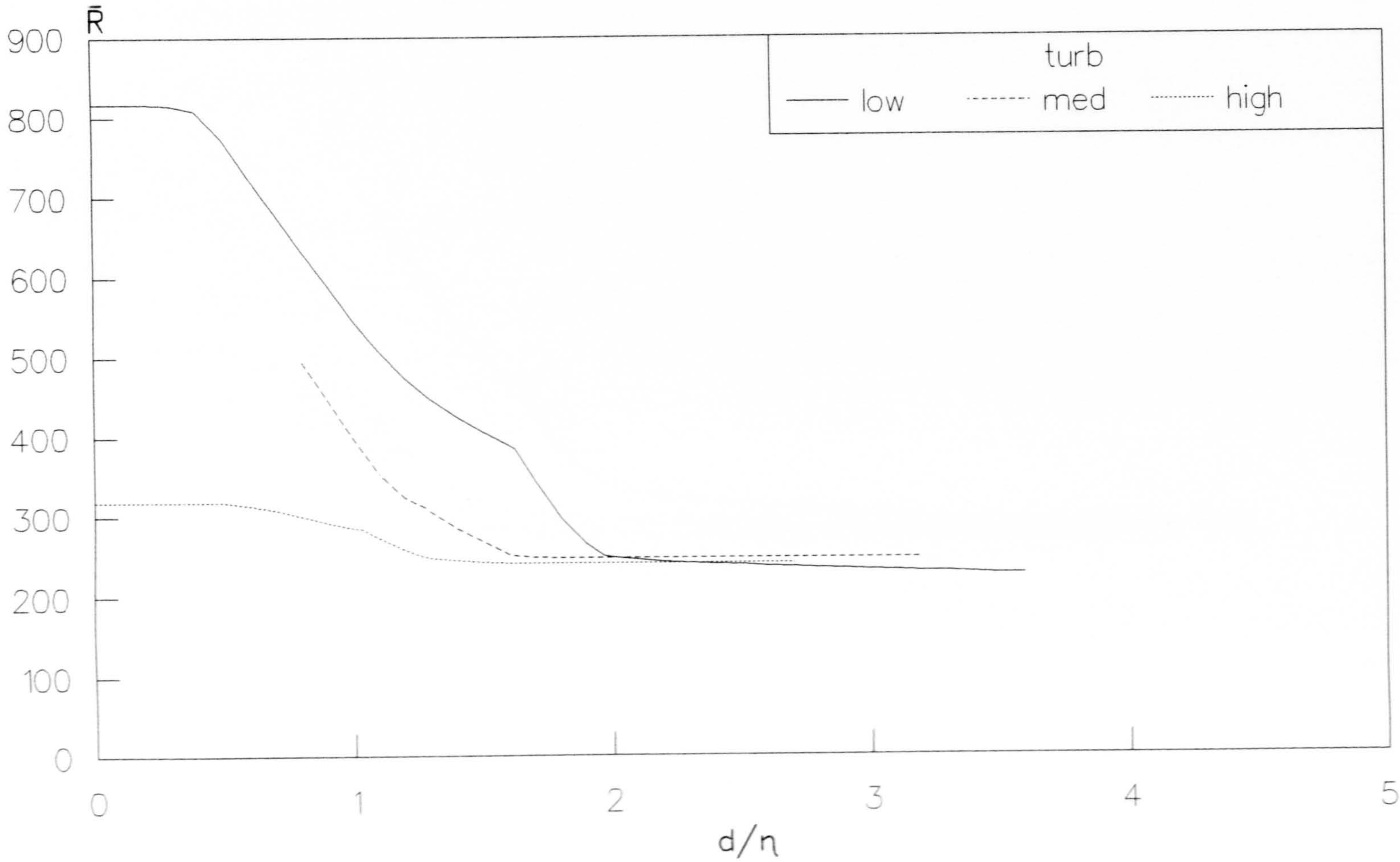

FIG 7.10
TRANSITION COMPLETION, $s/\eta = 2000$
2D TRIPS ; VARIOUS LEVELS OF FREESTREAM TURBULENCE

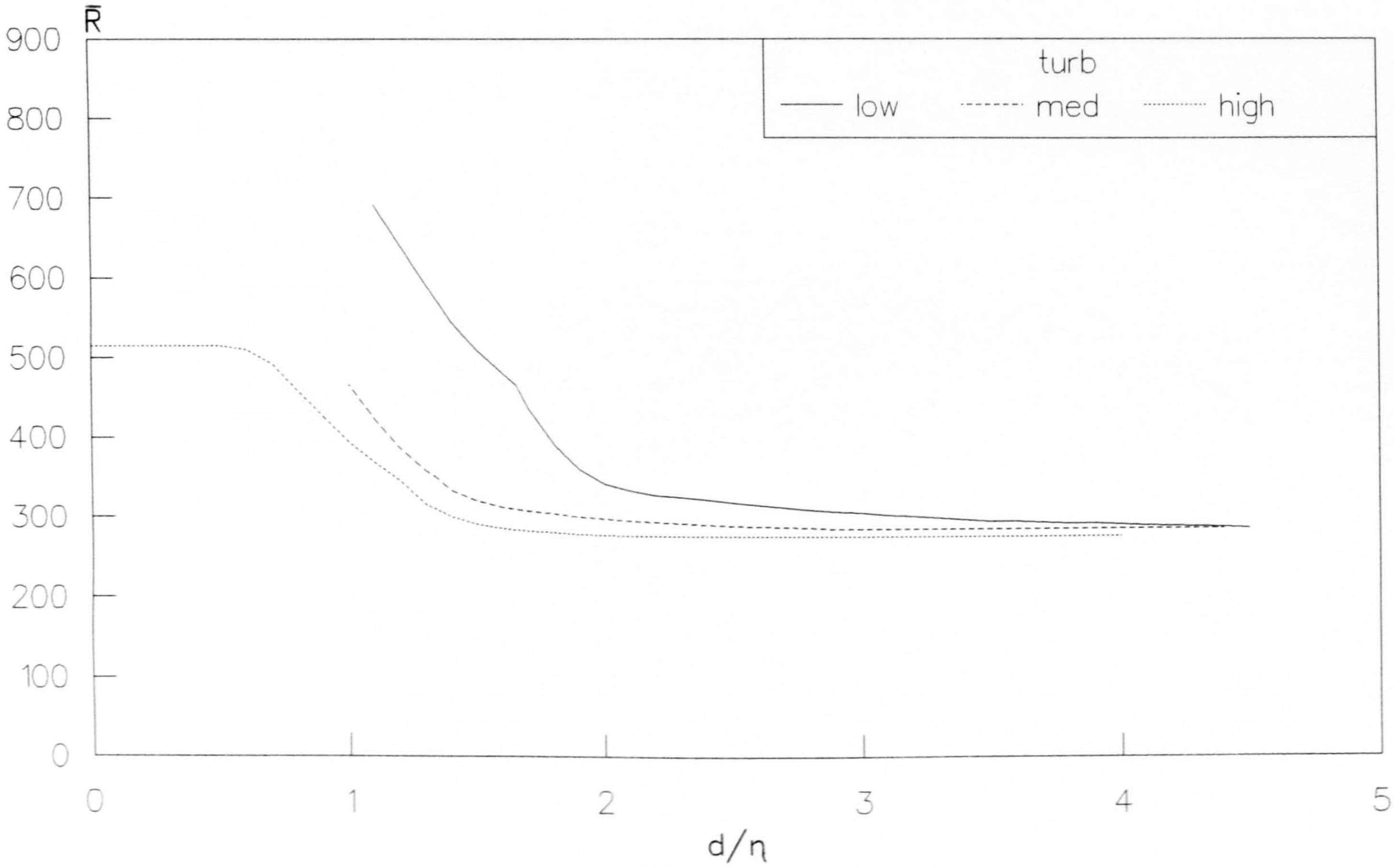

FIG 7.11
TRANSITION ONSET IN LIMIT AS s/η TENDS TO ZERO
2D TRIPS ; VARIOUS LEVELS OF FREESTREAM TURBULENCE

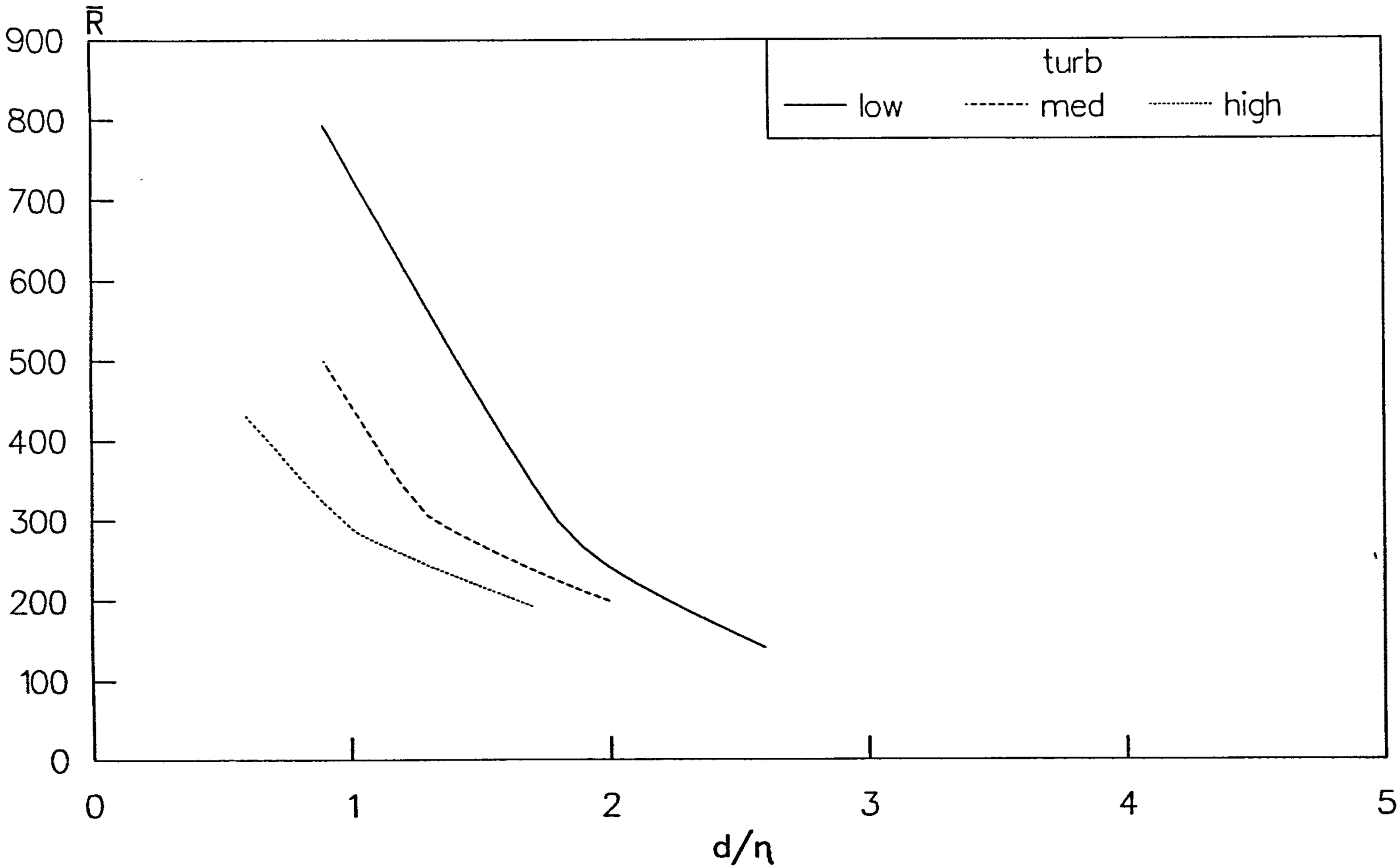

FIG 7.12
TRANSITION COMPLETION IN LIMIT AS s/η TENDS TO ZERO
2D TRIPS ; VARIOUS LEVELS OF FREESTREAM TURBULENCE

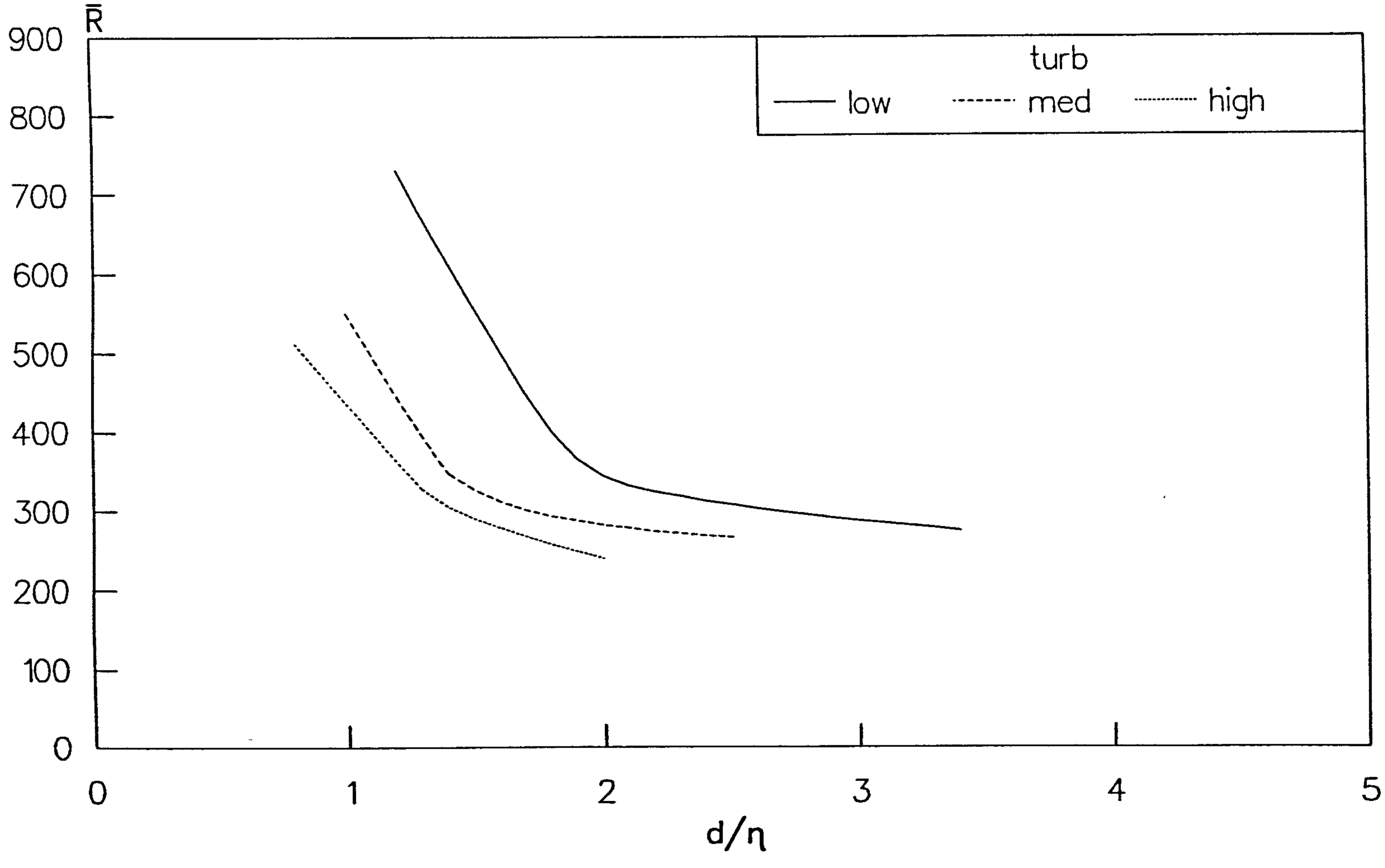

FIG 7.13
TRANSITION IN LIMIT AS s/η TENDS TO ZERO
2D TRIPS, MEDIUM LEVELS OF FREESTREAM TURBULENCE

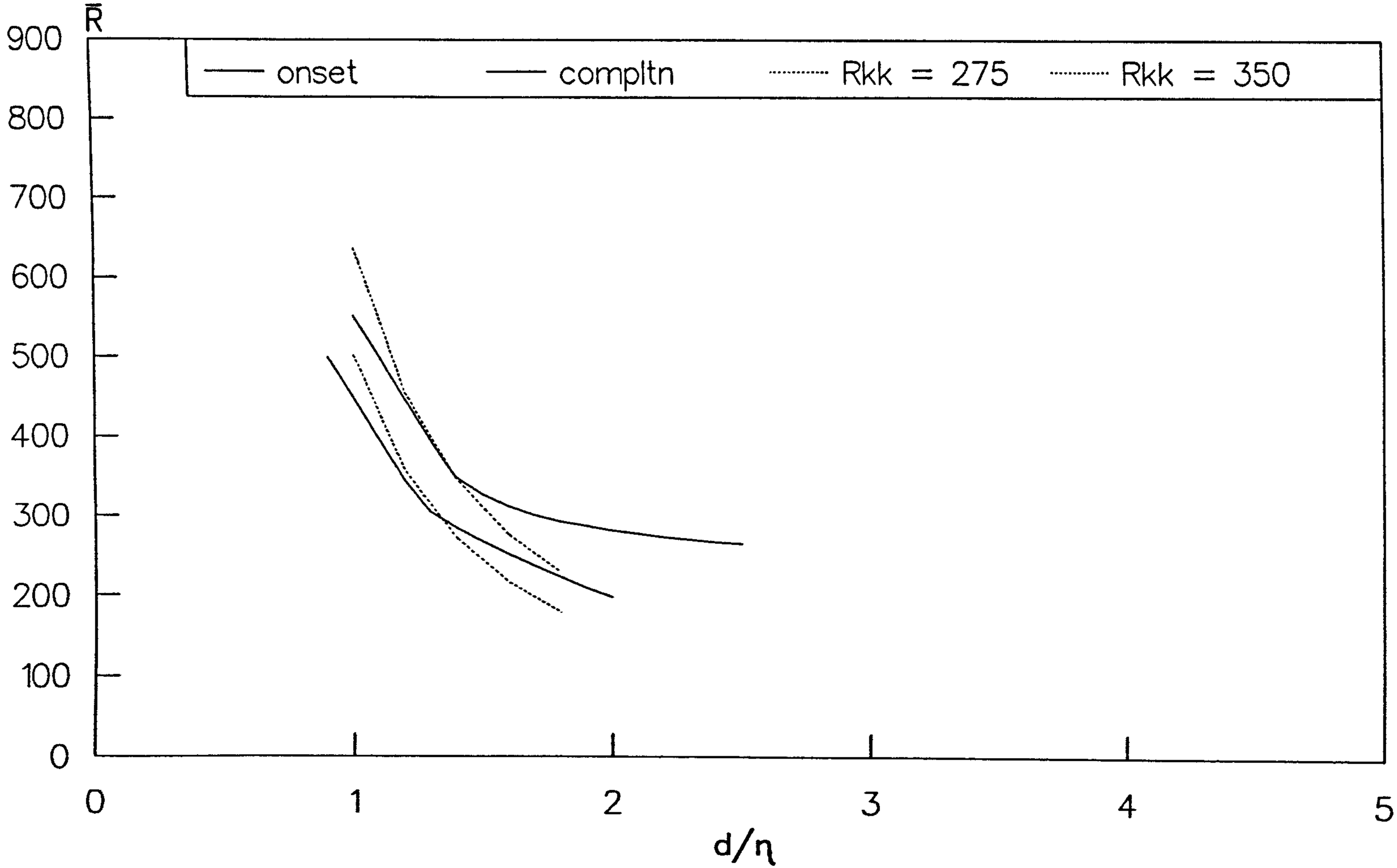

FIG 7.14
TRANSITION IN LIMIT AS s/η TENDS TO ZERO
2D TRIPS, HIGH LEVELS OF FREESTREAM TURBULENCE

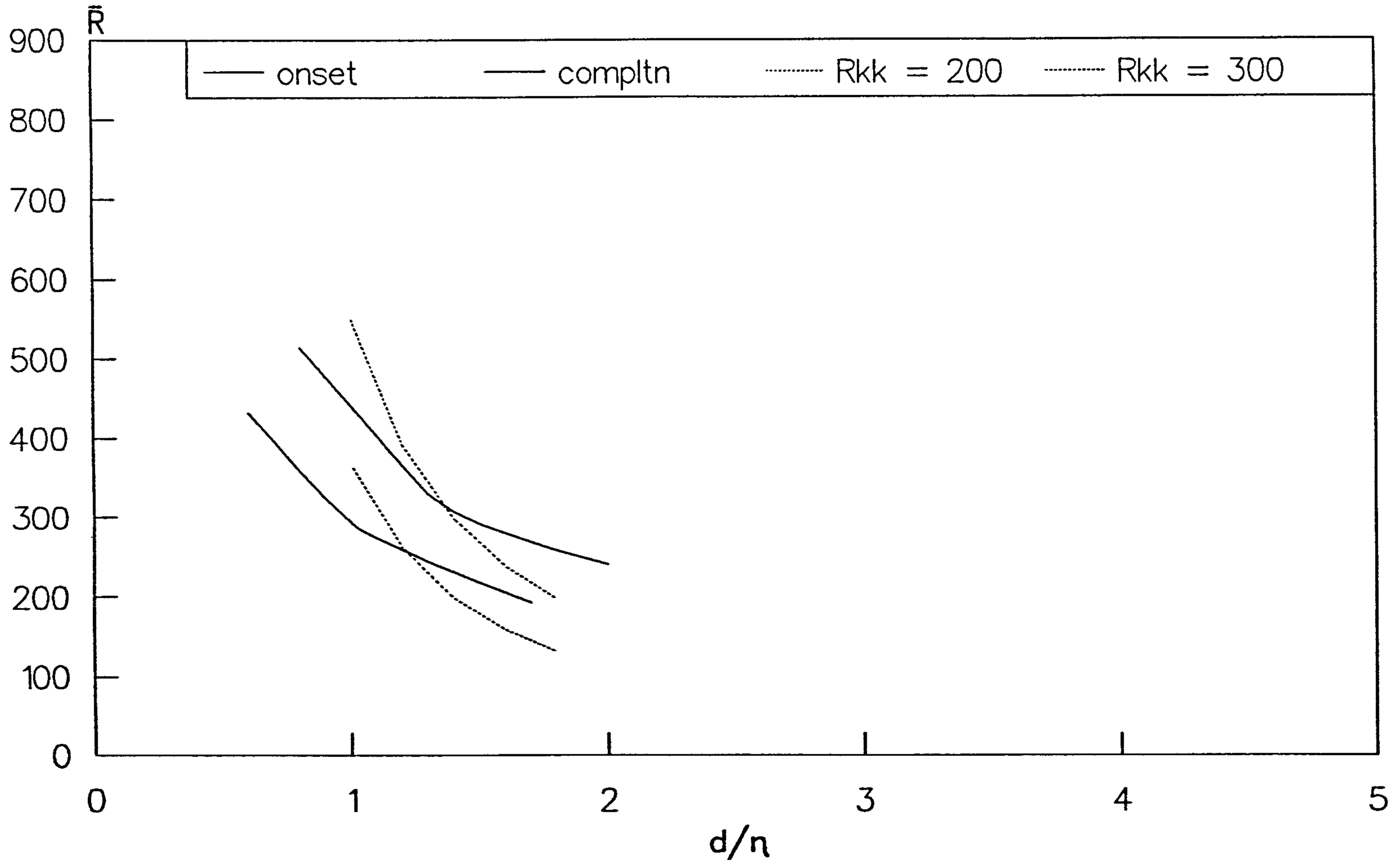

FIG 7.15
TRANSITION ONSET AT TRIP
VARIOUS LEVELS OF FREESTREAM TURBULENCE

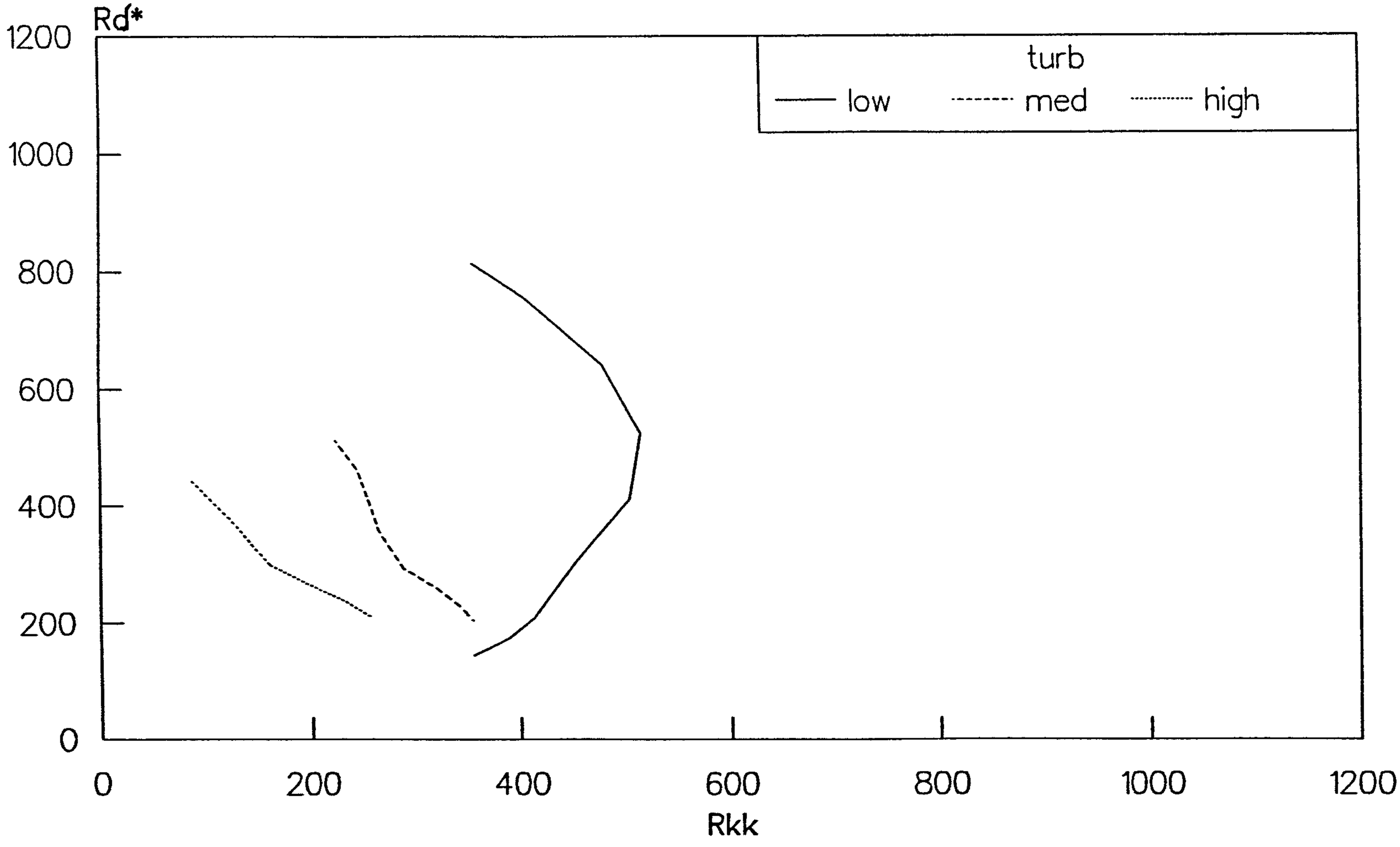

FIG 7.16
TRANSITION COMPLETION AT TRIP
VARIOUS LEVELS OF FREESTREAM TURBULENCE

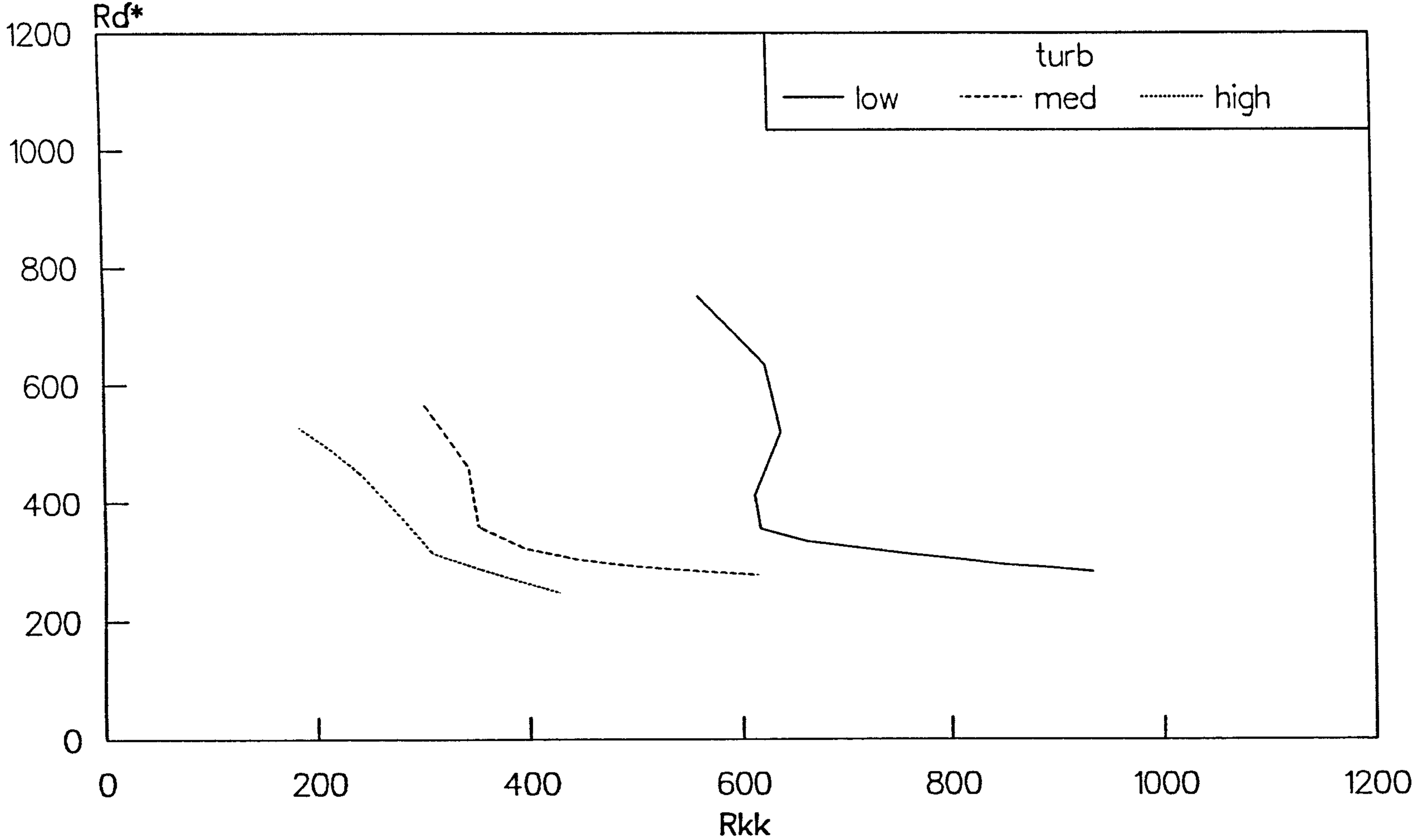

FIG 7.17
GENERAL INTERMITTENCY DISTRIBUTION
2D TRIPS ; MED & HIGH TURBULENCE

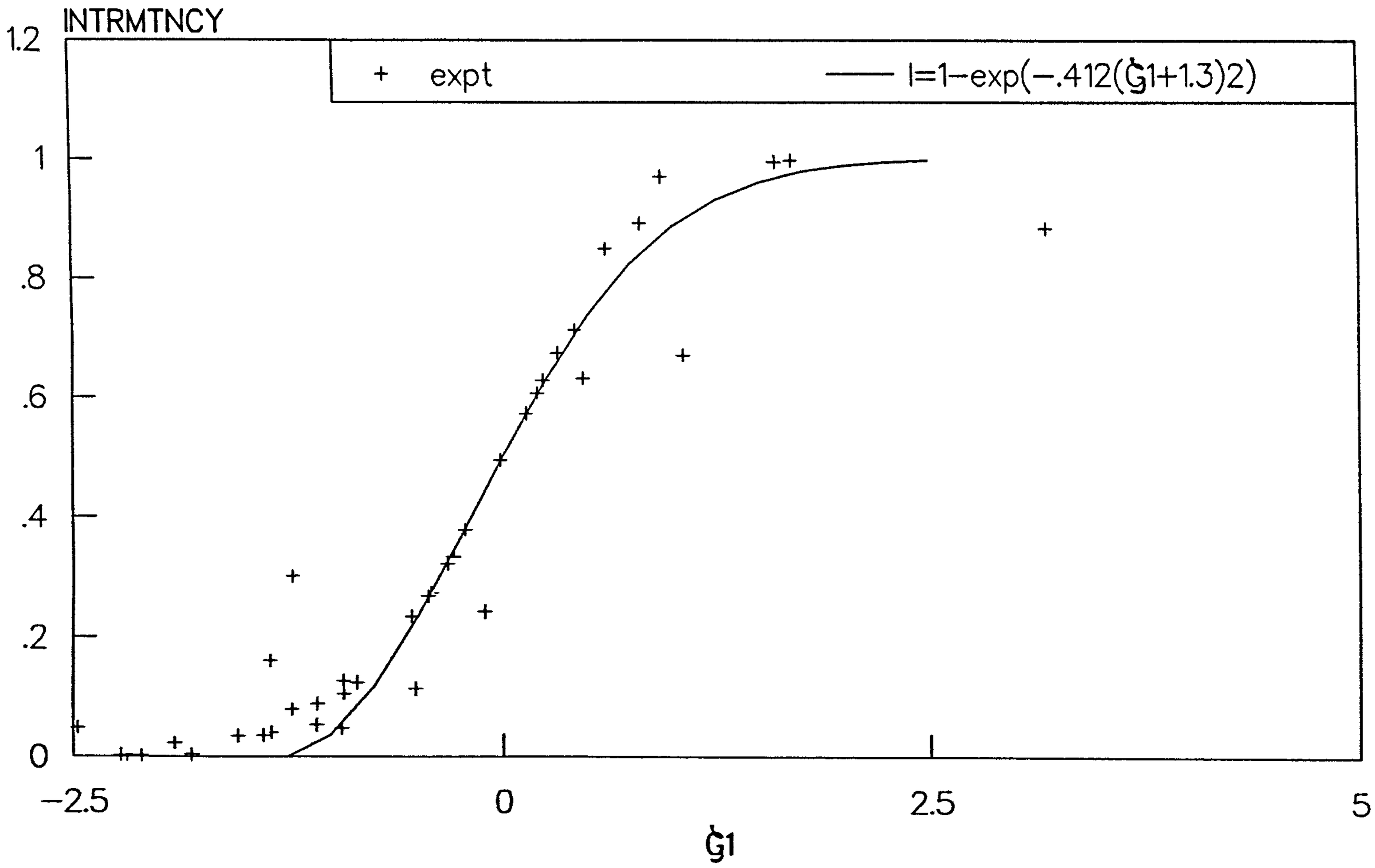

FIG 7.18
GENERAL INTERMITTENCY DISTRIBUTION
2D TRIPS ; MED & HIGH TURBULENCE

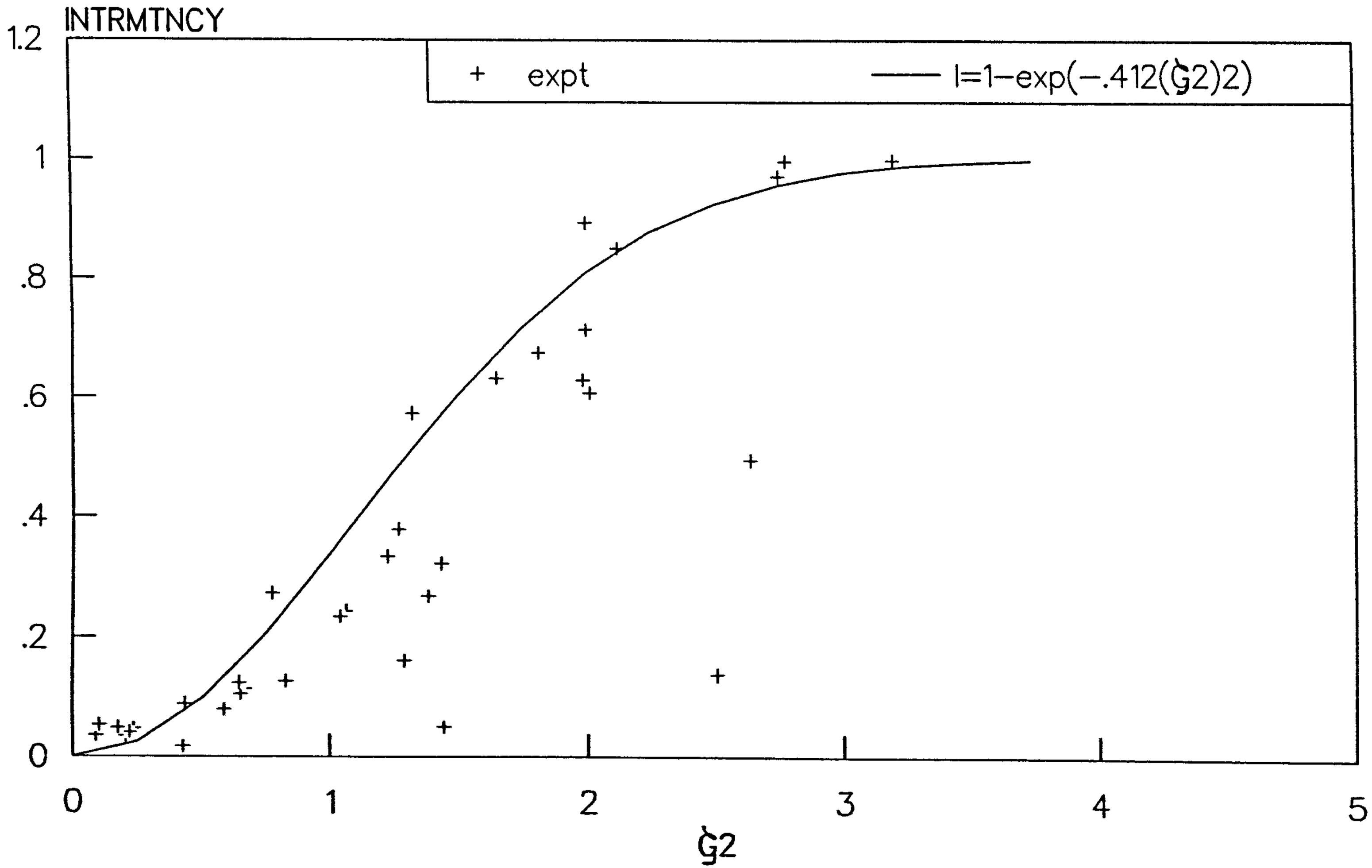

FIG 7.19
3D TRIPS , MEDIUM LEVELS OF FREESTREAM TURBULENCE
TRANSITION ONSET

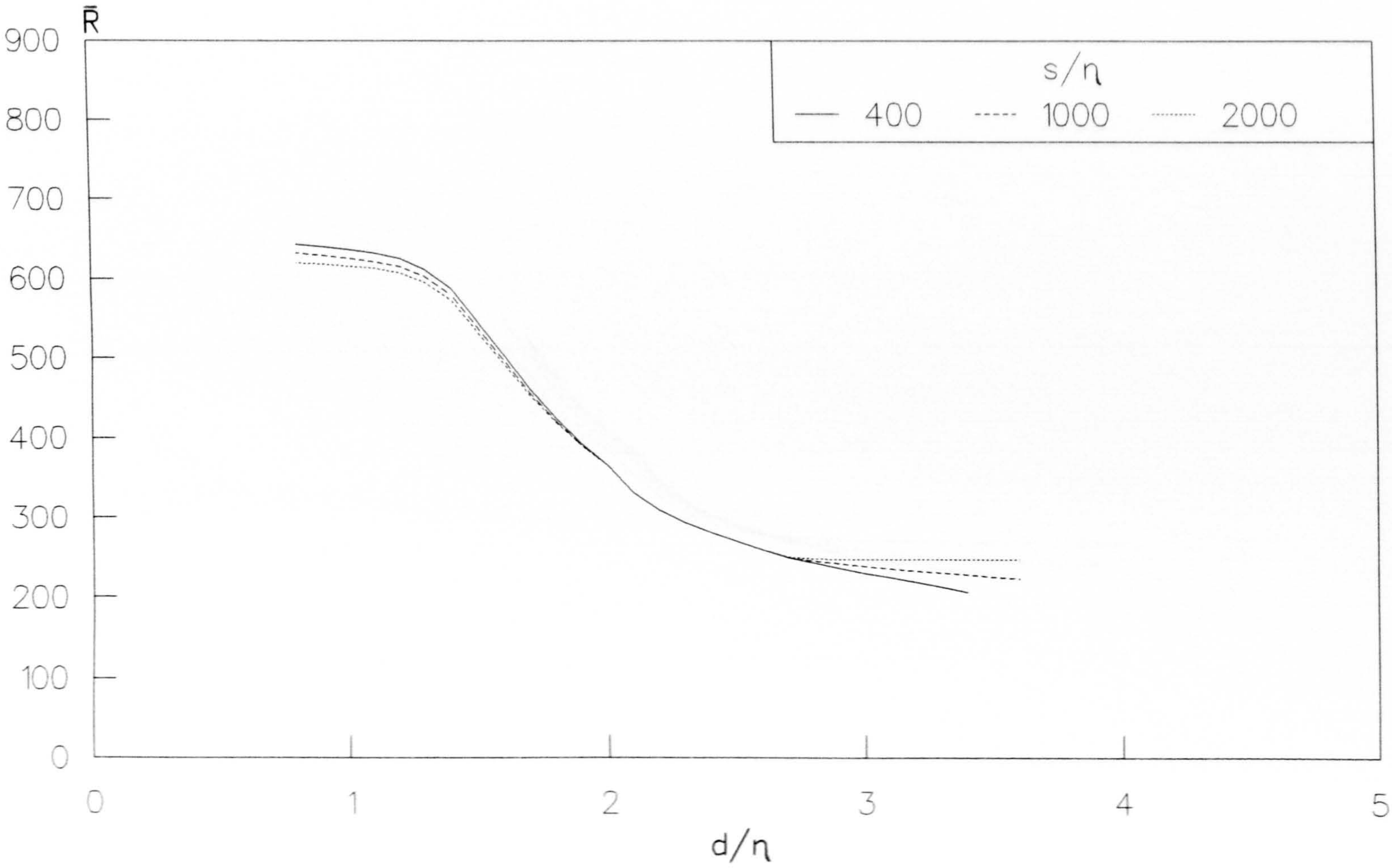

FIG 7.20
3D TRIPS , MEDIUM LEVELS OF FREESTREAM TURBULENCE
TRANSITION COMPLETION

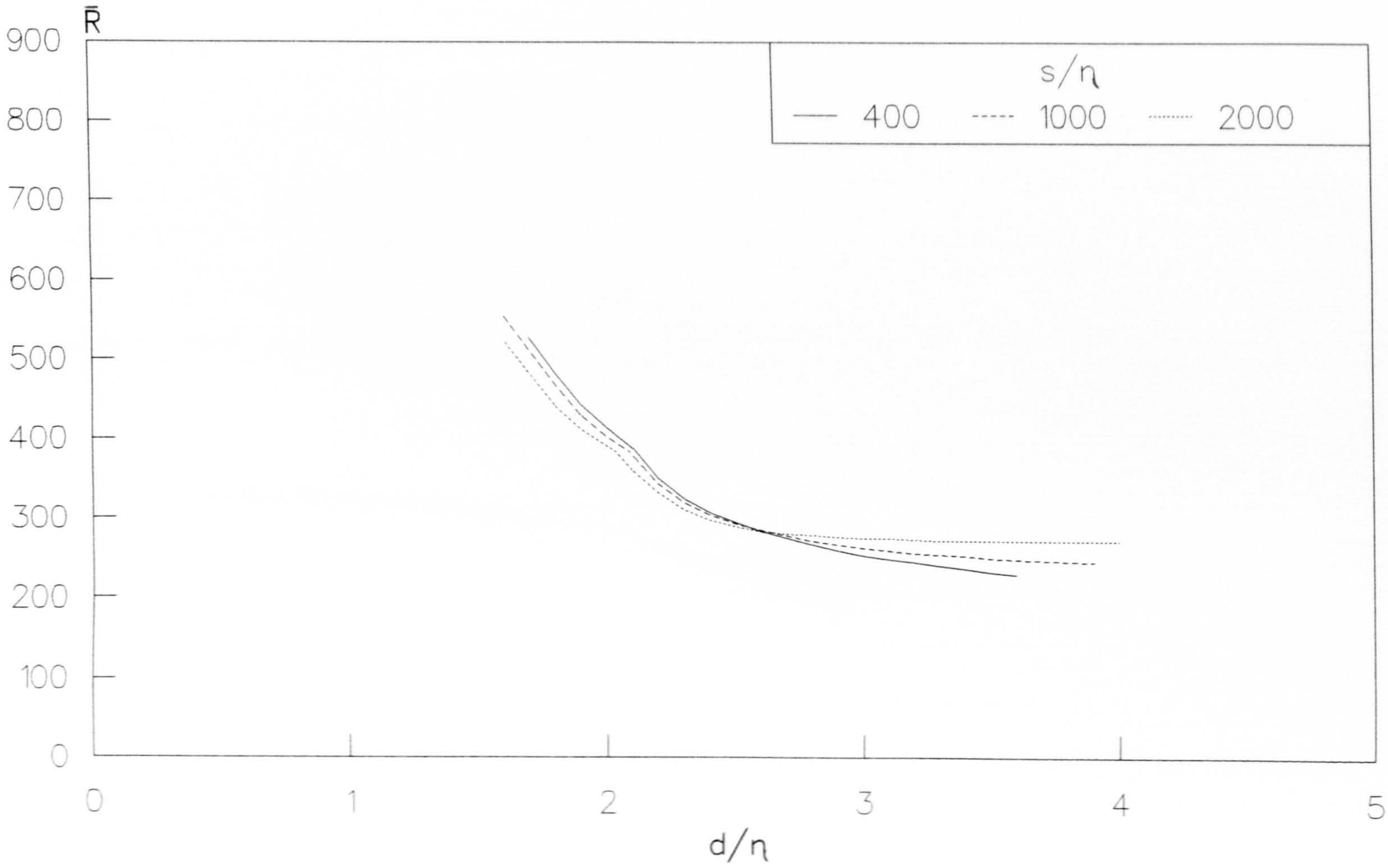

FIG 7.21
3D TRIPS, HIGH LEVELS OF FREESTREAM TURBULENCE
TRANSITION ONSET

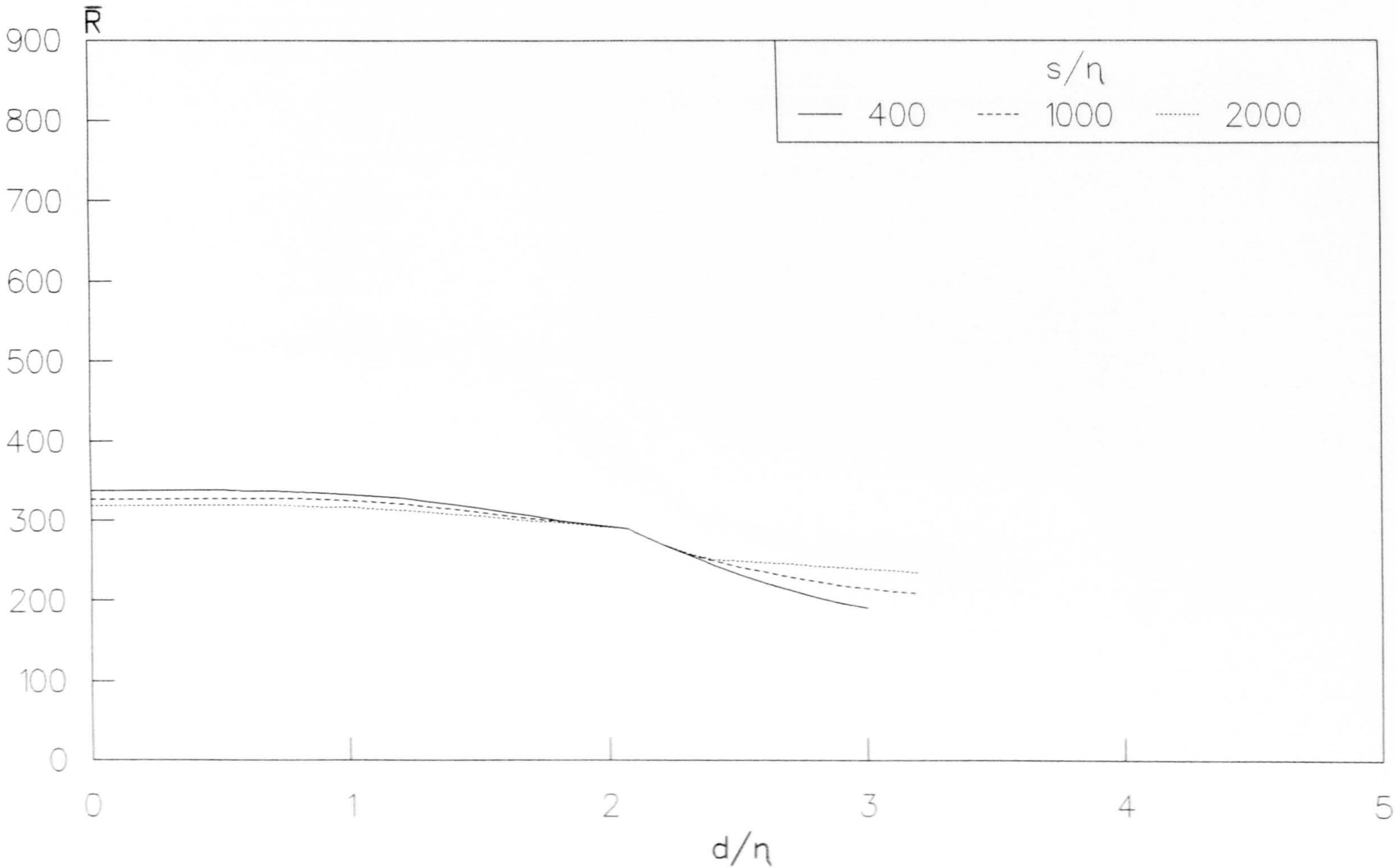

FIG 7.22
3D TRIPS, HIGH LEVELS OF FREESTREAM TURBULENCE
TRANSITION COMPLETION

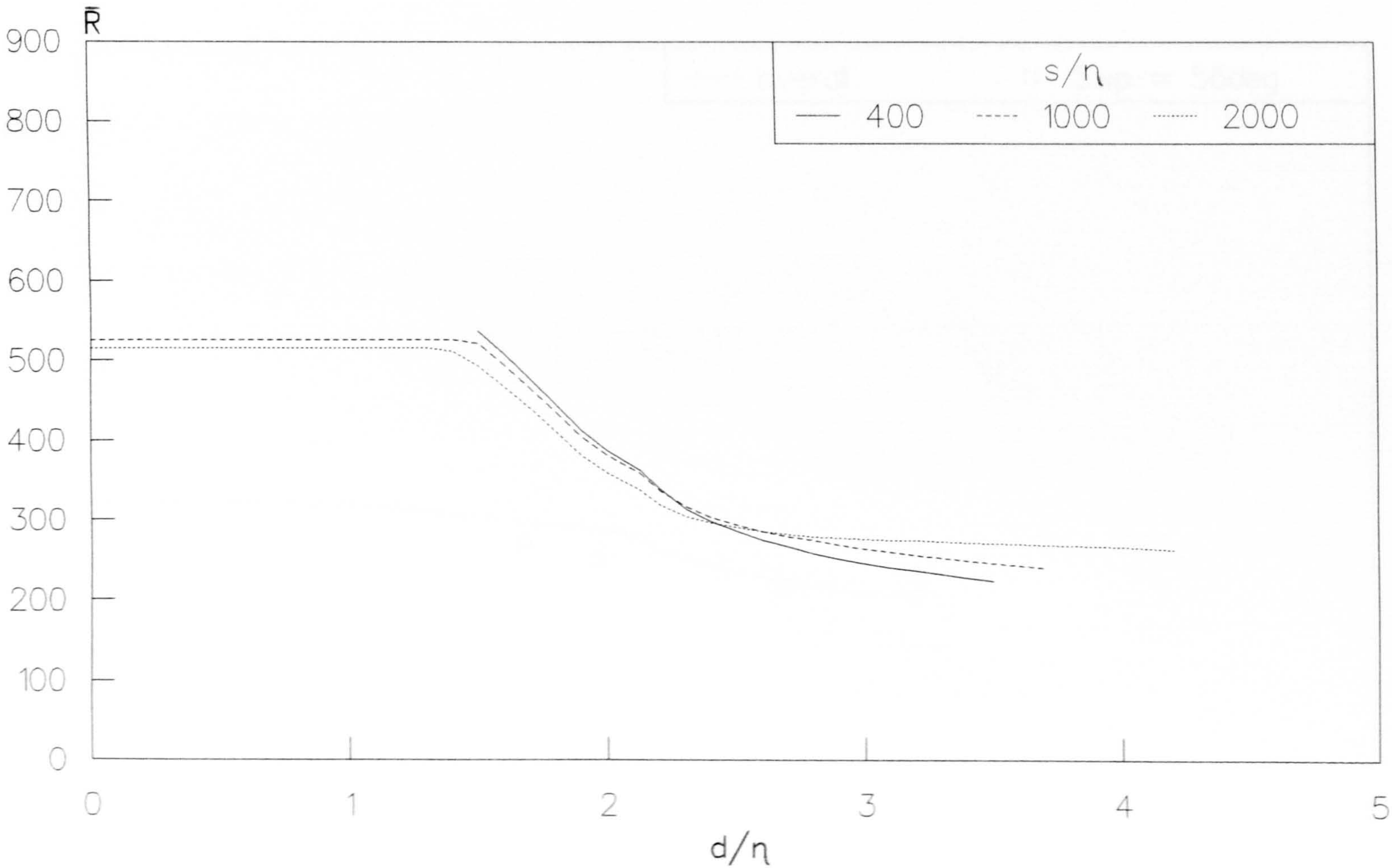

FIG 7.23
3D TRIPS, HIGH LEVELS OF FREESTREAM TURBULENCE
TRANSITION ONSET ; $s/\eta = 1000$

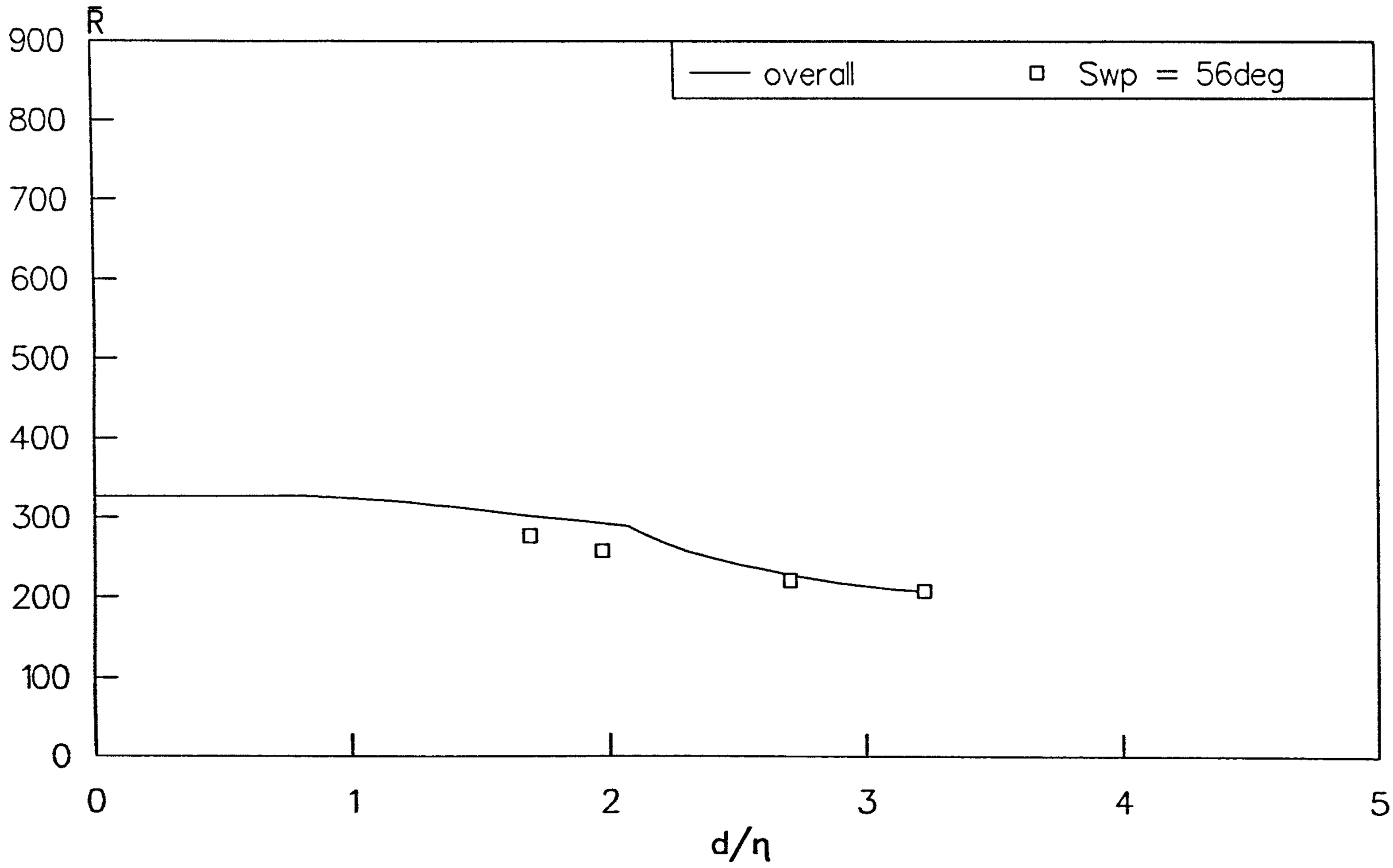

FIG 7.24
TRANSITION ONSET, $s/\eta = 2000$
3D TRIPS ; VARIOUS LEVELS OF FREESTREAM TURBULENCE

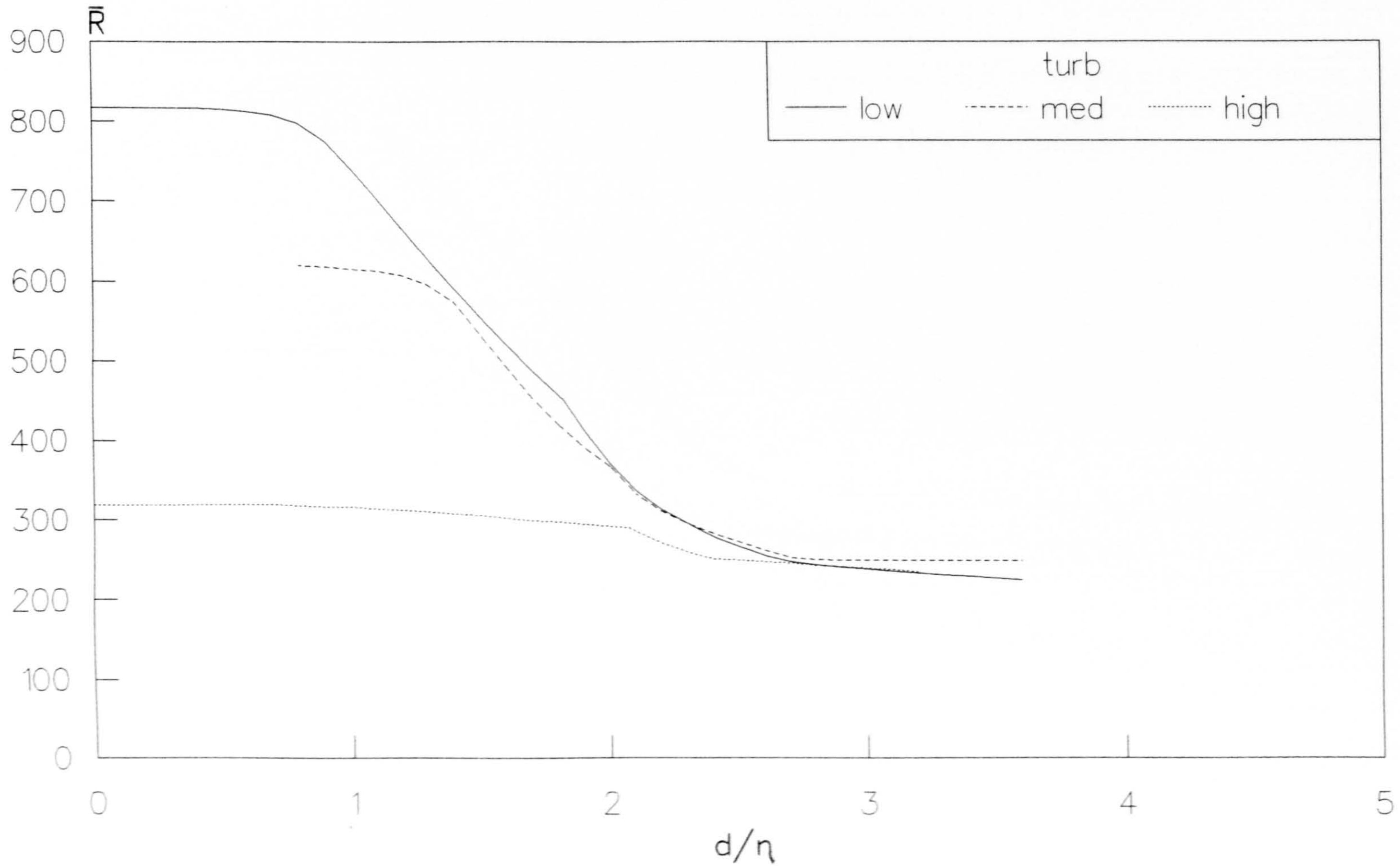

FIG 7.25
TRANSITION COMPLETION, $s/\eta = 2000$
3D TRIPS ; VARIOUS LEVELS OF FREESTREAM TURBULENCE

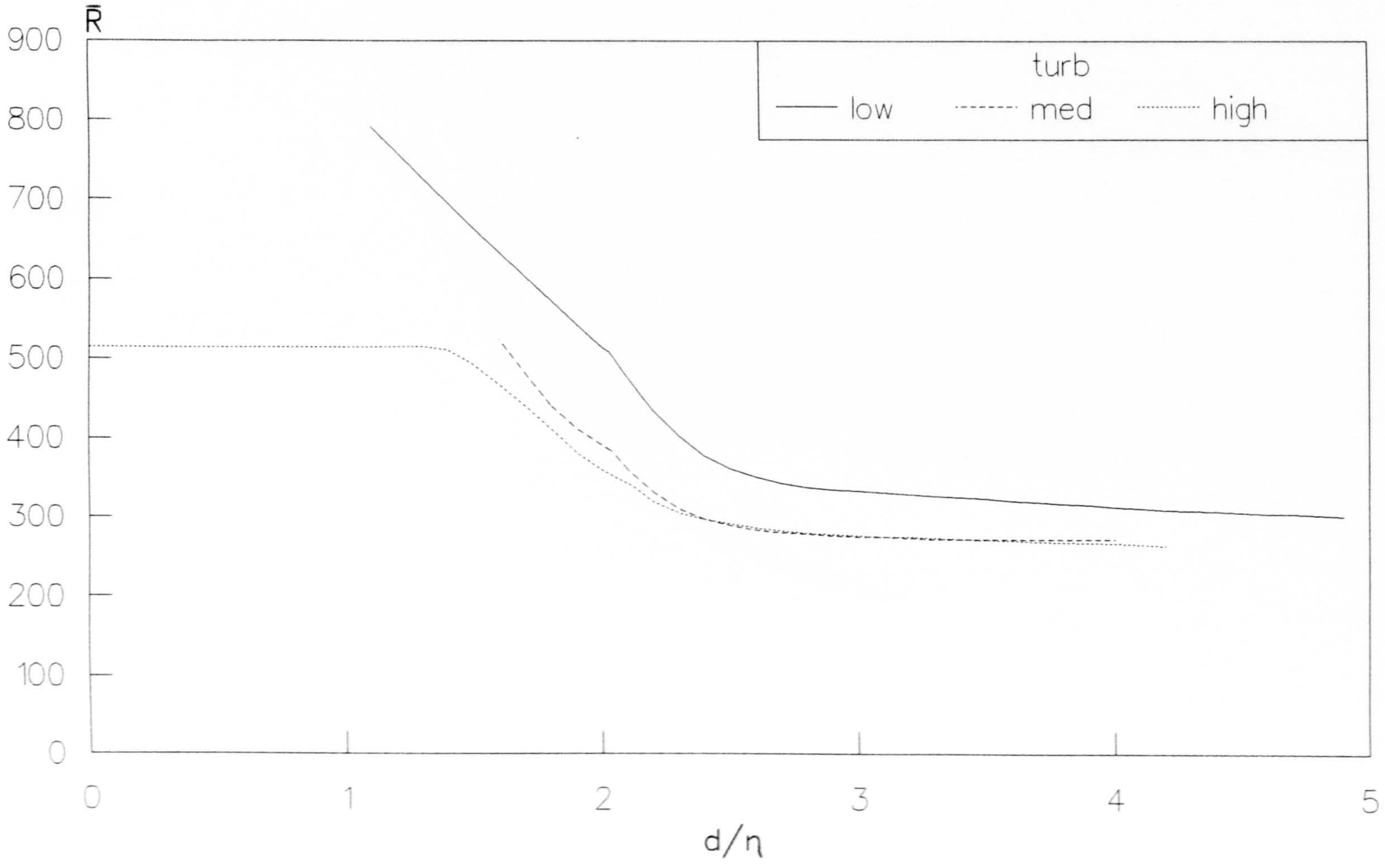

FIG 7.26
TRANSITION ONSET IN LIMIT AS s/η TENDS TO ZERO
3D TRIPS ; VARIOUS LEVELS OF FREESTREAM TURBULENCE

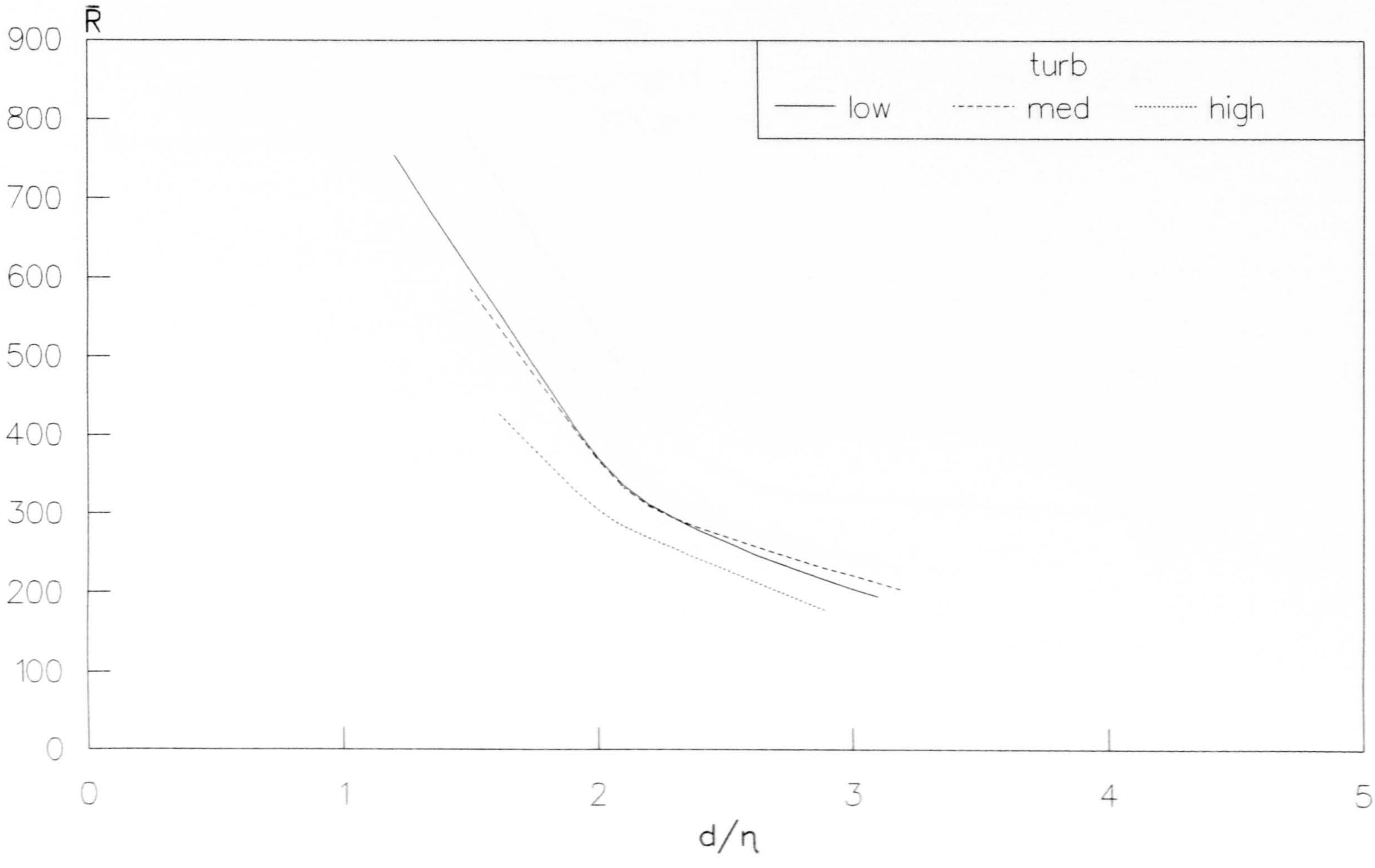

FIG 7.27
TRANSITION COMPLETION IN LIMIT AS s/n TENDS TO ZERO
3D TRIPS ; VARIOUS LEVELS OF FREESTREAM TURBULENCE

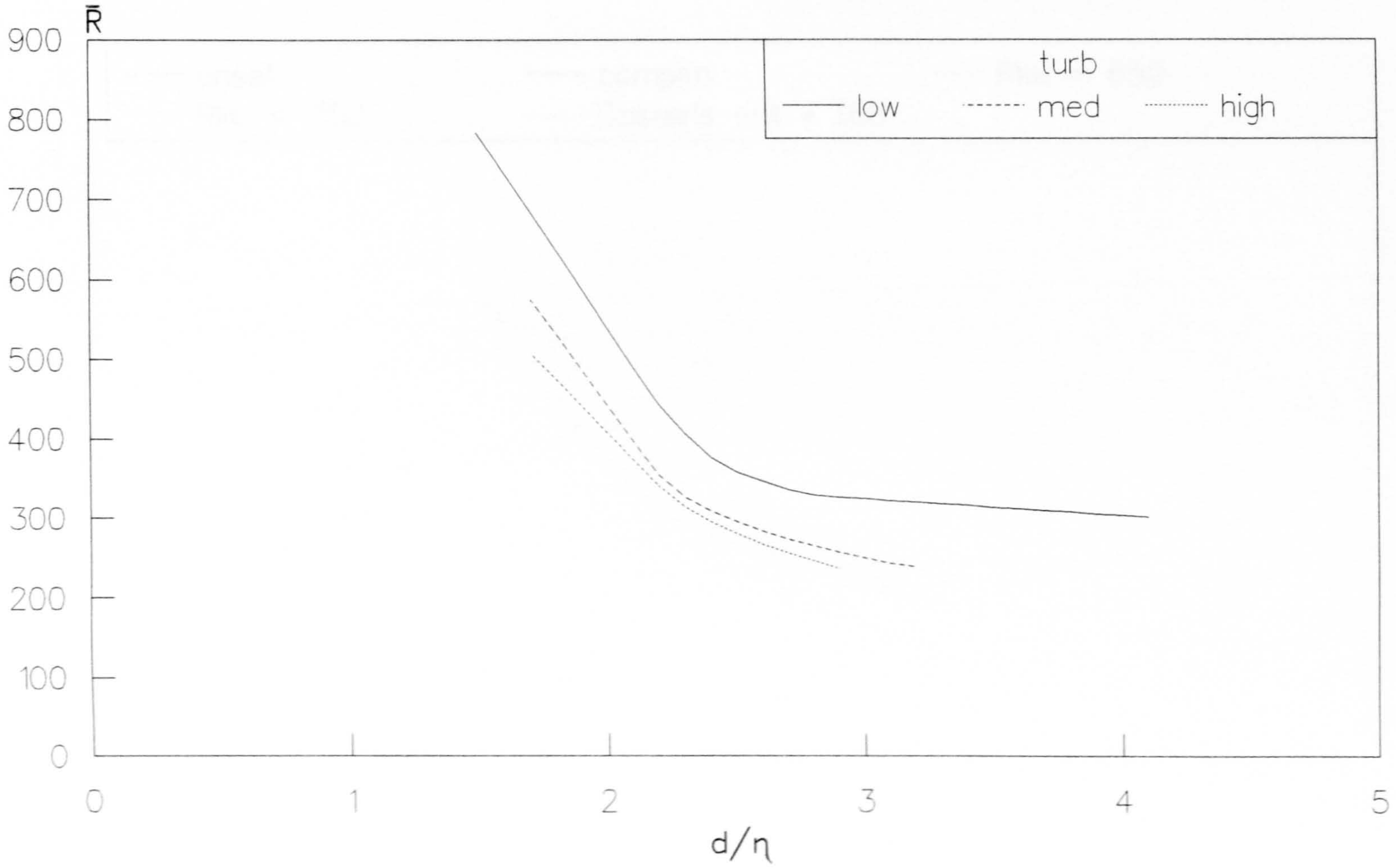

FIG 7.28
TRANSITION IN LIMIT AS s/η TENDS TO ZERO
3D TRIPS, MEDIUM TURBULENCE

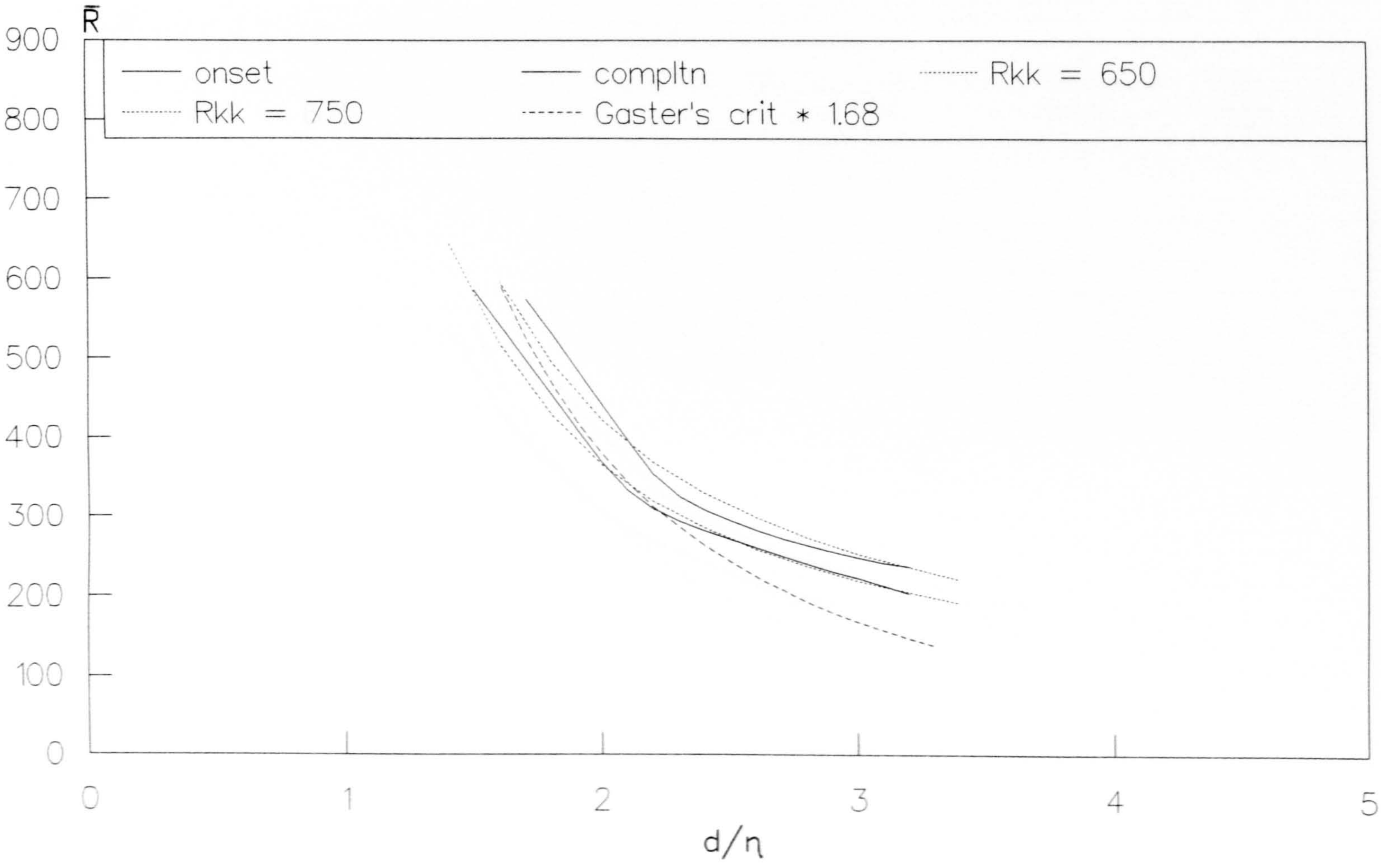

FIG 7.29
TRANSITION IN LIMIT AS s/η TENDS TO ZERO
3D TRIPS, HIGH TURBULENCE

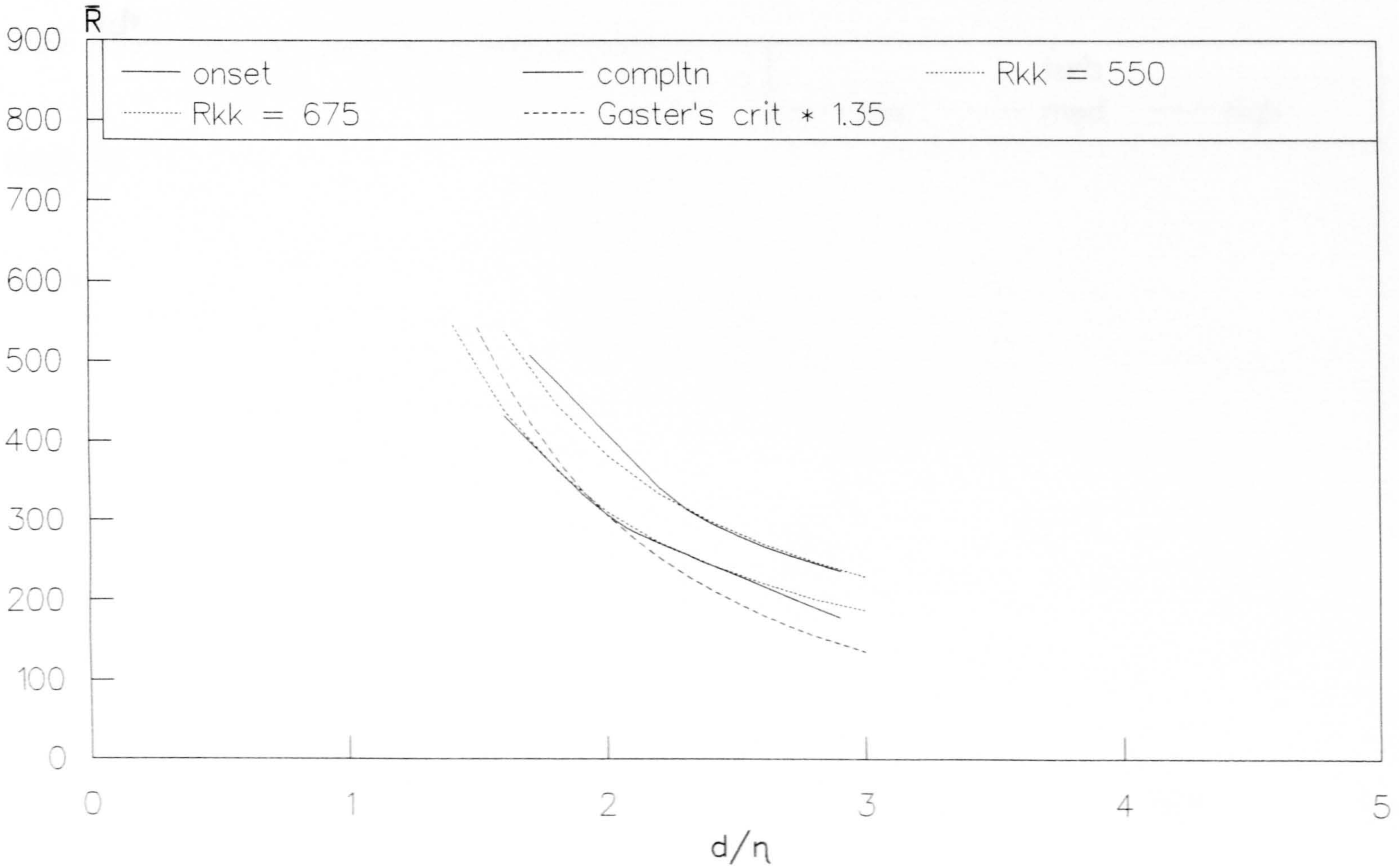

FIG 7.30
TRANSITION ONSET AT TRIP
VARIOUS LEVELS OF FREESTREAM TURBULENCE

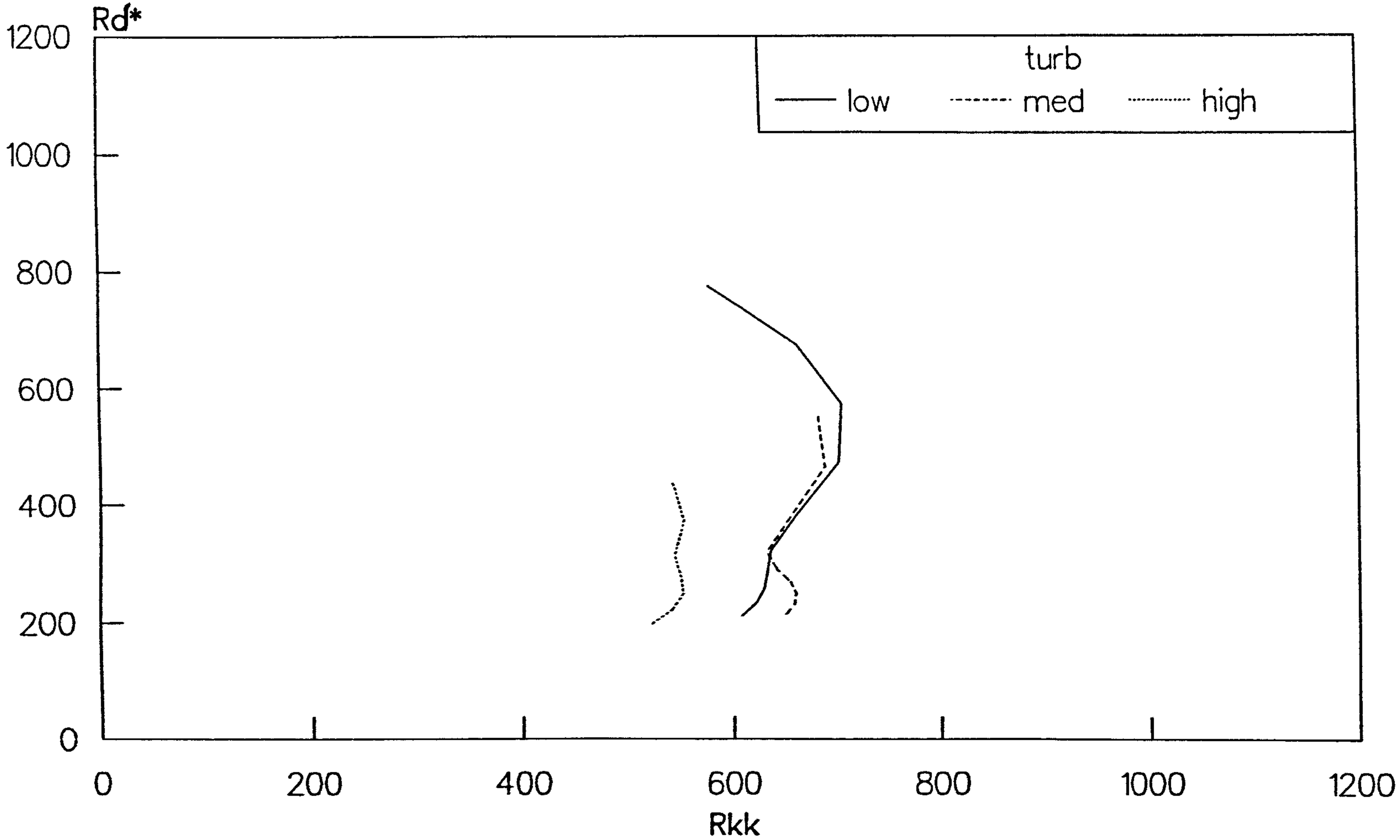

FIG 7.31
TRANSITION COMPLETION AT TRIP
VARIOUS LEVELS OF FREESTREAM TURBULENCE

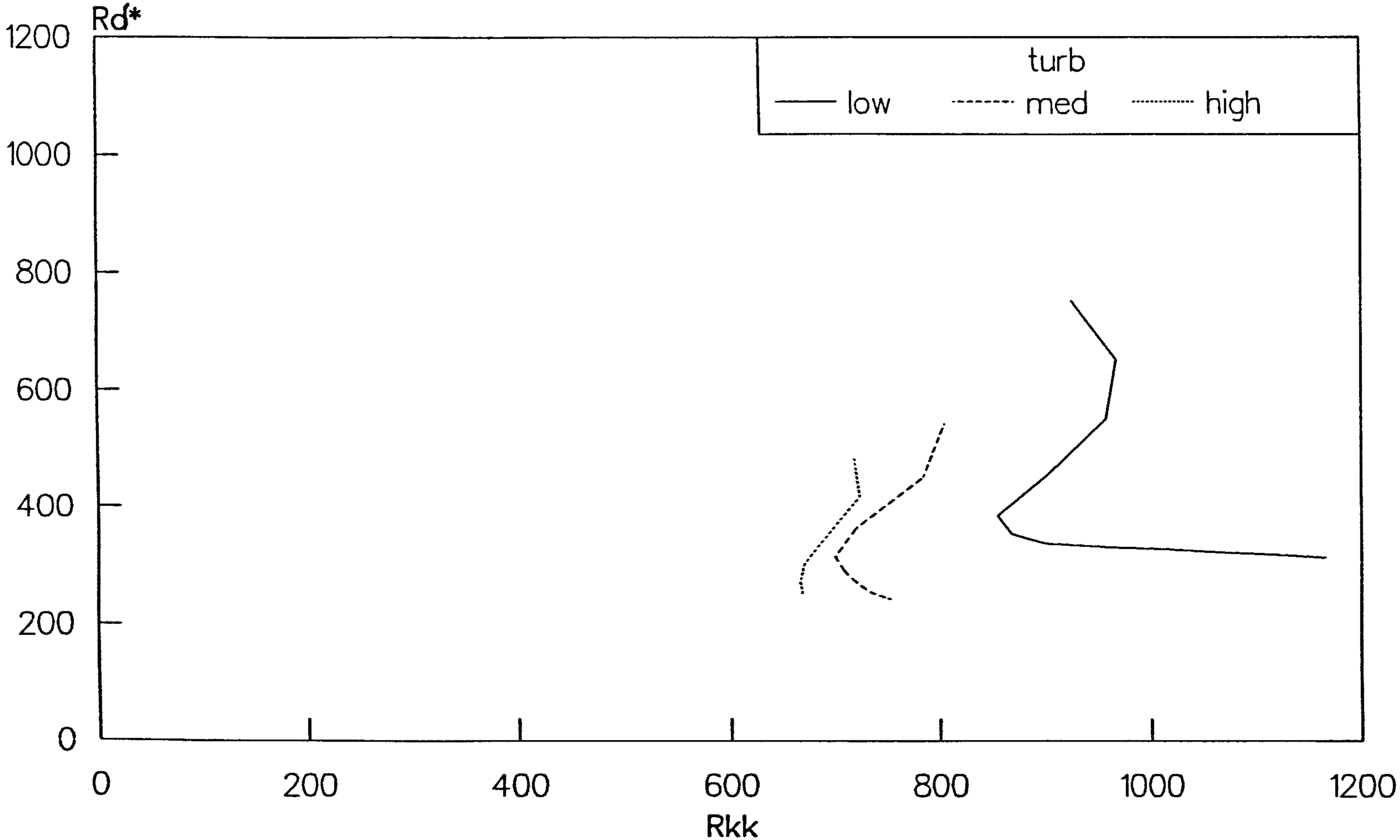

FIG 7.32
GENERAL INTERMITTENCY DISTRIBUTION
3D TRIPS ; MED & HIGH TURBULENCE

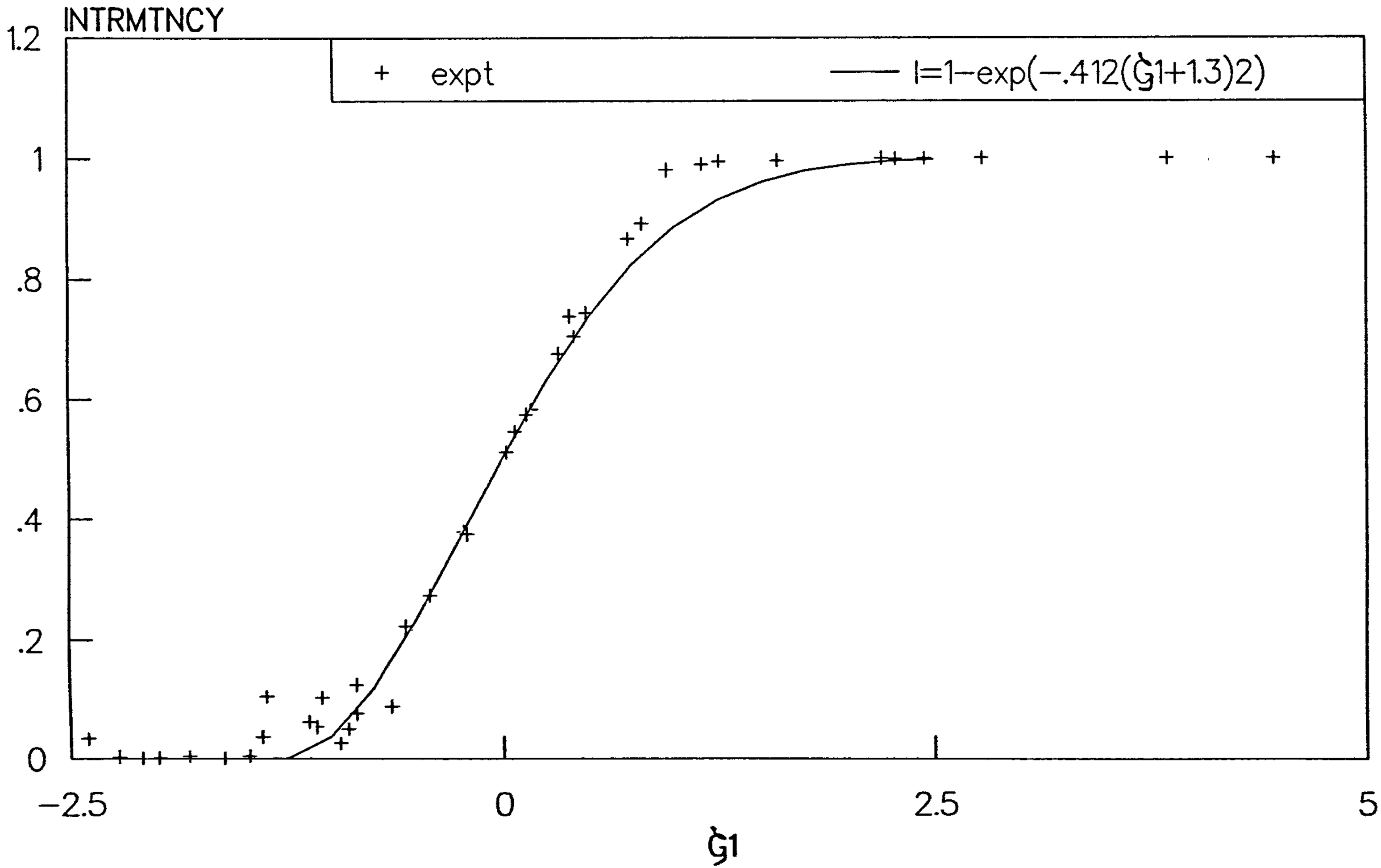

FIG 7.33
GENERAL INTERMITTENCY DISTRIBUTION
3D TRIPS ; MED & HIGH TURBULENCE

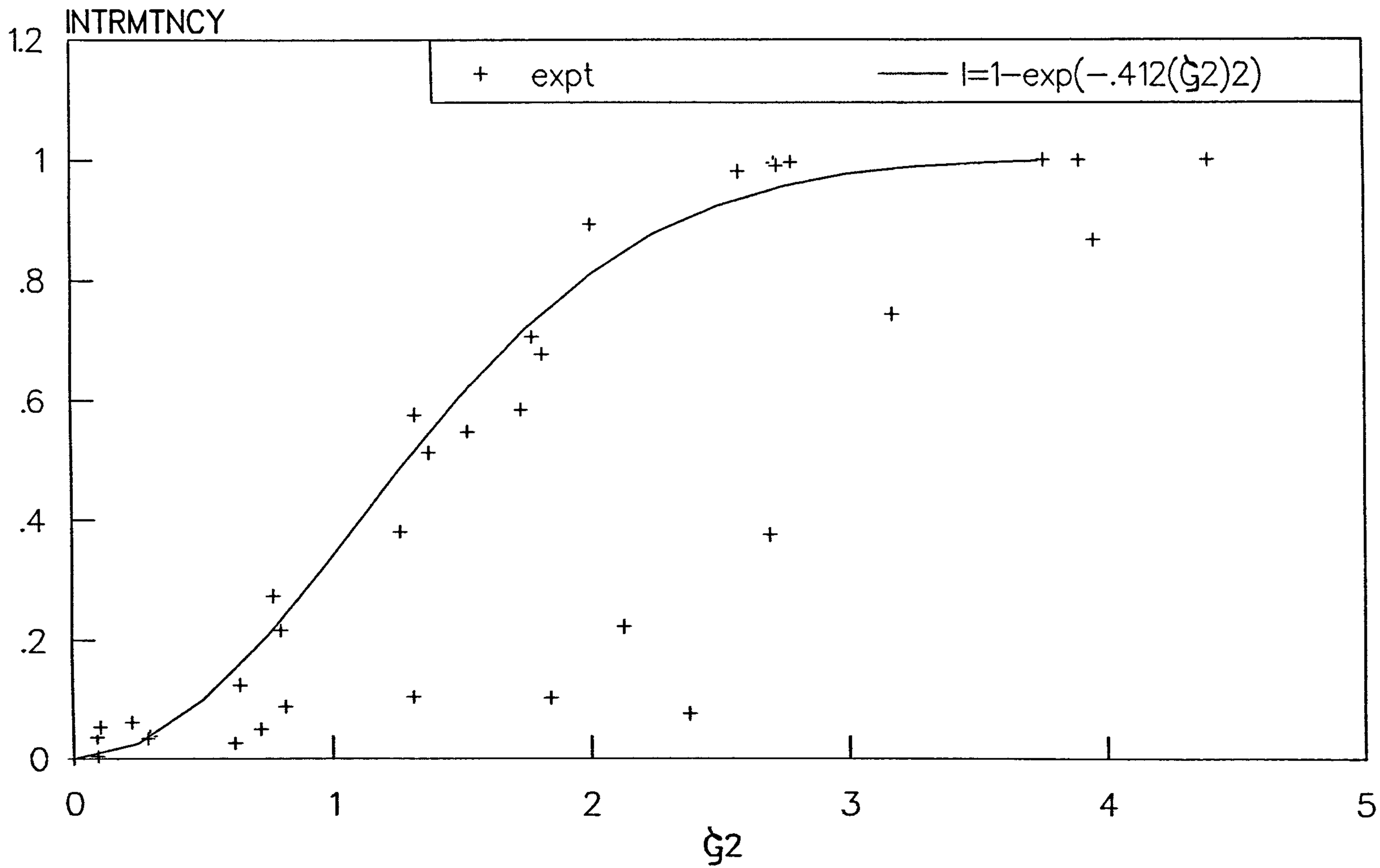

FIG 7.34
LIMITING VALUES OF $\bar{R}$
TRANSITION ONSET, 2D & 3D TRIPS

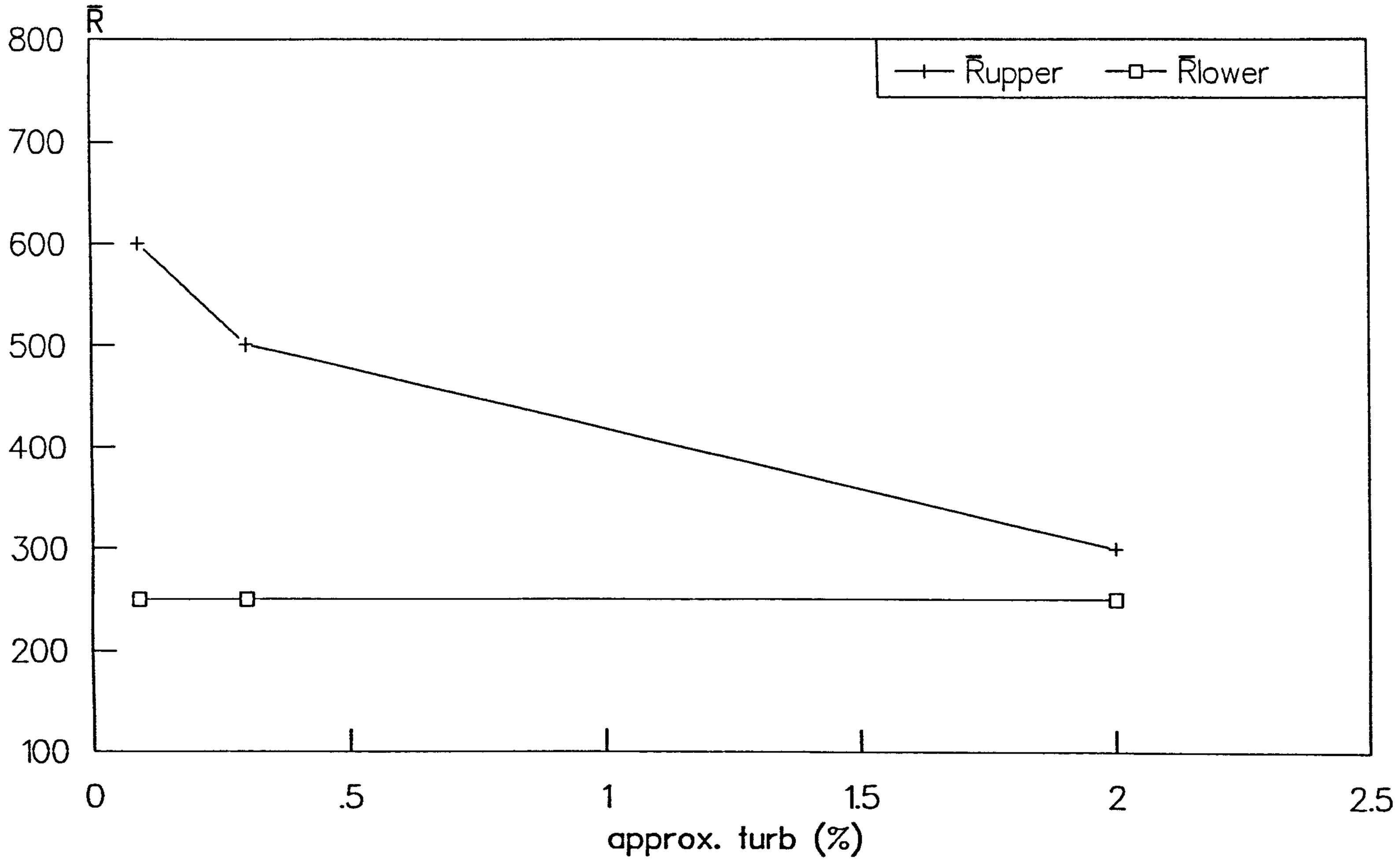

FIG 7.35
LIMITING VALUES OF d/η
TRANSITION ONSET

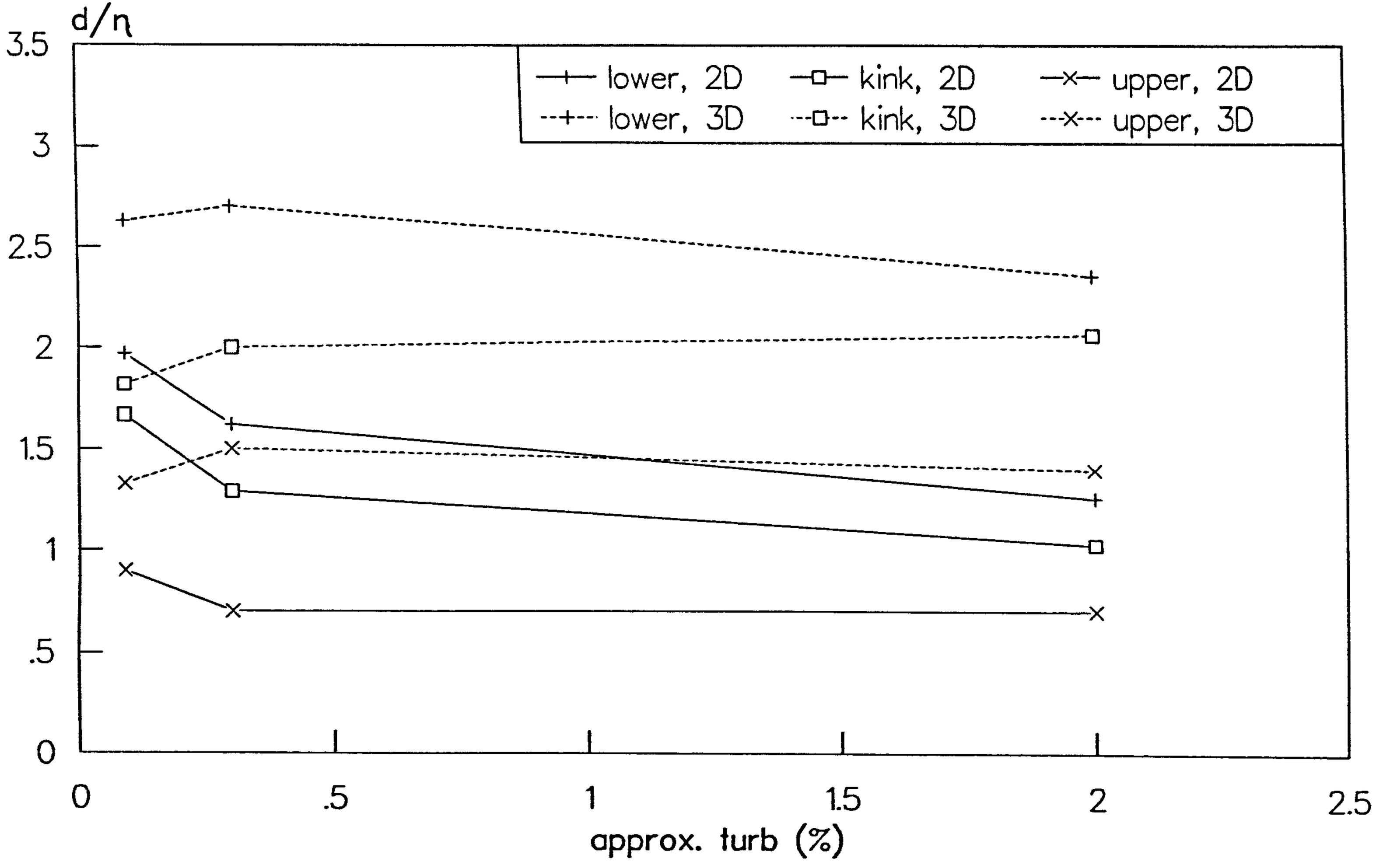

FIG 7.36
VALUES OF Rkk FOR FULLY EFFECTIVE TRIPPING
TRANSITION ONSET & COMPLETION

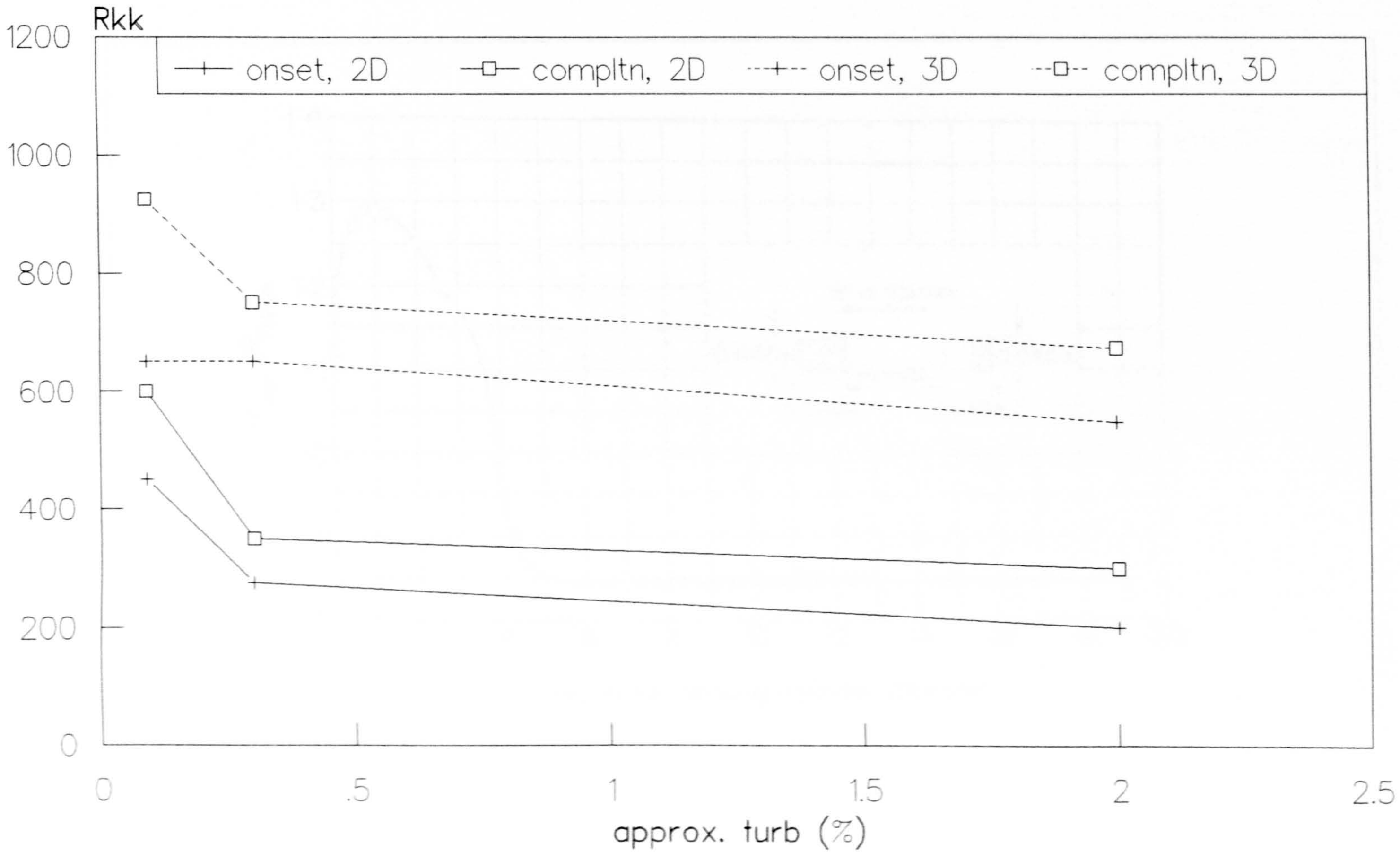

FIG 8.1
TRIP INTERACTION BETWEEN TWO CYLINDRICAL ELEMENTS WITH VARIOUS STREAMWISE SPACING ON A FLAT PLATE

FROM Von DOENHOFF'61

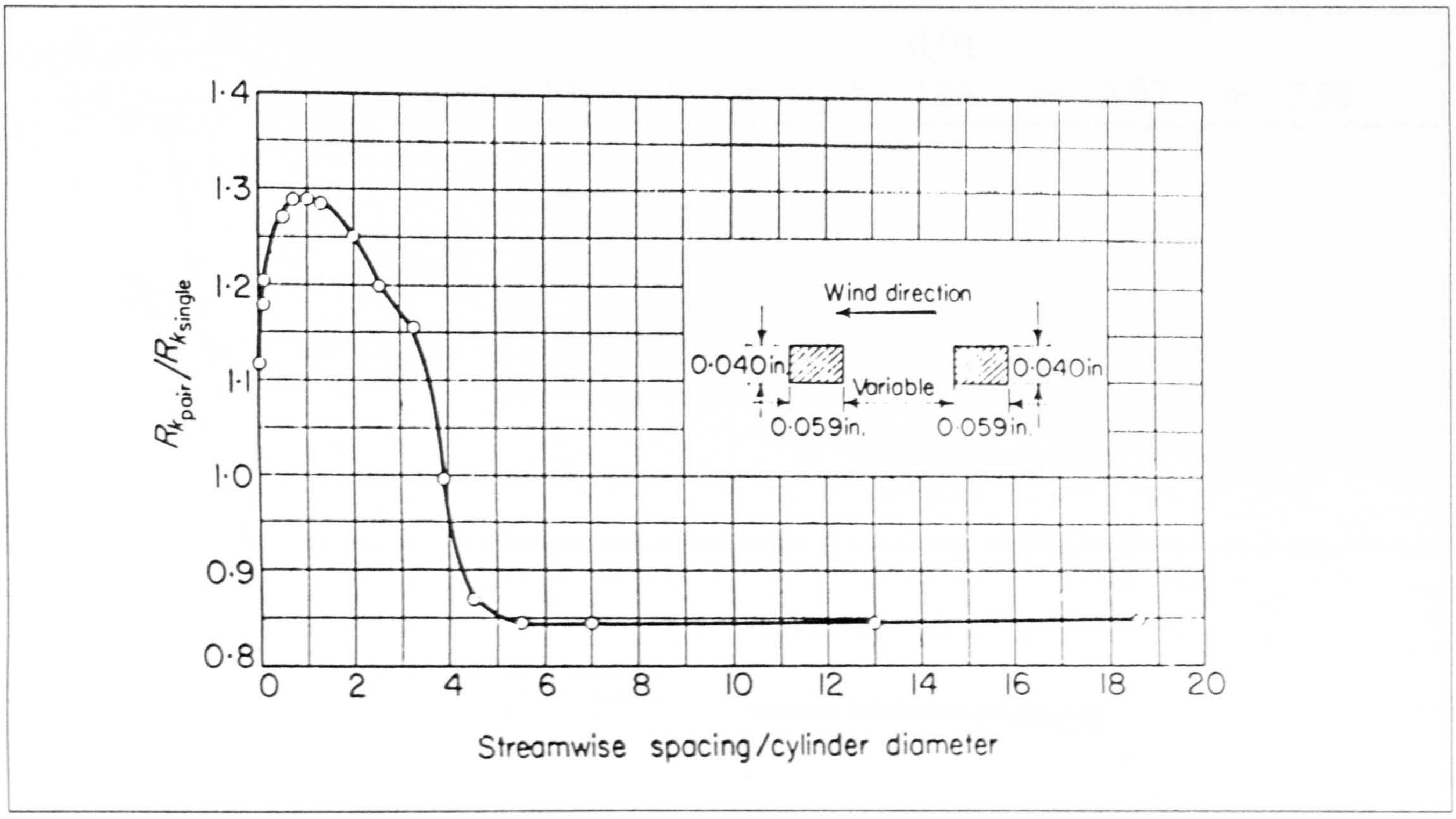

FIG 8.2a
3D TRIP INTERACTION, TRANSITION ONSET
TWO SIMILAR TRIPS SEPARATED BY s12

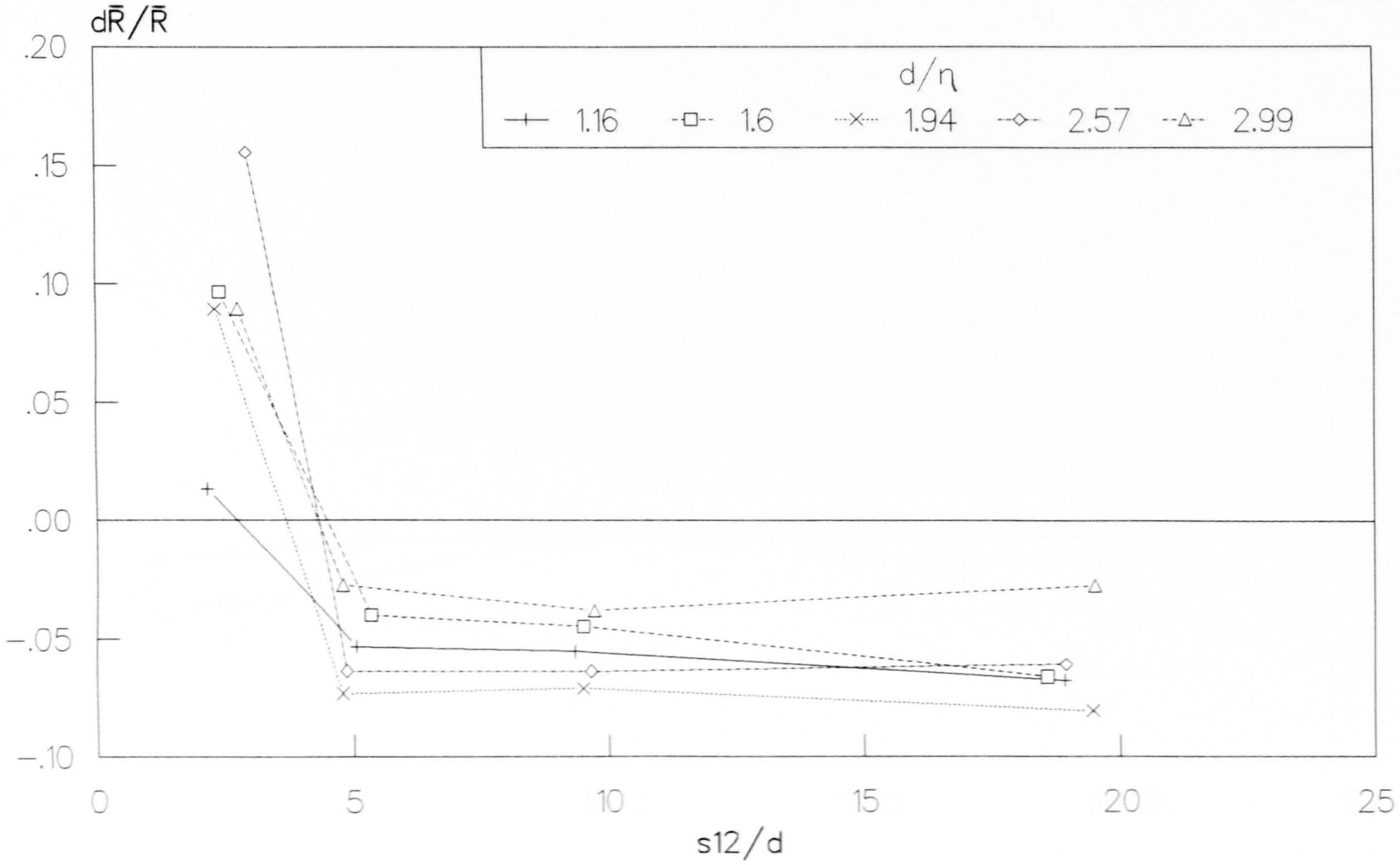

FIG 8.2b
3D TRIP INTERACTION, TRANSITION ONSET
TWO SIMILAR TRIPS SEPARATED BY s12

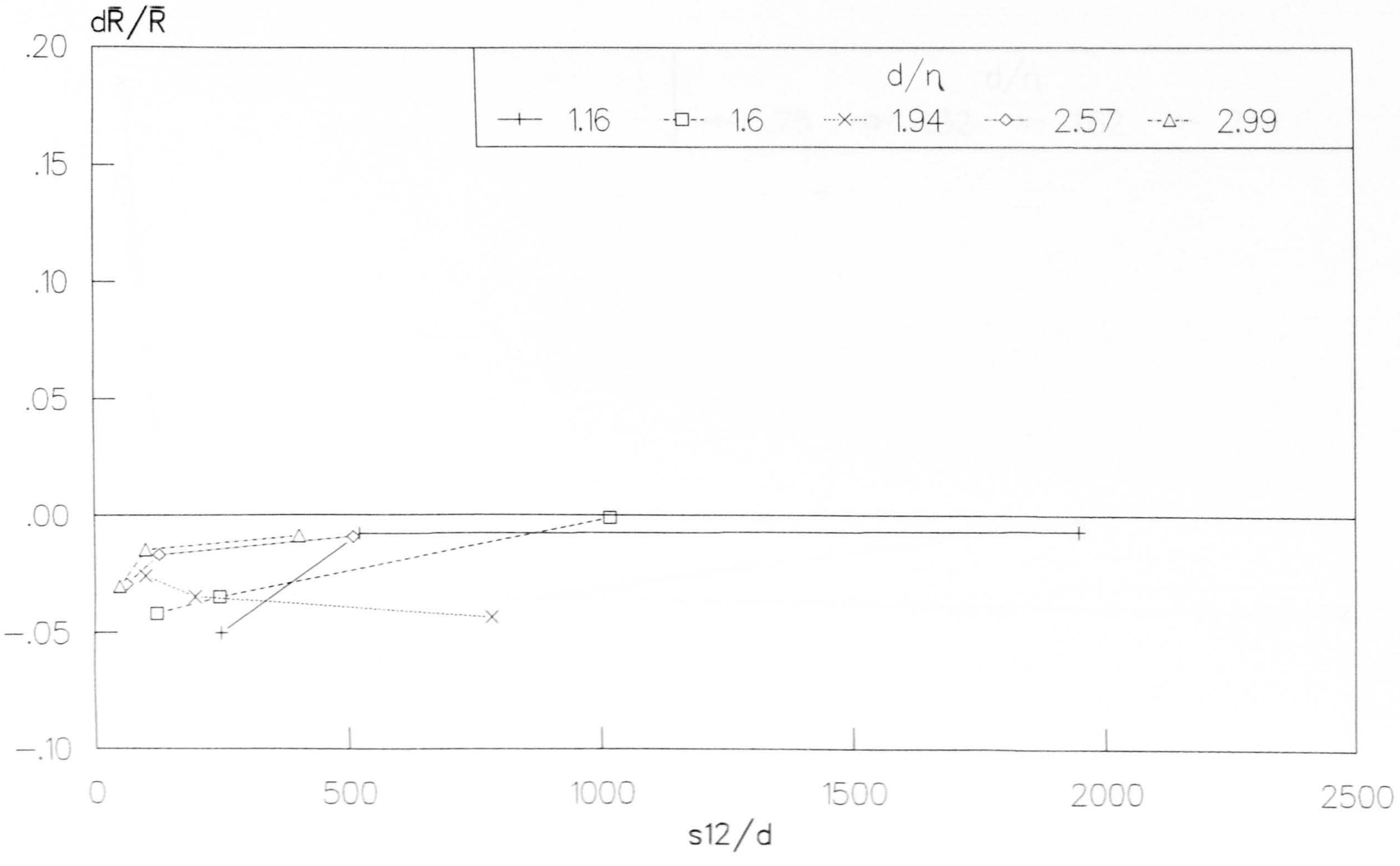

FIG 8.3
2D TRIP INTERACTION, TRANSITION ONSET
TWO SIMILAR TRIPS SEPARATED BY s12